

UNIVERSITY NORTH

ANALYTICAL AND NUMERICAL METHODS OF ISOTROPIC,
ORTHOTROPIC AND RIBBED PLATES CALCULATION

Authors: Prof. Yuriy L. Vynnykov, DSc
Assist. Prof. Aleksej Aniskin, PhD

Reviewers: Prof. Andrii Hryshyn, DSc
Prof. Yurii Kaliukh, DSc

Publisher: University North

For the publisher: prof.dr.sc. Marin Milković

Proofreading: Tina Smolković, Mag.phil.

Graphic editor: Assist. Prof. Aleksej Aniskin, PhD

Print: 100 examples

Publication was approved by the Senate of the University North ac.year. 2017/2018, KLASA:
602-04/18-02/03, Ref. No.: 2137-0336-09-18-8

The CIP record is available in the computer catalog of the
National and University Library in Zagreb under number.

No part of this book may be duplicated,
photocopied, or in any way be reproduced without
publisher's written approval.

1st edition

ISBN 978-953-7809-66-9

POLTAVA NATIONAL TECHNICAL YURI KONDRATYUK UNIVERSITY
/ UNIVERSITY NORTH

**PRACTICAL PROBLEMS OF
ANISTROPIC SOIL MECHANICS**

Yu.L. VYNNYKOV, A. ANISKIN

MONOGRAPH

**Poltava, Ukraine – Varazdin, Croatia
2019**

CONTENT

Preface	7
1. Analysis of the existing researches for soil anisotropy	9
1.1. Analysis of the existing methods for soil anisotropy parameters investigation	10
1.2. Results of the existing researches for soil anisotropy.....	10
2. Experimental methods for soil anisotropy investigations	15
2.1. Physical modelling methods for loose anisotropic strata.....	15
2.2. Field studies methods for natural and artificial (secondary) anisotropy for cohesive soils.....	33
3. Results of the experimental researches for soil anisotropy	39
3.1. Loose soils anisotropy parameters investigation	39
3.2. Field and laboratory studies results for cohesive soils anisotropy	47
4. Experimental studies of the horizontal pressure under different fill up conditions (different orientation of the anisotropy hodograph axis)	59
4.1. Description and calibration of the experimental device	59
4.2. Results of the experimental studies.....	71
5. Mathematical modelling of the soil mechanics anisotropic tasks	83
5.1. Elastic-plastic model of the isotropic and orthotropic soils compaction	83
5.2. General settings for soil compaction modelling software	97
5.3. Engineering tasks of the mathematical modelling for compacted soils anisotropic properties stress-strain state	109
6. Estimation of the homogeneous anisotropic strata interaction with building constructions (engineering tasks)	115
6.1. Calculation of the horizontal pressure from homogeneous anisotropic strata on retaining walls	115
6.2. Deformational anisotropy account with calculation of the soil bases and foundations settlements	143
Conclusions	149
References	151

PREFACE

Anisotropic soils and rocks (clay deposits of water, eolian, Eolian-glacial origin, peaty, frozen, solonetz and some other varieties) are quite characteristic of modern geotechnical practice. According to a number of experts, the anisotropy in soils is rather a rule than an exception.

However, in the scientific and normative literature, the results of experimental studies of soil anisotropy parameters, analytical and numerical solutions of the applied problems of the interaction of anisotropic medium with constructions presented insufficient. That is why the authors suggest to familiarize colleagues-geotechnicians with their work in this direction.

In particular, the current state of anisotropy studies of soils is analyzed in the first section of the monograph.

The author's methods of experimental studies of anisotropy of loose and coherent soils are described in Section 2.

The third section analyzes the results of laboratory and field studies of natural and induced anisotropy of loose and coherent soils.

Experimental studies of silo pressure under different conditions of filling (for different orientation of the anisotropy hodograph axis) are given in Section 4

The fifth section describes a phenomenological model of isotropic and orthotropic soil developed to evaluate the stress-strain state (SSS) of the fundamentals using the finite element method (ITU) and the stepwise iterative procedures, the main provisions of the software complex with the grid of variables in the form and on the the volume of curvilinear axisymmetric finite element oriented on the modeling of soil consolidation problems, as well as an example of the solution of such a problem.

Engineering solutions for calculating the lateral pressure of anisotropic soils on closely spaced walls and taking into account deformation anisotropy in determining the settling of foundations are given in Section 6.

Section 5, clauses 2.2, 3.2, 6.2 written by the dr. of tech. sciences, professor Yu.L. Vinnikov (Poltava National Technical University named after Yuri Kondratyuk, Ukraine), section 4, clause 2.1, 3.1, 6.1 by Associate Professor A. Aniskin, PhD (University of the North, Varazdin, Croatia), introduction, section 1 and conclusions written by the authors jointly.

The work is carried out within the international program Erasmus +.

The authors express their sincere thanks to the DSc, professor M.L. Zotsenko and DSc, professor A.V. Shkola for useful advice in their scientific work on the topic of work.

They are also sincerely grateful to the reviewers of the monograph DSc, professors A.V. Grishin, Yu.I. Kalyukha and V.G. Shapoval.

1. ANALYSIS OF SOIL ANISOTROPY STUDIES

If the properties of the soil sample do not depend on its spatial orientation in the array, then such a soil is called isotropic. In the opposite case, the soil is considered as anisotropic.

The idea of the unjustified widely distributed soil isotropy hypothesis and the possibility of using their anisotropic model in geotechnical problems is developed in the works of I.P. Boyka, O.K. Bugrova, FG Gabibova, G.O. Geniev, OI Golubeva, MN Goldstein, M.F. Drukovany, V.V. Kovtuna, O.A. Korobova, AP Krivorotova, V.V. Lushnikova, MO Molyeva, P.M. Nazi, O.V. Novsky, L.V. Nuzdina, OO Petrakova, AF Polaka, Yu.O. Sobolevsky, LM Timofeeva, S.Ya. Tsimbala, GI Chernoy, VG Shapovala, A.V. Shkola, LM Shutenka, V.B. Shvets, N.S. Shaw, B. Amadei, L. Barden, A. Casagrande, M. Cudny, I. Duncan, G. Gazetas, H. Kulatilake, J. Loc, J. Magnan, M. Molenda, H. Seed, J. Nielsen, K. Zhang and etc. [3, 9, 11, 12, 24, 31, 46, 52 - 54, 56, 58, 60 - 63, 69, 71, 78, 84, 87, 89, 92, 95, 119].

Designers are usually interested in the difference in the mechanical properties of the soil in different directions, or the so-called *mechanical anisotropy* (for example, deformation anisotropy, anisotropy of strength, anisotropy of swelling), and sometimes the difference in filtration properties, or *filtration anisotropy*.

The anisotropy of the mechanical properties of soils is explained by their ordered structure with the priority parallel orientation of the particles in some direction.

There are two types of anisotropy, the primary or natural anisotropy of the soil is caused by its natural structure (in particular, the ordered structure of the soil with the parallel orientation of the particles), origin, conditions of formation (in particular, the process of sediment accumulation), etc., and secondary, or given, anisotropy, nature and regularities which depend both on the natural structure of the soil and on the peculiarities of the technology of arranging artificial bases or foundations, for example, from the direction of squeezing of soil particles by a working body (a ram, a roller, a pneumopter), piles, blocks, explosion, etc. Interfundamental spaces and so on. al. [4 - 8, 17, 18, 32, 121 - 123].

Natural anisotropy is quite characteristic of all groups of rocks of its origin, in particular magmatic with crystalline structure, sedimentary with layered or shiny texture and metamorphic with dislocation metamorphism (with significant single-sided compression of rocks).

In soils, natural anisotropy is common in clay deposits of water (especially marine, lake) origin, forests, belt clays, and the like.

1.1. Analysis of methods for investigating the parameters of soil anisotropy

The mechanical properties of anisotropic soils are usually investigated by selecting their samples, in particular, by cutting rings that are clearly oriented at different angles (for example, $\alpha = 0; 45; 90^\circ$ etc) to the horizontal plane (it is often conventionally taken as an isotropic plane), followed by a test in odometers, cutting devices, stopwatches, penetrometers, etc. [1, 3, 4 - 8, 17, 32, 61, 121 - 123].

Penetration tests of the soil are carried out also in field conditions, for example, by field dynamometric penetrometers perpendicular to the sections, cleared in the array in different directions to the horizontal plane.

At each point of the array for all directions of research α of the characteristics relative to the horizontal plane with close variation coefficients, the value of the mechanical characteristics of the soil is conveniently presented in the form of *hodographs* or their *quadrants*, which are a graphical representation of the dependences of the values of mechanical characteristics of the soil on the angle α [1, 7, 18, 57 - 61].

The coefficients of anisotropy of soil mechanical characteristics are usually determined by formulas

$$n_{E,\alpha} = E_\alpha / E_- ; \quad (1.1)$$

$$n_{c,\alpha} = c_\alpha / c_- ; \quad (1.2)$$

$$n_{\varphi,\alpha} = \text{tg}\varphi_\alpha / \text{tg}\varphi_- ; \quad (1.3)$$

$$n_{R,\alpha} = R_\alpha / R_- , \quad (1.4)$$

where - E_- the module of deformation of the soil in the plane of isotropy from the action of stresses in the same plane (orientation of the rings at an angle $\alpha = 0^\circ$ relative to the horizontal plane); E_α – the same, for the plane, inclined to the plane of isotropy at an angle α ; c_- ; c_α ; φ_- ; φ_α – Specific grip and angle of internal friction of the soil in the plane of displacement correspondingly parallel ($\alpha = 0^\circ$) and inclined to the plane of isotropy at an angle α ; R_- and R_α – the specific resistance of the penetration, respectively, at angles $\alpha = 0^\circ$ and $\alpha \neq 0^\circ$ to the isotropy plane.

1.2. Results of soil anisotropy studies

In fig. 1.1 gives the quadrants of the hodographs of the properties of the strength of natural and bulky soils, built on the results of compression and displacement tests [60].

The most common dependence, which biSSS the characteristics of soil strength with the orientation of the cut plane, was developed by A. Casagrande and N. Carillo [69]

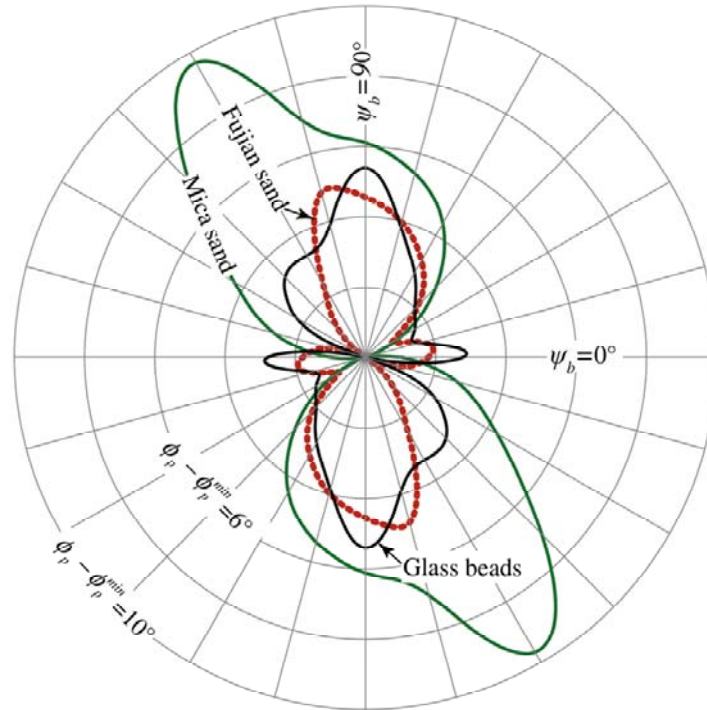


Fig. 1.1 Hodograph of the change of the angle of internal friction according to Z. Tong [115]

$$S_{\beta} = S_1 + (S_2 - S_1) \sin^2(\beta - \alpha), \quad (1.5)$$

where S_1 and S_2 are the boundary supports of the displacement along the orthogonal axes of symmetry, one of which is oriented at an angle α to the reference frame; β is the angle of the orientation of the sliding area.

A.V. Shkola [59] for assessing the degree of anisotropy of soils proposed the use of a dependence, which allows to integrate the anisotropy of the characteristics of strength in all directions of the implemented research

$$\mu = 1 - \frac{\Omega}{\pi \rho_{\max}^2}, \quad (1.6)$$

where $\rho(\beta)$ - index of resistance to the shift of soil; ρ_{\max} is the maximum value of ρ in the experimental hodograph.

The obtained function generalizes the known dependence of A. Casagrande and N. Carillo (1.5) and is proposed for use in practical calculations to determine the bearing capacity of anisotropic resistive impedance bases.

In a number of studies two types of anisotropy of soil foundation properties are distinguished. The first type of anisotropy is related to the texture of the soil, that is, with the layer, represented by soil layers with different granulometric composition, structure and physical-mechanical properties. He was described by N.V. Ornatsky [34] and M.E. Harry [49]. The second type of anisotropy is determined by the predominant orientation of the occurrence of particles in

space. In the theory of granular environments it was developed by N.V. Ornatsky [34], VV Genius [10] and II Kandaurov [19]. It is noted that under the influence of gravitational forces, unsymmetrical soil grains are arranged in arrays with a larger surface horizontally.

Experimental studies of the anisotropy of the strength of discrete environments, clay, mules and loose metiers were studied by O.A. Korobova [25], Yu.B. Osipov and AI Vayeykuny [35], Zh.E. Rogatkin [40], C.C. Sadovsky [41], Ye.M. Sergeev [111], B.A. Sokolov [43], VA Filimonov [48], S.Ya. Tsimbal [51], I. Arthur [64], Z. Ewertowska-Madej [74], R. Krizek [86], K. Lo et al. [88, 89], A. Loh [90], R. Yong and V. Sylvestry [118], Z. Bazant [65], I. Duncan and H. Seed [72], S. Nishimura [101], Z Yang et al. [117] M. Oda [106] et al.

In work P. Guo [79] studied the anisotropy of the strength of the sand by direct cutting in directions, in the range of angles of inclination of the plane of the occurrence of particles to the horizontal from 0° to 90° . Experiments used a special procedure for preparing the sample in a collector shifter (cut) in the size $60\text{ mm} \times 60\text{ mm} \times 45\text{ mm}$. Investigated loose materials from coarse and clumsy forms, crushed limestone (clumsy forms), Ottawa sand (wrapped) and glass beads.

The results of the experiment showed a change in the angle of internal friction in directions, for corn grains of crushed limestone at 16%, with the smallest friction angle observed at an angle of 30° , and the largest at 90° , for the ottawa sand Ottawa, the difference was less pronounced and amounted to 11% , the minimum and maximum angles φ were observed also at angles of occurrence of 30° and 90° . For beads, the difference was only 3%; in this case, the anisotropy can be neglected. It is argued that the anisotropy affects not only the angle of stacking, but also the shape of the grains, and the friction angle decreases with increasing vertical load.

Z. Tong et al. [115] analyze the results of experimental studies of the direct cut of three types of loose materials - two types of saSSS and a mixture of glass sharecks of different magnitudes. Experiments were carried out in a specially designed cut-off shear box of $60\text{ mm} \times 60\text{ mm} \times 43\text{ mm}$ with the ability to fill the samples in the shear box at various angles to the plane of displacement. 144 experiments were conducted. The angle between the plane of occurrence of the particles and the cut plane ψ_b was in the range from 0° to 180° , in a step of 15° . In experiments, the change in the peak internal friction angle φ was investigated for each material in relation to the angle ψ_b for various vertical stresses. As a result, a significant anisotropy of the internal friction angles has been approved. The value of the internal friction angle for the mica sand mixed with clumsy grains was in the range of $41^\circ - 52^\circ$, that is, the difference was 26.83%, for the quartz sand (long-tailed beans), $37^\circ - 43^\circ$, that is - 16.22%, and for glass beads - in the range from 30° to 36° , which was 20% (Fig. 1.1). The authors note that the smallest value of the internal friction angle is observed at the angles of the

orientation of the particles to the cut-off angle close to 0° and 180° , for the Fugianian sand - 150° , for the Mica sand - 15° , and for the glass beads - 165° . An interesting fact was found when testing glass beads. The difference in the angle of internal friction in the direction of the authors explained the imperfection of the form of balls and the anisotropic distribution of stresses in the formed array.

Works of A.V. Shkola and A. Haydar [50, 58] are devoted to the experimental study of the anisotropy of strength on the device of a straight cut of GHP-30. Experiments were carried out on three types of natural clay soils: saSSStone; macroporous loam; loam of brunette. Experiments were performed at normal pressures of 50 and 150 kN/m². Sampling was performed in directions at angles of 0° , 45° , 60° , and 90° to the horizontal. On the basis of the tests of 393 samples, homodographs of the internal friction angle $\varphi(\beta)$ and specific traction with $c(\beta)$ were constructed. The results confirmed the presence of anisotropy of strength in experimental soils, in addition, the effect of moisture on the samples was found, which significantly reduced the resistance to shifts, and the histogram changes.

The work of O.V. Novski is devoted to the laboratory research of the anisotropy of the indicators of resistance to the shift of the limestone-shell for the lateral surface of the models of drilling piles. Novsky [102]. Research in laboratory conditions is carried out in compliance with the main requirements of DSTU B B.2.1-1-95 "Soils, methods of field tests by piles". In tests, resistance was determined for a shift along the lateral surface of models of bored piles with a diameter of 21 mm. The tests were carried out with a pair of pile-widths, along and at an angle of 45° to the lamellity, and on the basis of their results, the coefficients of anisotropy were calculated as the ratio of the characteristics obtained during the loading along the layer and at an angle to the corresponding characteristics across the layer. The results of the conducted research showed that the resistance to shifts along the lateral surface of the drilling piles along the lamination is 16,28% smaller than the width, and at an angle of 45° to the lamination of 8,93% higher. In this case, the coefficients of anisotropy were respectively 0.86 and 1.08.

In work T. Dunstan [73] shows the results of tests on the shift (cut) of gravel in a natural deposit and sandy soils of various granulometric composition. Four types of saSSS were tested, and the strength parameters were determined in horizontal and vertical directions, with vertical loads of 71, 126 and 266 kN/m². The angle of internal friction at the cutting in the vertical direction was on average 10% higher than when slice along the layer. The author notes the effect of granulometric composition on the strength anisotropy indices.

Interesting experimental studies of wheat grain strength on shifts, depending on the technology of stacking grains, were conducted by M. Molenda and M. Stasiak [95].

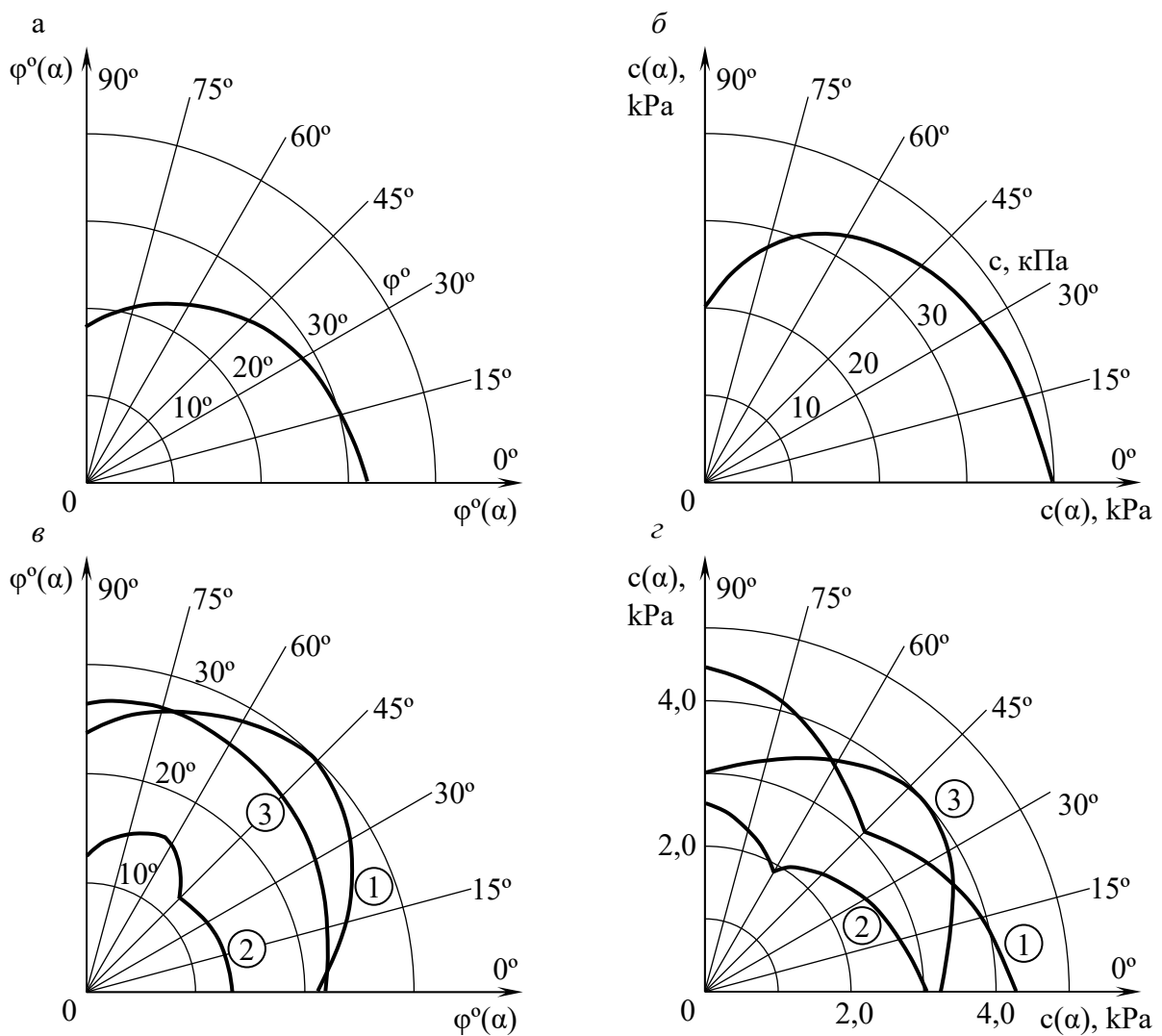


Fig. 1.2 – Examples of quadrants of hodographs of strength characteristics for soils with natural anisotropy: a, b - according to A.V. Shkola; c, d - according to M. Yu. Abelieva: 1 – loess loam in the natural state; 2 – loess loam in wet state; 3 - loess sand in the natural state

A sample of 25 cm x 61 cm was tested in a non-standard chamber of a straight cut. The wheat was covered in four different ways - a standard bucket, through a sieve, and under a slope to a cut plane, in which the long axes of individual grains were sharp and at a dull angle to the direction of displacement. As a result, the angles of internal friction with different orientations of grain in the zapypki differed by 16%, in addition, the nature of the shift curve also varied. The minimum angle of internal friction is obtained by filling at an oblique angle in the cut plane (25 °), and the maximum when filling through a sieve (29 °). The authors emphasize that the anisotropy strength characteristic is the result of a method of forming an array.

Examples [18, 57, 58] of such quadrants of hodographs for soils with natural anisotropy are given in Fig. 1.2.

2. METHODS OF EXPERIMENTAL RESEARCHES OF SOIL ANISOTROPY

2.1. The method of physical modeling of a loose anisotropic medium

Materials used. For anisotropy tests, two loose environments, long grain rice and a mixture of sand with flat particles of a beaten shells in certain ratio - a composite medium.

Rice - a loose anisotropic material. The rice was used to model the anisotropy of the bulk medium. The grain of rice is anisotropic in geometry, the average grain length is four times the thickness. In addition, rice grains are practically the same, that is, the composition of the medium is close to homogeneous. Using rice, it is possible to get a fairly good prevailing angle of orientation of grains (Fig. 2.1) with different technologies of filling the grooves of structures.

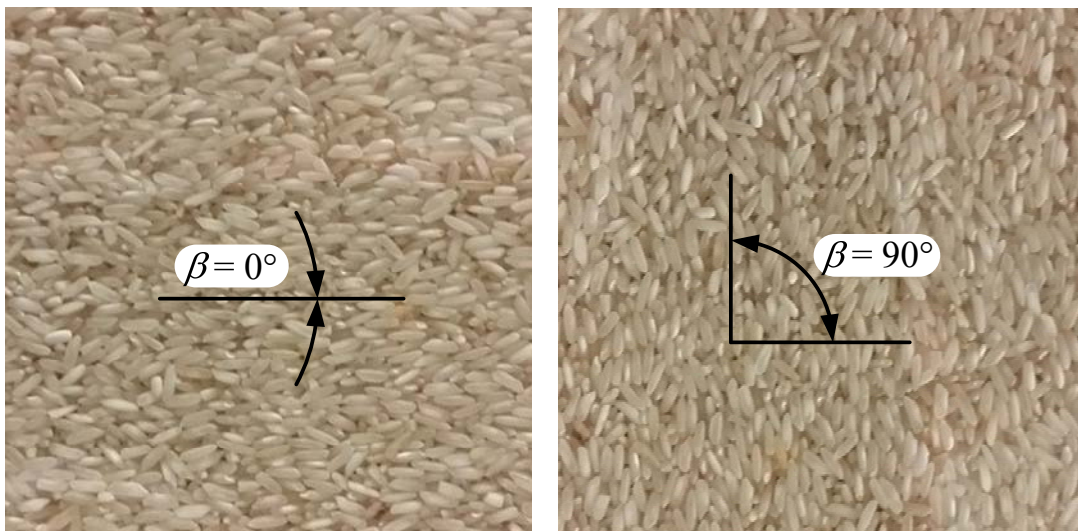


Fig. 2.1 - The preferred angle of orientation of rice grain to the horizontal

Under the filling technology, we will understand the sequence of operations in which, in the formed array, we obtain the desired angle of orientation of the grains (particles) of the material to the reference plane. This angle will be called the filling angle, and for filling in the shear box of the cut we will denote it β . In the literature, this angle is also called the angle of occurrence of the basis [115]. The reference plane is often horizontal.

It is known that for rice and other loose materials with anisotropic grain geometry, when filling from above on a horizontal surface, most grains fall in large size horizontally, that is, they occupy a more stable equilibrium state [34]. Thus, the rice test will allow us to estimate the effect of the grain orientation on the shift plane on the anisotropy of the parameters of strength c and ϕ . Test

results can be of interest to scientists - grain workers and builders who design silos and grain bins.

Long-grain polished rice has grains of white color, elongated shapes, similar to ellipsoids of average size 2 mm x 2 mm x 8 mm (fig 2.2).



Fig. 2.2 - General view of the model material - rice

For each shear, weighing of the volume was carried out according to the Croatian standard HRN U.B1.016. The obtained data is presented in the table 2.1.

It is important to note that rice grains are organic material, which in its composition contains water, the share of which is on average about 13%. Rice grains were tested in dry condition.

Table 2.1 - Basic physical characteristics of rice

Property	Standard	Value
Specific weight	HRN U.B1.016	$\gamma = 8,85 \text{ kN/m}^3$
Specific gravity of particles	HRN U.B1.014	$\gamma_s = 13,72 \text{ kN/m}^3$
Humidity	HRN U.B1.012	$w = 13,69 \%$.

Then the granulometric composition was tested in accordance with HRN U.B1.018. For this purpose a device for determining the granulometric composition of Model 15-D0403 of the Italian manufacturer Controls S.r.l was used. According to the standard, the sifting process lasted 10 minutes. Particle size curve for rice is shown in Fig. 2.3.

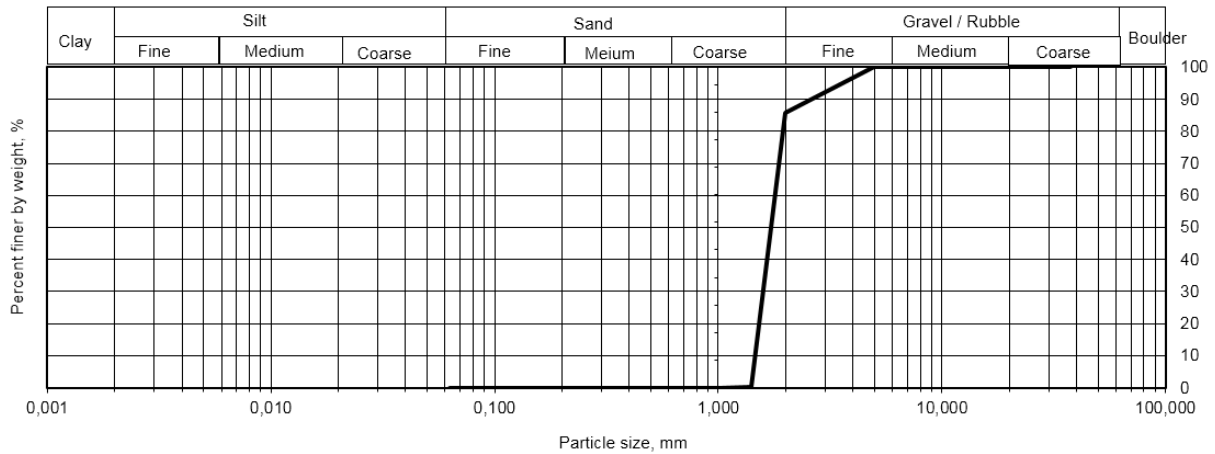


Fig. 2.3 - Granulometric curve of the model material - rice

The granulometric curve determined the effective diameters (D_{10} , D_{30} and D_{60}), coefficients of inhomogeneity (C_U) and curvature (C_C). The coefficient of heterogeneity was determined by the formula $C_U = \frac{D_{60}}{D_{10}}$, and the coefficient of curvature - by expression $C_C = \frac{D_{30}^2}{D_{10} \cdot D_{60}}$.

The smaller the heterogeneity coefficient, the steeper granulometric curve, indicating the homogeneity of the medium. Smooth curve indicates heterogeneity.

The coefficient of curvature characterizes the shape of the granulometric curve. The results are shown in Table. 2.2.

Table 2.2 - Characteristics of granulometric curve of rice

$D_{10} =$	1,6	$C_U =$	1,13
$D_{30} =$	1,7	$C_C =$	1,00
$D_{60} =$	1,8		

Composite medium. The first component of a dry composite medium is sifted sand from the basin of Drava river, a fraction of 0-4 mm. This sand is very often used in construction practice in Croatia. Grain - rolling, from the alluvial deposits of Draw (Fig. 2.4).

Large deposits of sand and pebbles in the Drava River basin are formed by the displacement and melting of glaciers with a weathered mountain rock from the Alps in the Holocene. The thickness of the layers in the fields is variable from 20 up to a maximum of 148 m [77]. A light fraction of sand makes up about 40% of quartz, 40% of rock, 12% of feldspar, carbonate grains and muscovite.



Fig. 2.4 - Sand - the first component of the composite medium

The main physical characteristics of dry sand ($w = 0\%$) are given in Table. 2.3, and granulometric curve - in Fig. 2.5.

Table 2.3 – Basic physical characteristics of the sand

Property	Standard	Value
Specific weight	HRN U.B1.016	$\gamma = 17,51 \text{ kN/m}^3$
Specific gravity of particles	HRN U.B1.014	$\gamma_s = 27,23 \text{ kN/m}^3$

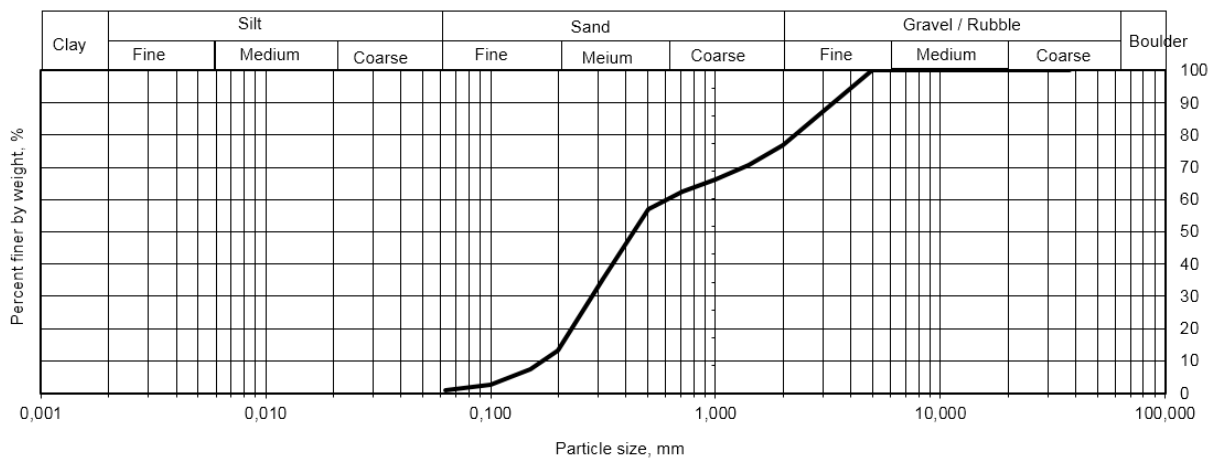


Fig. 2.5 - Granulometric curve of model sand material

Data obtained from the granulometric curve, are given in Table. 2.4.

Table 2.4 - Characteristics of granulometric sand curve

$D_{10} =$	0,17	$C_U =$	3,53
$D_{30} =$	0,28	$C_C =$	0,77
$D_{60} =$	0,6		

The second component of the composite material are flat particles of beaten shells of mussels (Fig. 2.6) sifted with a square sieve with a size of 7 mm. The shell particles in the composite mixture of their orientation cause anisotropy at different orientations in space [59]. All mussels were caught in the Krka River Delta near the port of Sibenik in Croatia



Fig. 2.6 - Parts of a beaten shell

The basic physical characteristics of a dry turtle ($w = 0\%$) are given in Table. 2.5.

Table 2.5 - Basic physical characteristics of the shell

Property	Standard	Value
Specific weight	HRN U.B1.016	$\gamma = 11,58 \text{ kN/m}^3$
Specific gravity of particles	HRN U.B1.014	$\gamma_s = 26,78 \text{ kN/m}^3$

The data obtained for the granulometric curve for a shell (Figure 2.7) is presented in Table. 2.6.

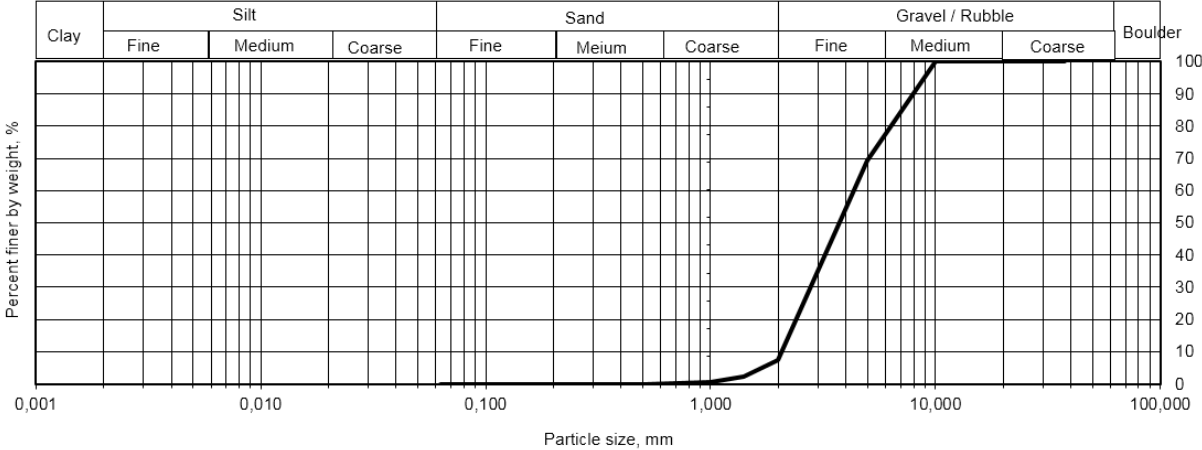


Fig. 2.7 - Granulometric curve of the model material – shells

Table 2.6 - Characteristics of the granulometric curve of the shell

$D_{10} =$	2,1	$C_U =$	2,10
$D_{30} =$	2,8	$C_C =$	0,85
$D_{60} =$	4,4		

To determine the bulk proportions of the components (sand and flat particles) of the shell of the composite medium, 18 experiments of direct cut in the following dry loose environments were performed:

- sand without a shell (6 experiments);
- a mixture of sand and shell in a volumetric ratio of 50% to 50% (6 experiments);
- Cutting of a shell without sand (6 experiments).

In the first 3 experiments for each medium, the orientation angle of the fill to the cut plane was $\beta = 0^\circ$, and in the next three - 90° . The graph of the dependence of the angle of internal friction on the volume content of the shell in the sand is shown in Fig. 2.8.

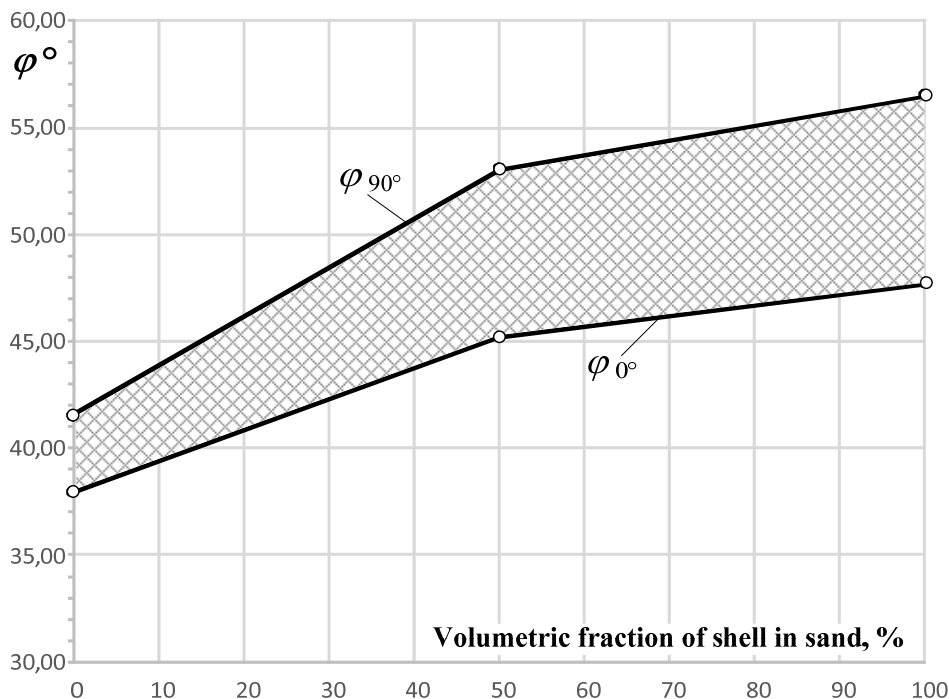


Fig. 2.8 - Graph of the dependence of the angle of internal friction on the volume fraction of the flat particles of the shell at $\beta = 0^\circ$ and 90°

From the curve on the graph (Fig. 2.8) it is evident that the difference in the friction angles at the angle of filling $\beta = 0^\circ$ and 90° increases with the increase of the shell's share in the composite. It is rapidly increasing from 9.45% for sand without impurities, up to 17.33% for sand and shell 1: 1, that is, with 50% volumetric content of the shell in the mixture. With the subsequent increase in

the shell's share, the difference significantly reduces its growth, and in the case of a pure shell, the difference is 18.30%. Both curves have a similar character, in the range of the shell size from 0% to 50%, the internal friction angle is increased by 19.18% for $\beta = 0^\circ$ and 27.76% for $\beta = 90^\circ$, and in the range from 50% to 100% curves more modest and growth is 5.52% and 6.40% respectively.

It can be concluded that when content of flat particles of a shell in the volume of more than 50% of the properties of composite material should be taken on the filler, that is, on the shells.

When choosing a bulk proportion, attention is drawn to such proportions of volumes in which there is a significant difference between the angle of internal friction with respect to the orientation of planar particles and that the chosen medium is encountered in practice (Fig. 2.9).



Fig. 2.9 - Components of the composite medium

Based on the obtained dependency schedules, it was decided to use a composite medium with a volume ratio of 70% of sand and 30% of shells, that is, in an approximate ratio of 2: 1. The material of this type is often found in underwater pitfalls of sea and river trade ports and is used to fill the sinuses of port hydrotechnical structures by dredging.

The basic physical characteristics of the dry composite medium ($w = 0\%$) are shown in Table. 2.7.

Table 2.7 - Basic physical characteristics of the shell

Property	Standard	Value
Specific weight	HRN U.B1.016	$\gamma = 16,81 \text{ kN/m}^3$
Specific gravity of particles	HRN U.B1.014	$\gamma_s = 27,00 \text{ kN/m}^3$

According to the granulometric curve (Fig. 2.10), the data are presented in Table. 2.8.

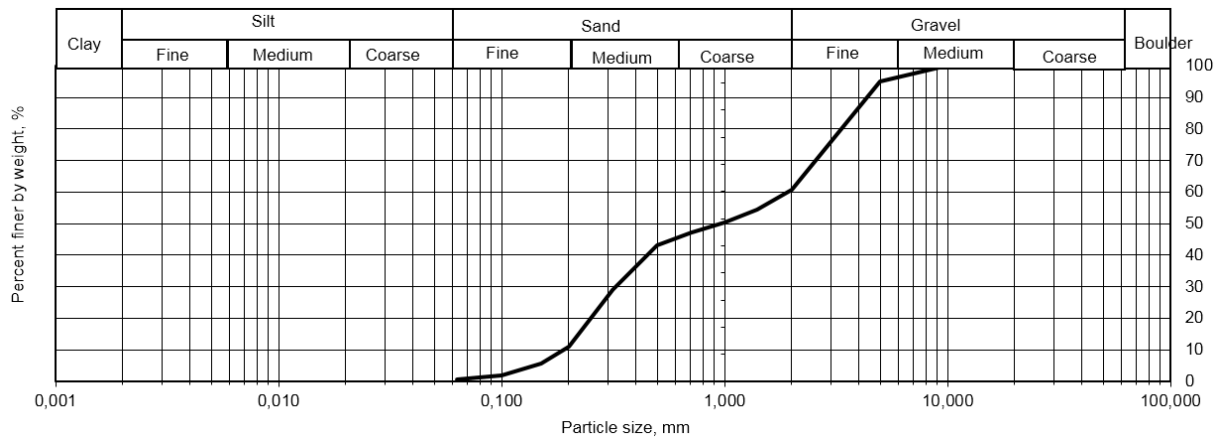


Fig. 2.10 - Granulometric curve of the composite medium

Table 2.8 - Characteristics of the granulometric curve of the shell

$D_{10} =$	0,19	$C_U =$	2,10
$D_{30} =$	0,32	$C_C =$	0,85
$D_{60} =$	2,10		

Method of experimental research. Direct shear device. To determine the resistance of the soil to the direct shear device was used which was manufactured by Slovenian enterprise " Ključavna delavnica Ljubljana " (Figure 2.11). The device allows direct shear at a constant set speed.



Fig. 2.11 – Прилад прямого одноплостинного зрізу

The lower box is driven by an electric motor, while the upper box rests in a dynamometer with a measuring range of 5 kN. During the experiment, the

horizontal force, the movement of the bottom of the box and vertical movements were measured. Horizontal and vertical movements were measured by clock indicators (Fig. 2.12) with a price of 0,01 mm to 10 mm graduation, which were pre-tested by the metrology service of the University of the North.

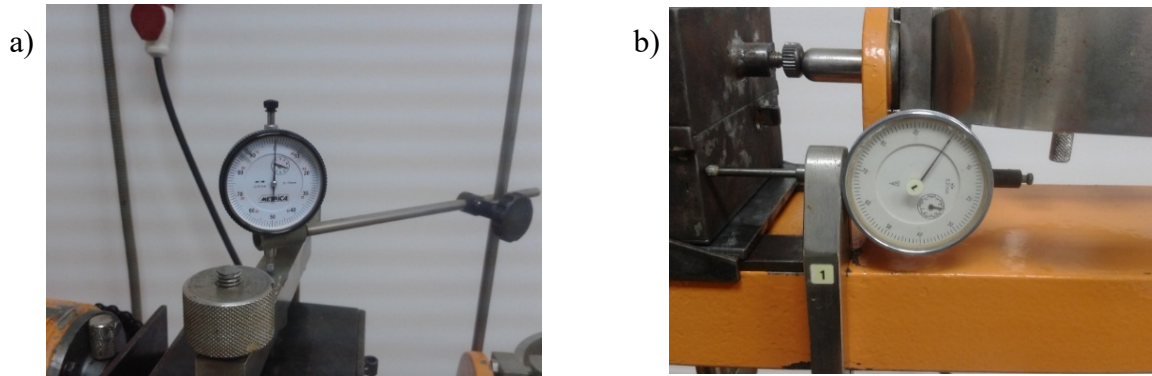


Fig. 2.12 - Indicators of vertical (a) and horizontal (b) displacements

The ring mechanical dynamometer was tare in the press (Fig. 2.13) by applying a vertical load with a step of increasing the force $\Delta F = 200$ N in the range from 0 to 2400 N.

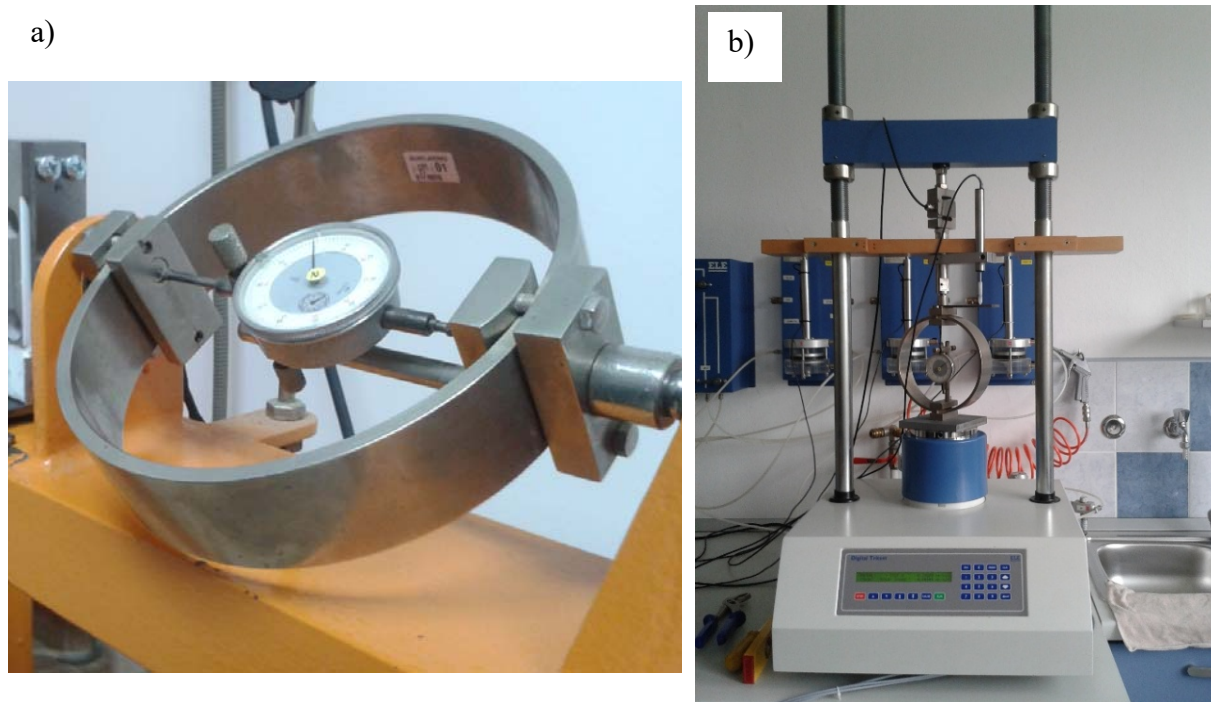


Fig. 2.13 - Calibration of the ring mechanical dynamometer: a) - dynamometer; b) - calibration in the press with the measurement of strength and deformation

In this interval, forces were recorded at trial shears. Tasting was carried out in three series. With each step of the step ΔF , the force lasted until the

stabilization of the clock indicator of the dynamometer. The compression values of the dynamometer were recorded. The results are shown in Table. 2.9.

Table 2.9 – Calibration results of the ring dynamometer

Applied force, N. F	Deformation of dynamometer, mm			Arithmetic Average of deformation, mm F	Rigidity coefficient, N/mm ε_1
	ε_1	ε_2	ε_3		
0	0	0	0	0	0
200	0,140	0,137	0,138	200	0,140
400	0,271	0,271	0,272	400	0,271
600	0,412	0,413	0,412	600	0,412
800	0,551	0,552	0,552	800	0,551
1000	0,688	0,690	0,688	1000	0,688
1200	0,823	0,825	0,826	1200	0,823
1400	0,960	0,957	0,960	1400	0,960
1600	1,089	1,092	1,092	1600	1,089
1800	1,234	1,235	1,233	1800	1,234
2000	1,378	1,375	1,378	2000	1,378
2200	1,516	1,513	1,517	2200	1,516
2400	1,657	1,654	1,657	2400	1,657
Average value of the rigidity coefficient					1456,310

The average value of the coefficient of hardness was calculated by the formula $K = \frac{F}{\varepsilon_{sr}}$ for each step by dividing the total force into the arithmetic mean of the corresponding compression. This approach is correct, since in the experiment the values of compression of the dynamometer ring were recorded for determining the tangential forces.

In the final calculation, for the determination of tangential stresses, the arithmetic mean value from the last column of table 2.9 was taken.

The shears were made in accordance with the British standard BS 1377; Part 7; clause 4 [67]. According to it's recommendations, the maximum speed of a drainage shear is determined by the formula $v = \frac{\delta_f}{12,7t_{100}}$ where δ_f – is the horizontal displacement of the shear box corresponding to the peak strength, t_{100} – is the time of 100% of the primary consolidation.

The time t_{100} is taken at the point of intersection of the tangent to the curve of the primary and secondary consolidation in the coordinate system with the square root of the abscissa with t (in t_{100} minutes) and the ordinate of the vertical settling Δh (Fig. 2.14). To determine δ_f , three trials of shifts were performed, where it was found that the mean value δ_f varies from 4 to 6 mm. In calculations, $\delta_f = 5$ mm is taken. From the schedule of the consolidation of experiments, the

time $t_{100} = 0,98$ min. When substituting to formula (2.3) we obtain the maximum cutoff speed $v = 0.41$ mm / min. For experimental loose dry materials, a speed of 0.2 mm / min was adopted.

Bulk materials were studied in a dry condition. For each sample, the specific gravity was measured. All experiments were conducted in well-controlled laboratory conditions with daily temperature and humidity measurements. The humidity in the laboratory varied from 35% to 45% and the temperature ranged from 21° C to 28° C.

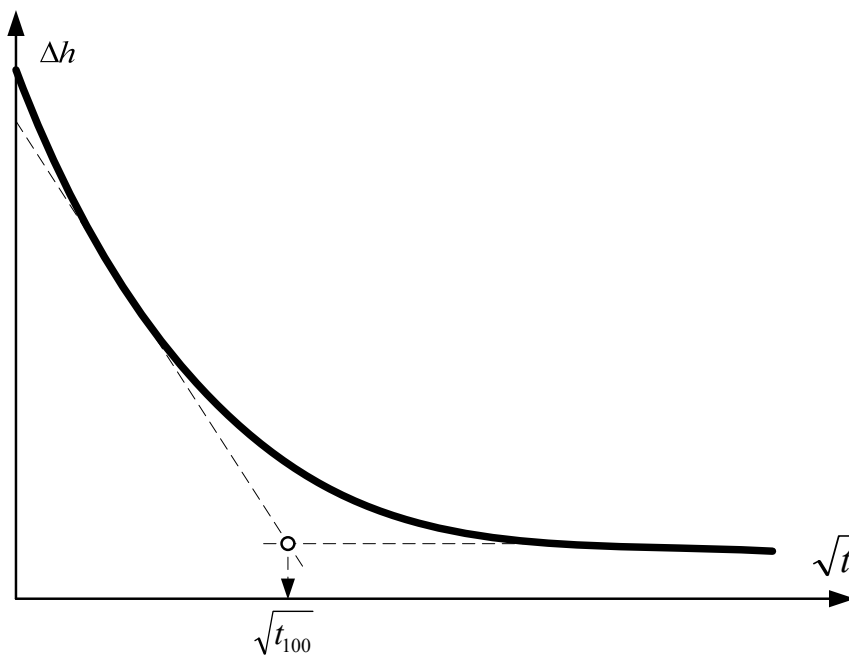


Fig. 2.14 - Determination of time t_{100}

In accordance with the standard BS 1377; Part 7 the maximum grain size of the material should not exceed 10% of the height of the cut-out chamber. Thus, the scale effect is overcome. The size of the grain of the tested rice and particles of the shell varied in the range from 7 to 9 mm, so the standard shear box of the cut in the kit of the cut-out, measuring 6 cm x 6 cm x 2 cm does not meet the requirements of the standard. According to the standard, the height of the wraps must be at least 9 cm. For cutting of rice and composite material, a 11 cm x 11 cm x 9 cm clasp is designed and manufactured (Figure 2.15). Due to the fact that the shifting shear box is non-standard, the accuracy of the shifts was confirmed by the conduct of 3 series (3 comparative sections) on the quartz sand of the fraction 1 - 2 mm. The obtained results of sections (Table 2.10) showed good convergence of results, the angle of internal friction differed only by 0,58°, that is, 1,43%.

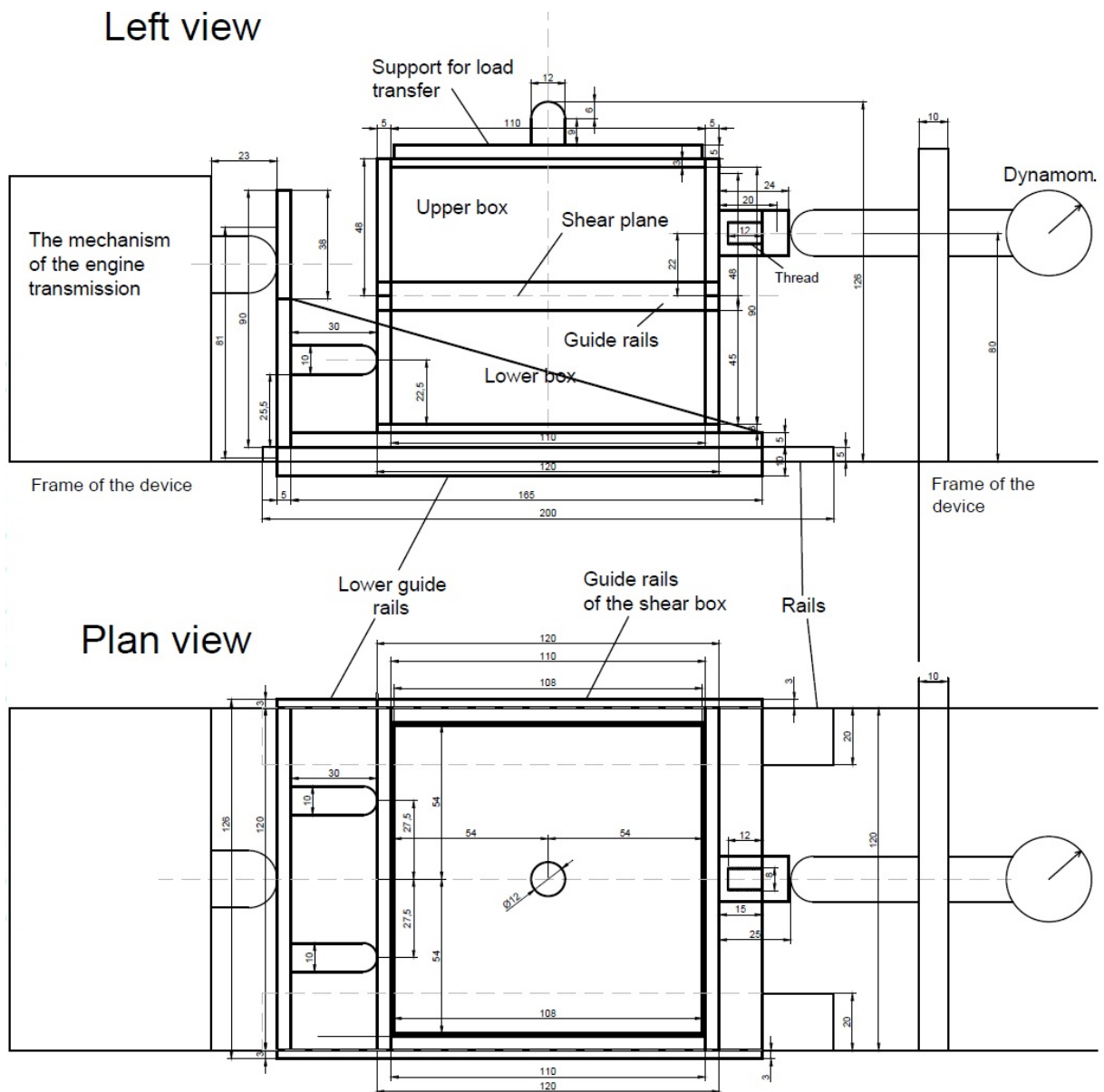


Figure 2.15 - Scheme of shear box with additional adapters

Table 2.10 - Results of calibration shears

Sample	Shear box 6 cm x 6 cm x 2 cm		Shear box 11 cm x 11 cm x 9 cm	
	$tg\varphi$	φ	$tg\varphi$	φ
1	0,8625	40,78	0,8787	41,31
2	0,8352	39,87	0,8543	40,51
3	0,9632	43,93	0,8695	41,01
Average	0,8870	41,52	0,8675	40,94

Experiments of the direct shear were carried out at different angles of orientation of the planar particles (rice and shells) to the cut-off plane $\beta = 0^\circ, 30^\circ, 60^\circ$ and 90° for both media (Fig. 2.16). To achieve the reliability of the results for each corner of the bulk, three series were conducted for three experiments. The experiment plan is shown in Table. 2.11.

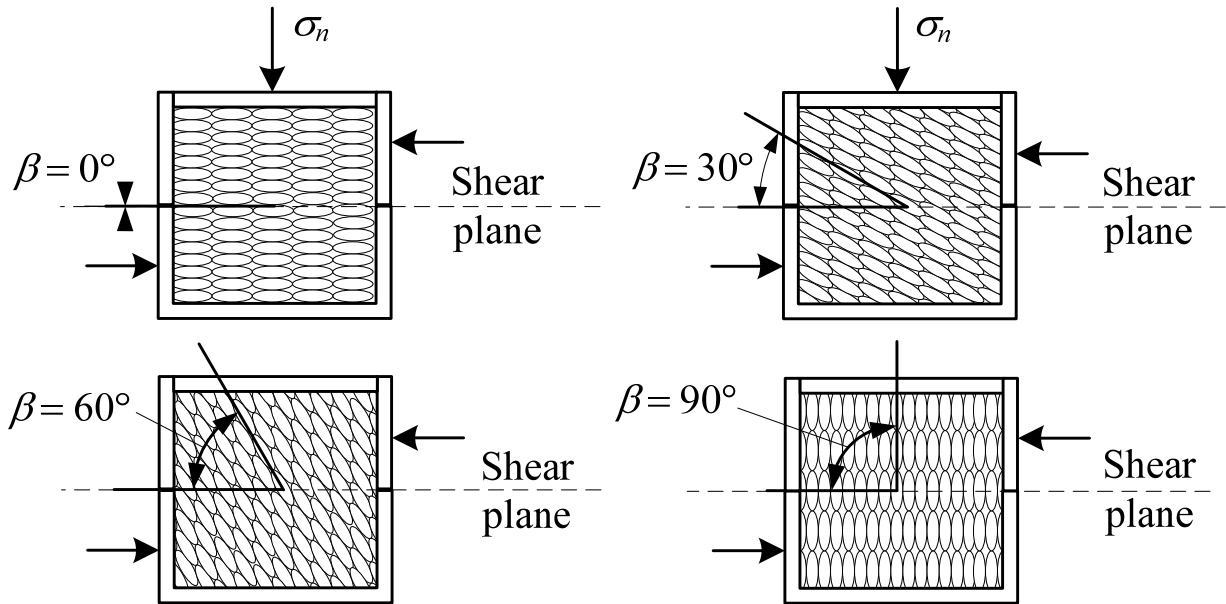


Fig. 2.16 Scheme of packing of model material in a shear box at angles $\beta = 0^\circ, 30^\circ, 60^\circ$ i 90°

Table 2.11 –Experiment plan

Material	The angle of the preferred orientation of the grain to the shear plane			
	0°	30°	60°	90°
	Number of experiments			
Long grain rice	9	9	9	9
Composite medium	9	9	9	9

The angle of orientation was achieved using specially developed technology of filling the material into the shear box (Fig. 2.17).

The sequence of the experiment. Both rice and composite material were dried before the experiment in a drying cabinet for 24 hours, rice at 80°C (organic material), and composite material at 105°C . The material was then cooled in a desiccator to a temperature of 25°C in the laboratory.

An inhomogeneous mixture of a composite medium was thoroughly blended before falling asleep into a direct shifter. The loose environment was always filled upright from the top by layers in the thickness of about 1 cm. To reach the angles $\beta = 30^\circ$ and 60° , the supports were fixed, which fixed the shear box at the desired angle (Fig. 2.17, b and c).

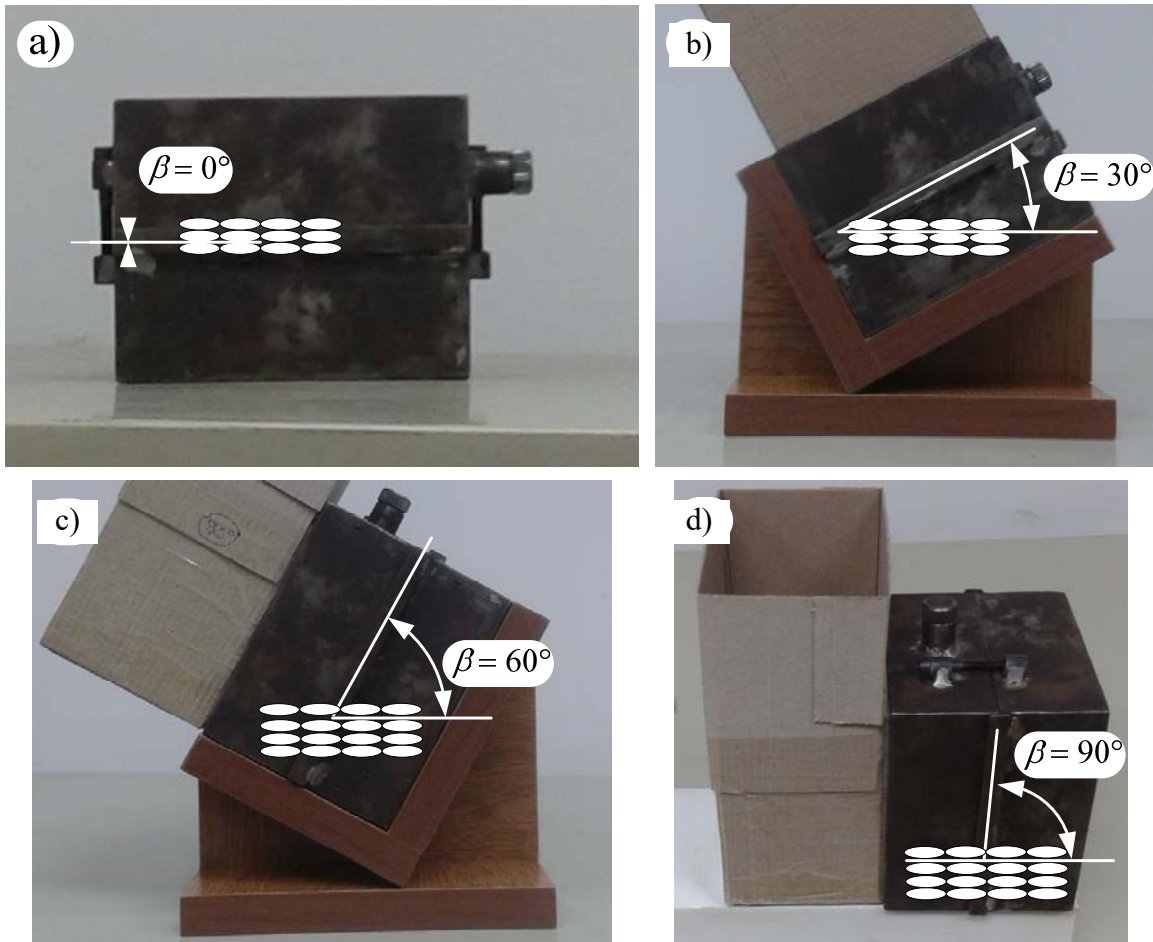


Fig. 2.17 - Additional equipment to achieve the desired angles of filling β : a) 0° ; b) 30° ; c) 60° ; d) 90°

In the case of $\beta = 90^\circ$ the shear box returned to 90° and laid the back wall in a horizontal position, while filling with a special cardboard insert (Fig. 2.17, g). After filling, each layer of the shear box was slightly shaken in a horizontal direction "from left to right" so that the planar particles lay in a horizontal position. After filling the shear box, it slowly and carefully returned to the horizontal position, and the protective cardboard insert was carefully removed. After this, the upper plane of the cartridges aligned, removed excess material, the shear box was weighed and calculated the proportion of material. Then the shear box with the material was installed in the cutter, applied vertical pressure for consolidation. Loose materials were tested under the following vertical pressures: rice at 9 kN/m^2 , 18 kN/m^2 and 36 kN/m^2 , and the composite medium at 10 kN/m^2 , 20 kN/m^2 and 40 kN/m^2 .

After several test consolidations within 24 hours, it was concluded that for complete consolidation of both bulk environments, it lasts 15 minutes. After the end of the consolidation, the connecting bolts were unscrewed and the drive was started.

During the experiment, measurements of the values of the deformation of the dynamometer ring and vertical movement for a horizontal displacement step

of 0.1 mm were recorded. Data was recorded in pre-prepared tables. The results of measurements are presented graphically in Fig. 2.18 - 2.25. After testing, the loose materials fell into plastic barrels that were tightly closed by the lid to prevent absorption of moisture from the air.

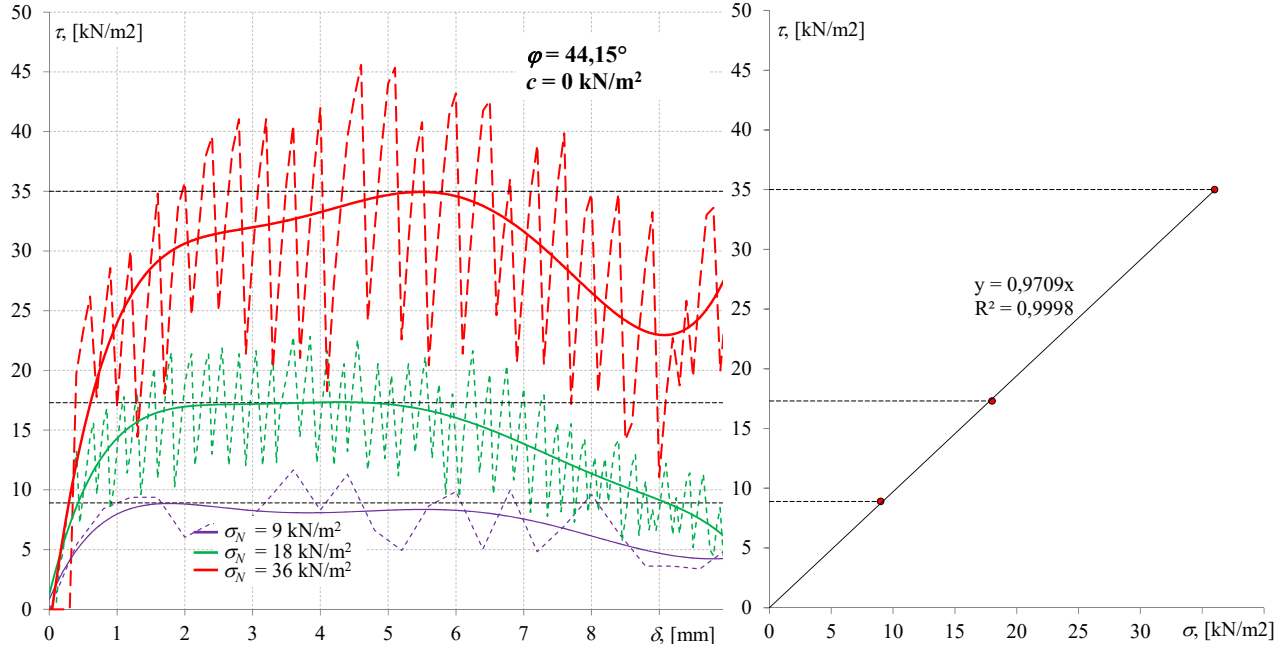


Fig. 2.18 –Measurement and analysis of the first series of experiments at $\theta = 0^\circ$

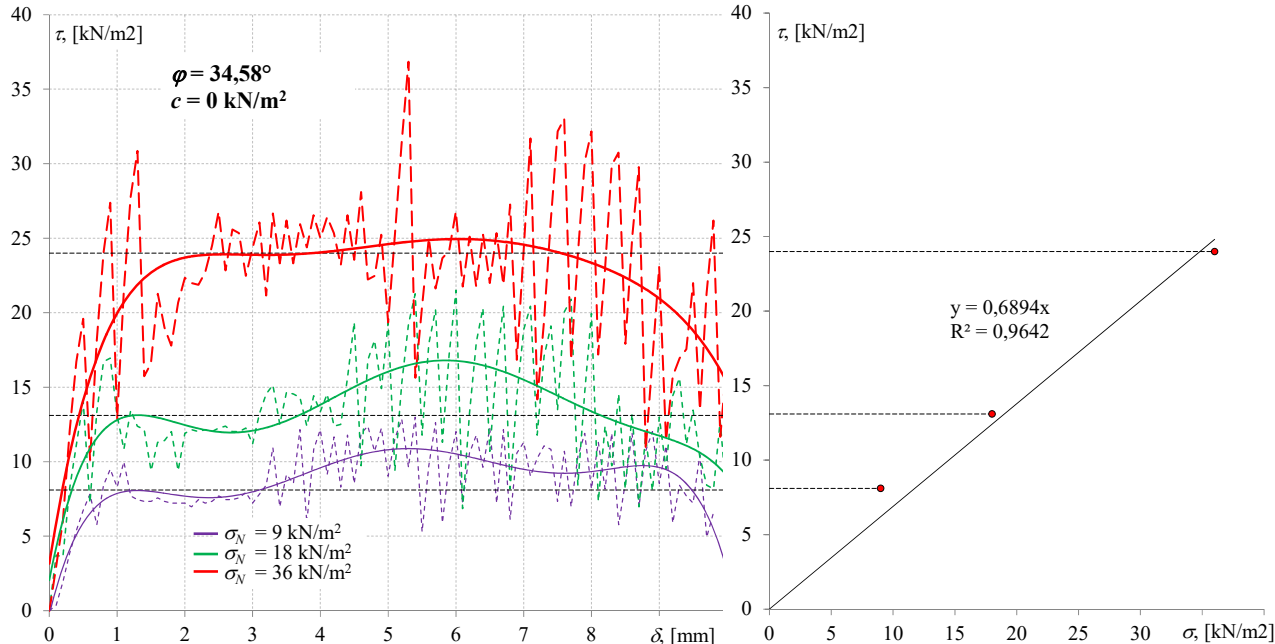


Fig. 2.19 –Measurement and analysis of the second series of experiments at $\theta = 30^\circ$

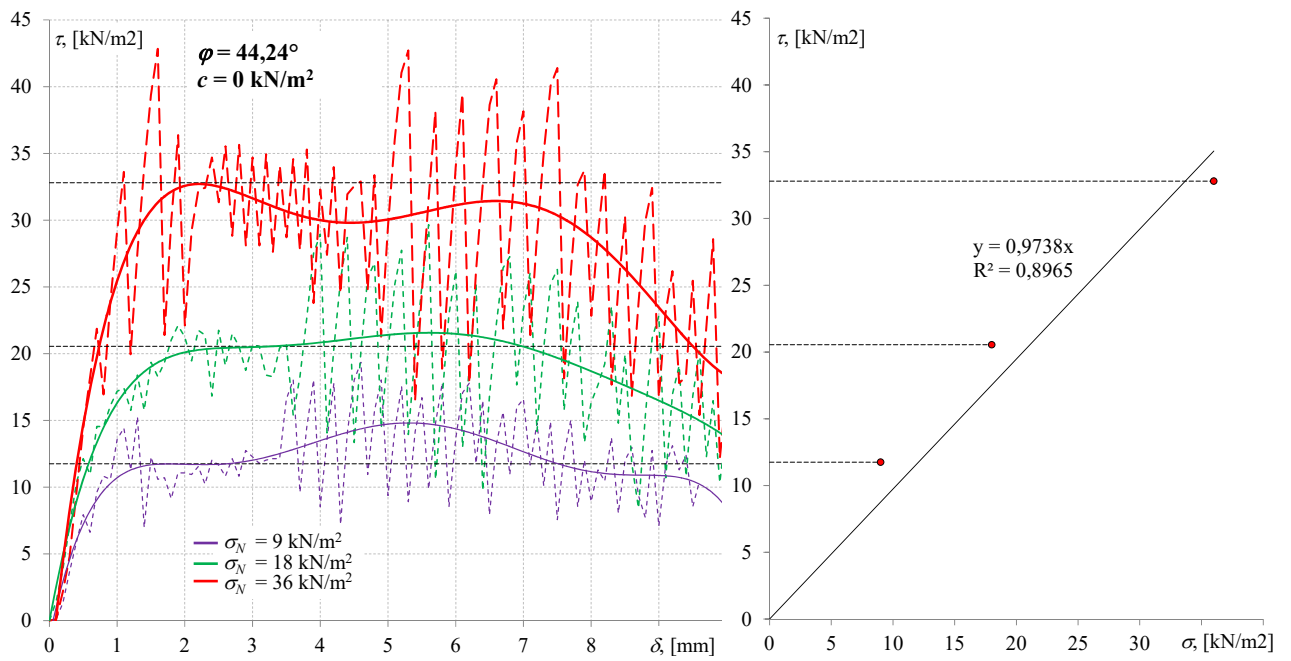


Fig. 2.20 – Measurement and analysis of the second series of experiments at $\theta = 60^\circ$

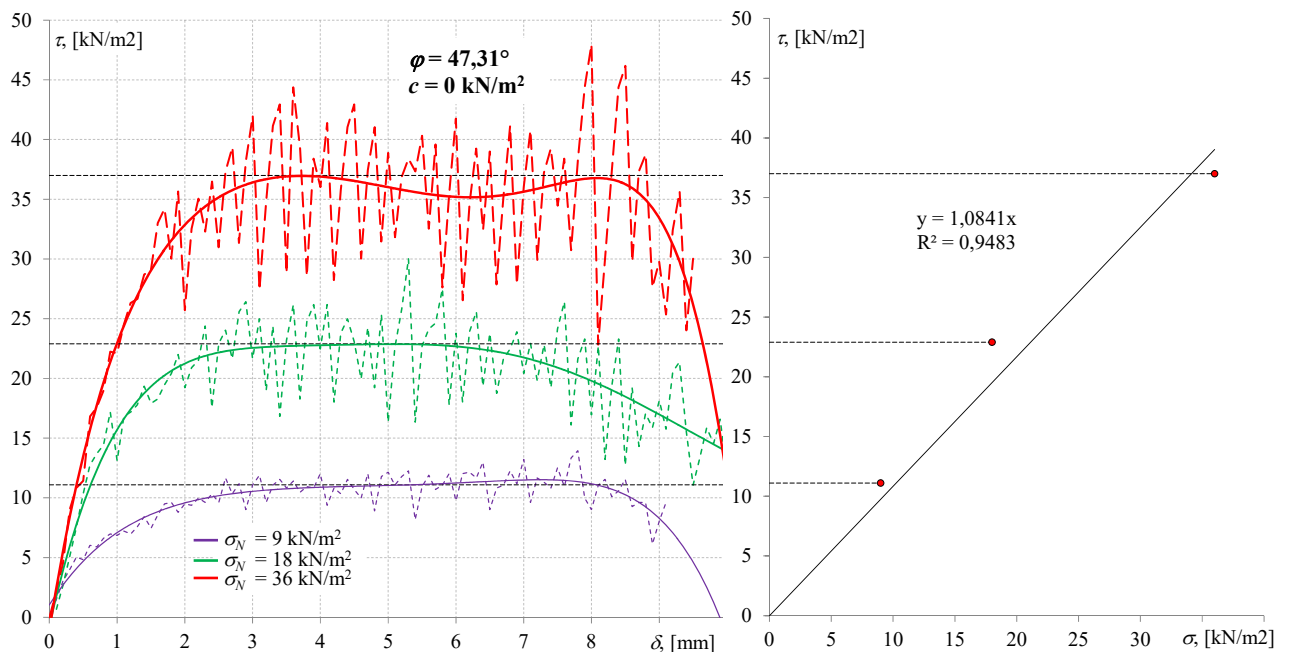


Fig. 2.21 – Measurement and analysis of the second series of experiments at $\theta = 90^\circ$

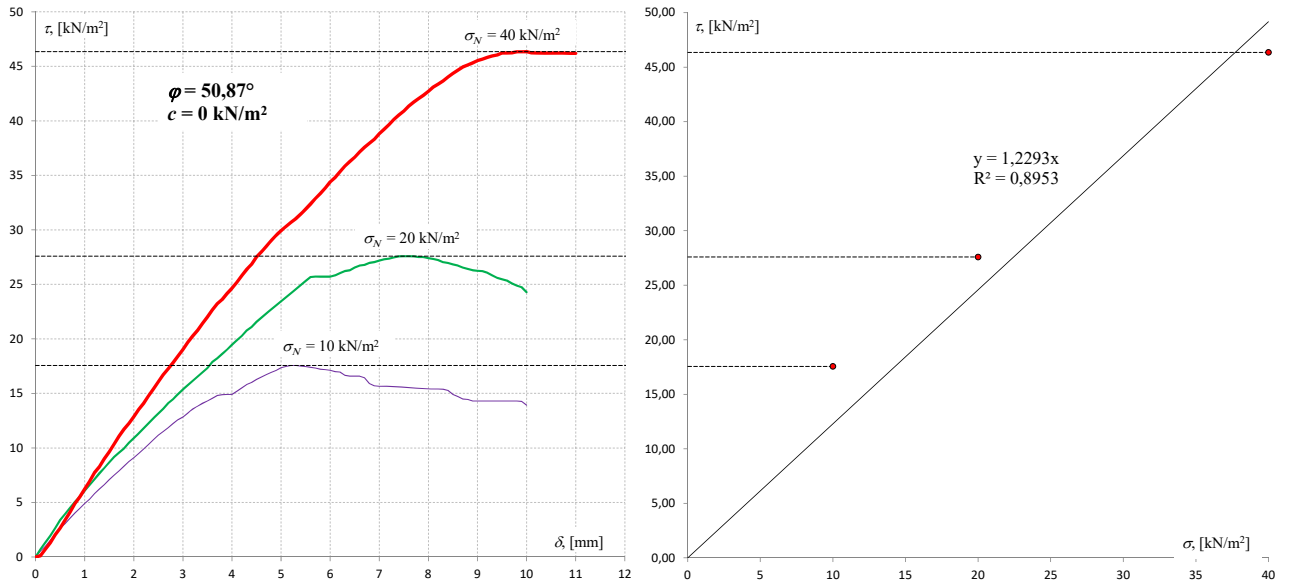


Fig. 2.22 – Measurement and analysis of the third series of experiments at $\theta = 0^\circ$

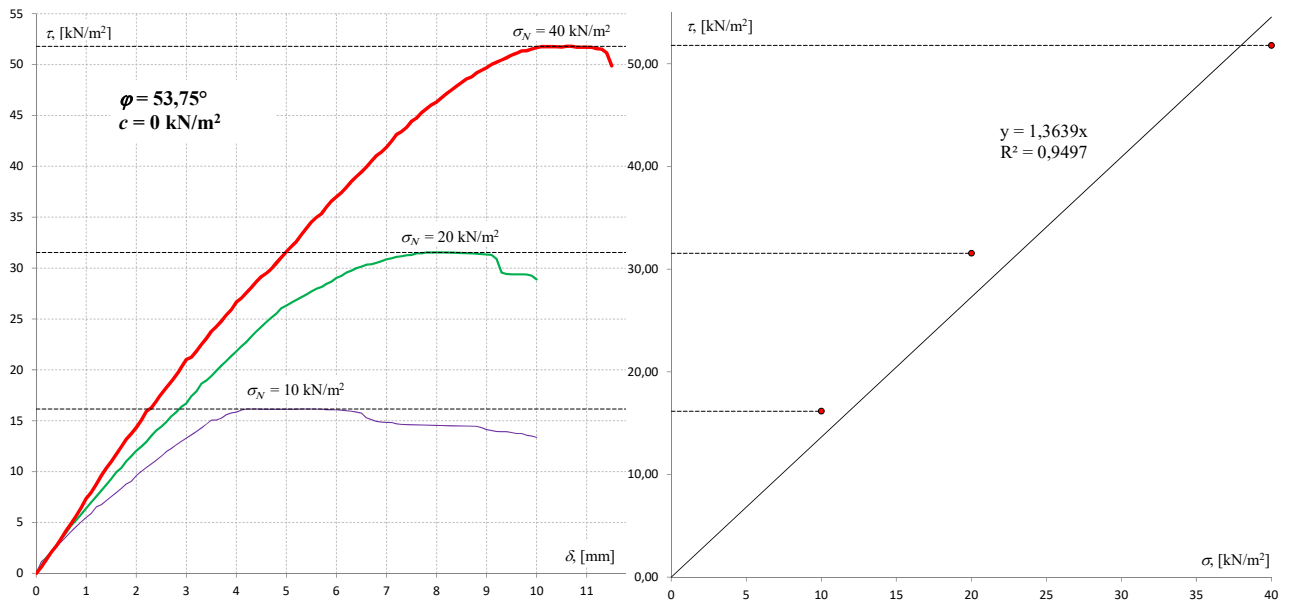


Fig. 2.23 – Measurement and analysis of the first series of experiments at $\theta = 30^\circ$

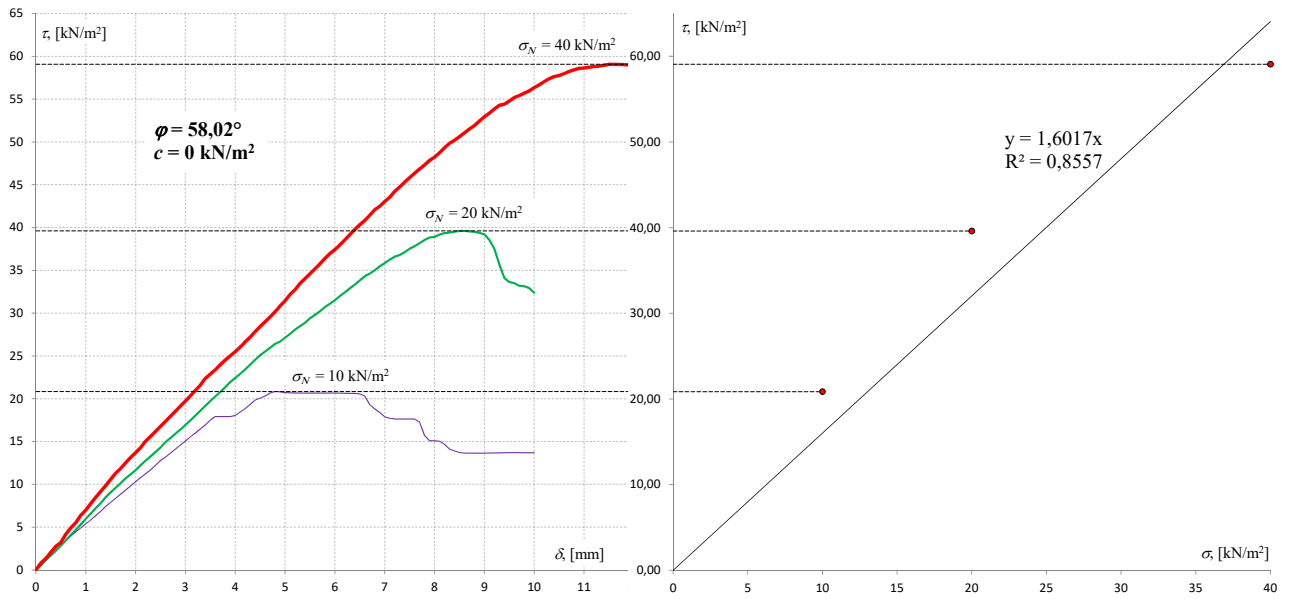


Fig. 2.24 – Measurement and analysis of the second series of experiments at $\theta = 60^\circ$

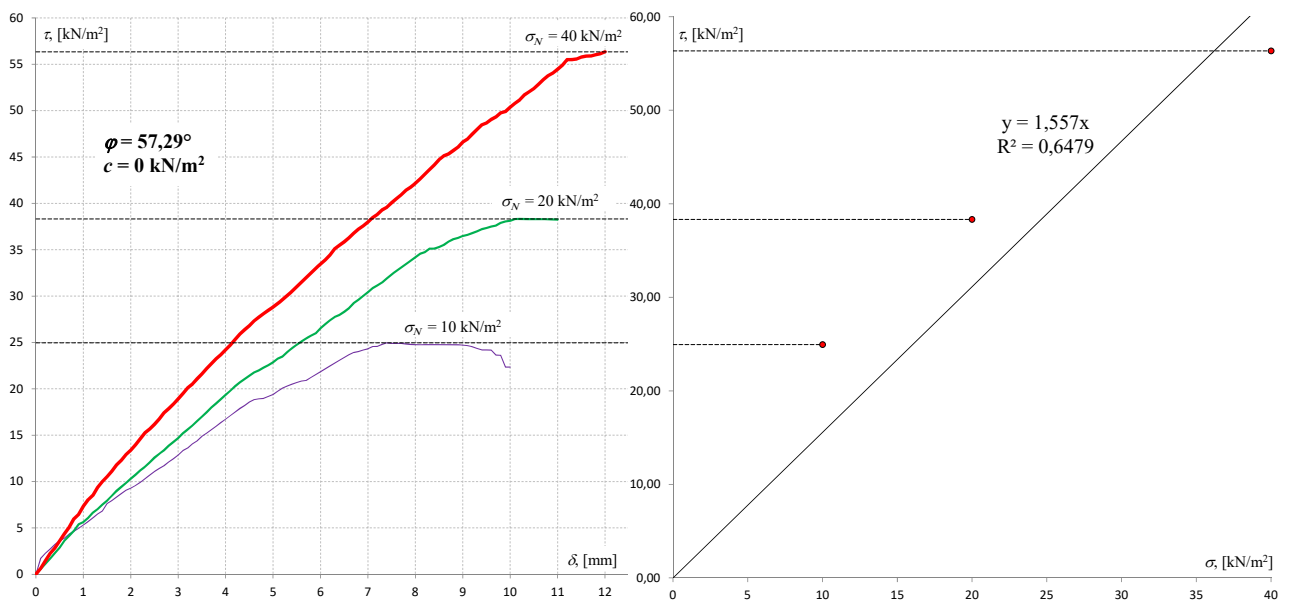


Fig. 2.25 – Measurement and analysis of the second series of experiments at $\theta = 90^\circ$

2.2. Methods of field research of natural and induced (secondary) anisotropy of coherent soils

The natural and indicated parameters of the ground of the bases with surface compacting were investigated in a layer with a thickness of each layer of soil 10 - 30, sometimes 50 cm. When studying the soil within the soil pillows samples were taken from the middle of each compacted layer after at least a week "rest" of the foundation after slipping. Samples of soil were taken from the middle of each compacted layer after at least a week "rest" of the base after slipping.

For each layer of soil in the field conditions [5, 7, 17] was performed:

- selection of standard rings of 40 cm in volume and 140 cm³ or 200 cm³ in thickness, which were usually precisely oriented at angles $\alpha = 0^\circ$, 45° and 90° (for studying the natural (primary) and induced (secondary) anisotropy of the soil) relative to the horizontal plane (three to six rings under each of the three corners);

- Seven penetration field dynamometer penetrometer PD-2M (or micropeople meter VSEGINGEO MB-2) with a conical tip with an angle at the top 30 in each of the three directions at angles $\alpha = 0^\circ$, 45° and 90° to the horizontal plane (isotropic plane);

- three control samples of the soil with 50 cm³ rings in order to determine the density and moisture content of the soil.

Measured geometric parameters of the natural and resulted bases, in particular, reduction of the surface of the array under a ramp (a cat); stamp tests of arrays before and after compression and static sounding them in the same sequence were performed.

Later in the laboratory, in addition to the density and humidity of the samples, were determined:

- compressibility of soil according to DSTU B V.2.1-4-96 [16] in single-side compression devices;

- resistance to the shift in accordance with DSTU B V.2.1-4-96 [16] in the tests of soil testing on a direct shift along a fixed plane of displacement PSG-2M;

- Specific resistance of soil penetration using laboratory penetrometer LP-1 with conical tip with an angle at the top of 30.

The results of the studies were presented in the form of charts changing the values of soil characteristics for the depth of the array or in its transverse direction.

The methodology [5, 7, 17] of the field investigations of the mentioned soil parameters of the bases and foundations (piles) created with its squeezing out from under different directions was also developed.

Usually the study of soil properties around such foundations was carried out after their static tests in a layer with a thickness of each layer of soil not more than 50 cm.

Consider such studies on an example of foundations (piling piles) in broken wells. The general view of them after tearing off and stripping is shown in Fig. 2.26, and the location of the soil layers - in Fig. 2.27.

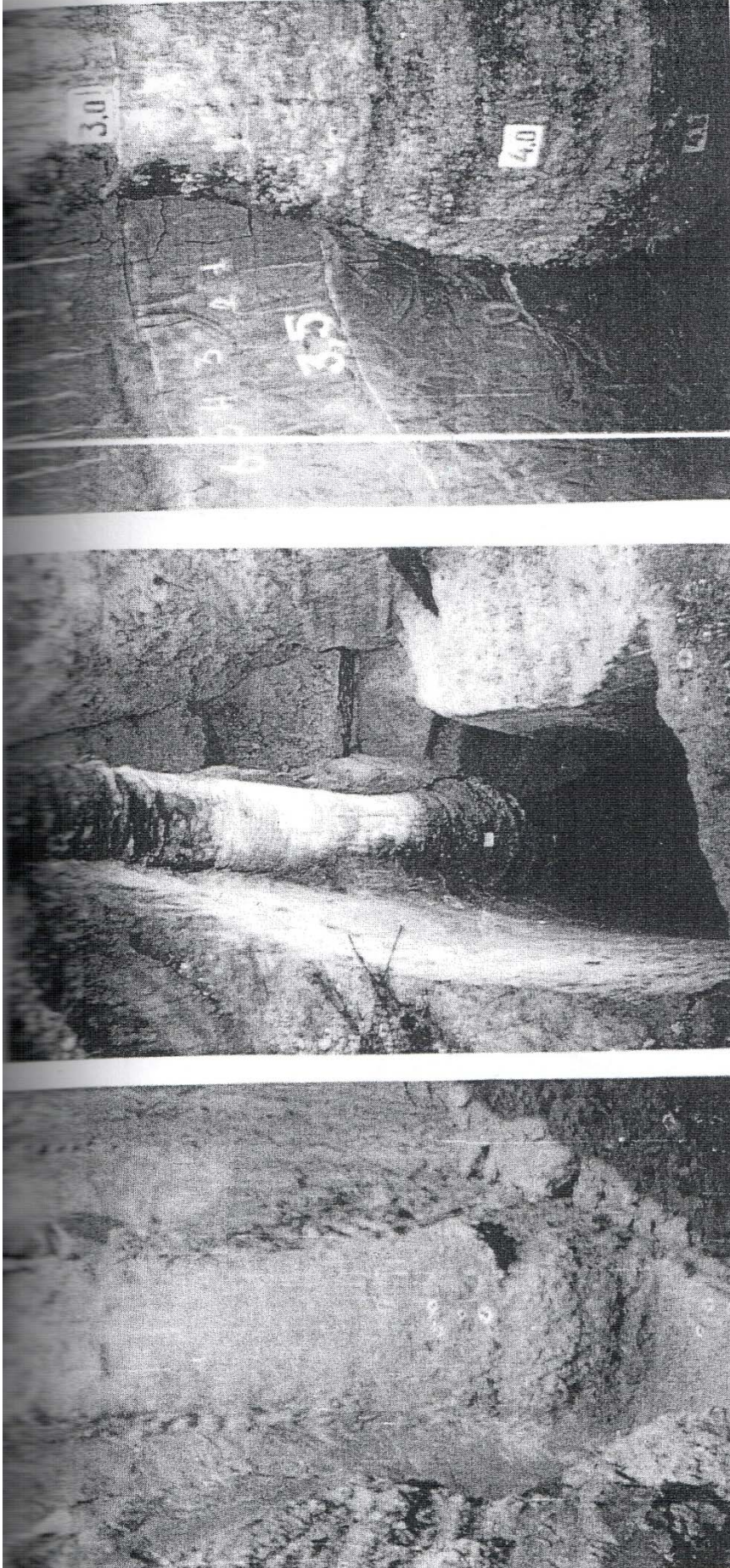
At the same time, the points of study or sampling of soil were located in circles of the radial to the vertical axis of the foundation. The radius of the first such circle exceeded the radius of the cross-section of the trunk or the extension of the foundation by 10 cm, the radius of each next round to the sixth inclusive was 10 cm more than the previous, from the seventh to eighth, by 20 cm, and from the ninth to the eleventh, 40 cm (Figures 2.27 and 2.28).

As it can be seen from Fig. 2.28 on each radial circle was performed:

- for seven penetrations with a field dynamometer penetrometer PD-2M with a conical tip with an angle at the vertex in each of the three directions at angles $\alpha = 0^\circ$, 45° and 90° , to the horizontal plane (the plane of isotropy);
- Seven penetrations of the MSPE-2 micropeopole meter with a conical tip with an angle at the vertex $17^\circ 40'$ in each of the three directions at angles $\alpha = 0^\circ$, 45° and 90° to the horizontal plane;
- by seven penetration micro-pectoral MV-2 with a tip with an angle at the vertex in each direction at angles, to the horizontal;
- three control samples of the soil with 50 cm^3 rings in order to determine the density and moisture content of the soil.

Thus, on each radial circle 63 penetration tests were performed, and on each layer of soil 693 penetration tests. Photos of examples of penetration tests of soil by penetrometers of different structures at angles, and to the horizontal plane are shown in Fig. 2.29.

The distance between the points of penetration was intended, based on: the exclusion of the mutual influence of neighboring tests, both under one, and at different angles to the horizontal plane, for which the distance between these points was designated not less than six diameters of the tip; Possibilities of sampling control in the cutting rings; the need to study both the compacted and the soil of the natural structure, located outside the compacting zone.



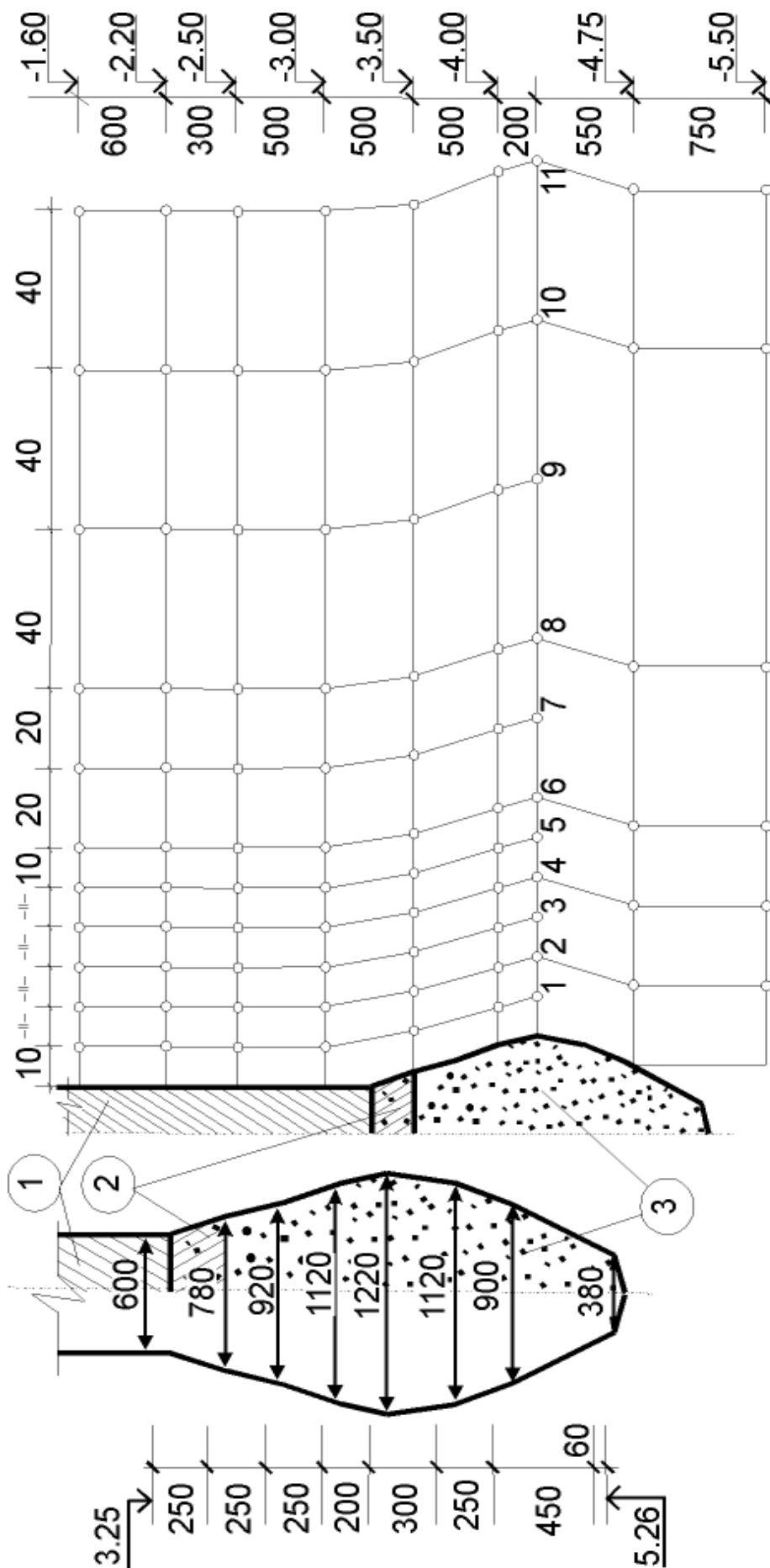
a

б

Fig. 2.26 – General view of piling piles in broken wells after tearing and stripping:

a - a platform in the city of Poltava - depth $h_k = 4.5$ m; volume of crushed stone, stamped in the expansion $V_{cr} = 1.25$ m³;

b - a platform in the city of Kobelyaky of the Poltava region - $h_k = 4.5$ m; $V_{cr} = 1.25$ m³



6

a

Fig. 2.27 – Example of measurements of the expansion and trunk of experimental piling piles in broken wells (a); Levels and points of soil study around the pile in height (b): 1 - body of the pile; 2 - transition zone; 3 - extension

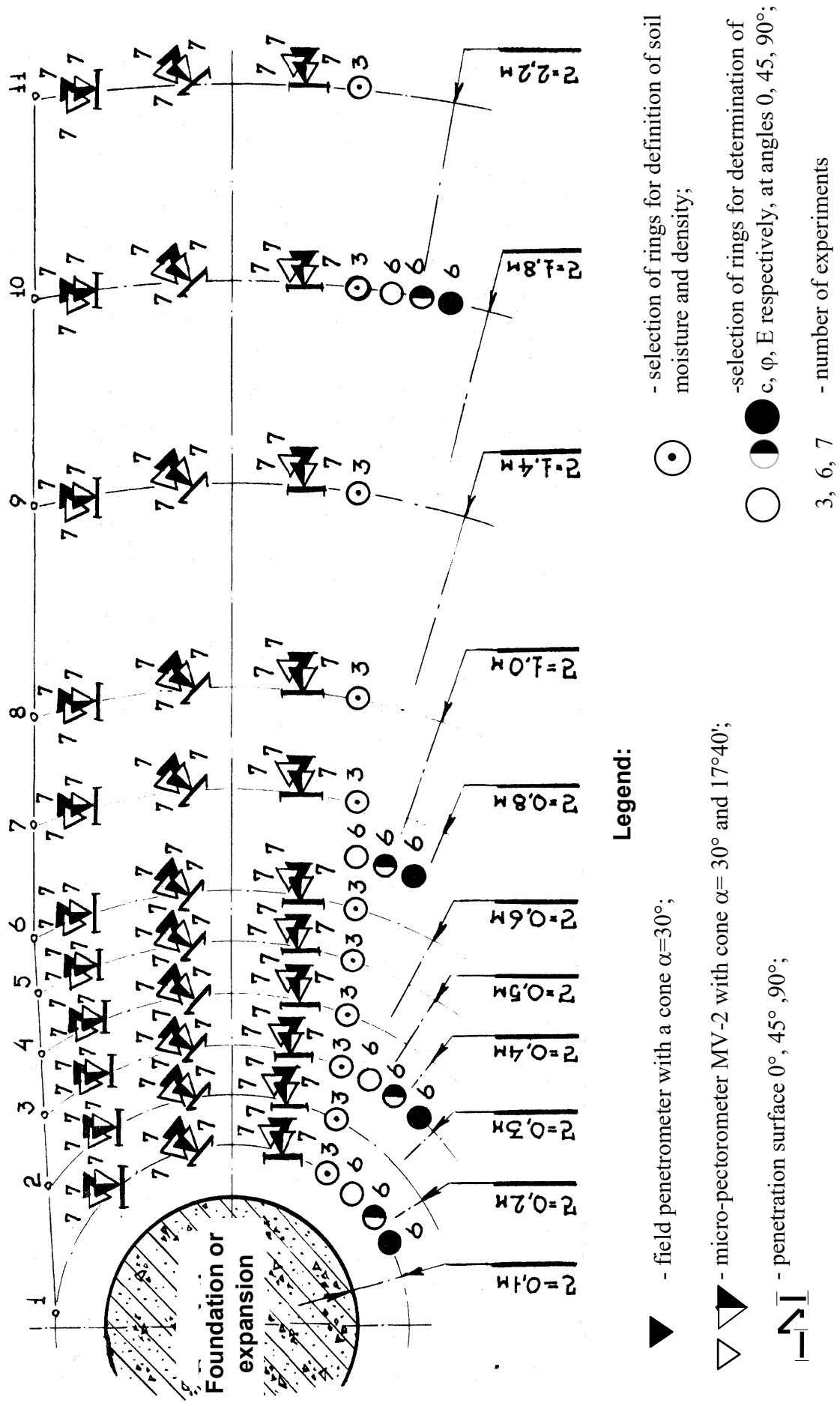
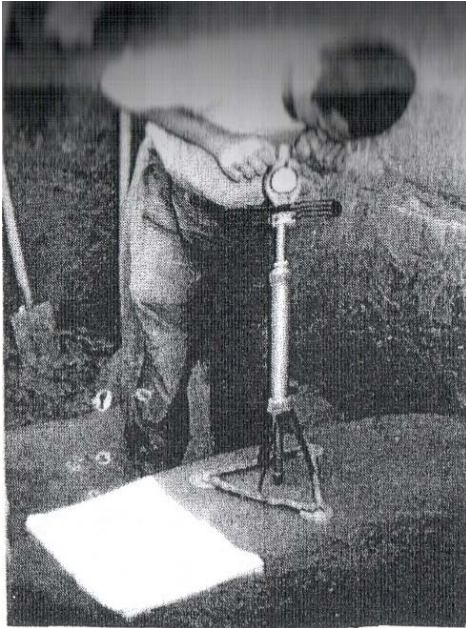
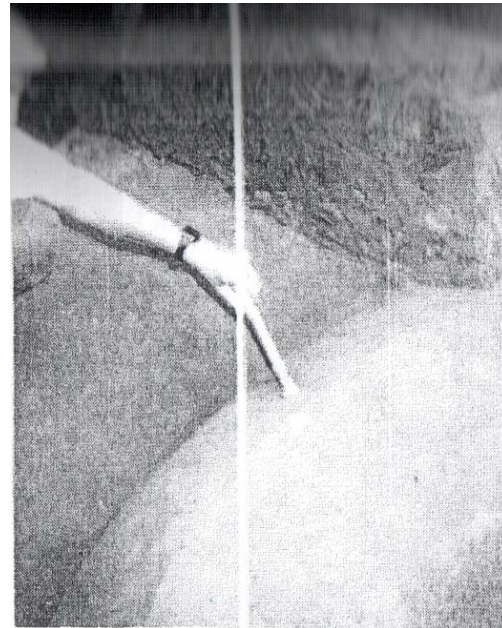


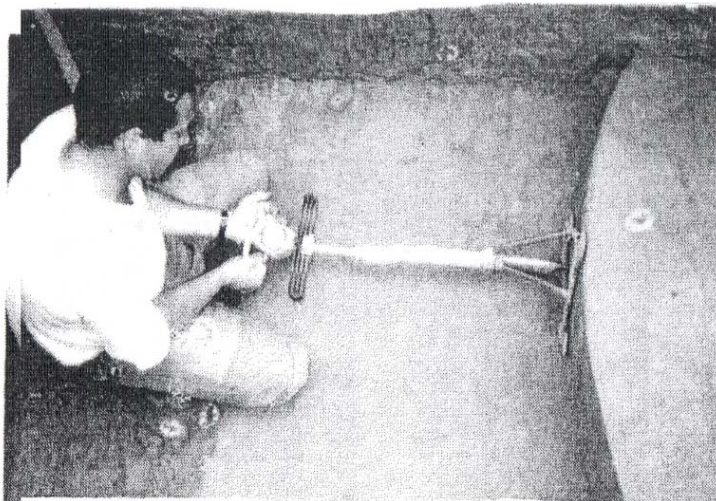
Fig. 2.28 – Scheme of placement of penetration points and sampling of soil for each layer of soil



a



b



B

Fig. 2.29 – Examples of penetration tests of soil: a, b - field penetrometer PD-2M at an angle α , respectively 0° та 90° and to a horizontal surface; b - Micropower meter MV-2 at an angle $\alpha = 45^\circ$

Four or five radial circles were pressed with standard 40 cm² rings centered on angles and relative to the horizontal plane (six below each of the three corners in each of the circles, as shown in Figure 2.28).

Compressibility of soil samples was determined according to DSTU B V.2.1-4-96 in single-axial compression devices, and resistance to shifts according to DSTU B V.2.1-4-96 in instruments for direct-shift testing with a fixed displacement plane of PSG-2M.

3. RESULTS OF EXPERIMENTAL STUDIES OF SOIL ANISOTROPY OF SOIL

3.1. Investigation of anisotropic bulk soils parameters

Analysis of research results. Angle of internal friction. In order to determine the difference characteristics of the shear strength according Coulomb, the tangential stresses from measurements were firstly calculated for the displacement by the formula (3.1). Then a standard shear plot was constructed in the coordinate system "movement δ - tangential stresses τ "(Fig. 3.1).

$$\tau = \frac{F_T}{A} = \frac{\delta_K \cdot K}{110(110 - \delta + \delta_K)}, \quad (3.1)$$

where δ_K - deformation of the dynamometer ring; K - coefficient of rigidity of the dynamometer ring; δ - move the bottom of the shear boxboard.

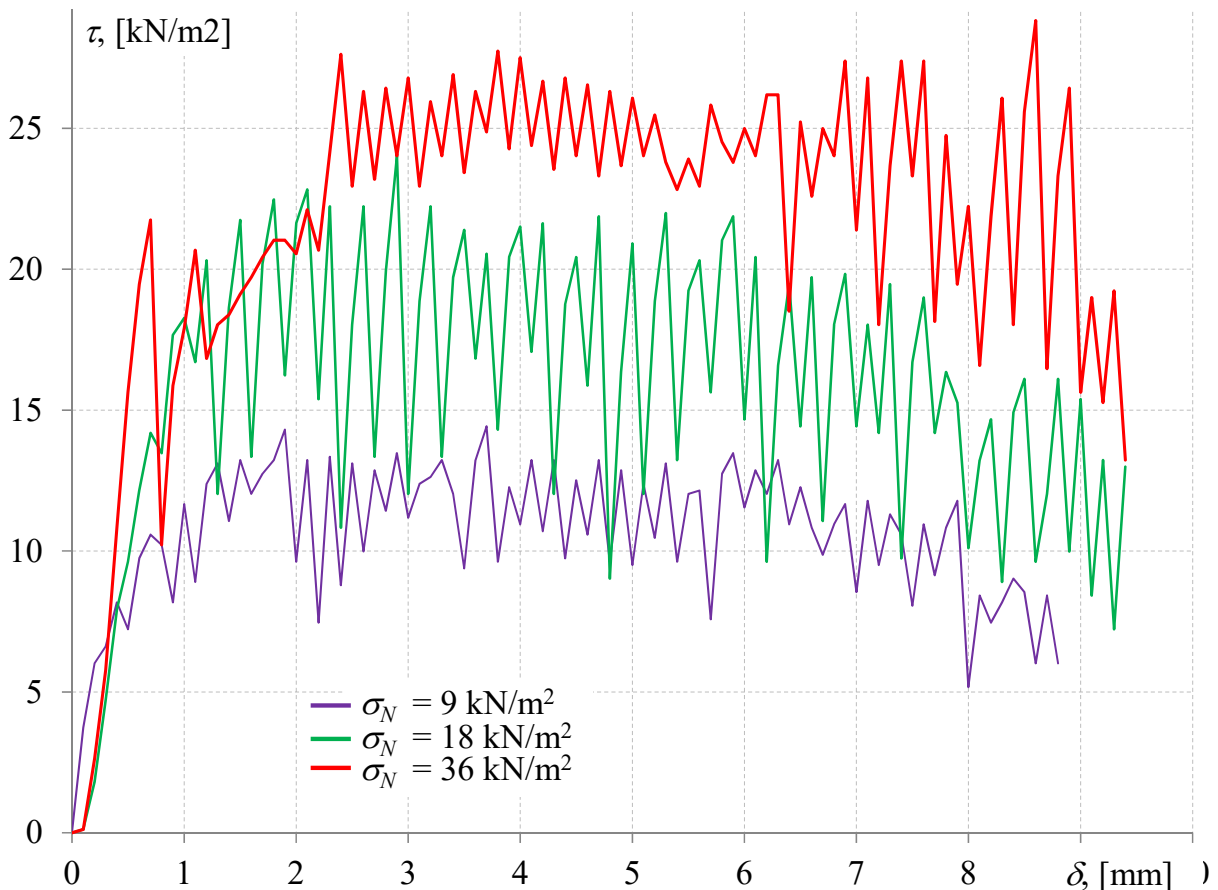


Fig. 3.1 – Shear plot for rice

The curves of the results of the rice shears (Fig. 2.18 - 2.21) are with stick-slip events. This phenomenon can be explained by the complexity of the process of cutting the rice, in which, in addition to friction, the particles on the cut plane rotate, pass one through one and break. The spin-like nature of the curves in the

case of different tests of the grain medium was obtained earlier in a number of authors [68, 98]. They concluded that the nature of the curve depends on the speed of the cut, and when the speed of the tests of the jumps are reduced.

When the composite medium shear, no marked jumps events were observed (Fig. 3.2).

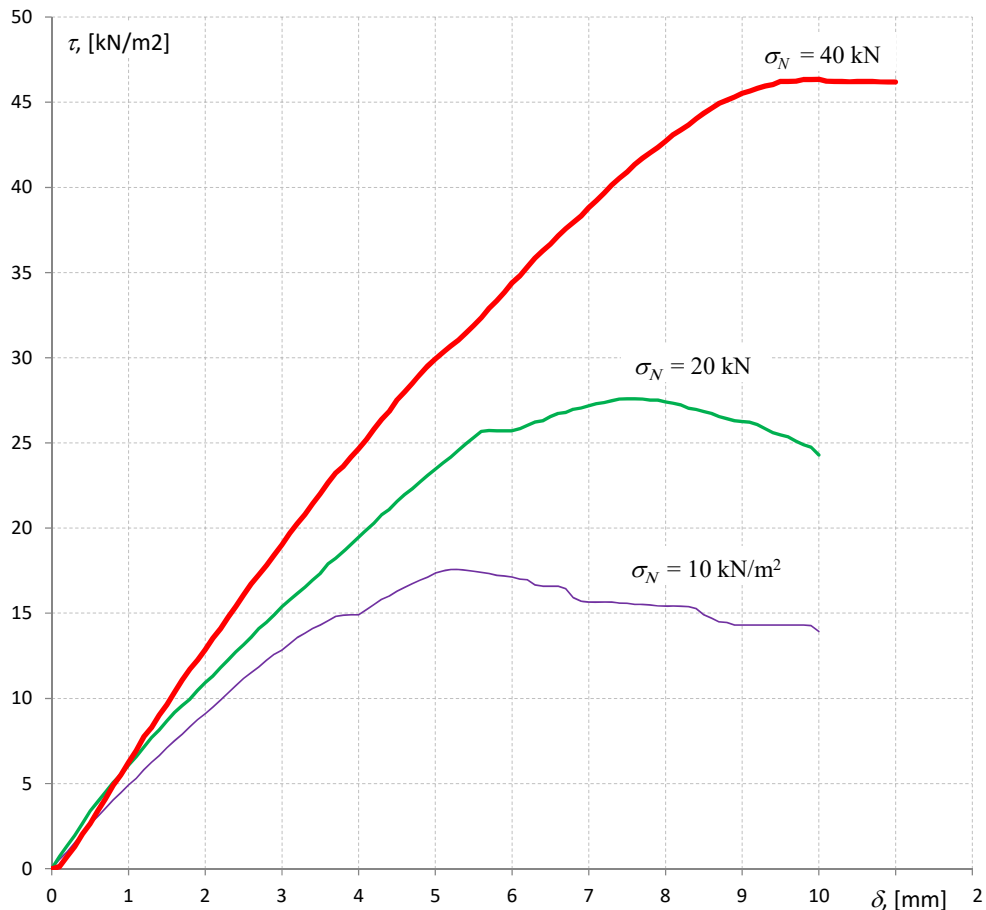


Fig. 3.2 – Typical plot of the composite medium

Processing of the results of rice tests required a special approach. In [91], we propose a method for processing spin-like curves, cut-off results, in which, in particular, the curve of mean values of tangential stress is constructed, and its peak value is determined from it (Fig. 3.3, a). We will use this rice data processing technique.

As a result, we obtain three peak values τ for each vertical stress σ , these values are reflected in the coordinate system (Fig. 3.3, b).

In work M.M. Sidorov [42] shows that the angle of internal friction of the sand is a value of the variable, inversely proportional to the growth of normal stress (Fig. 3.4). This dependence manifests itself sharply in the range of normal stresses up to 100 kN / m². At an area of 300-400 kN/m², the angle of internal friction practically does not change (Fig. 3.4, a).

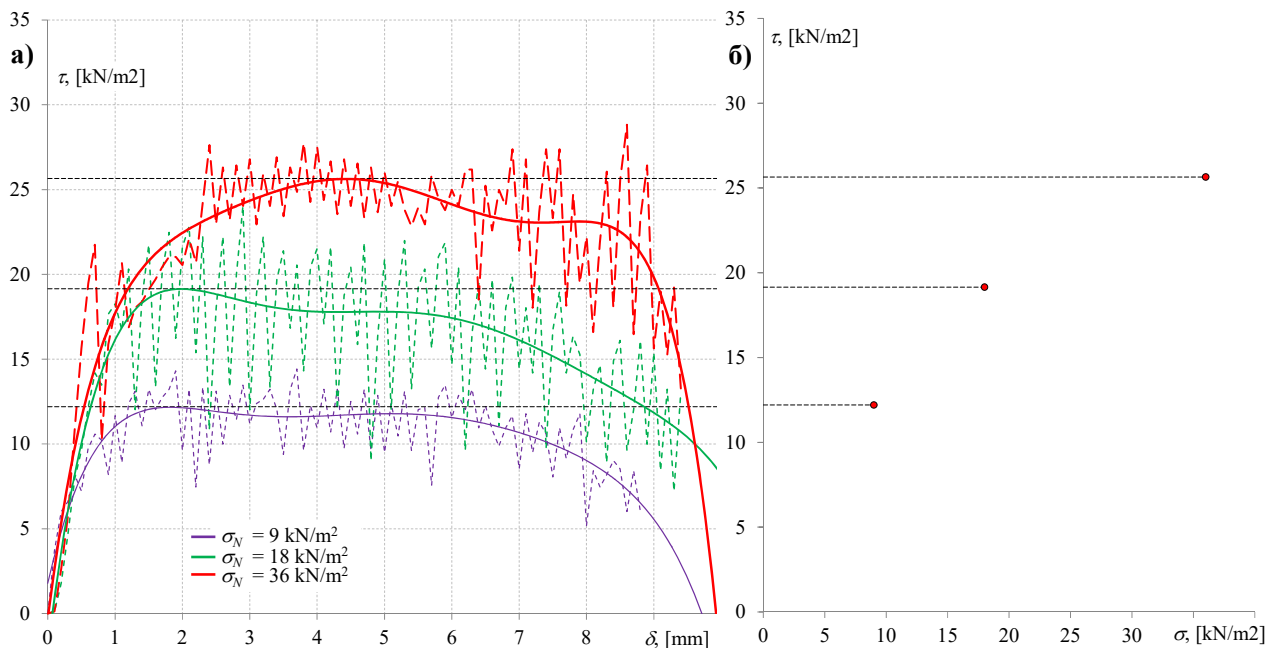


Fig. 3.3 – Data processing of the rice shear:
 a - processing data of rice direct shear; b - shear results

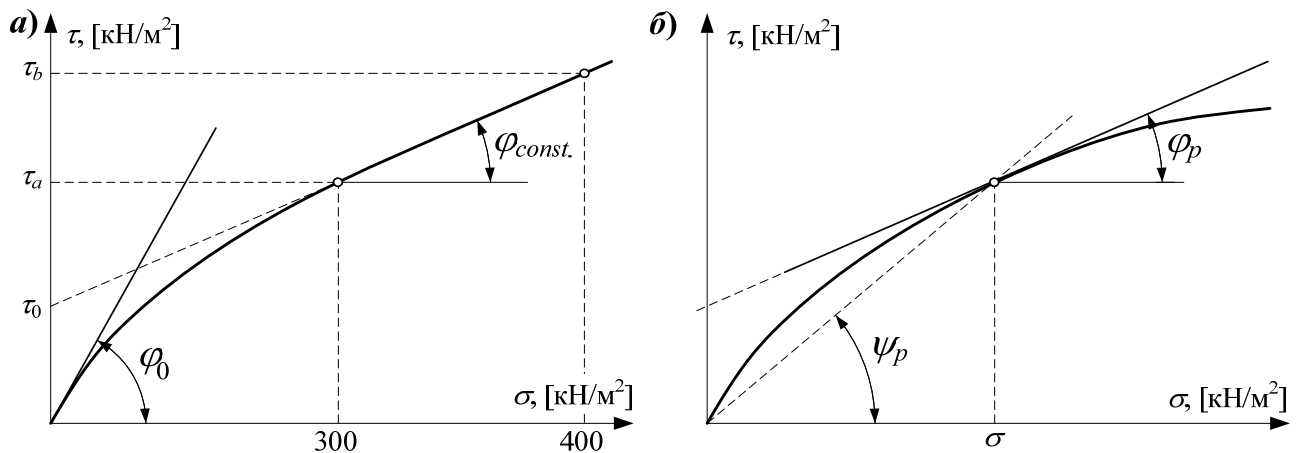


Fig. 3.4 - The boundary bending sand by M.M. Sidorov [2]:
 a) up to 100 kN / m²; b) up to 400 kN/m²

Based on the conclusions of MM Sidorov, G.G. Boldyrev [2] recommeSSS, at a normal pressure less than 100 kN/m², to use the decimal value of the internal friction angle $\varphi = \psi_p$ (Fig. 3.4, b). When processing the results of a cut in the plane $\sigma - \tau$, the recommendation of GG Boldyrev Using the method of least squares for a function of the first order, a straight line whose origin begins through the origin is obtained (Fig. 3.5). The angle that it forms with the abscissa is the angle of internal friction φ .

An analysis of the results of direct shear experiments for rice and composite medium is shown in Fig. 2.18 - 2.25.

From the analysis of 72 experiments on the shear of the bulk medium, the values of the angle of internal friction φ with respect to the angle of orientation of the bulk in the shear box to the shear plane β were obtained. The results are shown in Table. 3.1.

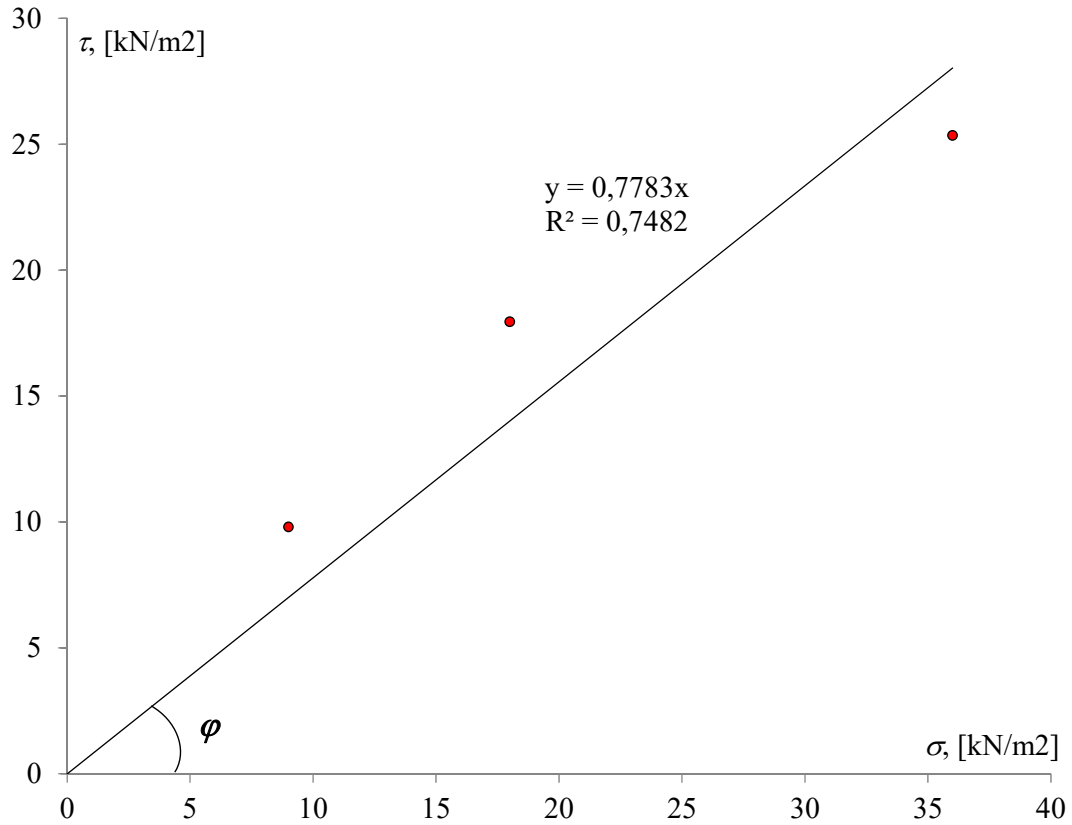


Fig. 3.5 – Internal friction angle φ

Table 3.1 –Results of direct shear

θ	№ of experiment.	Average specific weight, γ [kN/m ³]		φ , °			
		Rice	Composite medium	Rice	Avg.	Composite medium	Avg.
0°	1	8,90	16,61	44,15	40,35	51,31	51,46
	2	9,11	16,24	39,01		52,19	
	3	9,19	16,99	37,89		50,87	
30°	1	9,52	17,41	39,95	40,47	53,75	53,83
	2	9,42	17,28	34,58		53,46	
	3	9,25	17,26	46,89		54,28	
60°	1	9,57	17,33	42,31	43,65	57,00	57,46
	2	9,47	17,06	44,24		58,02	
	3	9,55	17,04	44,41		57,36	
90°	1	9,15	16,05	45,75	48,06	57,79	57,41
	2	9,36	16,36	47,31		57,29	
	3	9,40	16,41	51,11		57,15	

On the basis of tabular data one can construct the first quarter of the hodograph of the angle of internal friction (Fig. 3.6).

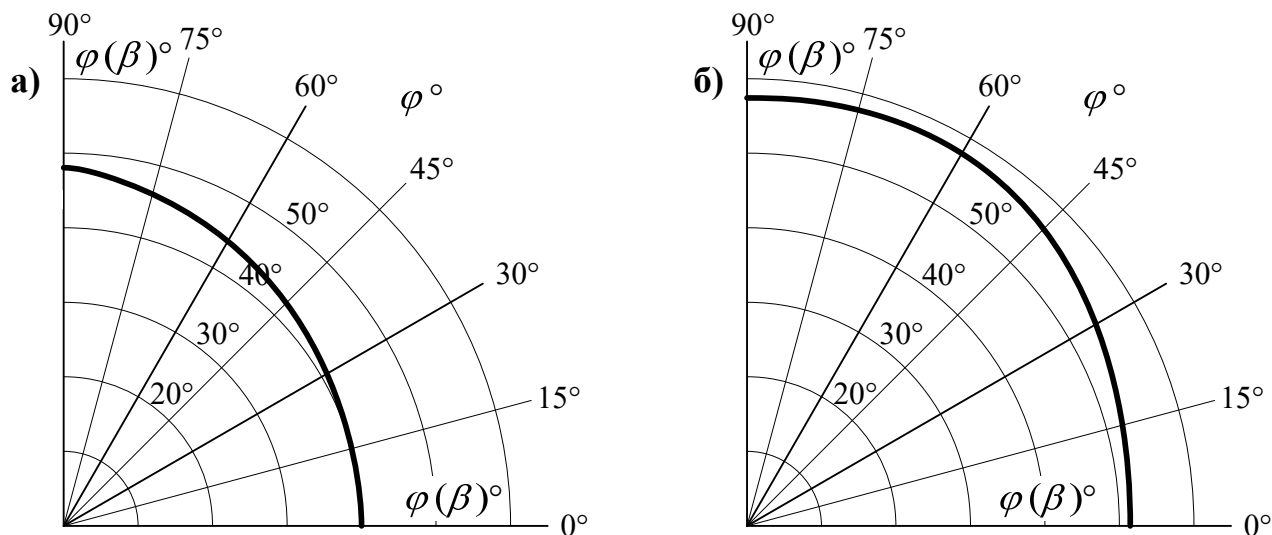


Fig. 3.6 – Hodographs of the angle of internal friction with respect to the fill angle β : a - rice; b - composite environment

At different orientations of particles β there is a significant anisotropy of strength properties. The maximum difference of the angle of internal friction φ falls on directions 0° and 90° , for rice it makes 19,09%, and for a composite material - 11,67%. The minimum angle φ was observed in the orientation of the grains $\beta = 0^\circ$ for both media, for rice $\varphi = 40.35^\circ$, and for the composite medium - $\varphi = 51.46^\circ$, while the maximum for rice appears with the orientation of the particles $\beta = 90^\circ$, $\varphi = 48.06^\circ$, and for the composite material at $\beta = 60^\circ$ and 90° the angle is almost the same $\varphi = 57,46^\circ$ and $57,41^\circ$.

These results represent the confirmation of the logical hypothesis Z. Ewertowska-Madej [74] that the soil particles, oriented at any angle β to the shear plane, are returned to the position at a cut to accept a position that agrees with the direction of the stresses of the cut. Of course, the larger the angle of rotation β , the more power needed to implement the cut. In samples perpendicular to the lamination, the soil particles turn at an angle of about 90° , which results in large values of shear resistance and deformations compared with samples cut parallel to the lamination.

In work A.V. Shkola [60] are recommended to take into account the anisotropic properties in practical problems when changing the strength characteristics of soils in the direction of adhesion not less than 10%, and the angle of internal friction is not less than 5%. One can conclude that the anisotropy of the parameters of strength at the tested loose media is significant, and therefore it can not be neglected.

Experimental investigations of friction of a bulk material on a metal wall. In order to calculate the side pressure on the closely spaced walls, in addition to the strength of the filler, it is necessary to determine the friction angle of the filling behind the model wall at different orientations of the particles relative to the wall. Experimental studies of rice and shell friction on steel were carried out in the conditions of gravity orientation of 0° and 90° froth.

The experimental research method was the same as in the removal of bulk media, except that the equipment of the direct cut was adapted - the upper casing was placed on a steel stand from which the wall of the model for measuring the side pressures was made (Fig. 3.7).

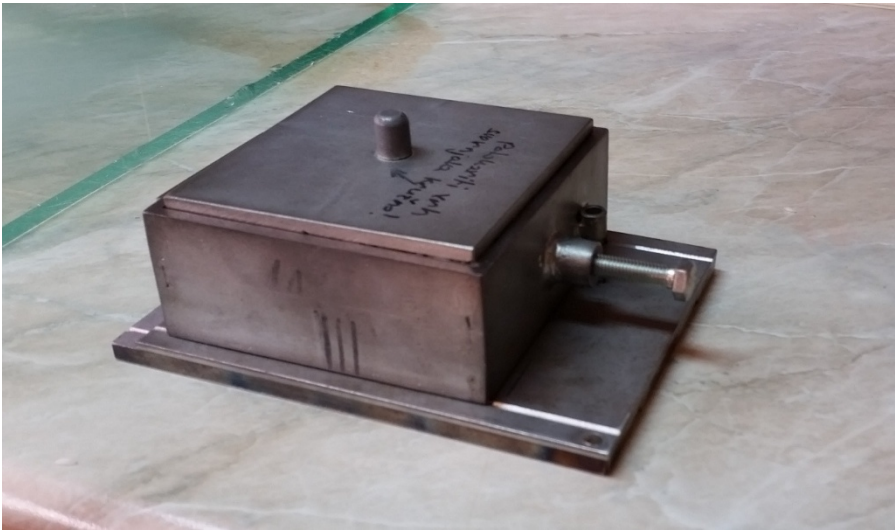


Fig. 3.7 – Adaptation shear box for testing the friction of bulk media on the steel

During the shears, the deformations of the dynamometer were measured, and tangential stresses were calculated from them. In tests, the vertical stresses $\sigma = 10 \text{ kNm}^2, 20 \text{ kN/m}^2$ and 40 kN / m^2 were applied.

Measured data with the analysis is shown graphically for rice in Fig. 3.8 and 3.9, and for the composite medium - in Fig. 3.10 and 3.11.

Data on friction angles of bulk materials on steel are given in Table. 3.2.

Table 3.2 – Angle of friction of bulk materials on steel under different packing conditions

Angle of filling, β	0°	90°
Rice	15,72	15,96
Composite medium	16,42	16,99

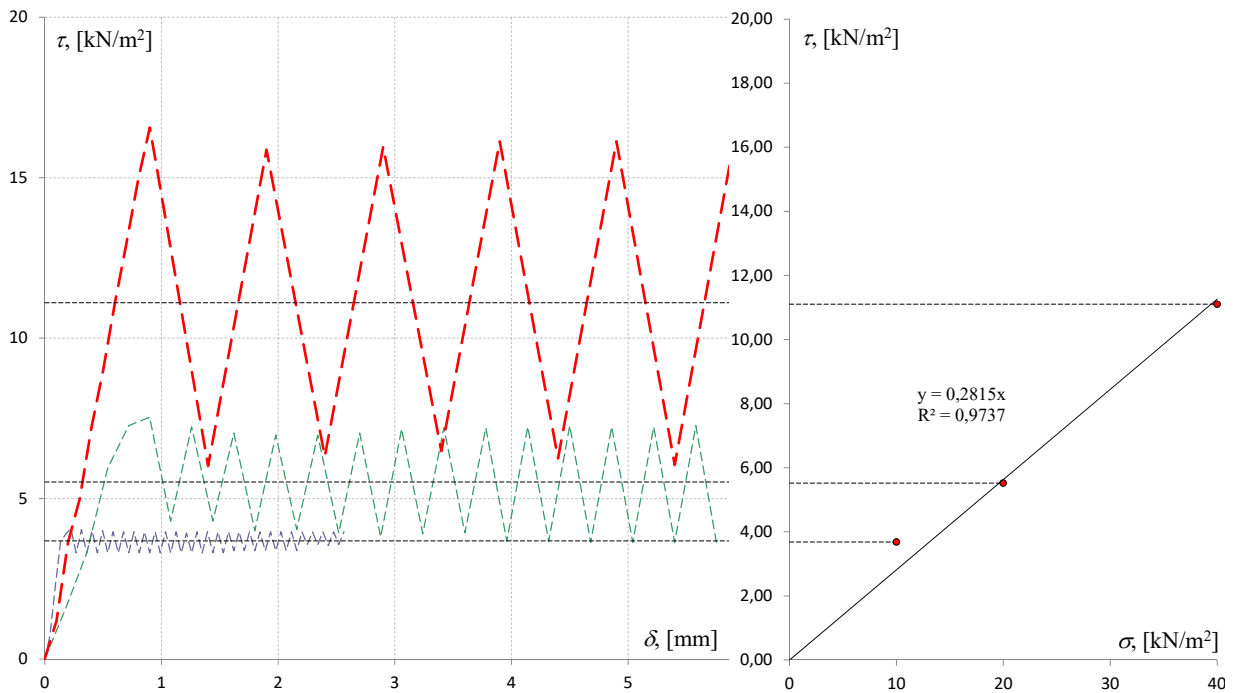


Fig. 3.8 – Analysis of measurement of friction of rice by steel for filling of rice 0°

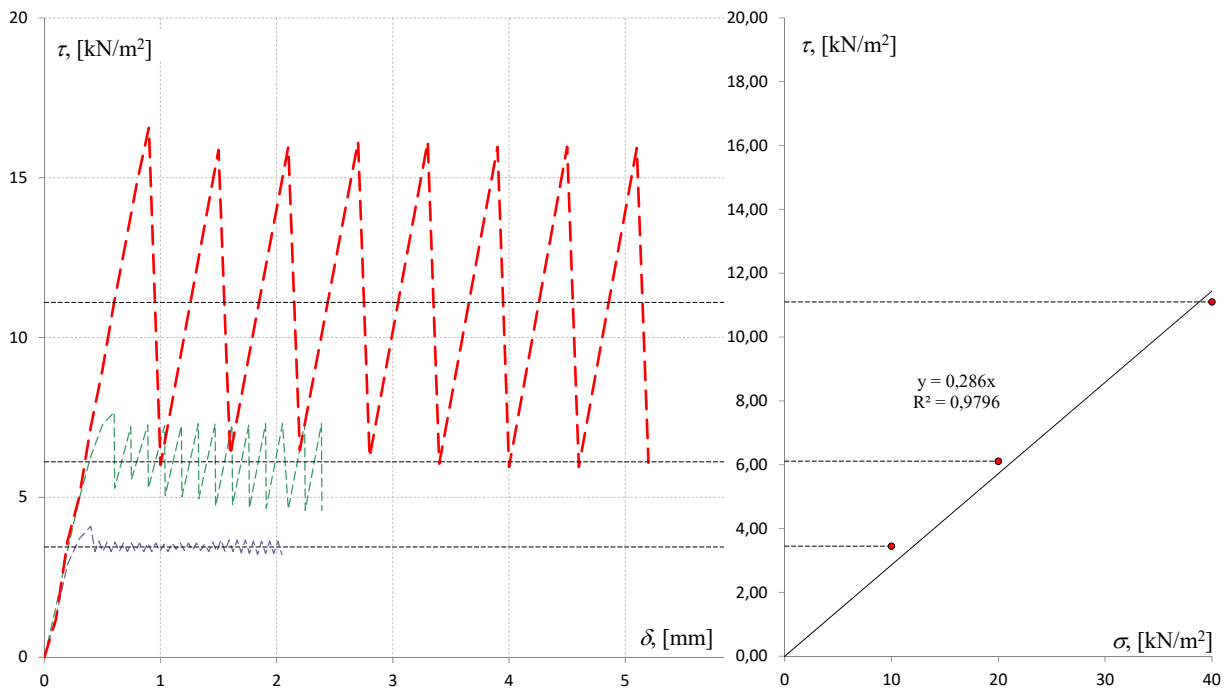


Fig. 3.9 – Analysis of rice friction measurements on steel for rice filling of 90°

The obtained data for the rice friction angles on steel at the angles of preferential grain orientation to the horizontal 0° and 90° differ by only 1.5%, and for the composite medium - by 3.5%, that is, the difference is negligible, which can be neglected. The explanation for such a difference is that when grabbing elongated bulk particles on the grain wall almost does not affect the wall as in the case of cutting in the medium layer, and therefore the rotation of the grains near the cut plane was insignificant.

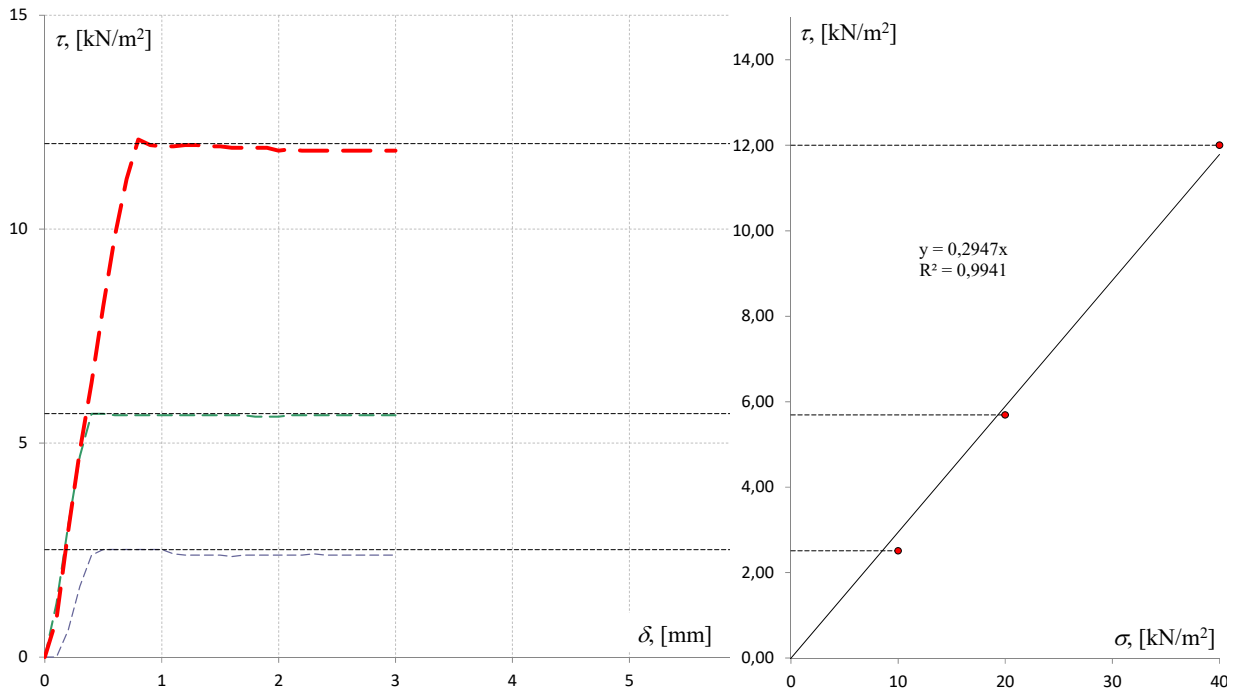


Fig. 3.10 – Analysis of the friction measurements analysis of the composite medium on the steel (0°)

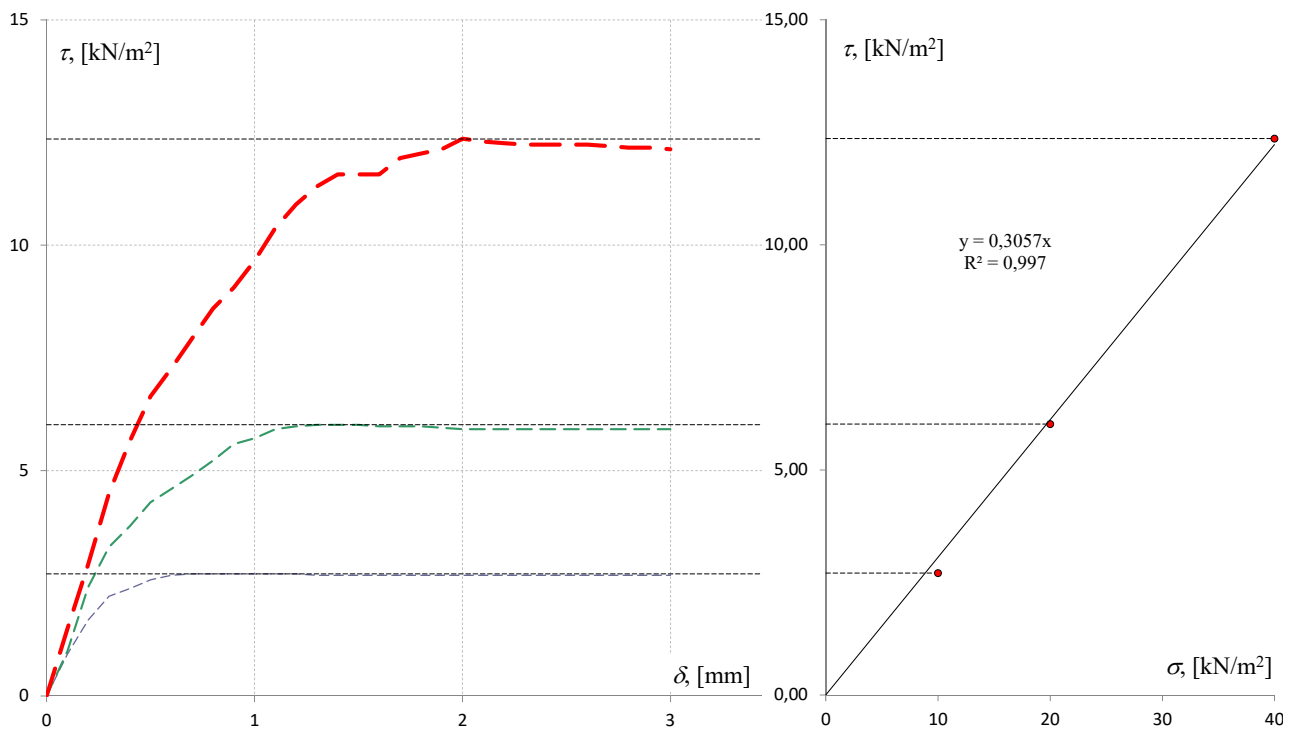


Fig. 3.11 – Analysis of the friction measurements analysis of the composite medium on the steel (90°)

A significant anisotropy of the properties of strength is determined by a direct shear at different angles of filling β . The maximum differences were recorded in the directions 0° and 90° , for the rice the angle of internal friction φ differed by 19.09%, and for the composite medium - by 11.67%. The minimum

angle φ was observed in the orientation of the grains $\beta = 0^\circ$ for both media, for rice $\varphi = 40.35^\circ$, and for the composite medium - $\varphi = 51.46^\circ$, and the maximum angle φ for rice appears in the orientation of the particles $\beta = 90^\circ$, $\varphi = 48.06^\circ$, and for the composite material at $\beta = 60^\circ$ and 90° the angle is almost the same $\varphi_{60^\circ} = 57.46^\circ$ and $\varphi_{90^\circ} = 57.41^\circ$

The friction angles of the bulk medium on the steel wall at the corners of the filling of 0° and 90° are measured. Experiments have shown that the angle of friction on the wall differs slightly, for rice 1,5%, and for composite medium, 3,5%. This change in practical calculations can be neglected. This phenomenon is due to the lack of interconnection between the grains and the steel sheet.

3.2. Results of field and laboratory research of anisotropy parameters of coherent soils

According to the method of field studies of heterogeneity of compacted soils artificial bases, one of the authors, together with M.O. Kharchenko [32] evaluated anisotropy of mechanical characteristics (internal friction angle φ and specific adhesion c) of compacted soils. For this purpose, for example, bulkly compacted soil pillow, rings were sampled with soil samples at angles $\alpha = 0^\circ$ (perpendicular) and 90° (parallel) to the horizon (the isotropy plane).

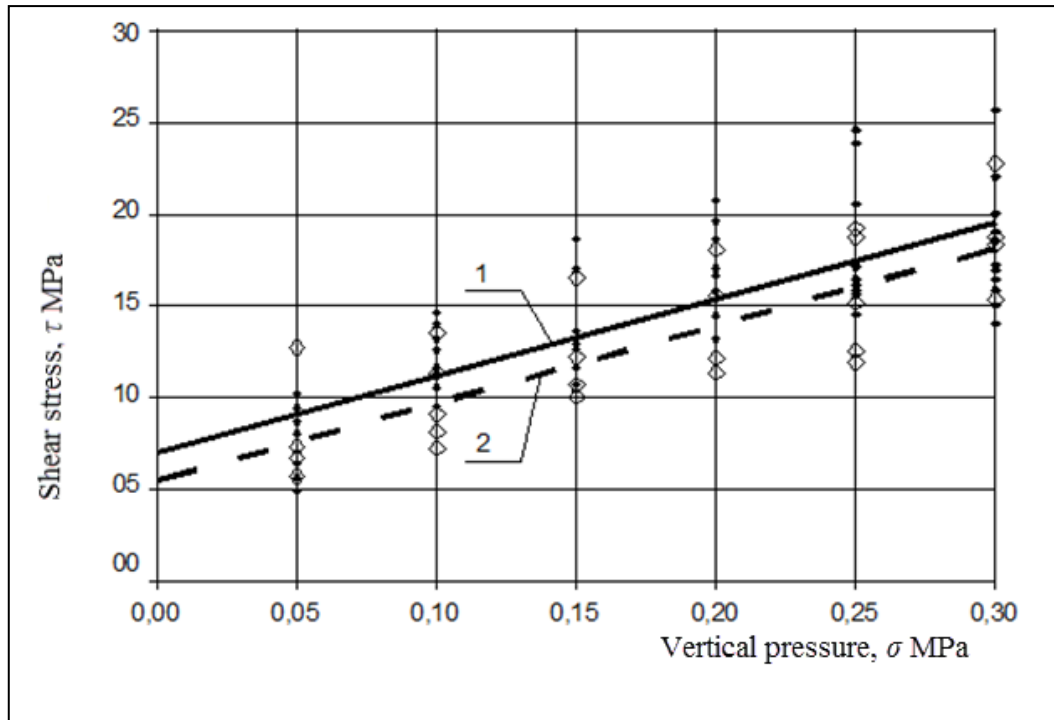
After this, in order to determine the characteristics of the strength of the compacted soil in the laboratory, a test was carried out in the device of a single-pitched shift of PSG-2M.

It was established [32] that the arrangement of a pad foundation of loess soil is characterized by the formation of anisotropic medium. In particular, the angle of internal friction of the soil in the horizontal rings (with the number of experiments and the coefficient of correlation $r = 0.81$) was $\varphi = 22.40$, and the specific clutch $c = 70$ kPa, and in the vertical - $\varphi = 21.90$ and $c = 70$ kPa (at τ) (Table 3.3).

Table 3.3 –The ratio of strength parameters of soil pad foundation

Ring orientation in relation to soil	Number of rings	Correlation coefficient, r	Angle of internal friction, φ°	Specific cohesion c , kPa
Horizontal	78	0,81	22,4 ⁰	70
Vertical	28	0,80	21,9 ⁰	61

In this case, the difference in the values of the mechanical characteristics obtained by sampling soil in different directions should be even greater, since the first sample included data for the upper (slightly "weaker") layer of the pillow (the vertical rings for him were not selected). The graphs of the relationship of tangential stresses from normal pressure by the results of the shift are shown in Fig. 3.12.



Legend

- - horizontally selected rings
- - - - - vertically selected rings
- ◇ - experimental points for vertically selected rings ($n=28$)
- - experimental points for horizontally selected rings ($n=78$)

Fig. 3.12 – Characteristic graphs of the dependence of the tension stress τ on normal pressure σ on laboratory studies of clayey soils of pad foundations:

- 1 - for horizontally selected rings ($n = 78$);
- 2 - vertically selected rings ($n = 28$) відібраних кілець ($n=28$)

Consequently, the strength of the compacted soil within the layered slipping of the pillow in a horizontal direction is slightly larger than in the vertical direction. That is, the arrangement of soil pillows is characterized by the formation of a given anisotropic medium. Artificial soils are characterized by anisotropy of their mechanical characteristics.

At each point of the natural and compacted array for the three directions $\alpha = 0^\circ; 45^\circ$ and 90° to the horizontal plane with close variation coefficients the values of the mechanical characteristics of the soil were represented in the form of quadrants of the hodographs. The coefficients of anisotropy of soil mechanical characteristics were determined by the formulas:

$$n_{E\perp} = E_{\perp} / E_{\angle} ; \quad n_{E\angle} = E_{\angle} / E_{\perp} ; \quad (3.1)$$

$$n_{C\perp} = c_{\perp} / c_{\angle} ; \quad n_{C\angle} = c_{\angle} / c_{\perp} ; \quad (3.2)$$

$$n_{\varphi\perp} = \text{tg}\varphi_{\perp} / \text{tg}\varphi_{\angle} ; \quad n_{\varphi\angle} = \text{tg}\varphi_{\angle} / \text{tg}\varphi_{\perp} ; \quad (3.3)$$

$$n_{R\perp} = R_{\perp} / R_{\angle} ; \quad n_{R\angle} = R_{\angle} / R_{\perp} , \quad (3.4)$$

where E_{\perp} – a module of deformation of the soil in the isotropy plane from the action of stresses in this plane, therefore, when orienting the rings at an angle $\alpha = 0^{\circ}$ relative to the horizontal plane;

E_{\perp} and E_{\angle} – the same, respectively, for the plane of the normal and inclined to the plane of isotropy, therefore, when $\alpha = 90^{\circ}$ and 45° ;

$c_{\perp}, \varphi_{\perp}, c_{\angle}, \varphi_{\angle}$ – Specific grip and angle of internal friction of the soil in the plane of displacement, respectively, parallel ($\alpha = 0^{\circ}$), perpendicular ($\alpha = 90^{\circ}$) and inclined ($\alpha = 45^{\circ}$) to the plane of isotropy;

$R_{\perp}, R_{\angle}, R_{\perp}$ – the specific resistance of the penetration test results, respectively, at angles, $\alpha = 0^{\circ}, 90^{\circ}$ and 45° to the horizontal plane.

The highest values of mechanical properties are characteristic for samples sampled at an angle of $\alpha = 0$ to the horizontal plane at the experimental sites, which comprise the loess loam of the natural structure ($w = 0.13 - 0.23$; $W_L = 0.29 - 0.33$; $W_p = 0.18 - 0.20$; $e = 0.83 - 0.99$) the smallest - at $\alpha = 45^{\circ}$ (coefficients of anisotropy were 0.6-0.9) [7, 8].

With the surface compacting by the ramps of this soil, the ratio of its mechanical characteristics in different directions was maintained, and sometimes somewhat strengthened (as with $\alpha = 45^{\circ}$ the magnitude of the coefficients of anisotropy decreased to 0.5) [7, 8].

A similar effect was observed for the soil below the bottom of the loaded bases at $p/R = 0.7 - 1.25$. The decrease in the values of the anisotropy coefficients by 5 - 10% is fixed, that is, we have some development of the horoscope hydrological characteristics [7, 8]. The construction of soil pillow from forest soil is characterized by the process of formation of anisotropic medium, by its nature similar to a natural forest or forest basis under the bottom of the bases of consolidation.

The material of the soil cushion of the experimental site in the city of Lubny, Poltava region, is represented by a loam of forest, heavy silty, with the following values of physical characteristics: $w = 0.17 - 0.20$; $W_L = 0.34$; $W_p = 0.19$; $\rho_s = 2.68 \text{ g/cm}^3$. The total capacity of the cushion is 1.40 m. The thickness of each layer of fallen soil is 25 - 30 cm. It was driven by loaded KrAZ cars for 10-14 tracks in one trail. The density of dry soil within the pillow reached $\rho_d = 1.71 - 1.87 \text{ g/cm}^3$.

After pouring the soil, of course, you can take for an isotropic medium, but after the slipping, he received certain anisotropic properties. As an example in Fig. 3.13 the quadrants of the hodographs given the mechanical characteristics of the clay soil within the compacted soil cushion: the deformation module (Fig. 3.13, a), specific gravity (Fig. 3.13, b), the internal friction angle (Fig. 3.13, c) and the specific resistance of the penetration Figure 3.13, d) in three directions to the horizontal plane at the characteristic point of the compacted layer [4, 7].

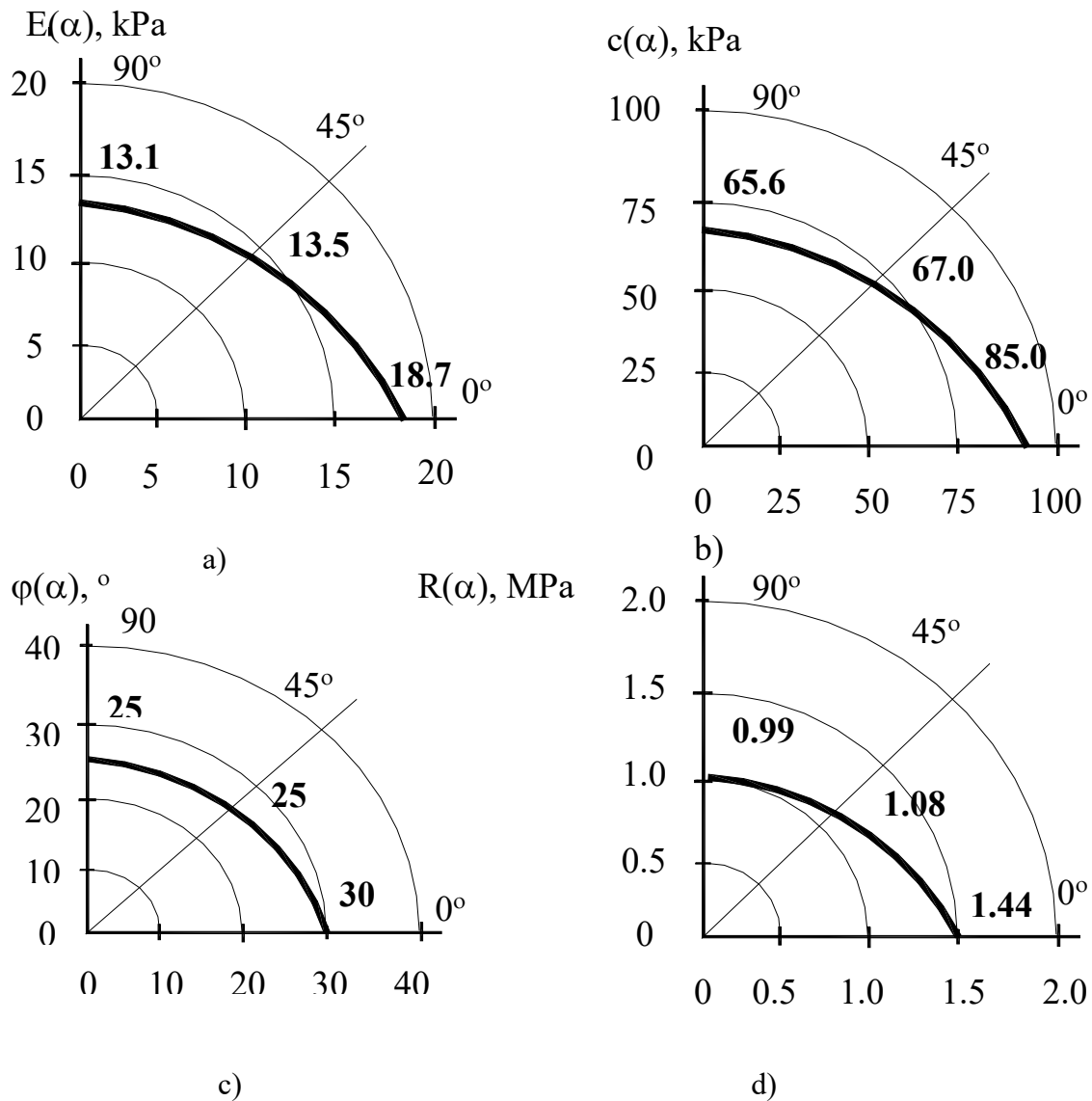


Fig. 3.13 Examples of hodographs of mechanical characteristics of forest loams in the characteristic point of a compacted layer of a soil pillow: a - deformation module; b - specific clutch; in - the angle of internal friction; Γ - specific resistance of penetration

The values of the mechanical characteristics of soil samples for $\alpha=0^\circ$ greater than those for $\alpha=0^\circ$ and 45° , which, in turn, are close together. Hence, as can be seen from Fig. 3.13, forms of the hodographs have a priority horizontal orientation. The values of anisotropy coefficients are less than unity and are in pairs close to each other $n_{E\perp} \approx n_{E\angle} = 0.62 - 0.89$; $n_{C\perp} \approx n_{C\angle} = 0.77 - 0.85$; $n_{\varphi\perp} \approx n_{\varphi\angle} = 0.81 - 0.90$; $n_{R\perp} \approx n_{R\angle} = 0.64 - 0.70$.

Investigations of bulk loams that were initially was isotropic showed that they also acquired anisotropic properties in their 10-40 years of compacting (in experiments, the anisotropy coefficients ranged from 0.65 to 0.95). Parameters of anisotropy of bulk soil to a certain extent depend on the duration of their self-compaction [7, 8].

It should also be noted that when *soaking* (and, incidentally, silication) of samples the loess soil became more isotropic: these coefficients usually ranged from 0.9 to 1.0 [7, 8].

Consequently, through field studies of bases that are compacted without and with limited ability of lateral extrusion, it is established that:

- with a long compression of the bases of buildings, a densely formed soil zone is formed which does not exceed half the width of the sole of the foundation, and the parameters of the soil are linearly dependent on the ratio of the average pressure under its sole to the calculated resistance of the soil of the natural structure;

- in case of superficial compaction of soil with heavy ramps, the thickness of a sufficiently densified layer and the change in the density of the dry soil at its depth can be determined by the linear function, depending on the natural value of the density of the dry soil and the size of the decrease of the surface of the array under the ramp;

- when creating a compacted array there is a process of formation of a given anisotropic medium with a priority direction of changes of the hodographs of its natural mechanical properties in accordance with the direction of squeezing the soil by the foundation or working body.

Let's consider also some typical examples of one of the authors of the field studies of the mentioned parameters of the ground of foundations and foundations (piles) created with its extrusion from under various directions [5, 121].

An example of studying soil characteristics around the basement is given for a research site in the city of Kobeljaki, Poltava region. Soils are represented by loam, bulk, hard ($W_L = 0.28$; $W_p = 0.19$; $w = 0.14$; $\rho_s = 2.64 \text{ g/cm}^3$; $e = 0.80$; $S_r = 0.47$). Parameters of the foundation in the pierced well: depth $h_k = 3.5 \text{ m}$; diameter $b_p = 0.5 \text{ m}$; The volume of rubble rubbed $V_{cr} = 1.25 \text{ m}^3$ (Fig. 3.14, b).

An example is the change in the specific resistance of penetration of the soil around the foundation (based on the results of tests by the pen-metrometer PD-2M) in three directions $\alpha = 0^\circ$, 45° and 90° in relation to the horizontal plane is given in Fig. 3.14. At each point of the array, the results of these studies are presented in the form of quadrants of the hodographs. In fig. 3.15 examples of quadrants of the modulus of deformation, specific gravity, internal friction angle and specific resistance of penetration in directions, $\alpha = 0^\circ$, 45° and 90° to the horizontal plane (at close variations of coefficients) at different distances from the lateral surface of the foundations are given.

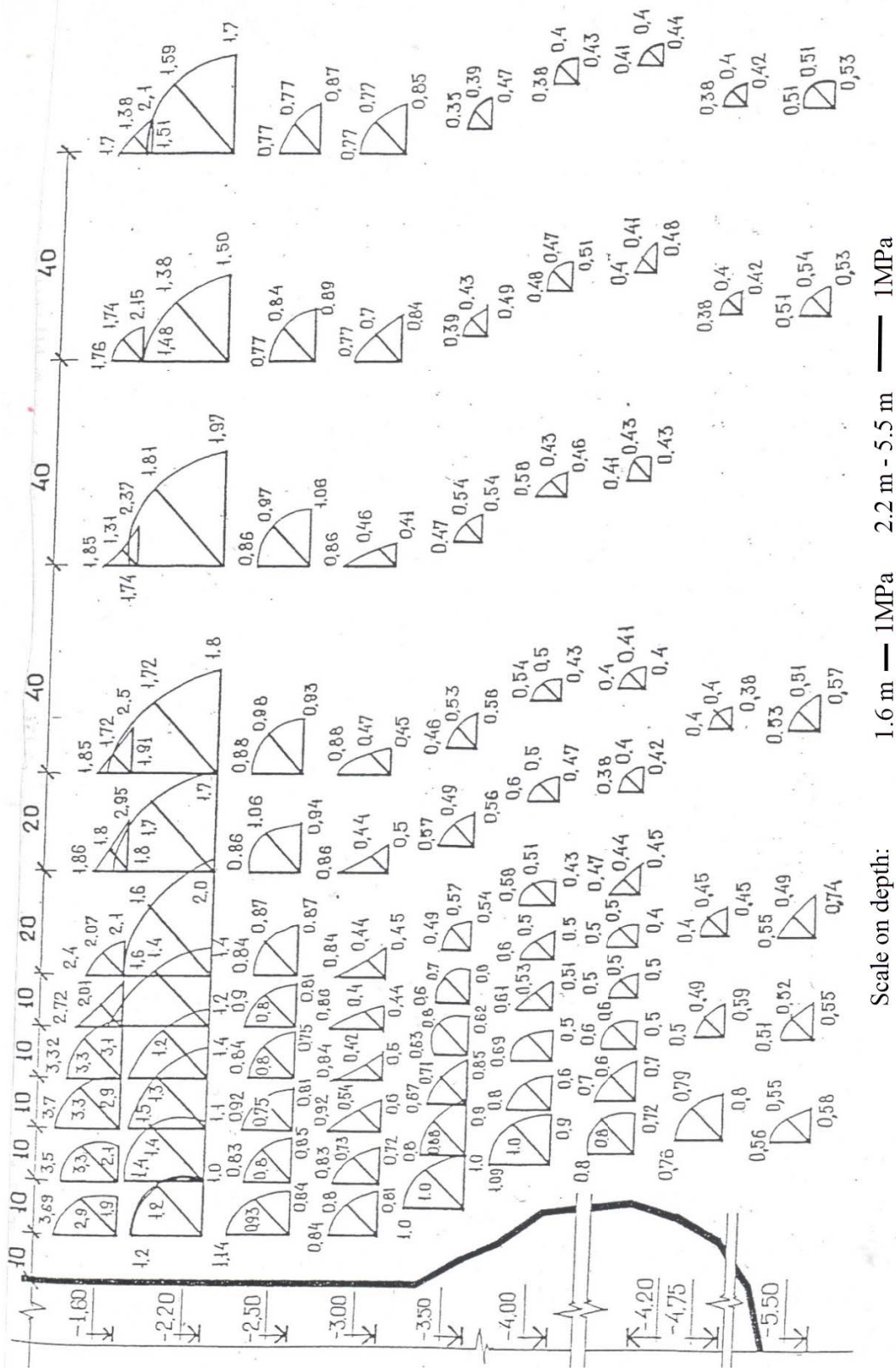


Fig. 3.14 An example of changes in the specific resistance to penetration of soil around the packing pile in the pierced well according to the tests of the field penetrometer PD-2m in three directions $\alpha = 0^\circ, 45^\circ$ and 90° and in relation to the horizontal plane

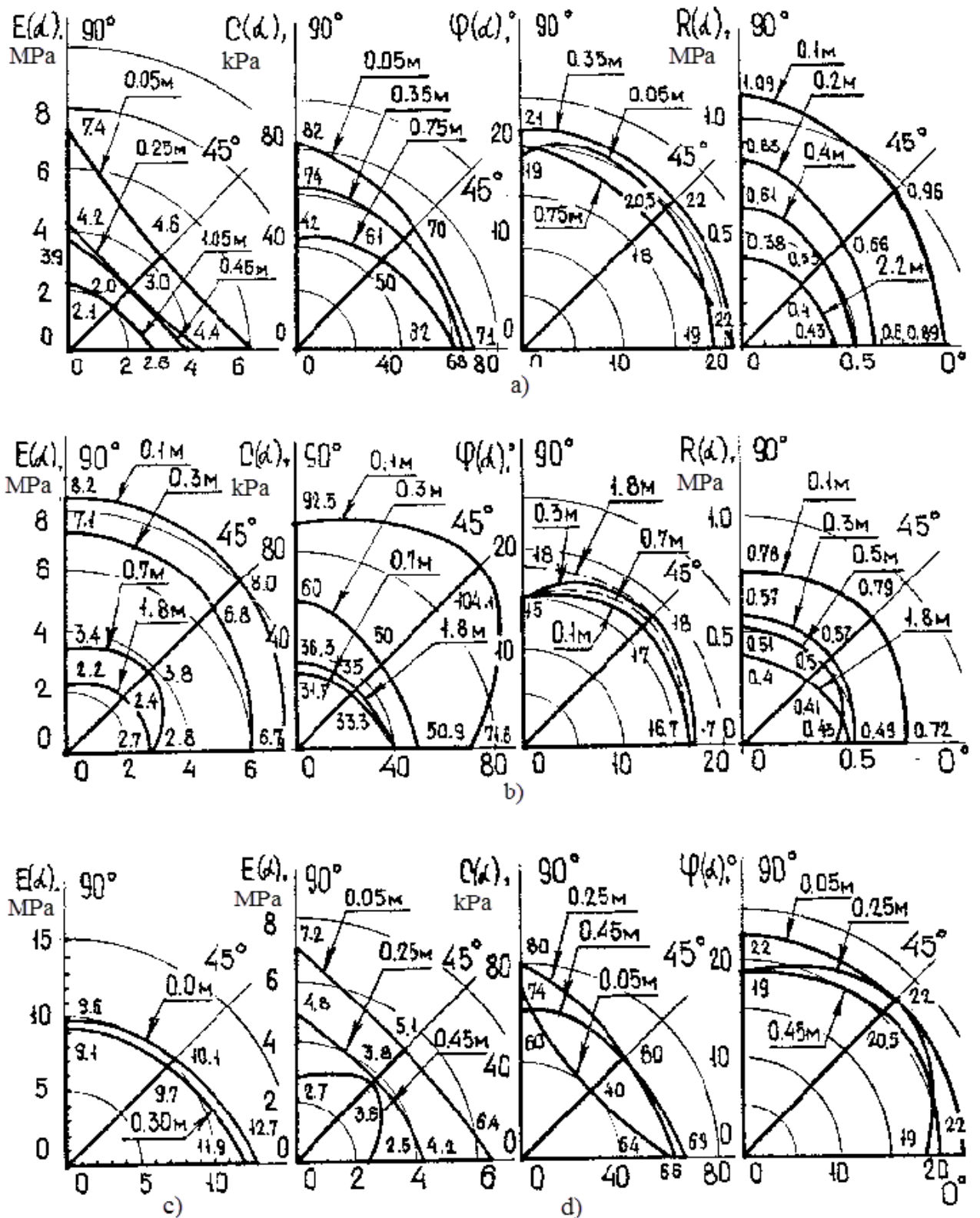


Fig. 3.15 Examples of quadrants of the hodographs of the mechanical characteristics of the soil: a) near the trunk and expansion of the stuffed piles in the broken wells; b) near the lower inclined surface of the expansion; in - at 0.5 m below the expansion; c) in the space between the piles of trunks ($l_w = 1.8$ m); r - distance from the side of the pile

For loess loams of natural composition, hence with primary anisotropy, higher values of the deformation module are characteristic when the rings are oriented at an angle $\alpha = 0^\circ$ to the horizontal surface, rather than at whose $\alpha = 90^\circ$ та 45° modulus of deformation are close. That is n_{E_\perp} and n_{E_\angle} the coefficients and smaller units of and $n_{E_\perp} \approx n_{E_\angle}$ (see, for example, the quadrants of the hodographs for the most distant from the lateral surface of the extensions of points in Fig. 3.15, a and b). With depth n_{E_\perp} and n_{E_\angle} somewhat decreasing: for the conditions of plots at a depth of 1 m from n_{E_\perp} and n_{E_\angle} the surface of $n_{E_\perp} \approx n_{E_\angle} = 0.85 - 0.9$, and at a depth of 4.0 - 4.5 m - already 0.7 - 0.8.

For the soil of the compacted zone, directly at the lateral surface and the pallet extensions, larger values are observed when the rings are oriented at an angle $\alpha = 90^\circ$ relative to the horizontal plane, rather than with $\alpha = 0^\circ$ and 45° the values E of samples taken under $\alpha = 45^\circ$ are the smallest of the three directions (Fig. 3.15, a), hence $E_\perp > E_- > E_\angle$. So for samples taken at a depth of 4 m directly at the trunk (Fig. 3.15, a) $n_{E_\perp} = 1.23$, $n_{E_\angle} = 0.77$. As the distance from the lateral surface of the foundations increases E_- , E_\perp , E_\angle , they decrease and level out (sometimes with a somewhat smaller or somewhat higher meaning).

It is possible to allocate the distance at which $n_{E_\perp} \approx 1$ (for the case shown in Figure 3.15 b, it is 0.4 - 0.45 m, and the case given in Figure 3.15, a, - 0.75 - 0.8), after which the coefficients n_{E_\perp} and n_{E_\angle} gradually return to values corresponding to the natural state of the soil. Under the bottom of the extensions $E_- > E_\angle > E_\perp$; and n_{E_\perp} та n_{E_\angle} less than one (in Fig. 3.15, in, in particular, $n_{E_\perp} = 0.76$; $n_{E_\angle} = 0.8 - 0.82$).). In the direction normal to the lower inclined surface of the expansion, the greatest values are and (Fig. 3.15, c). It should be noted that within the zone of sufficient compacting the soil deformation module was 2 to 4 times higher than its natural values.

It has been established that the shape of the hodographs of the characteristics of the strength (especially the specific clutch) in the natural state as a whole have a horizontal orientation (Fig 3.15, and b - for the most distant from the point extension.) In these cases: $n_{c_\perp} = 0.79$; $n_{c_\angle} = 0.83$ (Fig. 3.15, a) ; $n_{c_\perp} = 0.68$; $n_{c_\angle} = 0.8$; $n_{\phi_\perp} = 0.9$; $n_{\phi_\angle} = 0.8$ (Fig. 3.15, b). With depth n_{c_\perp} , n_{c_\angle} , n_{ϕ_\perp} , n_{ϕ_\angle} similarly n_{E_\perp} and n_{E_\angle} somewhat decreased.

The shape of the specific cohesion hodographs, samples taken at the lateral surface of the shafts (extensions), has a priority vertical orientation (for example, curves 1 in Figure 3.15, a, for which $n_{c_\perp} = 1.2$, $n_{c_\angle} = 1$ при $n_{\phi_\perp} = 1$, $n_{\phi_\angle} = 1.08$). In the direction of the normal to the lower inclined surface of the expansion, the greatest values are c_\perp and c_\angle Fig. 3.15, c), for which $n_{c_\perp} = 1.29$,

$n_{C\angle}=1.45$ at $n_{\varphi\perp}=0.9$, $n_{\varphi\angle}=1.02$. With an increase in the distance from the lateral surface of the foundations, the value c_{\perp} , c_{\angle} is reduced and aligned at very close values φ_{\perp} , φ_{\angle} . For the cases presented in Fig. 5.12, a and b, at a distance of 0.35 - 0.4 m – at $n_{\varphi\perp} \approx n_{\varphi\angle} \approx 1$. Consequently, the transition to the primary nature of the anisotropy of the strength of the soil is similar to the process for deformation anisotropy. Under the bottom of the extensions, the strength of the samples taken at the $\alpha = 0^\circ$ is the largest, that is, <1 and <1 ., $n_{c\perp} < 1$ and $n_{C\angle} < 1$. Within the zone of sufficient compacting, specific adhesion exaggerates 2-4 times the natural value.

In the interfoundation (interpile) space, the change of the anisotropy of the eastern soil with the transition from the compacted soil of the white surface of the foundation to the natural soil, but at the distance between the axes of the neighboring foundations smaller than three diameters of their cross-section, the primary values of the coefficients of anisotropy are not recorded.

Hence, the nature and patterns of the induced deformation anisotropy and the anisotropy of the strength of the soil are determined by its natural structure (primary anisotropy) and the direction of squeezing the soil by a ram and expansion in the arrangement of foundations, as well as the dimensions of the interfoundation space.

The regularities of the primary and induced anisotropy of the soil around the foundations for penetration tests, as shown in Fig. 3.15, correspond to its parameters of anisotropy of strength and deformability. Coefficients of anisotropy according to penetration data for natural soil $n_{R\perp}=0.74 - 0.96$; $n_{R\angle}=0.66 - 0.95$, and for compacted directly at the trunk or expansion – $n_{R\perp}=1.06 - 1.98$; $n_{R\angle}=1.08 - 1.58$.

Для встановлення взаємозв'язку між даними пенетрації та фізичними властивостями генетично однорідних ґрунтів за умов їх трикомпонентного стану викоФігтано рівняння взаємозв'язку В.Ф. Разорьонова [39]

An example of changes in the anisotropy coefficients of soil mechanical properties, depending on the distance to the lateral surface of the foundation, for individual layers of experimental sites in Kobeliaky region and "Sadi-3" in Poltava, is given in Fig. 3.16.

To establish the relationship between the data of penetration and the physical properties of genetically homogeneous soils under the conditions of their three-component state, the equation of the relationship by B.F. Razorionov [39] is used.

$$\lg \frac{R}{R_0} = \frac{W_R}{1/e_0} + \frac{\gamma_w}{\gamma_s} \cdot \frac{1 - M_{kpf}}{1/e_0} - w \frac{M_{kpf}}{1/e_0} - \frac{\gamma_w}{\gamma_d} \frac{1 - M_{kpf}}{1/e_0}, \quad (3.5)$$

where R – the specific resistance to penetration; $R_0 = 1$ MPa;

γ_d – specific weight of dry soil;

$1/e_0$ – the tangent of the angle of inclination to the axis of the ordinates of the dependency graph (3.5) constructed in coordinates "w – lg R" for the case of complete water saturation of the soil, that is, for $S_R=1$, and $w = W_{sat}$;

$M_{kpf} = 1 - ((1/e_0)/(1/e))$ - the coefficient in which $1/e$ the tangent of the inclination angle to the coordinate axis of the graph (3.5) constructed in coordinates " $W_{sat} - lg R$ " for the case of $w = const$;;

W_R - humidity of water-saturated soil at $R = 1$ MPa.

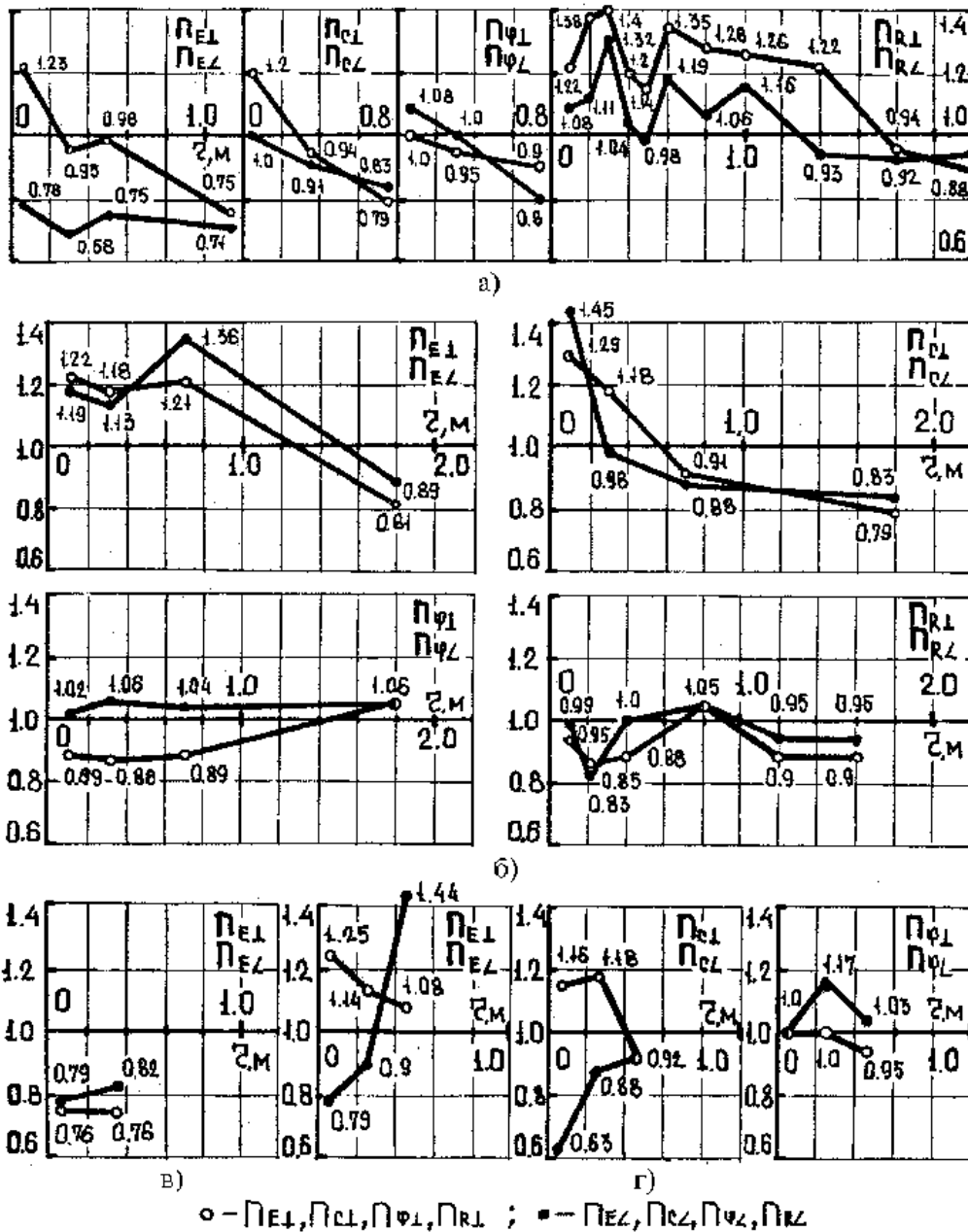


Fig. 3.16 Examples of changes in soil anisotropy coefficients depending on the distance from the lateral surface of the stuffed piles in the pierced wells: a, b, c, d - correspond to the same points as in Fig. 3.15

The equation of the relationship between the physical characteristics of the soil (both in the natural structure and within the compacted zone) and the results of penetration tests in different directions relative to the horizontal plane are summarized in Table. 3.4.

Table 3.4 Equation of the relationship between the physical characteristics of the soil and the results of penetration tests in different directions relative to the horizontal plane

Penetro meter	Angle at the top of the cone	Direction relative to horizontal plane	Empirical equations for determination:		The value of statistical characteristics		
			$\lg R =$	$\rho_d =$	r	v	D
ПД-2	30°	0°	2.59 - 4.94 W - 2.88 (1/ρ _d)	2.88 / (2.59 - 4.94 W - lg R)	0.96	0.09	0.003
		45°	2.12 - 4.12 W - 2.42 (1/ρ _d)	2.42 / (2.12 - 4.12 W - lg R)	0.92	0.12	0.006
		90°	1.54 - 2.67 W - 1.89 (1/ρ _d)	1.89 / (1.54 - 2.67 W - lg R)	0.92	0.12	0.005
MB-2	30°	0°	1.98 - 3.93 W - 1.99 (1/ρ _d)	1.99 / (1.98 - 3.93 W - lg R)	0.87	0.16	0.02
		45°	1.85 - 1.66 W - 2.47 (1/ρ _d)	2.47 / (1.85 - 1.66 W - lg R)	0.84	0.20	0.03
		90°	1.69 - 0.30 W - 2.62 (1/ρ _d)	2.62 / (1.69 - 0.30 W - lg R)	0.85	0.16	0.02
	17° 40'	0°	1.23 - 2.11 W - 1.80 (1/ρ _d)	1.80 / (1.23 - 2.11 W - lg R)	0.85	0.14	0.004
		45°	1.50 - 2.33 W - 2.15 (1/ρ _d)	2.15 / (1.50 - 2.33 W - lg R)	0.86	0.17	0.005
		90°	1.89 - 1.24 W - 2.98 (1/ρ _d)	2.98 / (1.89 - 1.24 W - lg R)	0.86	0.16	0.006

The values of the statistical characteristics of equation (3.5), also included in the table, indicates the close relationship between, the soil in all directions relative to the horizontal plane for both penetrometers and angles at the vertex of the cone.

Thus, on the example of formation of the indicated properties of the massif during the arrangement of the piling piles in the pierced wells, it has been experimentally established that the geometrical dimensions of the consolidation and depletion zones of the foundations, reduced by the possibility of squeezing the soil in different directions, and the parameters of the soil within them are significantly influenced by: I will become the soil; the directions of its displacement by the foundation (the palace, the working body); geometric dimensions of the foundations.

4. EXPERIMENTAL RESEARCHES OF SILO PRESSURE IN DIFFERENT CONDITIONS OF FILLING (FOR VARIOUS AXES ORIENTATION OF ANISOTROPY GODOGRAPH)

In the section is given experimental research lateral pressure on closely located rigid walls of the model at different angles of the orientation of the particles of the bulk medium to the horizontal. The purpose of the study is to determine the influence of the orientation of particles on the nature and distribution of lateral pressures.

Tests were conducted under the plane conditions. Two bulk media, rice and a composite medium were used for testing, whose physical-mechanical characteristics were investigated in the second section.

4.1. Description and calibration of the experimental installation

Experimental model, the general form of which is shown in Fig. 4.1, and the scheme - in fig. 4.2, is a parallelepiped of a steel sheet with an open top, with a size of 50 cm x 50 cm and a height of 105 cm. It consists of four walls and a bottom. The side walls, the front wall and the bottom are made of steel sheet in the thickness of 5 mm, and the rear side - from a steel sheet in thickness of 3 mm with transverse ribs (Fig. 4.2, b). All the walls except the rear are welded together.

Rear wall is mounting. With help of steel angular profiles 20 mm x 20 mm and a thickness of 4 mm, it can be installed at different distances from the front wall - 5, 10, 15 and 50 cm (Fig. 4.2, c). Angles are tight bolted to the wall of the model, and the rear wall is attached to them with bolts. The profiles of the rods further increase the longitudinal (vertical) stiffness of the back wall.

Five holes with a diameter of 50 mm, which are evenly distributed in height (Fig. 4.1, a), were made to measure the pressure in the middle of the front wall of the model. For fastening of sensors at each hole 4 threaded rods M6 are welded in length 20 mm.

On the side walls of the model installed on two handles and two pairs of threaded rods $\varnothing 20$ mm in length 40 mm on the side walls of the model.

In order to fill the bulk material in the cavity at an angle, the model can be installed at the desired angle, using a tray and steel supports. In the pallet there are holes in which the steel supports are screwed, the supports are fastened to the threaded pins $\varnothing 20$ mm (Fig. 4.3).

Five console load cells (Figure 4.2, a) of type-6530 made of aluminum, manufactured by the Chinese company Xi'an Ruijia Measurement Instruments Co. Ltd. were used to measure side pressures. Characteristics of the cells are given in Table. 4.1. The sensor operates on the Wheatson Bridge circuit.



Fig. 4.1 General view of the model: a) the front view; b) the rear view; c) view from above

The load cells were mounted on the front wall of the model. To the bottom of the sensor bolts fastened steel bar, and from the upper part - a steel cylinder (Fig. 4.4, a).

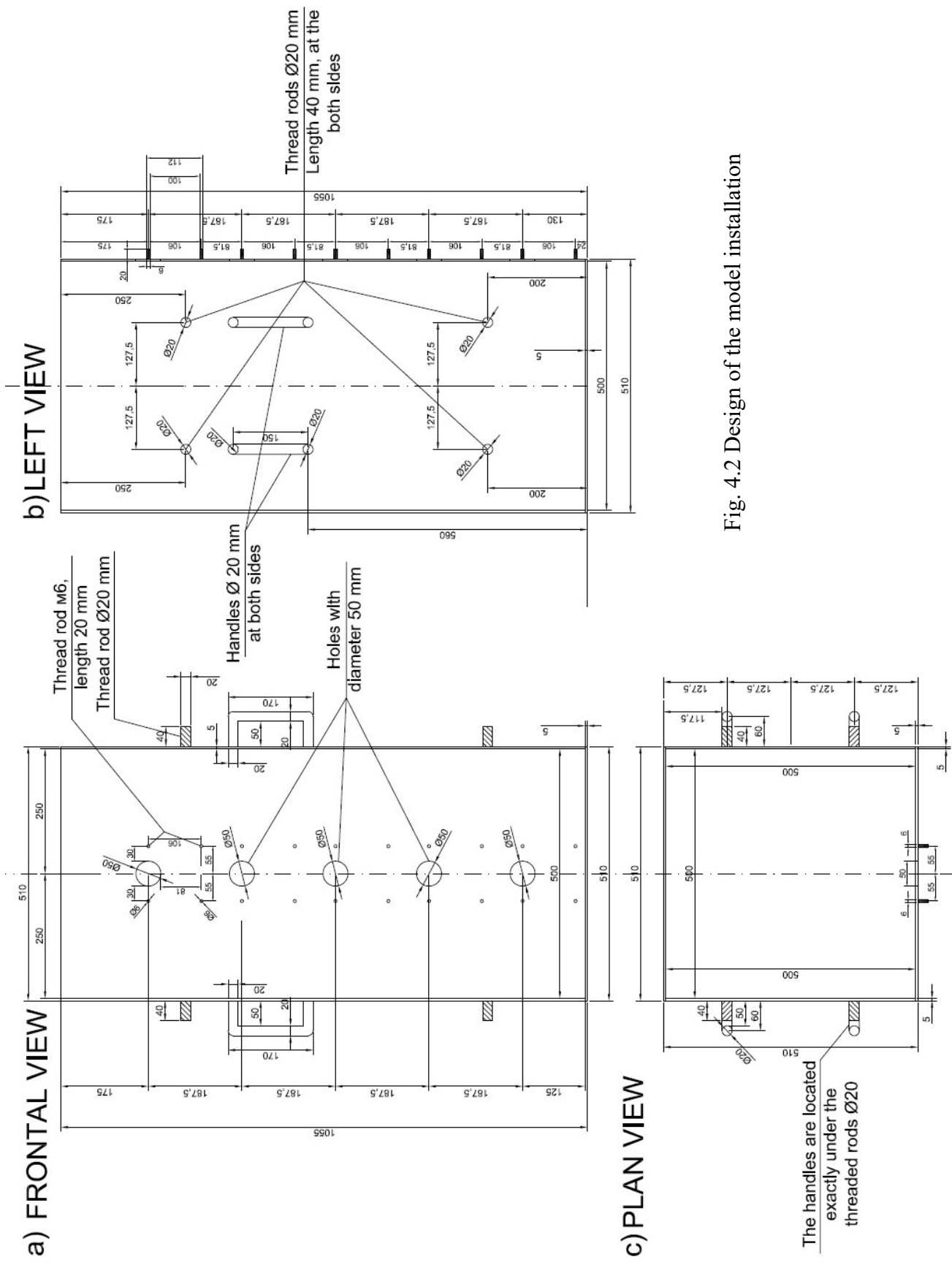


Fig. 4.2 Design of the model installation

Table 4.1 Characteristics of load cell 6530

Measurement limit	Kg	5		
Nominal coefficient of strain sensitivity	mB/B	2,0±0,15		
Total error	%FS	0,01	0,01	0,02
Creep	%FS (15 minute)	0,01	0,01	0,02
Input resistance	Ω	406±20		
Output resistance	Ω	350±5		
Insulation resistance	M Ω	≥5000 (100VDC)		
Measurement limit	%FS	±1		
Temperature coefficient signal level	%FS/10°C	0,02		
Temperature coefficient zero level	%FS/10°C	0,17		
Nominal operating temperature range	°C	-10~+60		
Maximum operating temperature range	°C	-20~+80		
Supply voltage, nominal	V	6~12		
Power supply, maximum	V	3~15		
Safe overload limit	%FS	120		
Limit overload	%FS	150		
Class of protection		IP65		
Material	Aluminum alloy			
Dimensions	22 MM x 30 MM x 130 MM			



Fig. 4.3 Installation of the model at an angle

In the steel bar are two holes, which exactly match on the threaded rods M6 (Fig. 4.4, b) on the front wall of the model, when secured with screw-nut, the cylinder which mounted on top, freely enter the hole (Fig. 4.4, c). The diameter of the cylinder was 48 mm, and the diameter of the hole was 50 mm, resulting in a ring gap, between the wall of the device and the cylinder, width of 1 mm. The gap contributed to the unobstructed movement of the cylinder in the opening under the action of even a small magnitude of force, thus friction between the cylinder and the walls was reduced to zero. To avoid getting small particles in the gap, a flexible, thin polyethylene membrane was used. A similar approach in measuring side pressure was used by E. Gallego [76] and H. Hsiao-Sung [82].

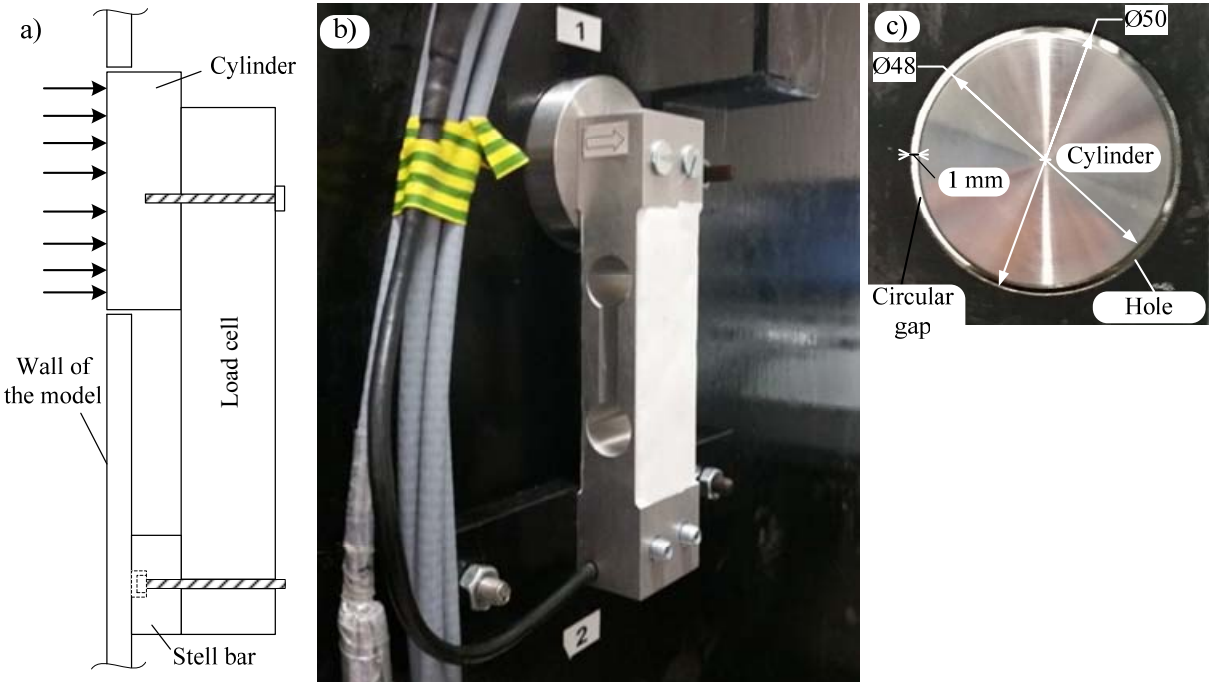


Fig. 4.4 Installation of the weight strain gauge on the model: a) the diagram of the mounting of the sensor; b) general view of the sensor; c) view of the measuring cylinder from the inside

The signals received from sensors were read using a universal 8-channel amplifier for the QuantumX MX840A, the German firm HBM (Fig. 4.6, a). The connection of load cells to the amplifier was conducted in accordance with the instructions for use, through the 15 pin connector. The diagram of connecting the sensor to the socket - the plug (see Figure 4.5).

Calibration of sensors. The qualitative calibration of the sensors of mechanical quantities and the creation of special tare devices and devices occupy one of the main places in the technique of the experiment [20]. When preparing sensors for work, the main attention is paid to the removal of stable amplitude characteristics.

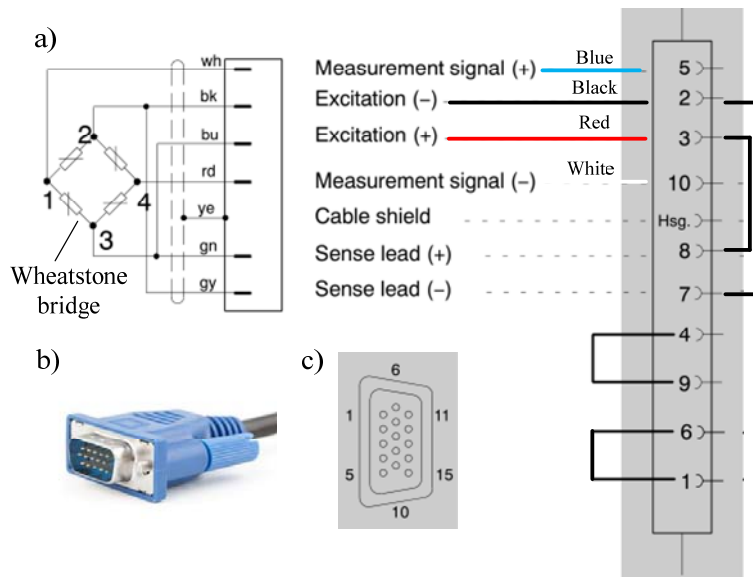


Fig. 4.5 Wiring diagram of the sensor connection to the jack: a) circuit diagram of the bridge of the bridge with the jacks; b) general view of the jack; c) scheme of the jack

The sensors were calibrated in the range of future measurements, which were determined using the theory of H. Janssen [85]. In particular, for rice, the interval of measurements ranges from 80 g to 260 g, and for sand - from 200 to 600 g. As a result, the interval of calibration from 20 g to 1000 g was adopted.

For this purpose standard weights of 20 g, 50 g, 100 g, 200 g, 500 g and 1000 g were used (fig. 4.6, b). The sensor was unilaterally rigidly fixed to the weighing machine (fig. 4.6, c), connected with the wire with the amplifier, and the amplifier to the PC (Fig. 4.6, g). The original software "Catman®Easy" cleared the sensor, and then the measurement process was started. Sensor sensitivity coefficient k_0 , given as nominal, according to Table. 4.1. Then the standard weights 20 g, 50 g, 100 g, 200 g, 500 g and 1000 g were individually placed on the sensor, measurements were taken for each weigh.

After that, the ratio of weight to weight and measured results was calculated, and the average ratio for the given interval of measurements was determined. This ratio is a factor in the correction of the nominal sensitivity of the sensor. The new, more accurate sensitivity of the sensor was determined by multiplying the correction factor by the sensitivity of the sensor (see expression (4.1)). The new sensitivity was introduced into the software (see Table 4.2). The weighing procedure was repeated anew. The gills were weighed again, for each operation the relative error was calculated, the total relative error for the measurement interval was calculated as the average of the arithmetic errors for each weight. On average, for all sensors, it did not exceed 0.4%.

$$k = k_0 \frac{m_{\text{meas.}}}{m_{\text{standard}}} \quad (4.1)$$

Table 4.2 Correction of sensors sensitivity coefficients k

№ sensor	The serial number	k_0	k
1	LB162554	2,00000	2,14762
2	LB162196	2,00000	2,17791
3	LB162624	2,00000	2,12765
4	LB162060	2,00000	2,08492
5	LB162124	2,00000	2,06875

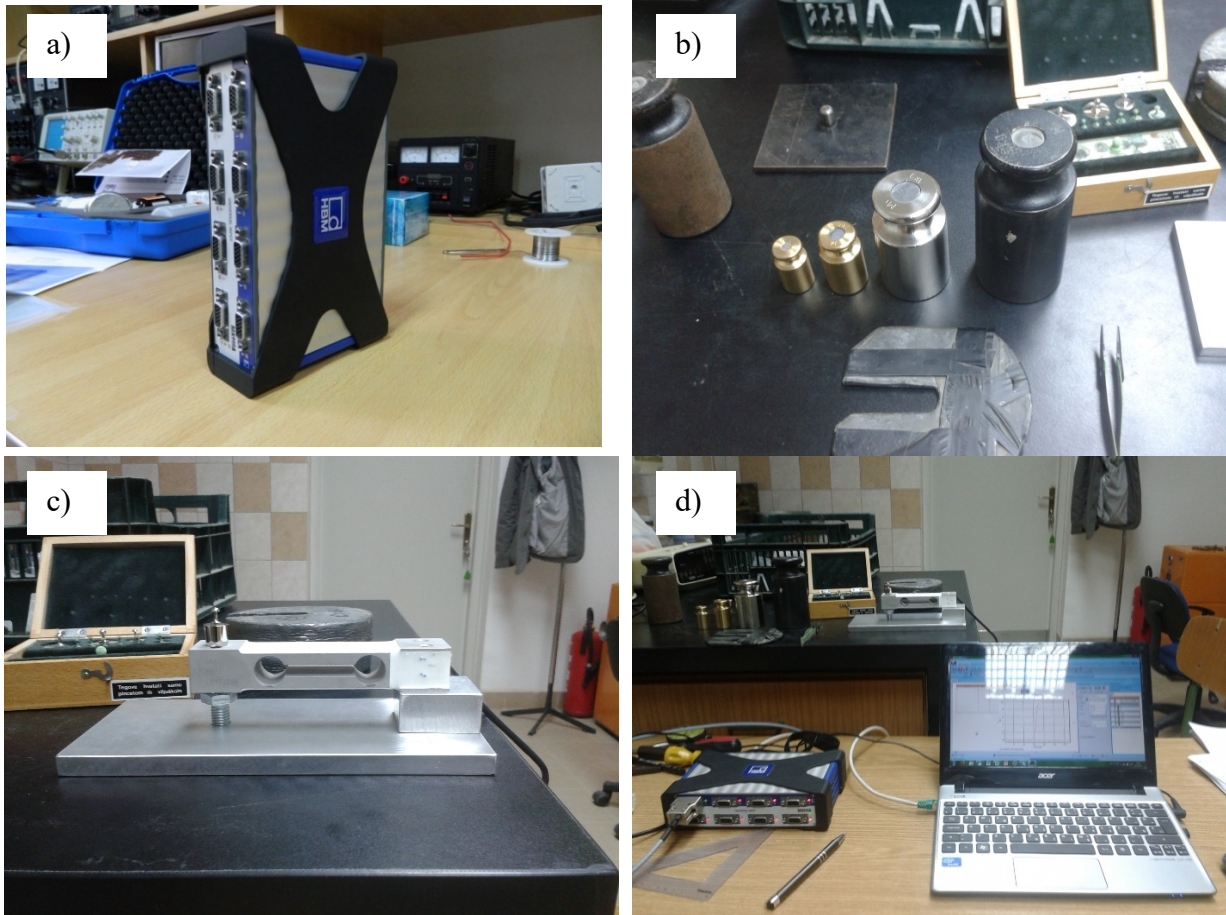


Fig 4.6 Calibration of sensors: a) an amplifier QuantumX MX840A; b) reference weights; c) a console installation for calibration; d) connection of the system sensor - amplifier on the PC

To test the performance in the whole working range, before the installation on the model, the sensors were exposed to loads to the measurement limit, that is, 5 kg. To do this, we used 2 lead weights of 2.5 kg, the load was carried out gradually to stabilize the weight of each of the weights, similarly, the sensor was unloaded. The cycle was repeated three times for each sensor. After calibration, the sensors were mounted on the front wall of the model, and on the inside of the model, glued elastic polyethylene membranes.

Calibration of the measuring system. Before the experiments began, the measuring system, the model with the installed sensors, was calibrated by measuring the hydrostatic pressure of water.

Calibration was done in the following order:

1. Indications of sensors were reset in the "Catman © Easy" software, then the measurement process was started;
2. In the cavity of the model water was poured with a hose to the mark of 1 m;
3. Waiting for stabilization of sensor indicators.

Calibration were repeated 3 times. The calculation of water pressure was carried out according to the standard formula $p = \rho_w g z = \gamma_w z$, and the measured average pressure was calculated as the ratio of the measured force to the cylinder surface.

Results of measurements are shown on Fig. 4.7, the line indicates the calculated theoretical pressure, and the crosses are measured values.

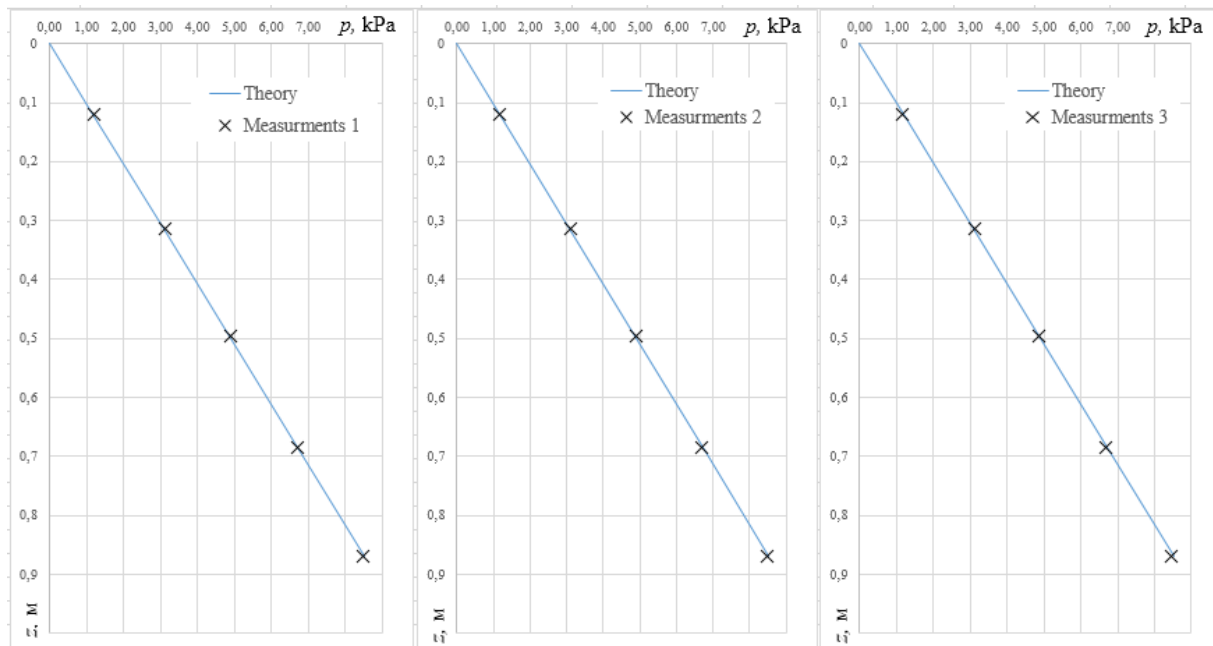


Fig. 4.7 Results of measurements of hydrostatic pressures

Details of the comparison of the measured values with the calculated ones are given in Table. 3.3. In this case, the relative error was calculated by the formula

$$\varepsilon = \frac{X_{pac.}}{X_{uzm.}} \cdot 100\% , \quad (4.2)$$

where is X_{calc} – calculated water pressure; $\bar{X}_{meas.}$ – the arithmetic mean of the measured values of the pressure.

Table 4.3 Comparison of measured and calculated values

Depth, z [m]	Estimated of magnitude	Measured values pressures, kPa			Medium	Relative error
		1	2	3		
0,000	0,000000					%
0,120	1,176840	1,19926	1,17342	1,15142	1,17470	0,18
0,315	3,089205	3,13860	3,12765	3,10780	3,11581	-0,85
0,495	4,854465	4,91165	4,88970	4,87000	4,88145	-0,55
0,685	6,717795	6,72492	6,68296	6,66505	6,69768	0,30
0,870	8,532090	8,46563	8,45949	8,44465	8,47546	0,67

The difference between the measured and calculated values of water pressure on average is 0.85%, and the spread of values around the arithmetic mean was $\pm 0.86\%$ on average.

Method of experimental research. In order to study the plane problem for experiments, the distance between the walls of 5 cm was chosen in the model. In this position, the ratio of the lengths of the sides of the model in the plan is 1: 5, and in the vertical longitudinal section 1:20. This condition of the walls necessarily leads to the effect of "H. Janssen ", that is, the deceleration of pressure growth with depth due to lateral friction of bulk material on the wall of the structure [85].

For filling in the cavity of the model, rice and composite medium were used, the physical and mechanical properties of which are defined in the second section.

Measurements were performed simultaneously on all five places of the device during the entire filling procedure. Experiments were conducted in laboratory conditions at an air temperature of 20°C and a relative humidity of 50%.

The amplifier connected to a personal computer, and the data was shot using the basic "Catman@Easy" software specifically designed for the HBM amplifier. As a raw data, the force was measured. In measuring the data, it was expected to stabilize the sensors, about a minute, and then the measurements were recorded (Fig. 4.8). As a result, the average normal stress was determined by the ratio of the measured force to the surface of the cylinder.

Material filling in the model was carried out in three different regimes, with different predominant angles of the orientation of the particles of the bulk fill to the horizontal (in the following text the filling angle, $\theta = 0^\circ, 45^\circ$ and 90°).

The model was filled with material up to a height of 1 m, and lateral horizontal pressure was measured without an additional load, only under the influence of the own weight of the fill.

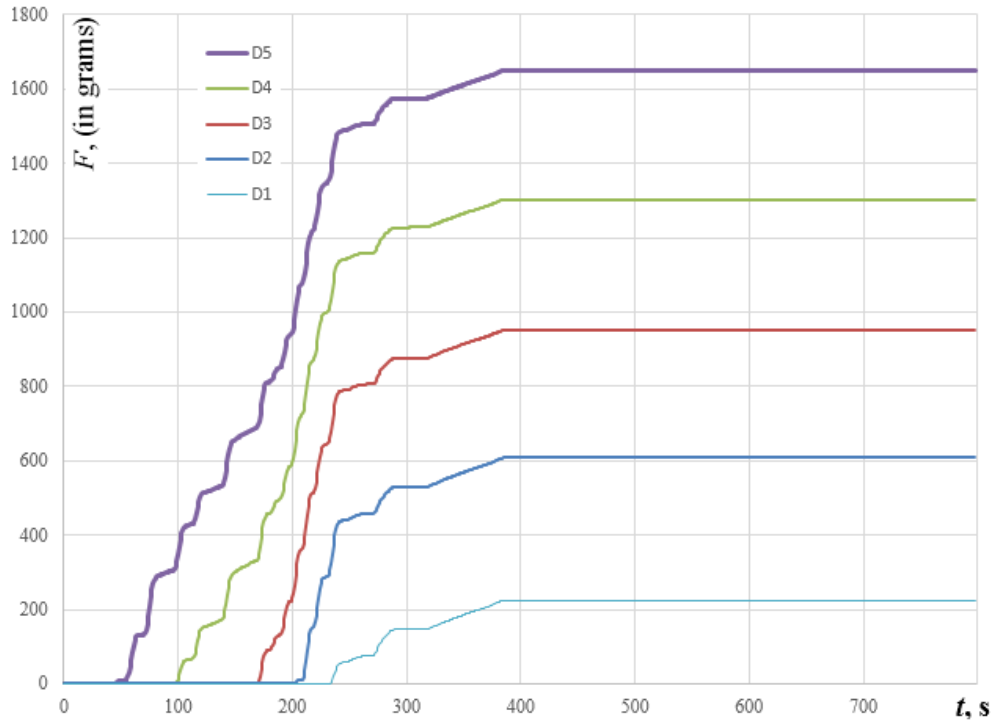


Fig. 4.8 Stabilization of sensor readings

The material was filled evenly, with layers approx. of 1 cm thick. The bulk medium was always filled from the top, and to achieve different fill angles θ the angle of the design model's position was changed.

Before the tests, a test was carried out in a tray with glass walls. As a result, a froth has been obtained with a clearly visible grain orientation in the filling (Fig. 4.9). In addition, after the experiment, a neat excavation of rice filling was performed at the angle of filling of 0° and 90° . At the same time, the angle of orientation of grains of rice is clearly distinguished (Fig. 4.10).

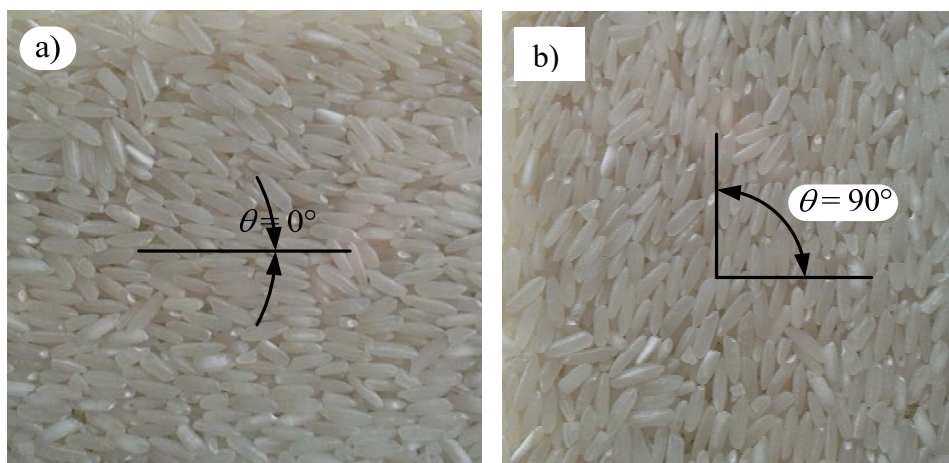


Fig. 4.9 The orientation of rice grains bedding angle

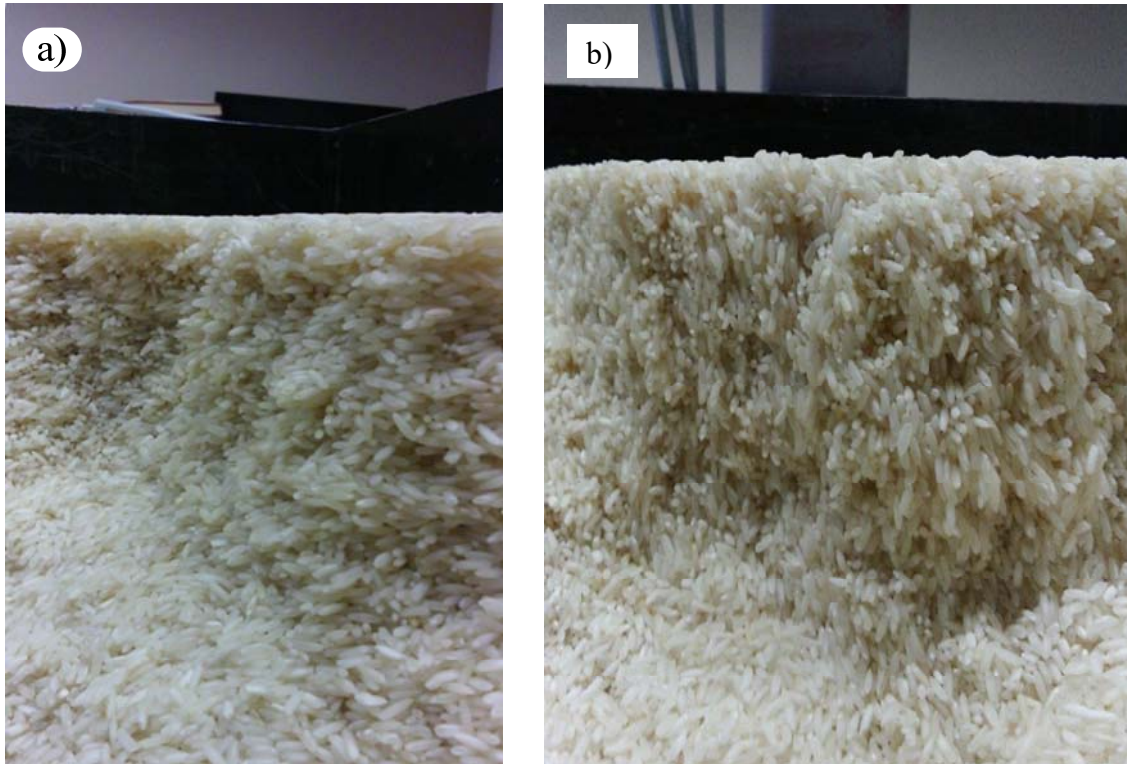


Fig. 4.10 Orientation of rice grain packing during excavation of a filling sample: a) 0°; b) 90°

The filling angle of 0° is achieved at the vertical position of the model designs (Fig. 4.11, a). Filling at angles of 45° and 90° is made using additional equipment - pallets, steel supports and two parallel wooden beams (Fig. 4.11, b and c).

For filling angle of 45°, the model is mounted on the floor with steel supports mounted beneath it to the horizontal in 45° (Fig. 4.9, b).

Then the model was filled up vertically from the top, and falling flat particles under the action of gravity basically lay in the position of stable equilibrium [34], that is, in a horizontal position. After the process of fill, the model was very slowly and gently returned to the vertical position.

Filling at an angle of 90° was carried out in the horizontal position of the model. The model was installed on two parallel wooden beams, with cross section of 15 cm x 15 cm (Figure 4.9, b), after which rear wall was dismantled, and in the upper part of the model, at a distance of one meter from the bottom, a special steel partition height in 5 cm was set to avoid the side rash of the material. After filling, the surface was thoroughly aligned with a long metal ruler, and the rear wall was set to its former position. Then the model slowly returned to the vertical position.

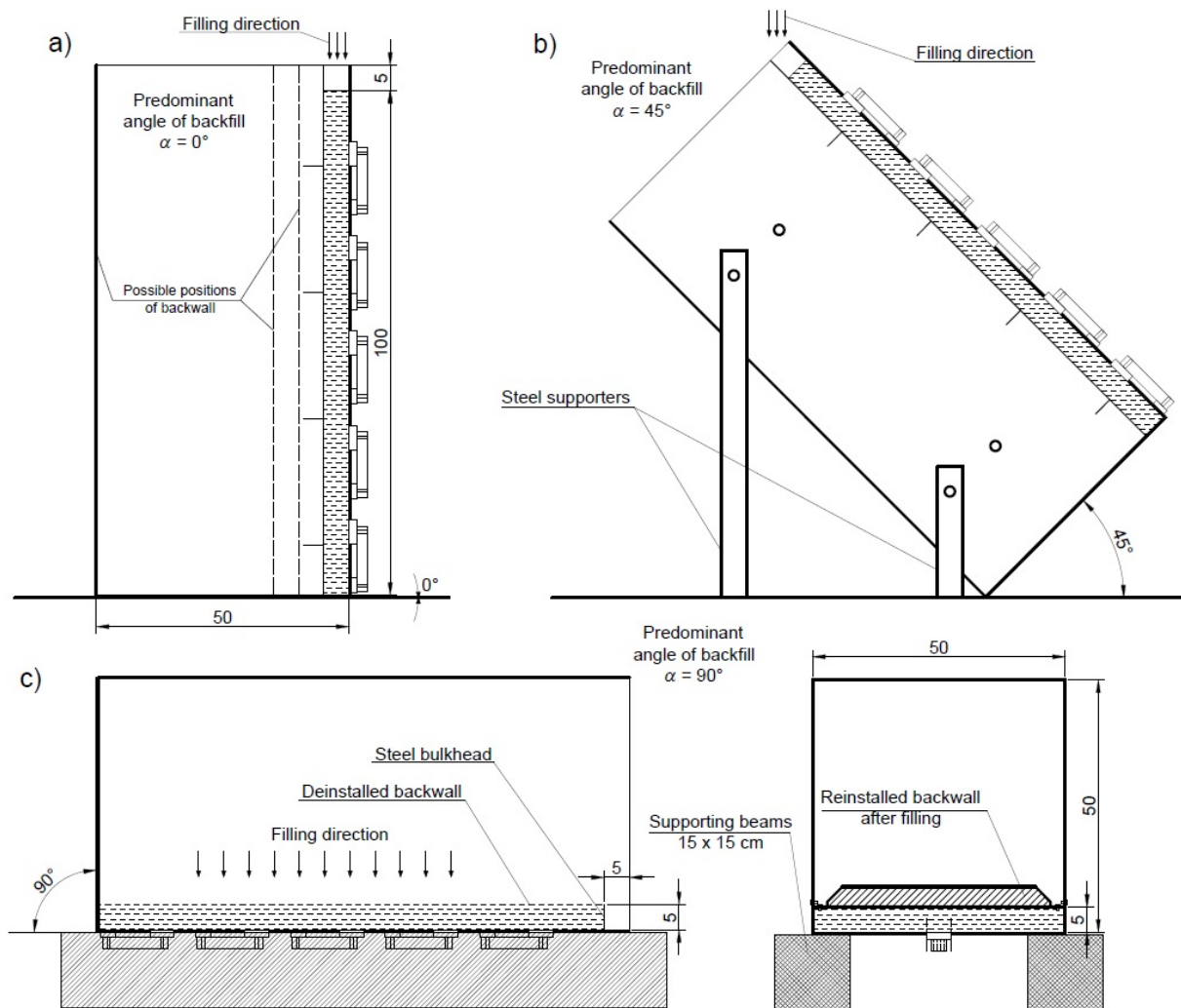


Fig. 4.11 The technology of filling the cavity of the model: a) 0°; b) 45°; c) 90°

For each test, the bulk density of a specimen was measured. All measured data for further processing and analysis were exported to the Excel table.

Each measurement procedure was carried out in the following sequence:

1. In the vertical position of the model functionality of each strain gauge in the software «Catman © Easy» was tested, the sensor readings was reset;
2. Measurement began in the vertical position of the model and monitored throughout the filling process;
3. Filling the cavity of the model was carried out uniformly, gradually and in layers, without abrupt movements;
4. After filling the model at an angle, it was very carefully turned to the upright position;
5. Measurements were recorded after stabilization of sensor reads, usually from 5 to 10 minutes;
6. The material was poured out, the weight of the material was measured to determine the bulk density, the sensors were cleaned.

4.2. Results of experiments

The purpose of the experiment was to determine the effect of the filling angle θ and the anisotropy of the strength of the bulk material on the nature and distribution of lateral horizontal pressures on rigid, closely spaced walls.

For this, measurements of pressure in five places, evenly distributed along the axis of the symmetry of the anterior wall were made.

The achievement of the reliability of the results for each variant of the given conditions and for each bulk medium was carried out by triple repetition of the experiment; in general, 18 experiments were carried out, not counting the calibration and erroneous measurements.

The plan of experiment is shown in the table. 4.4.

Table 4.4 Plan experiment

Material	Packing angle, θ		
	0°	45°	90°
	Number of experiments		
Long-grain rice	3	3	3
Composite medium	3	3	3

As expected, the values and characteristics of the curves of the lateral pressure differed significantly in different conditions of material filling angle.

In order to determine the nature and distribution of the side pressures of the bulk medium on the closely spaced walls under different filling conditions, for each experiment, the set of points of the lateral pressure σ (kN/m²) with depth z (m) was plotted in the coordinate system.

The measurement results are shown in Fig. 4.12 - 4.15 for rice, and for the composite medium - in fig. 4.16 - 4.19.

In addition, for each experiment, measurements of the specific weight of the samples were made, the results of measurements are given in Table. 4.5.

Analysis of experimental data obtained. A number of original experiments have been carried out in a specially developed model for determining the nature and distribution of lateral pressures at different angles θ .

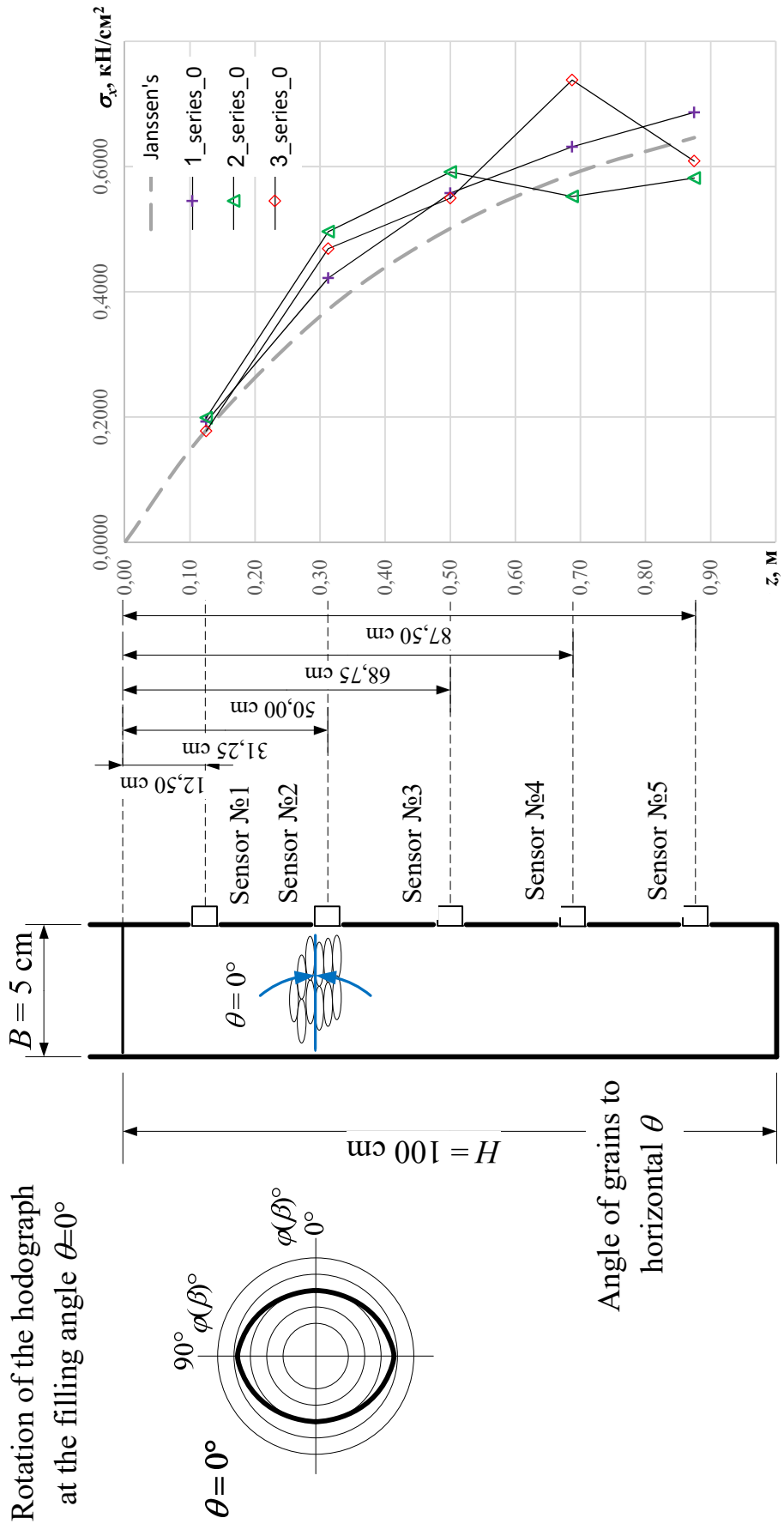


Fig. 4.12 Lateral pressures for rice at the filling angle $\theta = 0^\circ$

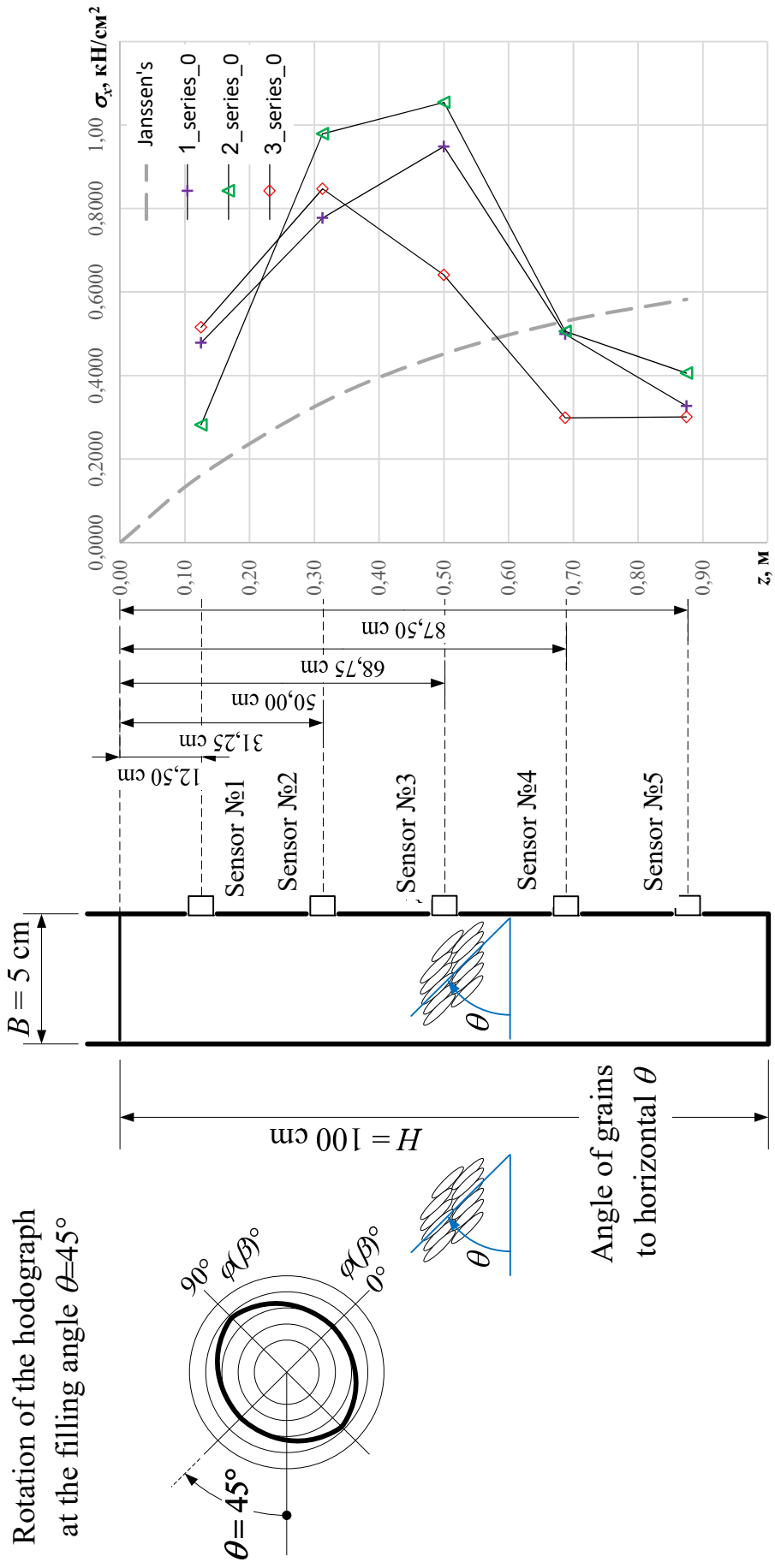


Fig. 4.13 Lateral pressures for rice at the filling angle $\theta = 45^\circ$

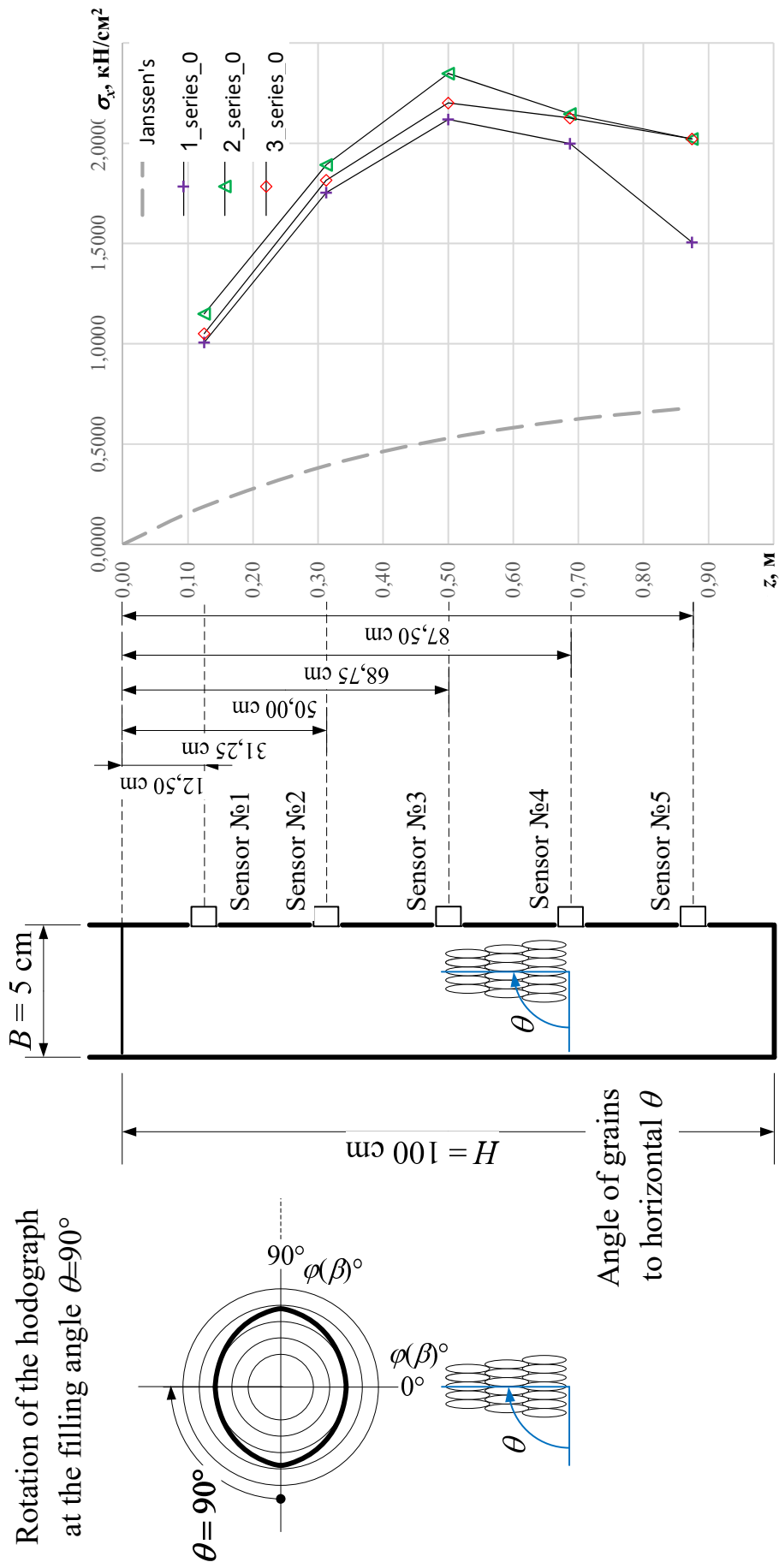


Fig. 4.14 Lateral pressures for rice at the filling angle $\theta = 90^\circ$

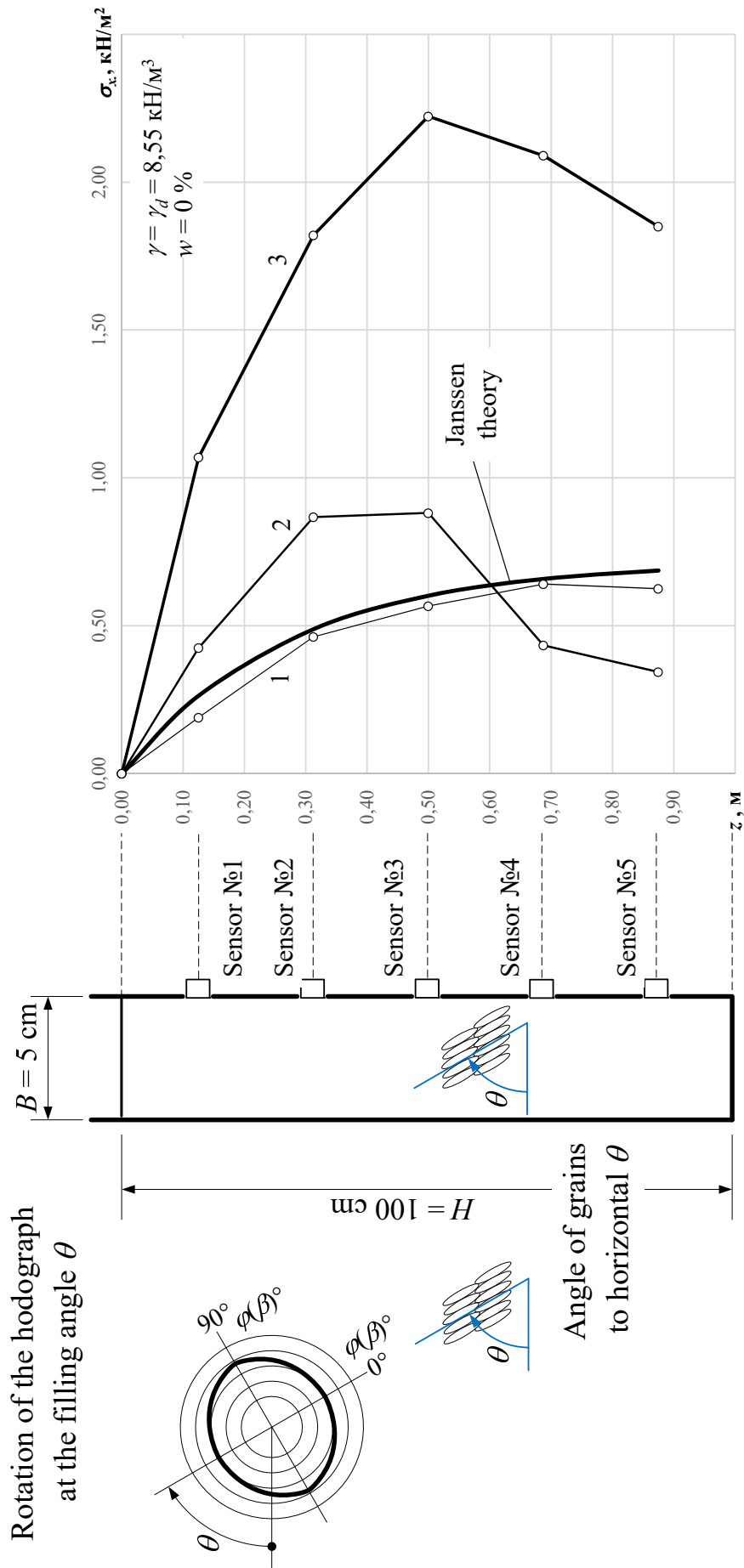


Fig. 4.15 Average lateral pressures for rice at the filling angle:

$\theta = 0^\circ$ (curve 1), 45° (curve 2) i 90° (curve 3)

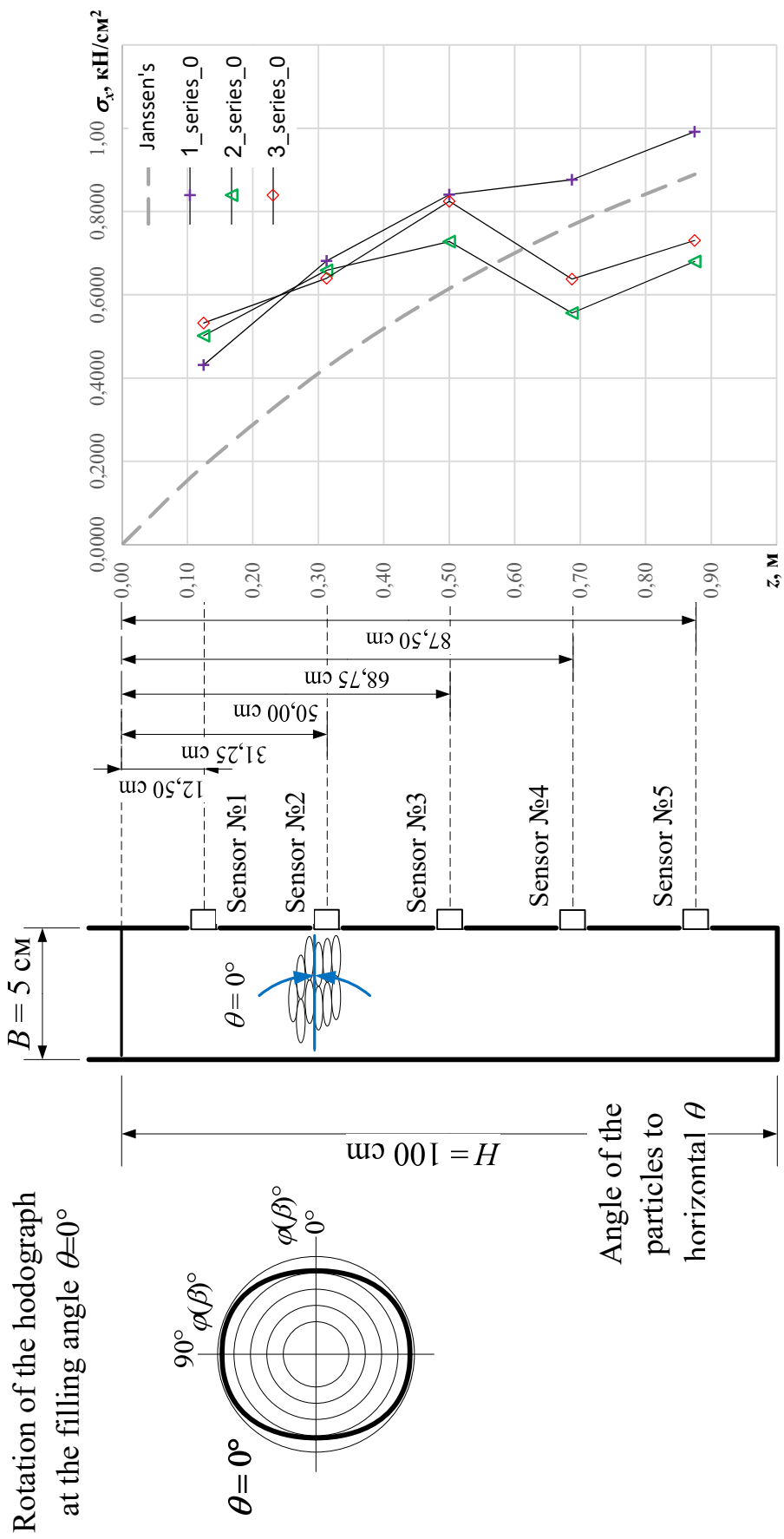


Fig. 4.16 Lateral pressures for composite medium at the filling angle $\theta = 0^\circ$

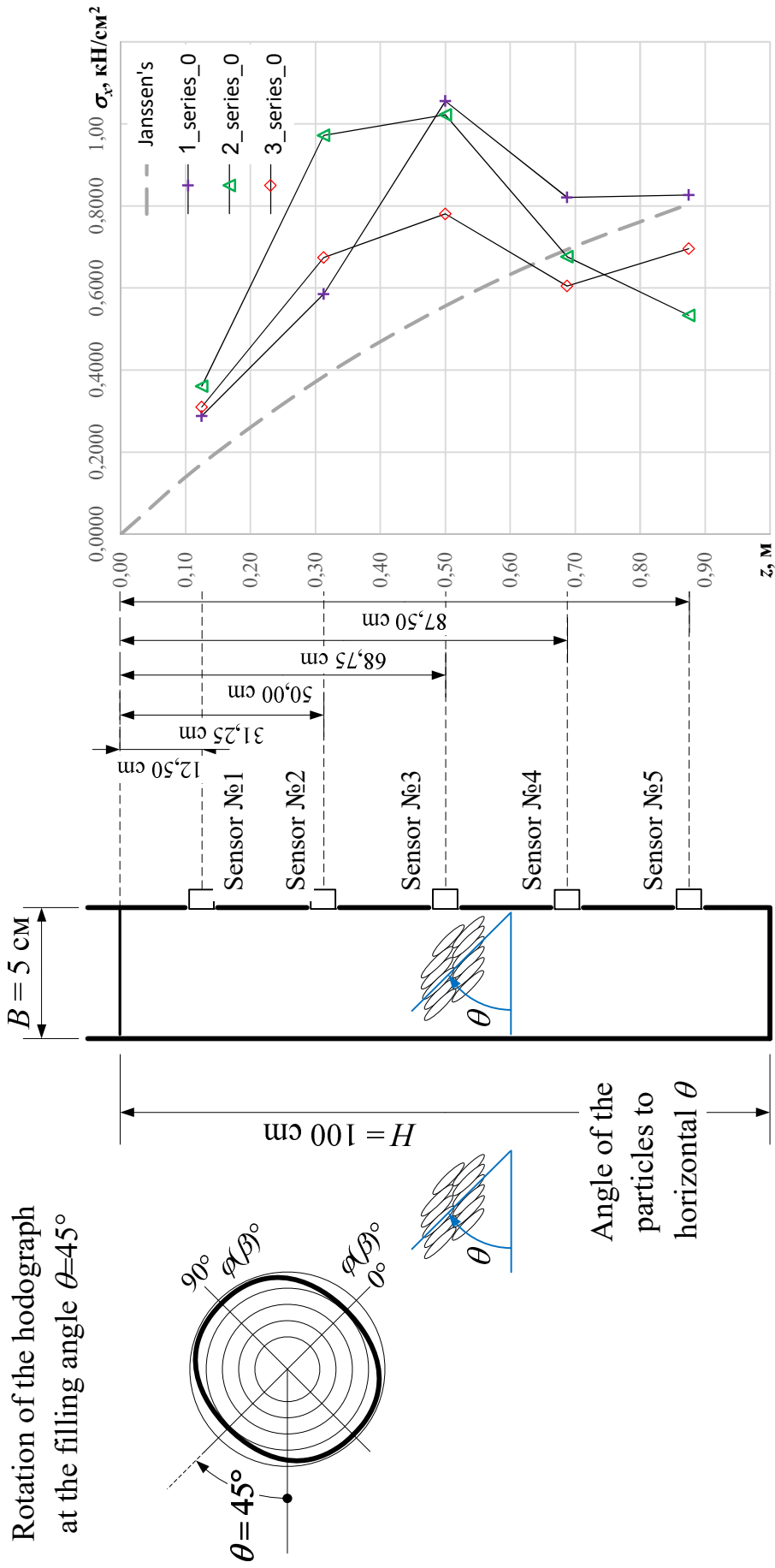


Fig. 4.17 Lateral pressures for composite medium at the filling angle $\theta = 45^\circ$

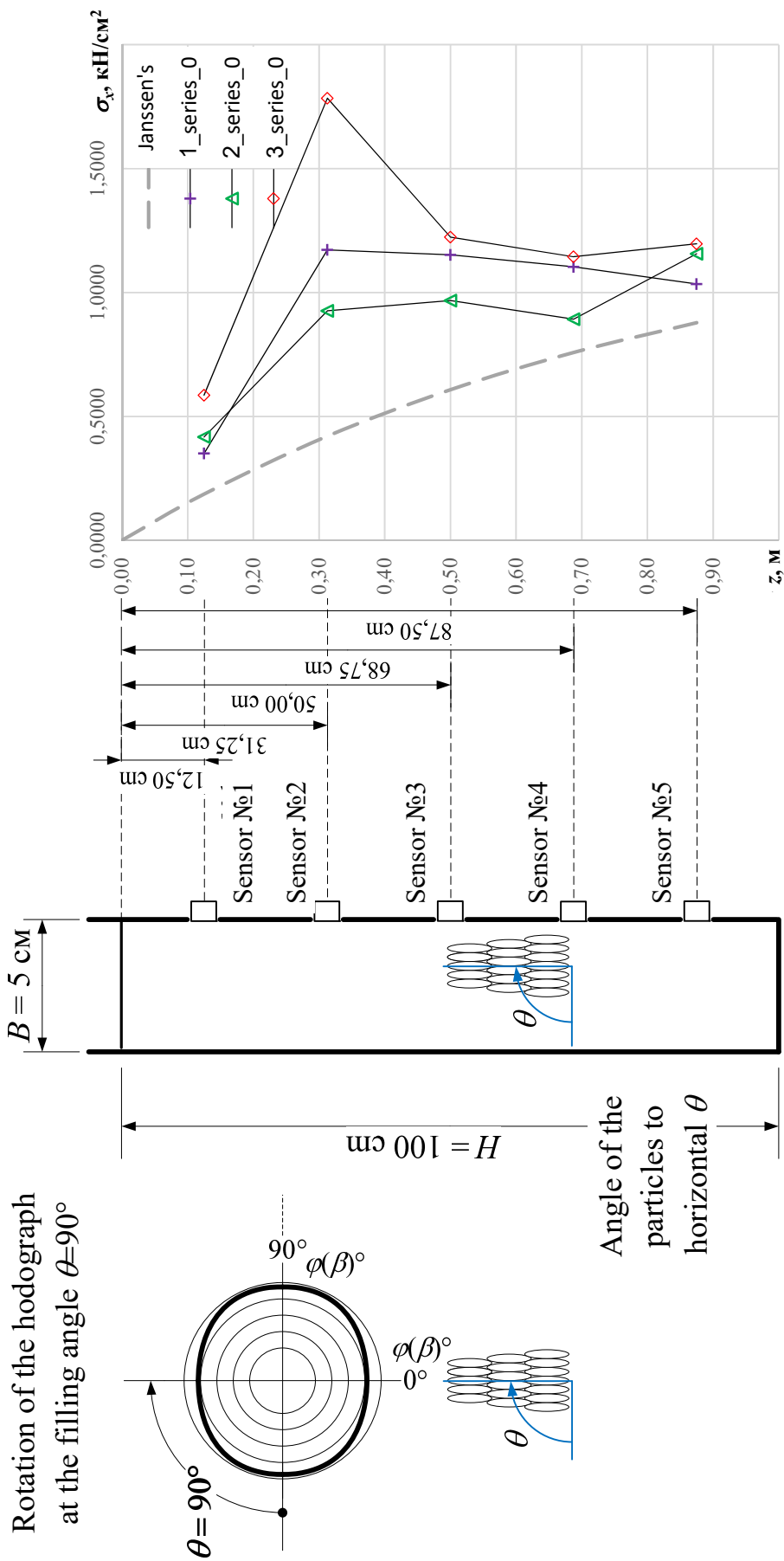


Fig. 4.18 Lateral pressures for composite medium at the filling angle $\theta = 90^\circ$

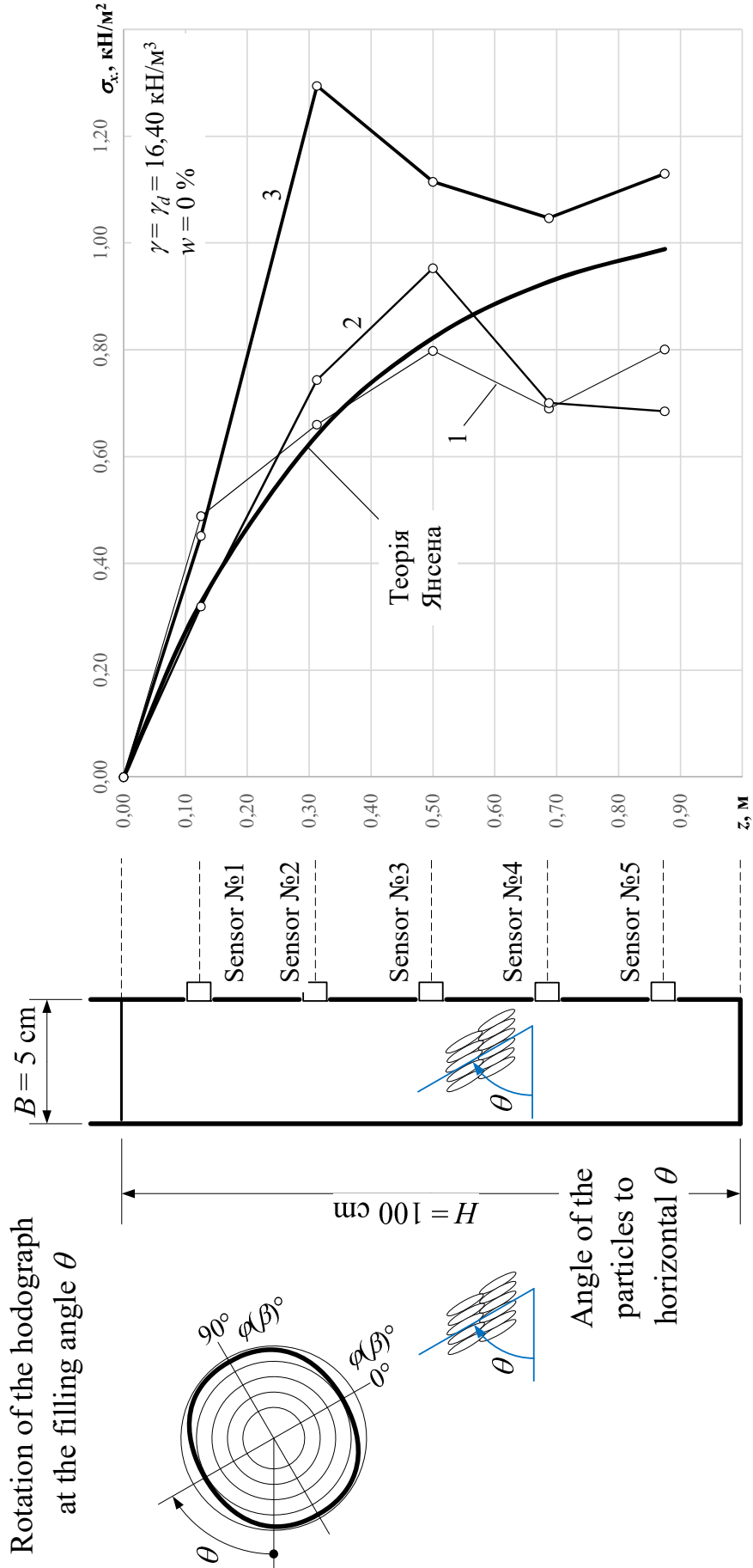


Fig. 4.19 Average lateral pressures for composit medium at the filling angle:

$\theta = 0^\circ$ (curve 1), 45° (curve 2) i 90° (curve 3)

Table 4.5 Specific weight of samples under different filling conditions

Material		Rice	Composite medium
№ exp.	Filling angle, θ	$\gamma = \gamma_d, [\text{kN/m}^3]$	$\gamma = \gamma_d, [\text{kN/m}^3]$
1	0°	8,74	16,47
2		8,58	16,19
3		8,71	16,52
Average		8,68	16,40
1	45°	7,88	14,49
2		7,74	14,97
3		7,84	15,02
Average		7,82	14,83
1	90°	9,07	16,34
2		9,32	16,29
3		9,09	15,95
Average		9,16	16,19

At different filling conditions, changes in the specific weight of samples of both bulk solids were observed. The data shown in the table. 4.5, indicate that the most compact sample of rice material was achieved at an angle of 90°, it was 5.57% higher than at 0°, while the most loose sample was observed at 45°, the difference on average, was 9.87%. For the composite medium, the difference in filling at 0° and 90° was small - only 1.24%, but at 45°, there was a similar tendency as for rice, the specific weight at 45 ° was on average less than 0° at 9.54%. The spread of measured values around the mean arithmetic for rice averaged $\pm 1.06\%$, and for the composite medium $\pm 1.34\%$.

Spread of the values of the lateral pressures measurements shown in Fig. 4.12 - 4.14 and Fig. 4.16 - 4.18, are shown in Table. 4.6.

Table 4.6 Spread of measured lateral pressures about arithmetic mean

Material Angle of filling, θ	Rice	Composite medium
0°	$\pm 8,05\%$	$\pm 12,66\%$
45°	$\pm 20,33\%$	$\pm 17,72\%$
90°	$\pm 6,61\%$	$\pm 18,00\%$

The obtained data testify to the accuracy of measurements of lateral pressures, taking into account the complex conditions of carrying out

experiments and the influence of dynamic factors when returning the model from the inclined position backward, to the vertical position, in cases with filling angles $\theta = 45^\circ$ and 90° .

The spread of the measured values at 20% at an angle $\theta = 45^\circ$ can be explained by the loose of the sample, whose specific weight was on average 10% less than at $\theta = 0^\circ$.

On fig. 4.15 and 4.19 are represented curves of mean values of lateral pressures of rice and composite medium at the angle of filling $\theta = 0^\circ$, 45° and 90° .

When filling angle $\theta = 0^\circ$ (Figures 4.15 and 4.19, curve 1), the measured data for rice differ from the theory of H. Janssen on average by only 6%, and for composite material 4.9%. The results obtained are comparable to those of well-known authors such as G.K. Klein [22], C. Brown [66], M. Reimbert [110], D. Schulze [112], etc., which further confirms the reliability of the results.

The lateral pressures for rice at an angle $\theta = 45^\circ$ (Figure 4.15, curve 2) are on average higher than at an angle $\theta = 0^\circ$ (curve 1) by 89.1% to about 0.6 m depth, and then decrease in the direction to the bottom, and on average less than 38.6%.

The nature of the changes in the lateral pressures for the composite medium qualitatively resembles similar curves for rice, at an angle $\theta = 45^\circ$ at a depth of 0.5 m, the pressure exceeds the pressure when $\theta = 0^\circ$ for 19%, with the increase in depth the difference decreases, and at a depth of 0.88 m pressure decreases by 15%. This fact can be explained by the influence of the hard bottom, which at 45° has the most expressed character.

For the rice pressure diagram at $\theta = 90^\circ$ (Figure 4.15, curve 3) distribution pattern is similar to the pressure diagram at $\theta = 0^\circ$ (Fig 4.15, curve 1), the maximum pressure is at half the depth. In the case of the composite material maximum is for $z = 0.3$ m. At the angle of filling of 0° and 90° for rice, the difference in lateral pressures was on average 294.4%, and for composite material -44.2%. Significant difference in lateral pressures at $\theta = 0^\circ$ and 90° can be explained by the influence of the preferential orientation of the rice grains, which contributes to the horizontal expansion (dislocation), which occurs due to indenting particles into the cavities (pore) between the grains under the action of gravity, as well as a partial inevitable effect dynamic factors when turning the model from the inclined position to the vertical.

Differences in lateral pressures, with rice filling, in cases of filling angle of 0° and 90° higher than in the case of a composite medium, which can be explained by a relatively greater homogeneity of bulking (the coefficient of heterogeneity for rice is only 1.13, and for the composite medium 2.10), as well as the influence of the form of rice grain, which, at $\theta = 90^\circ$ contributes more to the phenomenon of intergranular wedging.

With a change in the specific weight of the filling in range $\pm 10\%$, lateral pressure differs by about 300% for rice and 45% for the composite medium, indicating an increase in the lateral pressure $k = \sigma_3/\sigma_1$ with increasing angle θ .

In works of M. Molenda [96, 97] and Z. Tong [114] similar conclusions were drawn regarding the nature of the variation of the lateral pressure coefficient.

This experimental study has shown that the technology of filling in significantly affects the value of lateral (horizontal) pressure, which is significant in the construction of various anchored constructions, in which the filling procedures are used.

Accordingly, the technology and method of filling the material should be analyzed and adopted in the interests of reliability and economy, that is, in the direction of reducing load on the supporting structures or increasing the carrying capacity of artificial bases, using the optimum filling technology.

The nature of all plots of lateral pressure is curvilinear. The specific weight of the filling is different for different laying conditions, the most loose sample is recorded at $\theta = 45^\circ$ (the specific weight was less than in case of $\theta = 0^\circ$ for 9,87% for rice and 9,54% for the composite medium), and the most dense sample was observed at $\theta = 90^\circ$ (for rice, it was higher by 5.57%, and for the composite medium, the difference in specific weight was only 1.24%).

At the filling angle $\theta = 0^\circ$, the measured values of the pressure can be compared with the calculated pressure of the theory of H. Janssen, with an average difference of 6% for rice, and for a composite medium 4.9%. The lateral pressure of rice at $\theta = 45^\circ$ is on average 90% higher than at $\theta = 0^\circ$ to a depth of 0,6 m, and in other cases on average below 40%.

For a composite medium at $\theta = 45^\circ$ pressure to a depth of 0.6 m is an average of 1% higher, and in the remaining cases an average of 6% lower than at $\theta = 0^\circ$. At the angle of the filling $\theta = 90^\circ$, the lateral pressure of rice is by 294.4% higher on average than at $\theta = 0^\circ$, and for the composite medium by an average of 44.2%.

The difference in lateral pressures with rice filling in cases of a filling angle of 0° and 90° is approximately 6 times greater than in the case of a composite medium, which is explained by the more expressed effect of intergranular wedging of rice grains.

5. MATHEMATICAL MODELING OF MECHANICS OF ANISOTROPIC SOILS

5.1. Elastic-plastic model of compaction of isotropic and orthotropic soil

When constructing the model, we used known *hypotheses* of soil mechanics.

1. The soil (in each element) is taken for a homogeneous porous medium. At the stress state of as a result of irreversible deformations (compaction) the volume of solid particles remains constant, and the pores change (decreases).

2. The change in the values of the physical and mechanical properties of the soil, in other equal terms, is a function of the change in porosity and the rate of transfer of pressure.

3. Under deformations the integrity of the soil massif is kept.

4. Shaping deformations in the general case are nonlinear, that is, the connection between components of stress deviators and deformations is nonlinear.

5. Loads are simple (components of deviator stress increase proportionally to one parameter). Coexistence of stress tensors and deformations remains. As in other modern theories [3, 10, 13, 23, 33, 36, 38, 44, 45, 47, 55, 100, 103 - 105, 107, 108, 120], the connection between the components of bulk stress tensors and deformation tensors are nonlinear.

In general physical relations are written as follows:

$$\sigma_o = K\varepsilon_o'; \quad (5.1)$$

$$\tau_o = G\gamma_o', \quad (5.2)$$

where $\sigma_o, \tau_o, \varepsilon_o, \gamma_o$ - octahedral stresses and deformations; K and G - nonlinear functions of the volume module and the shear module.

$$\varepsilon_o' = 3\varepsilon_o; \quad (5.3)$$

$$\gamma_o' = 2\gamma_o; \quad (5.4)$$

$$\sigma_o = \frac{1}{3}(\sigma_x + \sigma_y + \sigma_z) = \frac{1}{3}(\sigma_1 + \sigma_2 + \sigma_3); \quad (5.5)$$

$$\varepsilon_o = \frac{1}{3}(\varepsilon_x + \varepsilon_y + \varepsilon_z) = \frac{1}{3}(\varepsilon_1 + \varepsilon_2 + \varepsilon_3); \quad (5.6)$$

$$\begin{aligned} \tau_o &= \frac{1}{3} \sqrt{(\sigma_x - \sigma_y)^2 + (\sigma_y - \sigma_z)^2 + (\sigma_z - \sigma_x)^2 + 6(\tau_{xy}^2 + \tau_{yz}^2 + \tau_{zx}^2)} = \\ &= \frac{1}{3} \sqrt{(\sigma_1 - \sigma_2)^2 + (\sigma_3 - \sigma_2)^2 + (\sigma_3 - \sigma_1)^2}; \end{aligned} \quad (5.7)$$

$$\gamma_o = \frac{2}{3} \sqrt{(\varepsilon_x - \varepsilon_y)^2 + (\varepsilon_y - \varepsilon_z)^2 + (\varepsilon_z - \varepsilon_x)^2 + \frac{3}{2}(\gamma_{xy}^2 + \gamma_{yz}^2 + \gamma_{zx}^2)} =$$

$$= \frac{1}{3} \sqrt{(\varepsilon_1 - \varepsilon_2)^2 + (\varepsilon_3 - \varepsilon_2)^2 + (\varepsilon_3 - \varepsilon_1)^2} . \quad (5.8)$$

The soil model is designed to evaluate stress – strain state (SSS) of the bases with the help of Fenete element method (FEM) and step-iterative procedures by a software complex focused on axial-symmetric problems of compaction of the soil massif (first stage), and its subsequent work under the action of static load (second stage). At the first stage, both geometric and physical nonlinearities of soil compaction are taken into account, and in the second one only the physical nonlinearity of its work is taken into account. In the calculations accepted that after the first stage the stresses in the soil relax, and the given physical and mechanical characteristics of the soil are preserved. The peculiarity of the model in the conditions of significant geometric and physical nonlinearity, in particular the process of compaction of the massif, is a description of changes in the physical and mechanical characteristics of the soil in explicit form (based on logarithmic dependencies) with its irreversible volumetric deformations, depending on the change in the porosity of the soil and the speed of pressure transference on it.

The peculiarity of the model in the second stage is that, in the case of complex SSS (compression with shear), the general deformations include linear (elastic) and plastic parts, and the plastic component of deformations occurs after the achievement of the SSS of the strength according to the Mises-Schleicher-Botkin condition. It is also possible to strengthen the soil in the same way as the first stage. Model parameters are established according to the data of close to standard soil tests under conditions of uniaxial compression and direct shear.

The analysis of the features of soil models that is possible to use in the first stage of the simulation of the grouSSS SSS, showed that for an adequate description of their behavior when compacted under different schemes of squeezing of the soil and the speed of pressure application, that is, in conditions of considerable physical and geometric nonlinearity (the result of which is the formation of a heterogeneous massif structure), the defining is the description of irreversible volumetric deformations of the porous body (hypothesis 1) with the definition of changes in its properties in this case (hypothesis 2). The value of soil porosity is always positive

$$n = e_0 / (1 + e_0) \geq 0, \quad (5.9)$$

Where e_0 - the initial value of the porosity coefficient of the soil.

The boundary condition of the soil skeleton, that is, at $n = 0$, may be determined by the dependence of "single-axis stress-deformation" in the form:

$$\bar{\sigma} / \sigma_y = \begin{cases} \bar{\varepsilon} / \varepsilon_y, & \bar{\varepsilon} < \varepsilon_y; \\ (\bar{\varepsilon} / \varepsilon_y)^N, & \bar{\varepsilon} \geq \varepsilon_y, \end{cases} \quad (5.10)$$

where σ_y - the limit of elasticity under stress; $\varepsilon_y = \sigma_y/E$ - the elastic limit of deformation; $\bar{\sigma}$ - effective stresses in the soil skeleton, and the plasticity condition of the porous material - in the record by A. Gurson [6]

$$F(\sigma_s, \sigma_o, n) = \left(\frac{\sigma_s}{\bar{\sigma}}\right)^2 + 2n \cdot q_1 \cdot \cosh\left(\frac{q_2 \sigma_o}{2\bar{\sigma}}\right) - 1 - q_3 \cdot n^2 = 0, \quad (5.11)$$

where $\sigma_s = \sqrt{3}\tau_i$ - the intensity of stresses; q_1, q_2, q_3 - constant material.

From the last expression it turns out that the condition of the plasticity of the medium depends significantly, and at $n=0$, it degenerates into the Mises condition.

Note, however, that due to the parity of the function of a hyperbolic cosine, the expression (5.11) is not sensitive to the sign of hydrostatic pressure and corresponds to the behavior of the material with the same resistance to compression and expansion, but the soils practically do not work for stretching. With the replacement of the hyperbolic cosine, the exponential function for positive values σ_o increases the soil yield point, and the negative - decreases, therefore this modification of the Gurson model already correctly reflects the physics of the soil (Fig. 5.1). Assuming that the rate of change of pore proportional to the volume of solid particles ($m=1-n$) and the rate of irreversible volume change ε_{pv} , and using the associated law of flow, we obtain the laws of deformation of the soil.

But this model requires three constants, and the change of the deformation module in the deformation of the soil is determined in an implicit form. Therefore, for the parameter of the model describing the irreversible volumetric deformations of the soil from forced displacement, a more universal and simple dependence of the deformation module on the volume of soil, in particular, on the element of the massif, the compression ring, the CE of the calculated region V_i , on the i -th stage movement (load):

$$\eta_i = E_i/E_o = f(V_i/V_o), \quad (5.12)$$

where E_o and V_o - the deformation module and the volume of soil at the initial load level.

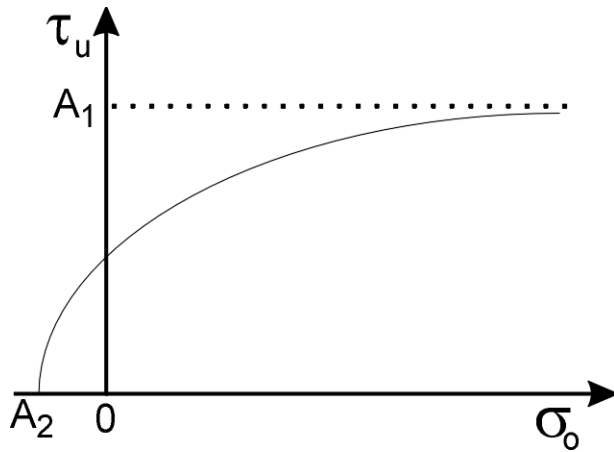


Fig. 5.1 – Condition for flowability (5.11)

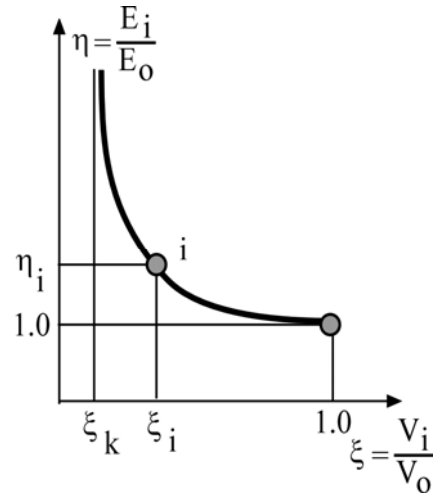


Fig. 5.2 – Schedule $E_i/E_o = f(V_i/V_o)$

Through hypothesis 1 and dependence E_i on the coefficient of porosity e_i under the same conditions: $E_i/E_o = f(e_i/e_o)$ – a similar expression (5.12) the form. The theoretical graph $E_i/E_o = f(V_i/V_o)$ is shown in Fig. 5.2. With a decrease

$$\xi_i = V_i / V_o, \quad (5.13)$$

the value E_i/E_o increases (indeed, the smaller the volume of the soil, the less its porosity, the greater the deformation module) and approaches the asymptotic

$$\xi_k = V_{\min} / V_o, \quad (5.14)$$

where V_{\min} – the minimum value of the volume of soil in a compressed state, for example, near the edge of the pile, expansion of the paved pit directly under the ramp, a boiler, a pneumatic fender, etc.

The value V_{\min} is a variable that depends on the physical properties of the natural soil, the class and the group of methods of its consolidation, in particular the transfer rate of the load on the soil. It can not be less than

$$V_{\min} \geq m \cdot V_o. \quad (5.15)$$

As numerous experimental studies show, the dependence of the deformation module E_i on the volume of soil at a significant range of pressure variation (greater than for the bases of traditional structures $\Delta\sigma = 0.1 - 0.3$ MPa) is described by variations of the logarithmic function. The whole range of graphics $E_i/E_o = f(V_i/V_o)$ on fig. 5.2 is described by a phenomenological expression

$$\eta_i = \frac{1}{b} \ln \left(\frac{\xi_i - \xi_k}{1 - \xi_k} \right) + 1, \quad (5.16)$$

where b - the empirical coefficient, which is equal to

$$b = \frac{1}{\eta_i} \ln \left(\frac{\xi_n - \xi_k}{1 - \xi_k} \right). \quad (5.17)$$

Determination of the parameters of the soil deformation pattern is carried out on the basis of standard compression tests at a pressure well exceeding the traditional, for example, up to $\sigma = 3$ MPa, and for a wide range of exposure time Δt of each degree (often $\Delta\sigma = 0.1$ MPa), load: from 1 to 2 sec to 1 hour. and conditional stabilization of 0.01 mm in 16 hours. for DSTU B V.2.1-4-96. That is, each group (subgroup, type) of the methods of sealing the bases, as well as their subsequent work under load, select their own regimens of laboratory tests.

The high statistical indicators also have another logarithmic function, which also describes the dependence of the deformation module E_i on the volume of soil V_i

$$E_i/E_o = 1 + a_o [V_i/V_o - \ln(V_i/V_o) - 1], \quad (5.18)$$

where a_o – the empirical coefficient.

Dependency $E_i/E_o = f(V_i/V_o)$ can be set in tabular form.

Consequently, in contrast to many models with fixed values of the deformation module, a real phenomenological model explicitly describes its changes in irreversible volumetric deformations, in particular, densification, depending on the change in the porosity of the soil and the rate of transfer of pressure on it. In this case, for each mode of transfer of pressure on the soil only one empirical coefficient must be determined.

To the features of the model at *the second stage of simulation* (work of an array under static load) due to relatively small deformations of the soil include the application of the apparatus of the theory of small elastic-plastic deformations [23, 36, 44, 55, 70, 100] belongs to the features of the model at the second stage of the simulation (work of the array under static load). Manifestations of nonlinearity include plastic deformation of mold changes with complex NS, unimpeded deformation during stretching. At a complex emergency (compression with a shift), general deformations include linear (elastic) and plastic parts. The plastic component of the deformation occurs after reaching the NP of the strength limit according to the condition Mises - Schleicher - Botkin:

$$\tau_o = \sigma_o \operatorname{tg} \varphi_o + c_o; \quad (5.19)$$

$$\operatorname{tg} \varphi_o = -\sqrt{3/2} \cdot \sin \varphi; \quad (5.20)$$

$$c_o = \sqrt{3/2} \cdot c \cdot \cos \varphi, \quad (5.21)$$

where φ – the angle of internal friction of the soil; - Specific grip of soil.

The Mises strength - Schleicher-Botkin defines the boundary relations of tangential and normal stresses on octahedral sites. The geometric interpretation of the accepted strength condition relative to the diagonal of the main stress space $\sigma_1, \sigma_2, \sigma_3$ is a cone (Fig. 5.3, a). It is built in a local cylindrical coordinate system. The points corresponding to the voltages a and lie in the middle of the boundary surface are in the prefrontal state, and the points on the surface correspond to the boundary neutron. The form of the projection of the boundary surface on the deviator plane (equal to all three main axes $\sigma_1, \sigma_2,$) by the Mises-Schleicher-Botkin criterion - circle (Fig. 5.3, b).

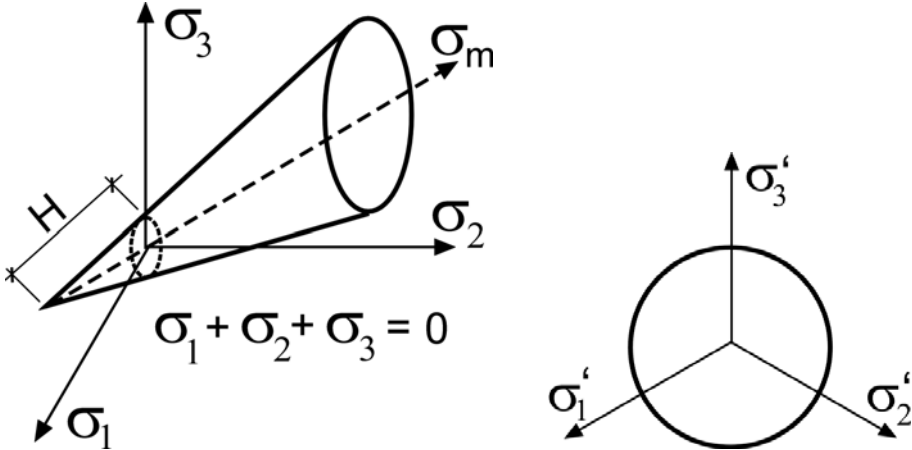


Fig. 5.3 - Geometric interpretation of soil condition: a – is the boundary surface $\sigma_1, \sigma_2, \sigma_3$ in space; b is the projection of the boundary surface on the deviator plane

For the one-axial NS it is possible to use the expression [29, 94]

$$\tau_o = \sigma_s \sqrt{2}/3. \tag{5.22}$$

To account for the influence on the nonlinearity of deformation of octahedral volumetric deformations, dilatations and other factors, the corresponding functions of nonlinearity were used in the formulation of S. F. Klovovich [23], in particular the phenomenological dependence of the apparatus on the theory of small elastic-plastic deformations between octahedral tangential stresses and shift:

$$\xi = \frac{\tau_o}{\bar{\tau}_o} = \frac{\lambda \eta}{1 + A\eta + B\eta^2 + C\eta^3}, \tag{5.23}$$

where $\bar{\tau}_o$ –the limiting value of the octahedral tangent voltage (correspoSSS to the exhaustion of the strength of the soil); η and λ - parameters of the deformation diagram of the soil forming

$$\eta = \gamma'_o / \bar{\gamma}'_o; \tag{5.24}$$

$$\lambda = G_o \bar{\gamma}'_o / \bar{\tau}_o, \tag{5.25}$$

where $\bar{\gamma}'_o$ – the limiting value of octahedral angular deformations (as and τ_o correspond to the exhaustion of the strength of the soil); G_o – initial value of the shear modulus; A, B, C – coefficients of the equation (5.23) [23].

Modifications to the deformation modulus in the second stage of the simulation are reflected in the same way as the first dependence $E_i/E_o = f(V_i/V_o)$, but for the regime of pressure transfer with conditional stabilization of deformations. Output parameters of the model are still the specific weight of the soil γ and the Poisson coefficient ν .

The parameters of the dependence of the deformation modulus on the change in porosity and the rate of transfer of pressure on it ($E_i/E_o = f(V_i/V_o)$) are determined from compression experiments, the mode of which is selected in accordance with the technology of laying the foundations and foundations (in particular, the speed of transfer of pressure to the soil), namely: at the time of exposure to pressure levels ($\Delta\sigma = 0,1$ MPa) from $\Delta t = 1 - 2$ sec to the conditional stabilization of deformations (0.01 mm for 16 hours) to the final pressure value of $\sigma \approx 3$ MPa. At the same time, "very fast" tests (Δt in seconds) correspond to a group of dynamic methods of consolidating bases (according to "Classification ..."), "fast" (Δt up to several minutes) - a subgroup of "fast" methods relating to a group of "static" densification methods, and "slow" ($\Delta t = 1$ hour to conditional stabilization of deformations) - subgroup "slow" from the same group of "static" methods. Interpretation of test results is used at the first stage of simulation.

Experiments with conditional stabilization of deformations also correspond to conditions of static tests of foundations and their exploitation. Their results are used in the second stage of the simulation. In order to avoid high friction of the soil behind the walls of the ring of a typical odometer, especially at high pressure, and to ensure the selection of samples of the undisturbed structure, which was impossible in the compressor device Kovtun-Bugaev, the design of the latter was improved: the "ring for testing soil in conditions of one-dimensional deformation" (Patents for: invention No. 58642 and industrial design No. 4016).

In the design of the ring (Fig. 5.4 and 5.5), the placement of the clips in the middle of the cylindrical sleeve with the cutting edge ensures the possibility of selecting the soil of the natural structure, which increases the accuracy of the determination of the deformation properties of soils [6, 7]. The device comprises a ring 1 consisting of metal rings 2, between which there are elastic pads 3. Outside the ring 1 is placed on a cylindrical sleeve 4 having a cutting edge on one lateral, and on the opposite lateral there is a thrust ring 5 pushed by a one-way sleeve 6. The device comprises a ring 1 consisting of metal rings 2, between which there are elastic pads 3. Outside the ring 1 is placed on a cylindrical sleeve 4 having a cutting edge on one lateral, and on the opposite lateral there is a thrust ring 5 pushed by a one-way sleeve 6. Fastening a one-sided coupling on

a cylindrical sleeve 4 is carried out on a carving. The taring of the ring is carried out prior to penetration into the soil by applying vertical force to its upper face in the pressure range characteristic of the compression tests.

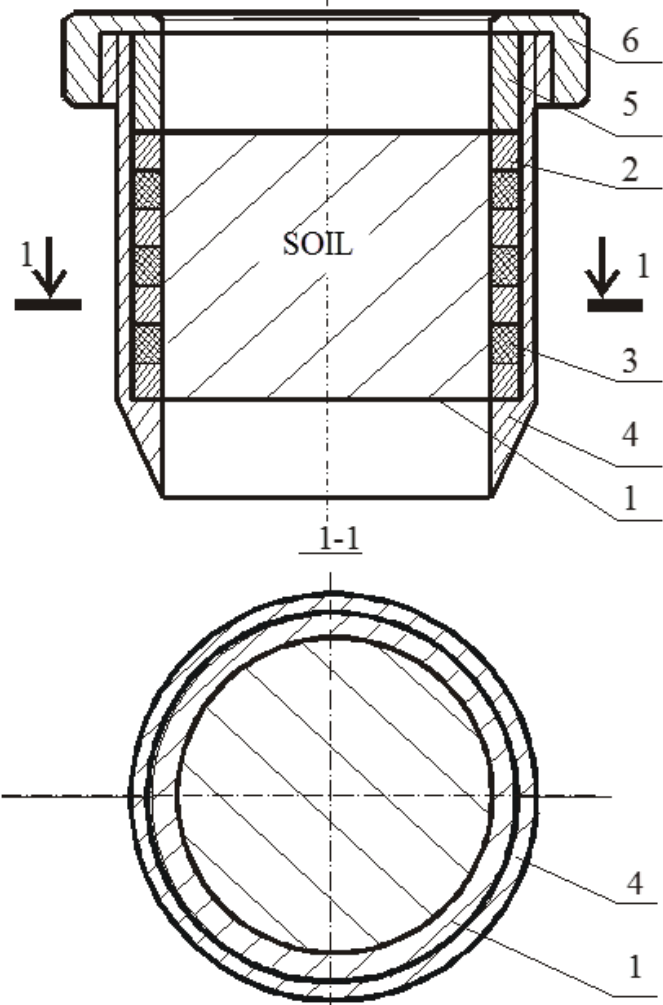


Fig. 5.4 – Design of a ring for soil testing in conditions of one-dimensional deformation:
 1 – ring; 2 – thin metal rings; 3 – rubber linings; 4 – cylindrical sleeve with a cutting edge on one side; 5 – thrust ring; 6 – one-sided coupling



Fig. 5.5 - Ring for testing of one-time deformation batches

The device is arranged by the cutting edge of the cylindrical sleeve on the surface of the soil. The pressure to the one-sided coupling device is pushed to the ground to a state when the surface of the soil inside exceeds the top of the ring. To facilitate the depression of the device, the cutting of the outside of the cutting edge is performed. To remove the device from the soil after the intake, the soil is cut below the cutting edge. In order to prepare a sample for testing under conditions of one-dimensional deformation, a one-sided coupling and a stop ring are removed, after which the ring 1 with the soil sample of the undamaged structure is removed from the cylindrical sleeve, the leaves of the soil outside the ring 1 are cut off, and further tests are carried out by the load of the die, which is based simultaneously on a sample of the soil and the upper edge of the ring.

The ring is made of (Figure 5.5) steel rings with an external diameter of 82 mm, an internal diameter of 70 mm, a thickness of 0.5 mm from a steel of 65 g. Elastic gaskets are made in the form of rubber rings and have the same dimensions as steel rings. Between the rings and rubber gaskets are bonded with synthetic glue. Overall height of the ring is 36.5 mm. Such dimensions provide the conditions for conducting soil tests in accordance with current standards. All of these elements are made of steel 45. The thickness of the walls of the cylindrical sleeve is 2 mm, and the total height of the assembly is 70 mm, the angle of inclination of the cutting edge is $15 - 25^\circ$. The design of the ring provided the possibility of selecting the soil of the undisturbed structure, which increases the accuracy of determining the deformation properties of the soil by 10 - 50% depending on the type and condition of the soil. It is possible to bring pressure up to $\sigma = 2.5-3$ MPa.

Tests were also carried out in a compressor device KPr-1 using rings of 40 cm² in volume and 140 cm³. The maximum load on the traction cable was 1080

kg instead of 600 kg per passport, and therefore its cross section was increased from 10.02 mm² to 17.85 mm². We will consider the method of determination of dependence parameters $E_i / E_o = f(V_i / V_o)$ on the example of tests in a unit of uniaxial compression of samples of loam of forest, heavy dusty, semi-solid with the following characteristics: $\gamma = 18.3 \text{ kN} / \text{m}^3$; $w = 0.24$; $W_L = 0.39$; $W_p = 0.23$; $e = 0.86$; $S_r = 0.77$, - taken from a depth of 1.7 m.

The program included compression soil tests at the time of exposure to each load level Δt : 15 sec; 1 min.; 5 min.; 1 year and to conditionally stabilize the deformation 0.01 mm for 16 hours. Load levels were: 0.05; 0.075; 0.1; 0.2; 0.3 ... 2.7 MPa. Each series of experiments included tests of six samples, and only tested thirty samples in five series [6].

The data of compression studies were presented in the coordinates "pressure σ – relative deformation of the sample" ($\varepsilon = \Delta h / h$, where Δh – absolute deformation of the sample; h – sample height to the test) in the form of five graphs for different times of exposure to each load level. An example of a series of tests is shown in Fig. 5.6 [6].

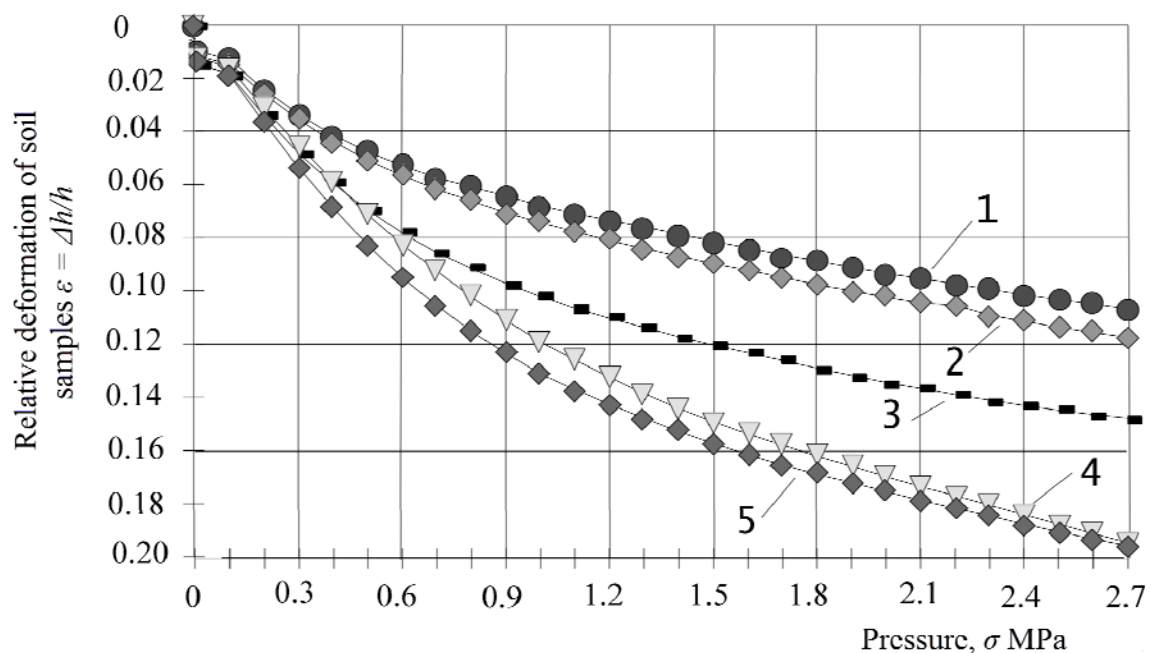


Fig. 5.6 - Graphs of the relative deformation of soil samples from the pressure σ for different times of exposure to each load level Δt : 1 - 15 sec; 2 - 1 minute; 3 - 5 minutes; 4 - 1 hour; 5 - to conditional stabilization of the deformation

With the increase in the shutter speed of each load, the shape of the graphs $\varepsilon = f(\sigma)$, becomes more steep. The lowest position of the curve $\varepsilon = f(\sigma)$ corresponds to the exposure time of each degree to the conditional stabilization of the deformation. This is explained by the fact that with an increase in the time of exposure to each degree of loading, the proportion of the irreversible

component of the deformation of the soil increases due to the creep of its skeleton. Dependence $\varepsilon=f(\sigma)$, given on fig. 5.6, is approximated by a logarithmic or step function with correlation coefficients $r=0.85 - 0.96$.

According to the graphs $\varepsilon=f(\sigma)$, the deformation modules of the soil were determined in the pressure interval $\sigma_i \dots \sigma_{i+1}$ and the dependency graphs were constructed $E=f(\sigma)$ for different times of exposure to each load level. The experimental data in the range of stresses 0-2.7 MPa of each graph $E=f(\sigma)$ can be approximated by linear dependence from $r=0.82$ to 0.97 . Therefore, in general, the graphs of dependence $E=f(\sigma)$ for different times of exposure to each load degree have the form close to a beam of straight lines, the angle of inclination of which to the axis the greater σ , the less time to withstand the load Δt .

Figures of dependencies of deformation module on pressure $E=f(\sigma)$ and time of endurance of each load level $E=f(\Delta t)$ are used to determine the parameters of the phenomenological dependence of the module of deformation of the soil on the change in porosity and the rate of transfer of pressure on it. First they were presented in coordinates "the ratio of volumes of soil sample at i -th degree of load V_i to the original sample volume V_0 – the ratio of values of soil deformation modules at the i -th degree of load E_i and at initial load E_0 ", an example of which is given in Fig. 5.7.

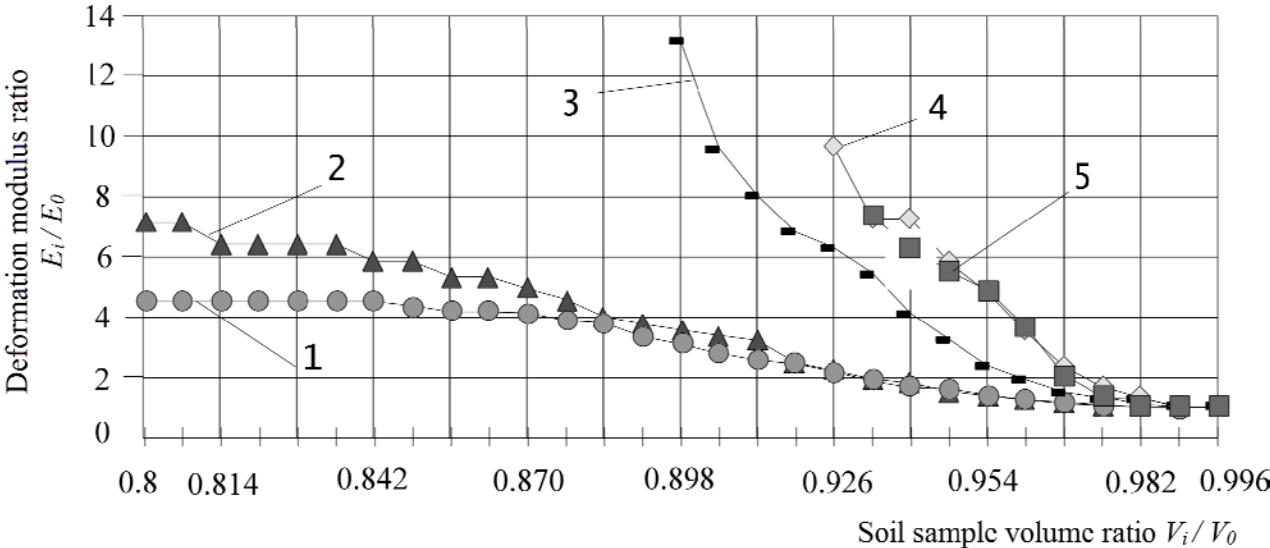


Fig. 5.7 - Graphs of the relationship between the values of the deformation modules of the soil at the i -th degree of loading E_i and at the initial load of the ratio E_0 of the corresponding volumes of the soil sample V_i/V_0 for different times of exposure to each load degree Δt : 1 - to conditional stabilization of the deformation; 2 - 1 year; 3 - 5 minutes; 4 - 1 min; 5 - 15 sec

Similar graphs were constructed in coordinates "the ratio of the values of the soil porosity coefficient for the i -th degree of loading e_i and the initial coefficient of porosity of the same sample - the ratio of deformation modules at the i -th degree of loading E_i and at the initial load level E_0 ".

From their analysis it was established that:

- with a decrease in the porosity coefficient (sample volume) an increase of the deformation module of the soil occurs under some curvilinear laws;

- reduction of sample volume occurs mainly due to reduction of its porosity; so there is no fundamental difference, which dependence:

($E_i / E_0 = f(V_i / V_0)$ or $E_i / E_0 = f(e_i / e_0)$) to use;

- at the "rapid" application of pressure ($\Delta t = 15$ sec, 1 min, 5 min), the value of the ratio of the deformation modules of the soil increases much faster than with the "slow" ($\Delta t = 1$ hour before the conditional stabilization of the deformation), which affects the difference in the process deformation of the soil when the foundation is laid and its work under load. So, in dynamic methods of sealing ("rapid" deformation of the base) the soil has a greater degree of consolidation than with static methods or the static loading of the foundation ("slow" deformation of the foundation);

- in general, dependencies $E_i / E_0 = f(V_i / V_0)$ or $E_i / E_0 = f(e_i / e_0)$ are described by the logarithmic function of the form (5.16) or (5.18).

In particular, for the above-discussed example of the experimental data, the empirical coefficients in equation (5.16) have the meanings:

- at "fast" load ($\Delta t = 15$ sec, 1 min.): $b = -0,06$; $\xi_k = 0,62$ - with correlation coefficients $r = 0,95$ and variation of $v = 0,09$;

- at "slow" load ($\Delta t = 1$ hour and to conditional stabilization of the deformation): $b = -0.43$; $\xi_k = 0.78$, at $r = 0.95$ and $v = 0.08$.

In case of use of dependence (5.18) for the same data we have:

- at "fast" load: $a_0 = 1144.0$, - at $v = 0.09$;

- at "slow" load: $a_0 = 220.7$, - at $v = 0.12$.

To establish the strength conditions, the boundary ratios of the tangential and normal stresses $\tau = f(\sigma)$ were determined by soil tests on a direct shift with a fixed displacement plane according to the DSTU B.V.2.1-4-96 in the range of normal stresses, similar to the one-axial compression experiments (usually $\sigma = 0.05 \dots 2.00$ MPa). This kind of destruction was considered as a special case of the spatial NS of the soil.

The graphic representation of the approximation of experimental data of $\tau = f(\sigma)$ linear dependence (corresponding to the Kulona-Mora strength condition Kulona-Mora) and parabolic functions in different pressure ranges for the same soil is shown in Fig. 5.8.

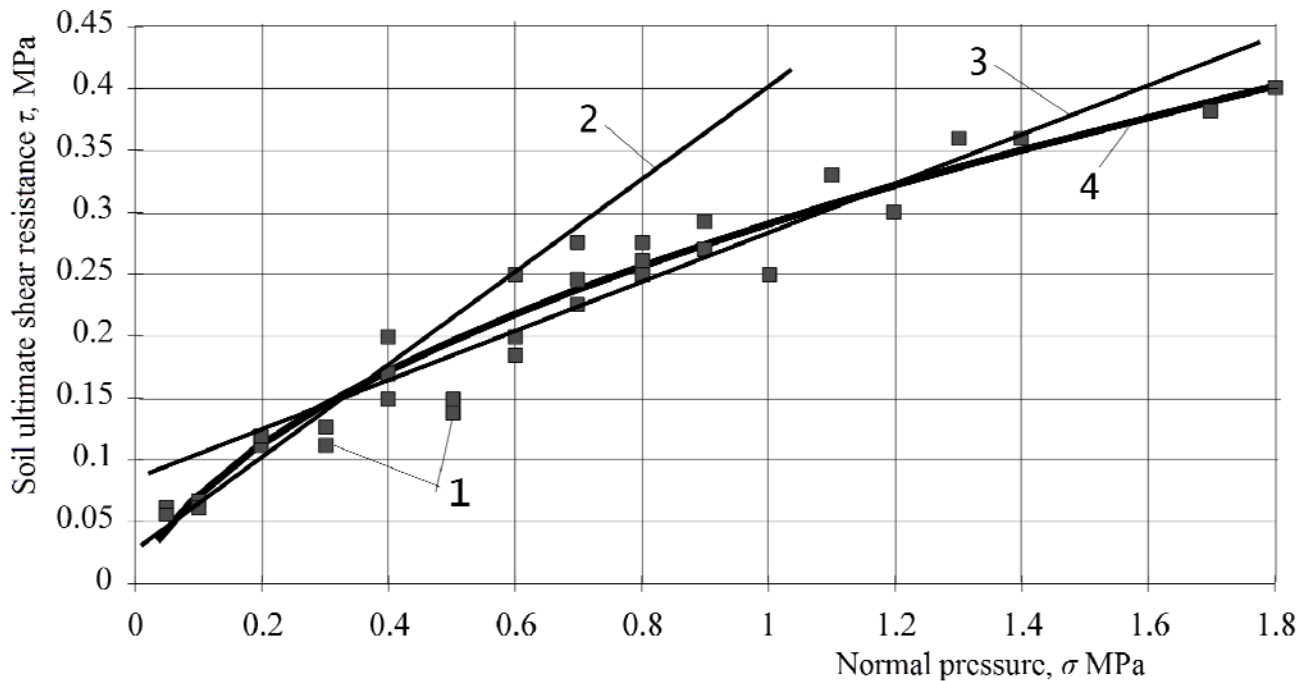


Fig. 5.8 - Charts of the dependence of the boundary resistance τ of the soil on the displacement from normal stresses: σ : 1 - experimental data; 2 - linear approximation of these data in the range of pressure $\sigma = 0.05 - 0.4$ MPa; 3 - the same for $\sigma = 0.05 - 1.4$ MPa; 4 is a parabolic approximation of data for $\sigma = 0.05 - 1.4$ MPa

Linear approximation in the range of pressure $\sigma = 0.05 \dots 0.4$ MPa (item 2 in Figure 5.8) gives good results for this segment. For larger values, the calculated values τ under such approximation have significantly higher values than the experimental ones.

The linear approximation of data in the range of $\sigma = 0.05 \dots 1.8$ MPa (item 3 in Figure 5.16) also takes additional errors in the calculations, because at $\sigma = 0.05 \dots 0.3$ MPa and $\sigma = 1.2 \dots 1.8$ MPa gives an inflated value compared to the experimental value τ , and at $\sigma = 0.3 \dots 1.2$ MPa - understated. The best statistical indicators ($r=0.98$ and $v=0.12$) have an approximation of the dependence $\tau = f(\sigma)$ of the parabolic function (item 4 in Figure 5.8) in the form

$$\tau_o = a_1 + a_2 \sqrt{\sigma_o / \sigma_o^\circ}, \quad (5.26)$$

where a_1 and a_2 – empirical coefficients; $\sigma_o^\circ = 1$ MPa.

Other functions less well describe the dependence $\tau = f(\sigma)$ throughout the range of pressure σ : for $\tau_o = a_1 + a_2 \cdot \lg(\sigma)$ – $r=0.93$ and $v=0.20$; for $\tau_o = a_1 \cdot \sigma^{a_2}$ – $r=.92$ and $v=0.21$; for $\tau_o = a_1 + a_2 \cdot \sigma$ – $r=0.95$ and $v=0.16$.

Due to the specificity of the anisotropy of the primary (natural) mechanical (deformation, strength) clay deposits of water origin, forests, and clay deposits caused by their natural structure (an ordered structure with a priority parallel orientation of particles or pores in some direction), origin, conditions of formation (in particular, the process of sediment accumulation), etc., and

secondary (induced) anisotropy, the nature and patterns of which depend both on the natural structure of the soil and on the features of the foundation technology, namely: from the direction of squeezing of soil particles by the working body, piles, blocks, etc .; the sizes of the interfoundation space [7, 116], - it may make sense to use in their model known physical relations anisotropic, especially orthotropic, medium.

Parameters describing these bodies (in the cylindrical system of coordinates - its scheme in Figure 5.9) are: modules of deformation in the plane of isotropy E_r and E_θ , as well as the direction perpendicular to it E_z ; corresponding coefficients Puasson coefficients $\nu_{r\theta}$, ν_{rz} , $\nu_{\theta z}$. In the case of a transversally-isotropic body, a model is adopted $E_\theta = E_r$.

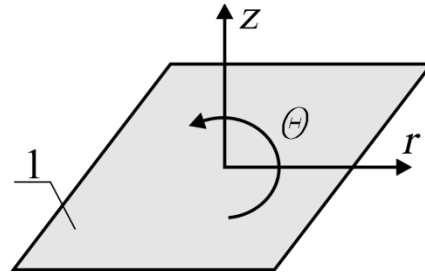


Fig. 5.9 - Cylindrical coordinate system:
1 - isotropic plane

The mechanical properties of anisotropic soils were studied by selecting the samples with cutting rings oriented at different angles ($\alpha = 0^\circ$; 45° ; 90° and others) to the horizontal plane (taken for the plane of isotropy), followed by testing in odometers, cutting devices, penetrometers.

The coefficients of anisotropy of mechanical parameters were:

$$n_{E,\alpha} = E_\alpha / E_- ; \quad (5.27)$$

$$n_{c,\alpha} = c_\alpha / c_- ; \quad (5.28)$$

$$n_{\varphi,\alpha} = \text{tg}\varphi_\alpha / \text{tg}\varphi_- ; \quad (5.29)$$

$$n_{R,\alpha} = R_\alpha / R_- , \quad (5.30)$$

where E_- – the module of deformation of the soil in the plane of isotropy from the stresses in the same plane (orientation of the rings at an angle $\alpha = 0^\circ$ to the horizontal plane); E_α – the same, for the plane, inclined to the plane of isotropy at an angle α ; c_- ; c_α ; φ_- ; φ_α – Specific grip and angle of internal friction of the soil in the plane of displacement correspondingly parallel ($\alpha = 0^\circ$) and inclined to the plane of isotropy at an angle; and α ; R_- i R_α – the specific resistance of the penetration at angles $\alpha = 0^\circ$ and $\alpha \neq 0^\circ$ to the isotropy plane.

Thus, for cases, *when the values of the soil anisotropy coefficients differ significantly, the accuracy of $n_\alpha = 1.0$, calculations of the bases of SSS can be increased by the use of an orthotropic or transversally isotropic medium in their physical ratios.*

5.2. Basic installation of software for simulation of soil consolidation tasks

Based on classification of soil consolidation methods and phenomenological elastic-plastic model of soil, a software complex "PRIZ-Pile" was created, in which the solution of an axisymmetric elastic-plastic task of the MCE (method of displacements) was implemented by the step-iterative methods in a physically and geometrically nonlinear formulation. The designer is able to model: 1) various geometry, the pattern of squeezing of the soil, the nature and speed of pressure on it to process the laying of bases and foundations with consolidation of the soil, resulting in the SSS of the array and the values of physical and mechanical characteristics of soils; 2) the subsequent work of these bases and foundations under load [6, 7, 17, 83].

The language of computational part "FORTRAN-77", service "Turbo Pascal". The data between them exchanges files on the hard disk. Sections are written using dynamic structures and compiled to work in protected mode. Therefore, the dimension of tasks is limited only by the available RAM of the PC. The complex has three sub directories: \ INPUT (output information, calculation results), \ SCR (table preparation of output data), \ GRAPHER (output of settlement results in the form of isolines, graphs, surface). A graphical representation of the output data and simulation results created the Pile Graphic program package. Eight-nodular iso-parametric equally-symmetric CEs with quadratic description of geometry and displacement fields per section (with four points of integration) are used. This makes it possible to use, besides the rectangular grid of the CE, also curvilinear.

The problem of rigidity characteristics for isotropic and anisotropic materials is possible. When the soil is represented by an isotropic medium, the physical equations of the NS in the matrix form have the form:

$$\begin{Bmatrix} \sigma_r \\ \sigma_\theta \\ \sigma_z \\ \tau_{rz} \end{Bmatrix} = \frac{E}{\Omega} \begin{bmatrix} 1 & \frac{\nu}{1-\nu} & \frac{\nu}{1-\nu} & 0 \\ \frac{\nu}{1-\nu} & 1 & \frac{\nu}{1-\nu} & 0 \\ \frac{\nu}{1-\nu} & \frac{\nu}{1-\nu} & 1 & 0 \\ 0 & 0 & 0 & \frac{1-2\nu}{2(1-\nu)} \end{bmatrix} \begin{Bmatrix} \varepsilon_r \\ \varepsilon_\theta \\ \varepsilon_z \\ \gamma_{rz} \end{Bmatrix}; \quad (5.30)$$

$$\Omega = [(1+\nu)(1-2\nu)]/(1-\nu), \quad (5.31)$$

Where σ_r , σ_θ , σ_z , τ_{rz} – normal and tangential stresses in CE in cylindrical coordinates; E – deformation module of the soil of the same CE; ν – Poisson coefficient of soil CE; ε_r , ε_θ , ε_z , γ_{rz} – axial and angular components of relative deformations in CE.

In the case of the representation of the soil by an anisotropic (orthotropic) medium, the physical equations of the NA in the matrix form have the form:

$$\begin{Bmatrix} \sigma_r \\ \sigma_\theta \\ \sigma_z \\ \tau_{rz} \end{Bmatrix} = \frac{1}{\Omega} \begin{bmatrix} E_r(1 - \nu_{\theta z}\nu_{z\theta}) & E_r(\nu_{r\theta} + \nu_{rz}\nu_{z\theta}) & E_r(\nu_{rz} + \nu_{r\theta}\nu_{\theta z}) & 0 \\ E_\theta(\nu_{\theta r} + \nu_{zr}\nu_{\theta z}) & E_\theta(1 - \nu_{rz}\nu_{zr}) & E_\theta(\nu_{\theta z} + \nu_{rz}\nu_{\theta r}) & 0 \\ E_z(\nu_{zr} + \nu_{\theta z}\nu_{z\theta}) & E_z(\nu_{z\theta} + \nu_{r\theta}\nu_{zr}) & E_z(1 - \nu_{rz}\nu_{\theta r}) & 0 \\ 0 & 0 & 0 & \Omega G_{rz} \end{bmatrix} \begin{Bmatrix} \varepsilon_r \\ \varepsilon_\theta \\ \varepsilon_z \\ \gamma_{rz} \end{Bmatrix}; \quad (5.32)$$

$$\Omega = 1 - 2\nu_{\theta r}\nu_{rz}\nu_{z\theta} - \nu_{r\theta}\nu_{\theta r} - \nu_{\theta z}\nu_{z\theta} - \nu_{rz}\nu_{zr}, \quad (5.33)$$

where E_r , E_θ , E_z – modules of deformation of soil in appropriate directions; $\nu_{r\theta}$, ν_{rz} , $\nu_{\theta z}$ – are the corresponding Poisson's coefficients, which are defined as:

$$\nu_{\theta r} = \frac{E_r}{E_\theta} \cdot \nu_{r\theta}; \quad \nu_{zr} = \frac{E_r}{E_z} \cdot \nu_{rz}; \quad \nu_{z\theta} = \frac{E_\theta}{E_z} \cdot \nu_{\theta z}. \quad (5.34)$$

For a transversally isotropic body $E_\theta = E_r$.

G_{rz} – module of the shift, which according to the formula S.G. Lehnitsky [27] is equal

$$G_{rz} = \frac{E_r E_z}{E_z + E_r(1 + 2\nu_{rz})}. \quad (5.35)$$

For the soil of each layer (stiffness) determine:

- initial stiffness - depending on the attribute of anisotropy account. In the case of the presentation of the soil by an isotropic material, the rigidity characteristics are given in the form of the initial deformation module and the Poisson coefficient ν . When representing the soil, the orthotropic medium adopts deformation modules for the characteristics of rigidity E_r , E_θ , E_z , and the corresponding Poisson coefficients $\nu_{r\theta}$, ν_{rz} , $\nu_{\theta z}$. It is possible to accept the hypothesis of a transversally isotropic body [3]. Then $E_\theta = E_r$; $\nu_{\theta z} = \nu_{rz}$ [27];

- dependence of the deformation module on the volume (or porosity) of the soil $E_i/E_o = f(V_i/V_o)$ in the form of the analytical expression (5.12) or (5.18) or the table. For the first stage, this dependence is given for the application speed of the load, which corresponds to the technology of laying the foundation, and for the second - the static load;

- dependence of the soil resistance on the displacement from normal stress $\tau = f(\sigma)$;

- the specific weight of the soil γ .

In addition to the geometric sizes resulting from the first stage of simulation, the initial parameters of the foundations on the second take the physical-mechanical characteristics of their materials (specific weight, angle of internal friction, specific weight, deformation module), as well as the coefficients of lateral pressure of the soil λ and the influence of the slipping of the lateral surface the foundation on the soil deformation module (from 0 to 1). In the case when the foundation has several components (and, consequently, the types of stiffness), for example, the body of piles in a broken well of concrete (a mixture of crushed stone with clay) and its expansion from crushed stone

(gravel, hardness, sand, etc.), then the listed parameters determine for each component of the foundation.

The calculation is carried out in two stages. The first simulates the formation of a cavity under the foundation, burn, artificial basis. In this case, the axis of the cavity coincides with the axis of symmetry of the calculated area. External influence is given in the form of forced vertical and horizontal displacements of the nodes of the CE grid, which lie on the axis of rotation, the upper boundary of the calculated area, or occupy another position that simulates the process of squeezing the pile of soil (block, trambike, bucket, punch). These displacements, in general, lead to a decrease in the volume of the CE, and hence a decrease in the porosity of the soil and the growth of its deformation and strength module, although the reverse process - loosening of the soil, in particular, when it is drilled to the surface of the array, is possible. It is possible to simulate the effects characteristic of the process of arranging bases and foundations with soil compaction, such as: the formation of an elastic ground core under the stamp (the edge of the palle), the separation of the surrounding soil with this nucleus, the bumping of soil to the lateral or to the surface of the array, etc.

Since the forced displacements are compatible with the size of the CE, at each step the calculation scheme is corrected by specifying the coordinates of the nodes, taking into account the movements obtained in the previous step. With the change of coordinates, the volumes of CE vary, which makes it possible to specify the deformation modulus of soil in each CE for (5.12) or (5.18) for the rate of application of the load, which corresponds to the technology of the foundation. The coefficient of soil porosity in each CE is

$$e_i = e_o - (1 + e_o) \left(1 - V_i / V_o\right). \quad (5.36)$$

The result of the first stage (and each of its steps) is the new coordinates of the nodes of the CE, the characteristics of the soil (more often, the density of the dry soil, the porosity coefficient, the deformation module), the displacement (for which the moving of the nodes of the CE network), the stresses (in particular the vertical (isobars σ_z) and radial (bursts σ_r) normal stresses), presented in the form of tables, charts, isolines.

Since the calculation in the first stage is related to the stepwise solution of the problem to the given displacement and is carried out according to the deformed scheme at each step, then, as a rule, there is a significant change in the form of the CE, which can lead to the degeneration of the CE (that is, the Jacobian transforms the coordinates becomes non-positive) To avoid this, it is necessary to specify the movement of nodes no more than the value of the product of the size of the element and the porosity of the soil in this CE or appropriately select the size of the CE. If you still need to calculate for larger displacements, you need to set them in steps in steps, the number of which is set in the control data.

The calculated characteristics of the soil and the SSS of the array make it possible to proceed to the second stage - modeling the work of the foundation under load. The cavity obtained by squeezing the soil, filled with structural material, set its parameters, introduces additional CE simulating the foundation. For the soil, a new dependence is given $E_i / E_o = f(V_i / V_o)$, which corresponds to the rate of application of static load (time of degree of endurance - to conditional stabilization of deformations). The external load is applied by steps in the form of a concentrated force to the axial node of the upper face of the foundation or evenly distributed load to the upper edge of the foundation or its area. It is also possible to set displacements to the nodes. External loads can be applied separately and in combinations of loading steps. The external load is applied by steps in the form of a concentrated force to the axial node of the upper face of the foundation or evenly distributed load to the upper edge of the foundation or its area. It is also possible to set displacements to the nodes. External loads can be applied separately and in combinations of loading steps.

It is accepted that within the cone, which is the spatial geometric form of the Mises-Schleicher-Botkin condition, the soil is elastic. It takes into account its further consolidation and increase the value of the deformation module (due to reduction of the volumes of CE). With the achievement of the limit of strength, the law of the flow of soil is considered equal. Again, account is taken of its further seal-dissolution. The possibility of slipping the lateral surface of the foundation (pali) relative to the soil is realized by monitoring the tension stresses τ_{rz} in the soil of the CE located on the contact of «ground-to-ground». Condition is checked

$$\tau_{rz} \leq (\sigma_r + \gamma h \lambda) \operatorname{tg} \varphi + c, \quad (5.37)$$

where σ_r – radial stresses; h – distance to the surface; λ – lateral pressure factor.

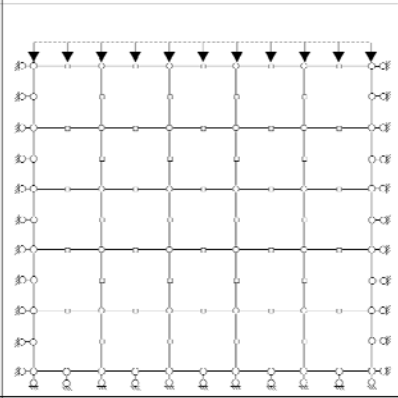
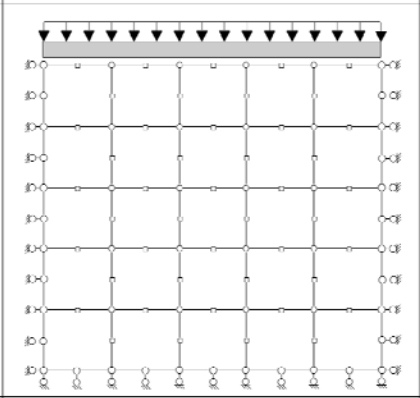
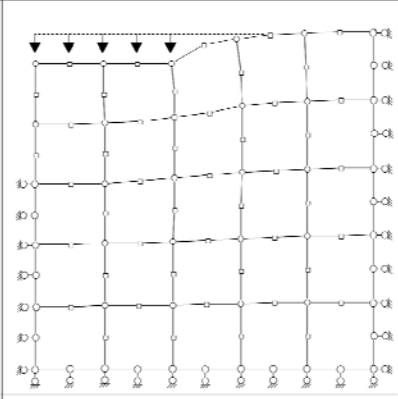
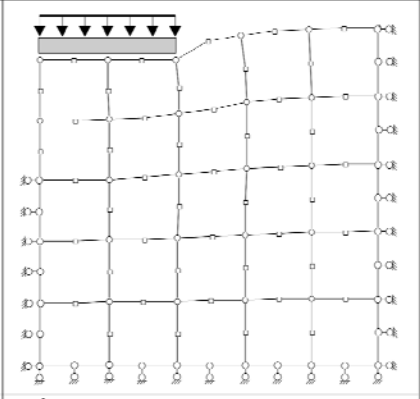
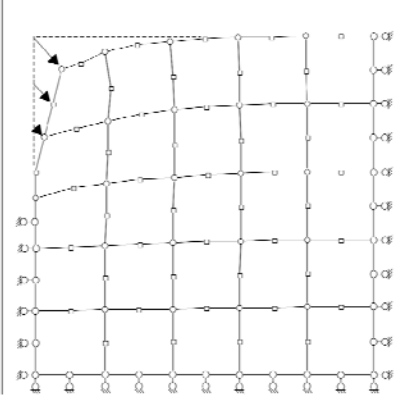
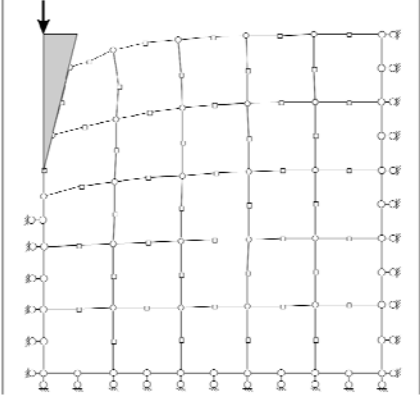
In case of violation of this condition, the module of soil movement in the CE in contact with the foundation is assumed to be zero. A lowering coefficient is introduced into the module of longitudinal deformations, which reflects the influence of the violation of the structure of the soil due to the slipping of the lateral surface of the foundation. At subsequent levels of loading over the CE surface adjacent to the soil, a uniformly distributed load is applied from the friction forces of the foundation on the ground intensity $p = \gamma h \lambda \operatorname{tg} \varphi$.

The result of the second stage (and its steps) is: the dependence of the subsidence of the foundation on the load; movement of each node of the CE; tension in the array; transition of soil into the fluid state in separate CEs; the characteristics of the soil are given, - are displayed in the form of tables, graphs, isolines, messages about the transition of the CE into the fluid state.

The calculation schemes of the ITU of soil compaction (soil compaction) when creating bases and foundations for different classes of soil consolidation methods and their subsequent loading [6, 7, 18] are given in Table. 5.1.

Creating the foundations and foundations of class 1 "The work of the soil without the possibility of its lateral displacement from the working body or foundation" ("compression problem") simulates the task of only forced vertical displacements of nodal points of the upper boundary of the calculated area (shown by the vertical arrows in Table 5.1).

Table 5.1 - Schemes of work (consolidation) of soil when creating and loading foundations, piles or artificial bases

№ class	Foundation creation (soil base)	Foundation work (soil base)
1		
2		
3		

At the same time the possibility of squeezing the soil in other directions is absent. For the bases and foundations of class 2 "Work of the soil with limited possibility of its lateral displacement from the working body or foundation" ("the task of immersion of a rigid flat stamp"), forced displacements are also set

in one direction (vertical arrows), but there is a squeezing of the part him in others.

For the bases and foundations of class 3 "Work of the soil with the possibility of squeezing it out from a working body or foundation in different directions" ("the task of immersing the penetration tip") forced displacement is set in different directions (inclined arrows).

The eight-node isoparameter symmetric CE, given in the curvilinear coordinate system (ξ, η, ζ : $-1 \leq \xi \leq 1$; $-1 \leq \eta \leq 1$) in Fig. 5.10, belongs to the KE of the 2nd order, which determines the degree of interpolation polynomial and the number of nodes.

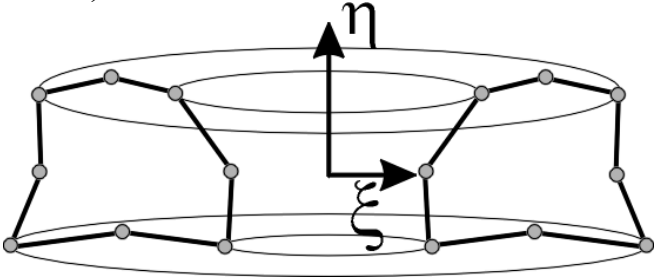


Fig. 5.10 - Scheme of the eight-node isoparametric equilibrium CE

The mathematical apparatus of the step-iterative solutions of the nonlinear solving equations of the ITU complex "PRIZ-Pile" is presented in [54].

The calculated area of the axisymmetric problem most often represents the cylinder (Fig. 5.11, a), obtained by the inversion of the rectangular calculated zone (Fig. 5.11, b) around the axis of symmetry of the OA, although a more complicated form of this zone is possible (for example, for a short pyramidal piling, the combination of a rectangle and a rectangular trapezoid (Fig. 5.12, b)), and hence another form of the calculated region (a combination of a cylinder and a truncated cone (Fig. 5.12, a)). The axis of symmetry coincides with the axis of the future foundation.

The dimensions of the calculation zone are set as follows:

- the lateral boundaries of the OA and the aircraft are taken respectively on the axis of symmetry and sufficient distance from the displacement site to maximize the effect of the condition of the prohibition of horizontal displacements, the concentration of stresses and soil consolidation on contact with the external boundary of the calculated zone. Experience shows that for the purpose of this condition it is usually sufficient to take for the diameter of the calculated area not less than, where b_p – the lateral of the cross-section or the diameter of the expansion of the foundation;
- the upper boundary of the OV is placed on the surface of the foundation pit;
- the lower horizontal boundary of the AU is in a layer that does not have special properties and is suitable as a natural basis; for the depth of the calculated zone, you can accept the lower boundary of the compressed layer [55].

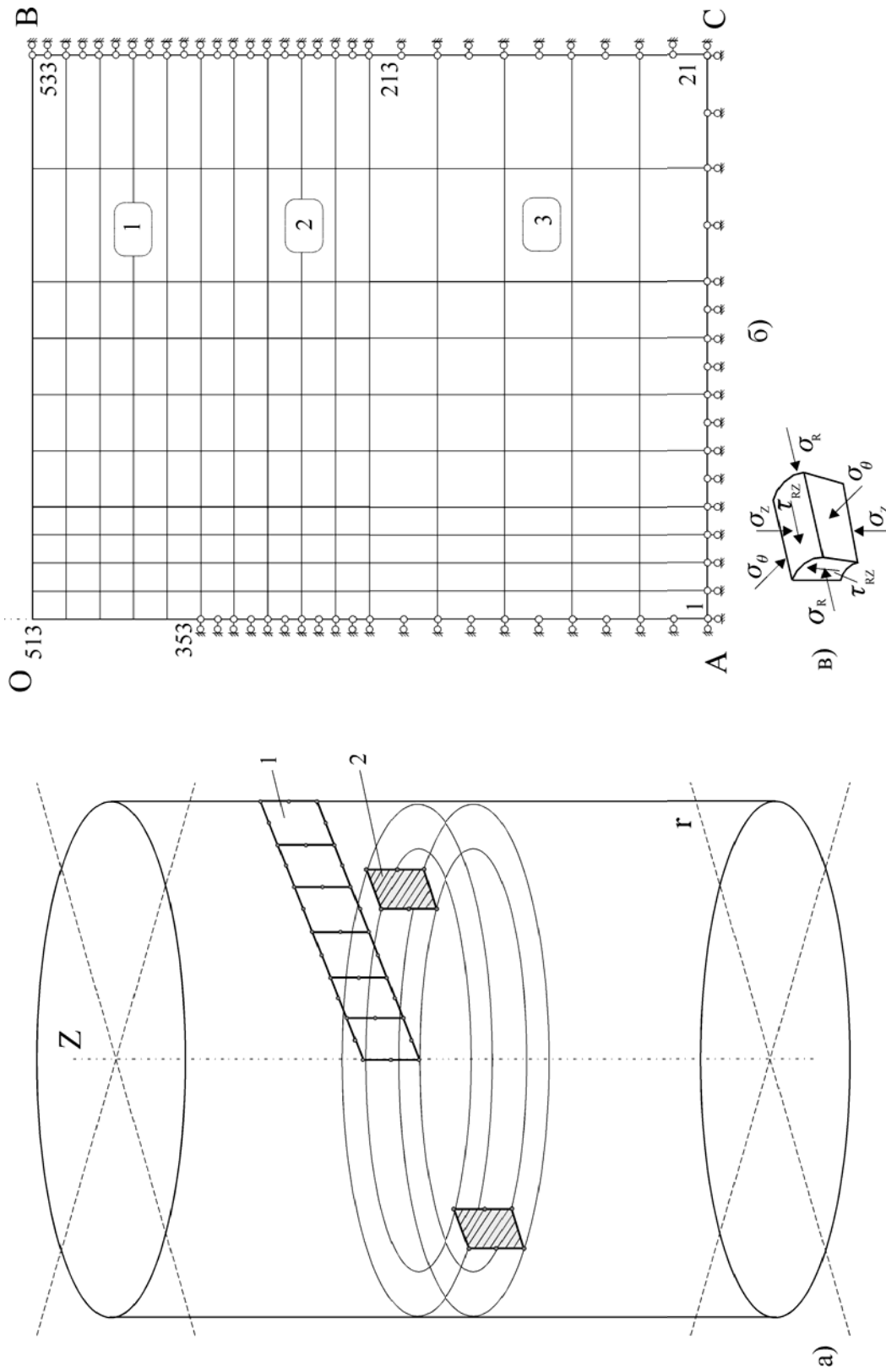


Fig. 5.11 - Output calculated area of an axisymmetric problem in the form of a cylinder: a - the calculated region; b - a rectangular design zone; c - voltage components; 1 - fragment of the division of the calculation area; 2 - CE

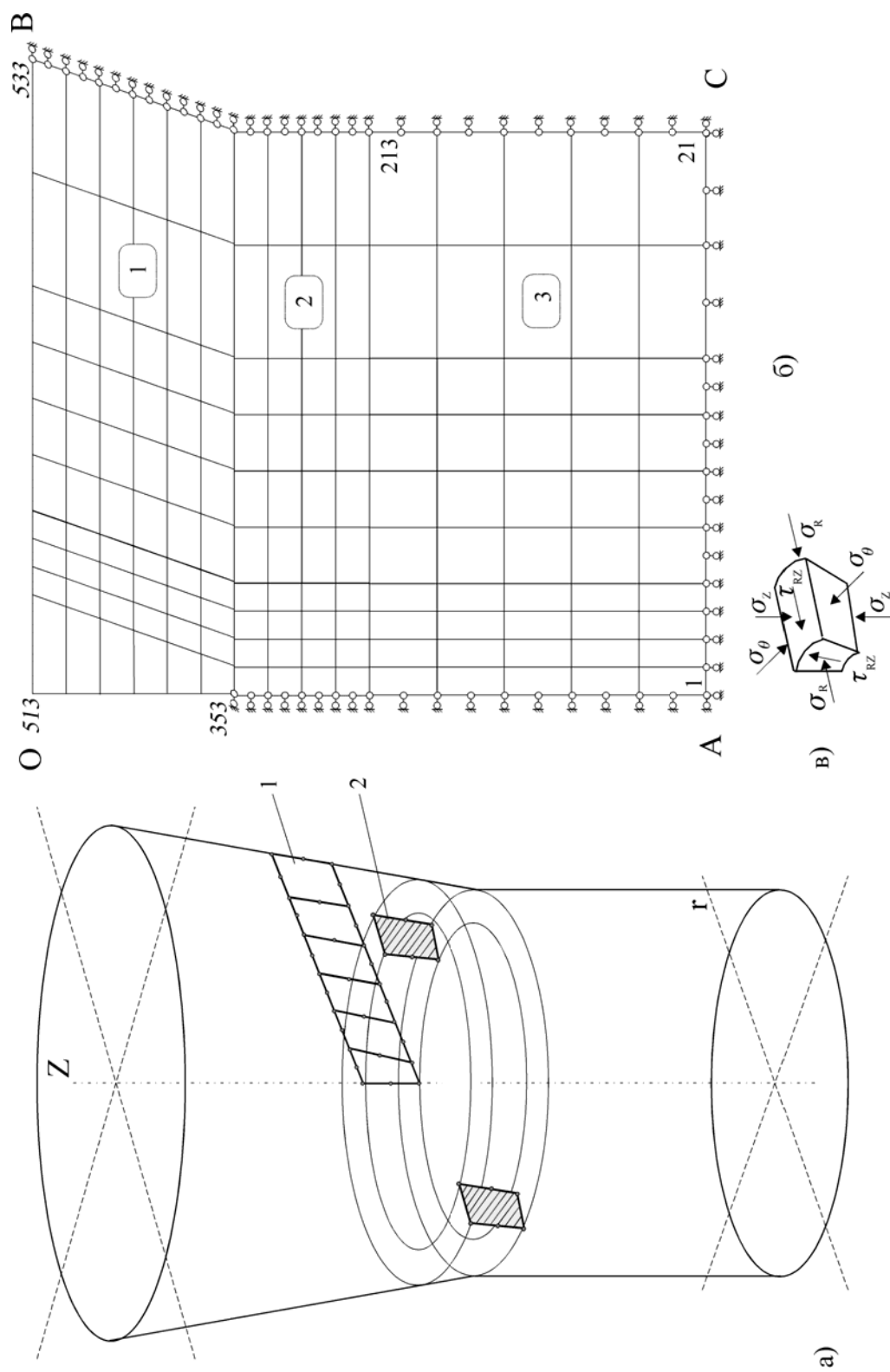


Fig. 5.12 - Initial calculated region of an axisymmetric problem in the form of a combination of a cylinder and a truncated cone:
 a - calculated area; b - the calculated zone in the form of a combination of a rectangle and a rectangular trapezoid;
 c - voltage components; 1 - fragment of the division of the calculation area; 2 - is a finite element

Use sequential numbering of nodes and elements. They are numbered, starting from the lower and from the axis of symmetry. The dimensions of the CE are adopted, mainly, taking into account the values of forced displacements in the first stage of simulation, as well as the size of the future foundation and the position of engineering geological elements. Generally, the grid of CE thickens (their sizes are reduced) in places where the first stage involves the largest forced displacements (hence the substantial change in the physical and mechanical characteristics of the soil and the SSS array), and the second - the movement of soil and the concentration of stress in it.

After assigning the size of the calculated zone and its division into CE, establish the boundary conditions that correspond to the physical conditions of the formation and operation of the bases and foundations under load, namely: all nodes located on the lower boundary of the AU, are fixed immutable; The nodes of the lateral boundaries of the OA and the Sun can not have horizontal displacement, except those nodes, which in the first stage are assigned forced displacements and are close to the latter (usually they lie on the axis of the OA).

In the upper part of the outer boundary of the Sun, several nodes may be released from horizontal boSSS (in situ, this correspoSSS to the formation of a ring fissure around the foundation) to avoid tensile forces in this area and reduce the calculation time without practically distorting the values of stresses and deformations.

As a result of calculations in the first stage, the movement of nodal points, the new coordinates of the nodes of the deformed circuit, the deformation, the volume, the new values of the deformation module in each CE, are changed due to the decrease (sometimes increase) of its volume. A fragment of this deformed scheme is shown in Fig. 5.13, a.

The generated cavity is divided into an additional group of CE. The number of nodes and CE increases, but already existing nodes located on the cavity contour, are used to construct new CEs. The order of the numbering of additional nodes and CE is usually taken in the same way as the first stage. The new CE defines the properties of the foundation material. A fragment of the breakdown of the foundation on CE is offered in Fig. 5.13, b.

All work with the program complex "PRIZ-Pile" is carried out through the main menu, shown in Fig. 5.14, which has seven main points:

1. "Cipher" - the choice of object modeling. The new task assigns a name to it or invokes the output data of the previously solved task for editing.
2. "Soil" - input or edited raw data for the calculation of the first stage. Forms data files on the hard disk in the subdirectory \ INPUT.
3. "Pale" - input or edited raw data for the calculation of the second stage. Forms data files on the hard disk in the subdirectory \ INPUT.

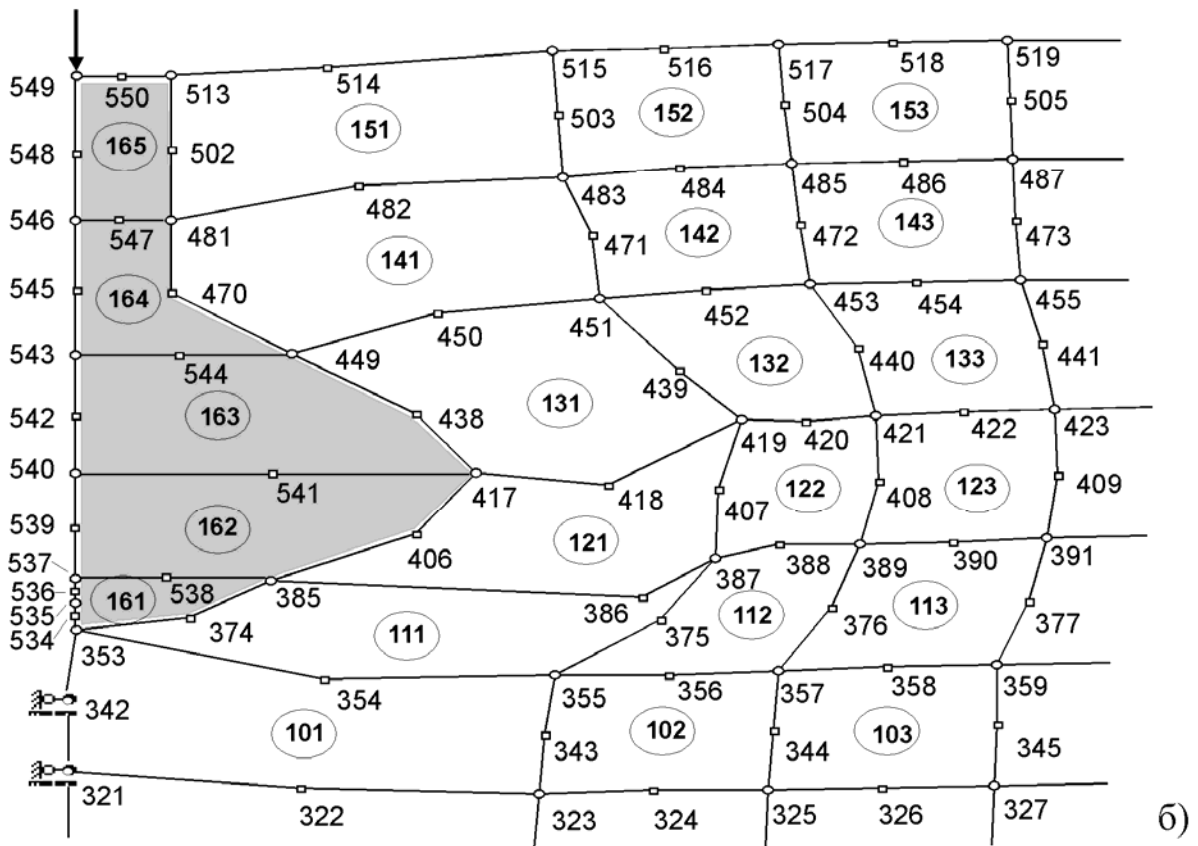
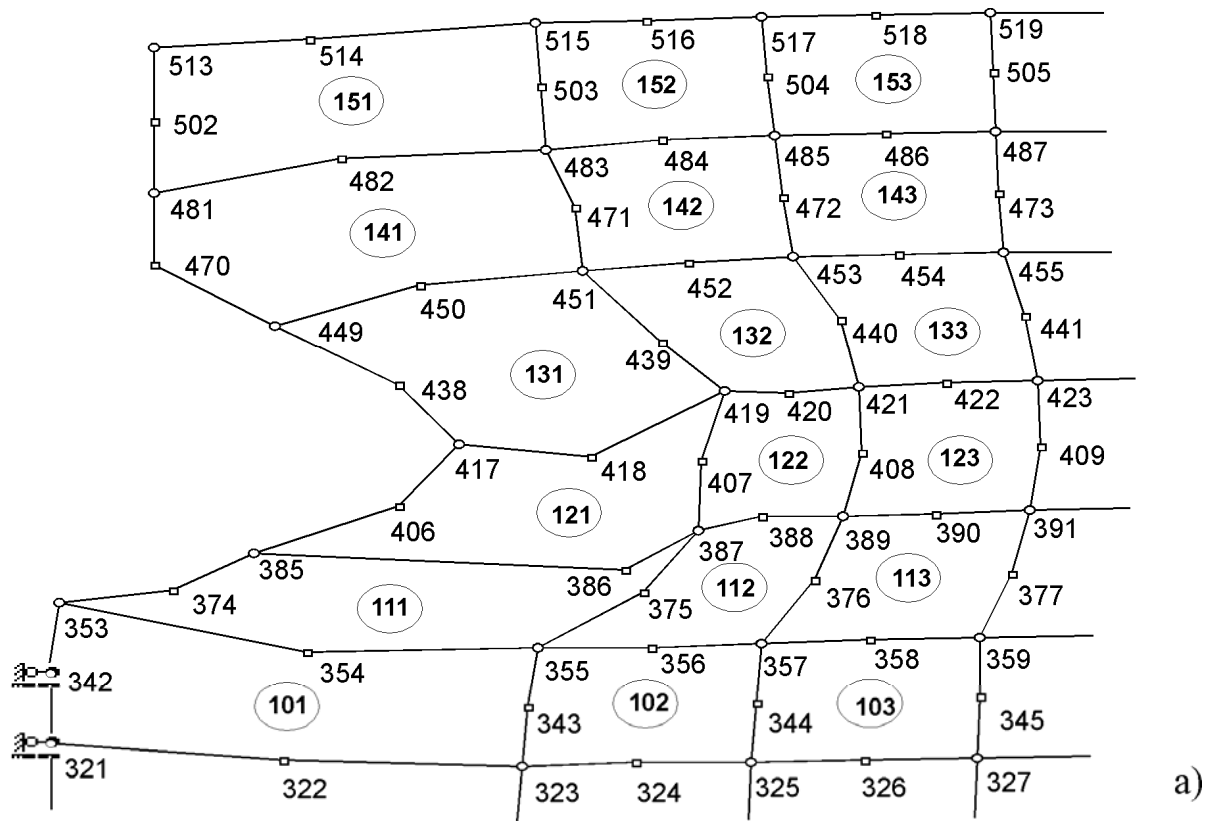


Fig. 5.13 - Fragment of the ITU scheme: a - deformation of the basis (completion of the first stage); b - foundation (second stage)

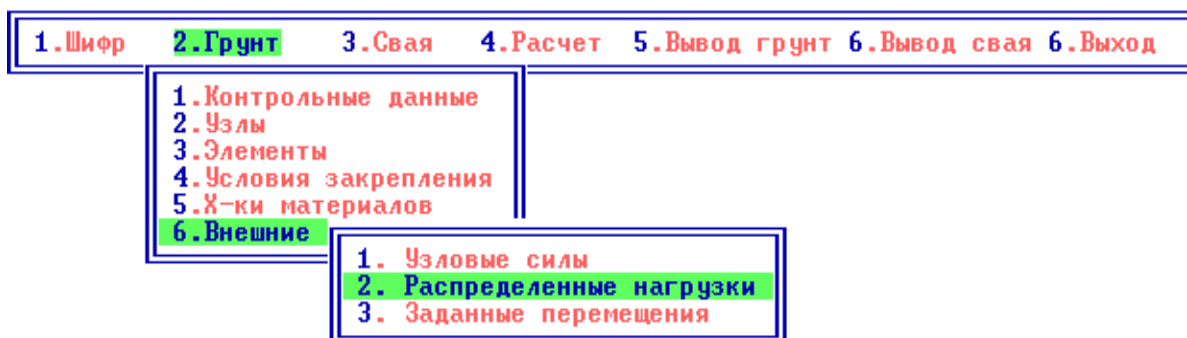


Fig. 5.14 - Main menu and content of the "Ground" item of the "PRIZ-Pile" complex

4. "Calculation" - the calculation for stages 1 and 2 is carried out.
5. "Output of soil" - intended for displaying and obtaining a solid copy of the tables with the data of calculations, calculation and deformed schemes of the first stage.
6. "Output Pile" - similar to paragraph 5, but for the second stage.
7. "Exit" - the return to the system is carried out.

For the convenience of entering the source information, a spreadsheet editor was developed. It allows interactive mode to enter and edit source information files. His tables are accompanied by explanatory inscriptions and drawings. For regular structures, a convenient form of duplication of individual fragments of a table is provided for the required number of times with a given step, as well as the possibility of removing unnecessary strings. The input of the initial numeric information for stage 1 of the calculation "Soil" is carried out from the table editor of item 2 of the main menu, the sequence and the general contents of which is given in Fig. 5.14:

1. "Control data" - contains control information about the number of: nodes of the network grid; elements in it; Types of stiffness; fixed nodes; downloaded nodes in all downloads; downloaded items in all downloads; nodes with specified displacements in all downloads; loading rates, as well as for taking into account or not taking into account anisotropy; Form of the task of porosity characteristics (graph or table); the number of steps to calculate.

2. "Nodes" - data for each node: its number and coordinates in the circular cylindrical coordinate system (ta).

3. "Elements" - data for each CE: its number; the numbers of each of the 8 nodes in the mandatory sequence (see Figure 5.15); type (serial number) of the CE hardness.

4. "Terms of fixing" - the number of the fixed node and the conditions of its attachment along the axes R and Z and.

5. "Characteristics of materials" - has two points: 1) initial stiffness (for isotropic materials, this is the deformation module and the Poisson coefficient, and the orthotropic deformation modules E_r , E_θ , E_z and the corresponding Poisson coefficients $\nu_{r\theta}$, ν_{rz} , $\nu_{\theta z}$); 2) taking into account the influence of

porosity on the soil deformation module can be carried out in the form of the analytical expression (5.12) or (5.18) or the dependency table $E_i/E_o = f(V_i/V_o)$.

6. "External influence" -the task of external influences: concentrated forces; evenly distributed load; forced (forced) movement of nodes in directions and. Each type of external influence can be applied separately as well as in combinations of load steps.

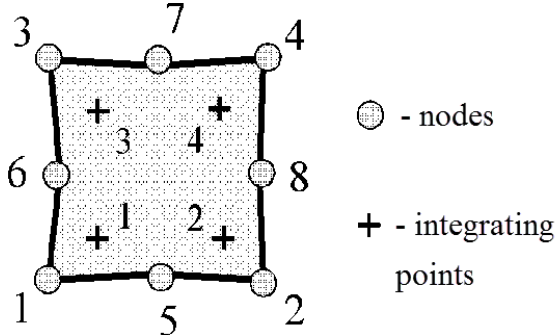


Fig. 5.15 – Node numbering CE

By filling all the tables to make sure that the information entered is correct, go to the menu item "Output of the soil - graphics - calculation scheme", where the calculation scheme, which is built on the data entered automatically, is displayed. In case of discrepancy with the accepted scheme, one should once again apply to the table editor and enter the necessary corrections.

By the option "Calculation - immersion of the pile in the soil" the calculation of the formation of the cavity in the array is performed.

In order to prepare the source information of the second stage in the main menu, there is the item "Pala", the content of which is close to the point "Soil", and it refers only to additional CEs that simulate the work of the foundation. In particular, "Control Data" contains information on the number of: additional nodes, elements, types of rigidity; fixed nodes; downloaded nodes and items in all downloads; loading rates, as well as taking into account or not taking into account the slipping of the lateral surface of the foundation.

By filling in all the tables of the "Pala" item in the main menu, you must make sure that the calculation scheme is correct based on the item "Output - Pile - Graphics - Scheme", then make the second calculation under the item "Calculation - Pile Load". Its results are displayed in the form of tables and in graphical form by the items in the menu "Output - Pale - tables", "Output - Pale - Graphics - Movement".

For the automatic representation of the results of each step of forced displacements and static loading of the bases and foundations in the form of calculation schemes of ITU, tables, graphs and isolines of the given characteristics of soils, displacements and voltages in the array, a package of programs "Pile Graph" [6] was developed. Appointment of these programs:

- "Scheme" - construction of the calculation schemes of ITU arrays to create the foundation, and after each step its formation and load;
- "Scheme" - construction of the calculation schemes of ITU arrays to create the foundation, and after each step its formation and load;

- "Soil deformation" - approximation of soil test data in a compressor for (5.18), the construction of tables and charts for them, preparation of data for the presentation of the results of deformation (compaction) of the soil in the array;

- "Grunt" - a program for representing the output and the given values of the characteristics of the CE (coordinates of the center of weight, the ratio of volumes) and soils (the deformation module, its ratio to the initial value, the density of the dry soil, the coefficient of porosity) in accordance with the results of simulation in tabular form ;

- "Horizontal graphs" and "Vertical graphs" - programs for constructing horizontal and vertical graphs of the values of given and natural characteristics of the soils of the massif in accordance with the results of simulation, as well as their comparison with the data of field research;

- "IsoLines" - a program for representing the simulated above characteristics of soils, displacements and stresses in an array in the form of isolines;

- "Picture Viewer" - a quick view of drawings and tables.

At the same time, the packages of the program are functionally interconnected.

5.3. Applied problems of mathematical modeling of stressed-deformed state of compacted soil of anisotropic bases

Features of the preparation of raw data for the simulation of the bases of foundations of the foundations that can be represented as anisotropic, in particular, transversally isotropic, medium, set forth in sections 5.1 and 5.2.

Initial conditions (soil layers, geometric and technological parameters of the pile) and calculation schemes for a packing pile with a leading well and the expansion of the crushed crushed stone were adopted for the initial data of the visual problem.

An example of a baseline separation scheme on the CE after the installation of a leading well with a diameter of 0.50 m and a depth of 5.00 m for simulating the VAT of a loading pallet with a crushing extension [116] is given in Fig. 5.16 (the borehole is limited to nodes 865, 867 and 1186). The scheme contains 369 CE with sizes from 0.25x0.25 to 0.80x1.00 m and 1204 nodes (150 fixed). The calculated area is a cylinder with a diameter of 9.1 m and a height of 15.0 m.

The scheme is designed for a pile of piles on the site of the restoration of the Holy Assumption Cathedral on the Ivanovo Hill in Poltava. To a depth of 1.5 m, the loam is heavily dusty, solid ($w = 0.21$; $\rho_d = 1.41 \text{ g / cm}^3$), in the range 1.5-3.5 m, loam is loose, solid ($w = 0.14$; $\rho_d = 1.49 \text{ g / cm}^3$; 5.8 MPa), and below is light clay loam, solid ($w = 0.215$; $\rho_d = 1.54 \text{ g / cm}^3$; $E = 14 \text{ MPa}$).

When using the output simulation data of the expression (5.18) to describe the dependence $E_i/E_o = f(V_i/V_o)$ of the value of the coefficient $a_o = 155.3$.

The expansion of this pallet was arranged by dumping the crushed stone = 1.5 m³ (= 0.25 m³) with a cylindrical tram diameter of 430 mm.

The extension has the form of an ellipsoid of rotation with half-lengths: horizontal = 0.65 m and vertical 0.70 m (defined by the "Guide ..." [37]).

His formation was modeled by the task of forced horizontal and vertical displacements of eight nodal points (from 865 to 983), located along the contour of the bottom of the well. A fragment of the scheme of deformation of the base at the arrangement of expansion is given in Fig. 5.17. The simulated pattern of consolidation of soil around the pile with a leading well and the expansion of the rubble crushed stone is presented in Fig. 5.18. The seal around the well is absent

The largest consolidation of the soil is directly next to the expansion. For example, at a distance of 0.15 m from the lateral expansion surface, the magnitude increased from 1.54 g / cm³ to 2.07 g / cm³. The radius of the zone of sufficient seal, where $\rho_d = 1.60$ g / cm³, according to the simulation was $r_s \approx 1.00$ m, and according to the experimental-analytical method, created on the basis of a large number of field experiments, 0.96 m (by the way, for the same pile, but without a lead well, 1.06 m)

The value of the soil deformation module at the boundary of the sufficient sealing zone increased by 2.3 times, and its value in the middle of this zone was 3.5 times. The characteristics of the percolator soil are given, its VAT is used to simulate the work of this pallet under load at the second stage of the calculation. The cavity, obtained by perturbation and decomposition, is "filled" with structural materials (gravel and concrete) and introduces additional CEs and nodes (in this example, respectively, 13 and 43), simulating the pulley trunk and expansion. Load is applied steps (first - 300 kN, and then - 100 kN) in the form of concentrated force to the axial node of the upper edge of the palm.

A comparison of the simulated graph of the dependence of the loading of this packing pulley on the load $S = f(P)$ with the data of its static tests is presented in Fig. 5.19. From it it is seen that the deposition on the results of modeling by 15 - 20% exceeds the data of static tests, but with increasing load, this difference significantly decreases. It should also be noted that the pilot palletising capacity of its bearer has not been exhausted, and in the simulation of soil, no CE has become flowing.

From rice 5.19 it can be seen that the stagnation of the modeling by 15 - 20% exceeds the static test data, but with increasing loading, this difference decreases. It should be noted that the pile bearing capacity has not exhausted, and in the simulation of soil, no CE has entered the boundary state [116]

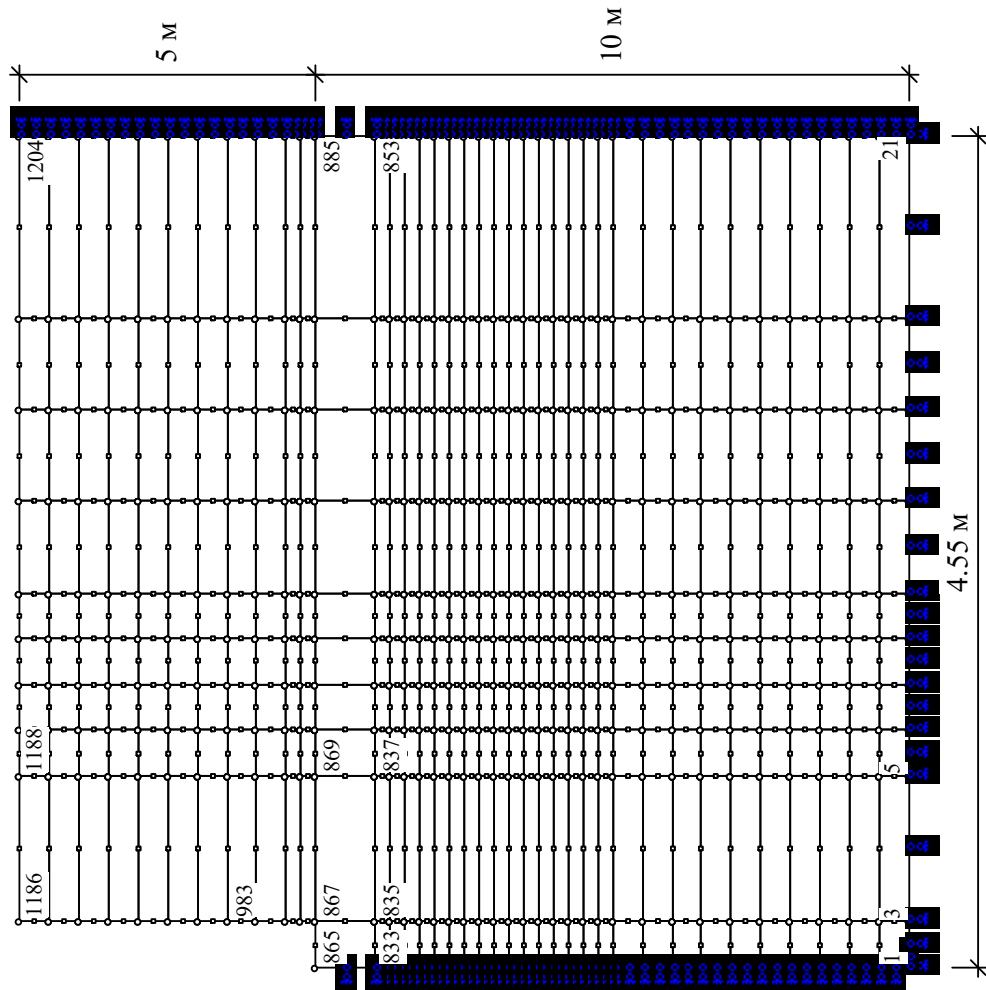


Fig. 5.16 - Example of the output scheme of the division of the calculated zone of the array to the finite elements after the formation of the leading wells and upgrades

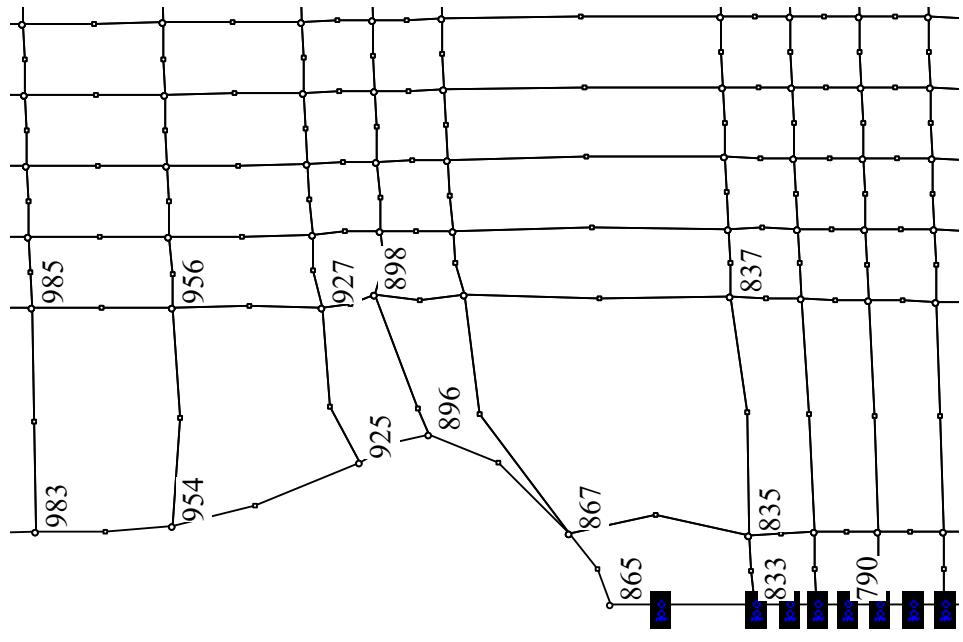


Fig. 5.17 - Fragment of the scheme of the first stage simulation of the deformation of the pile base with the lead well after expansion

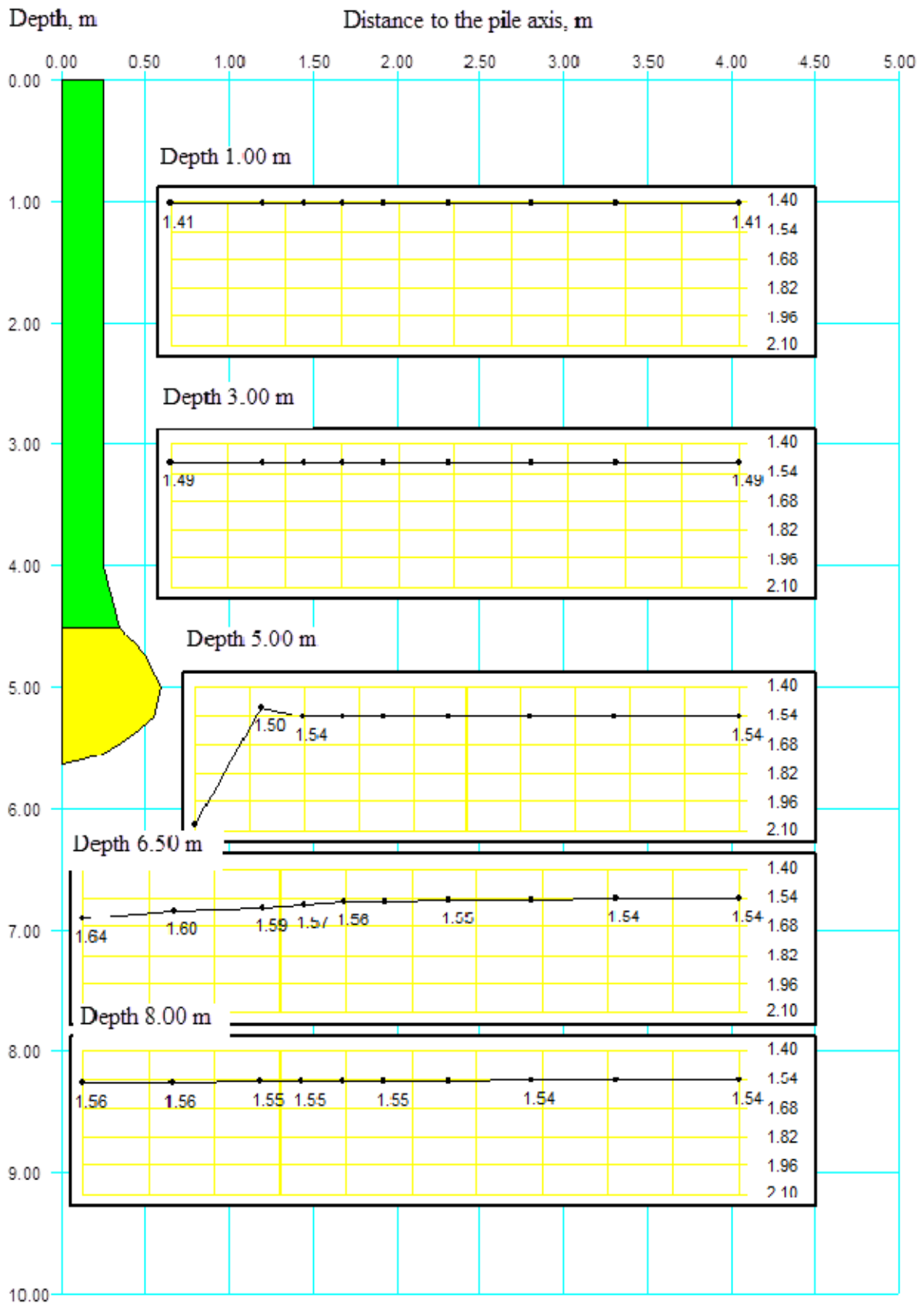


Fig. 5.18 - Seal the soil around the packing pile with the leading well and extension of the crushed stone for modeling

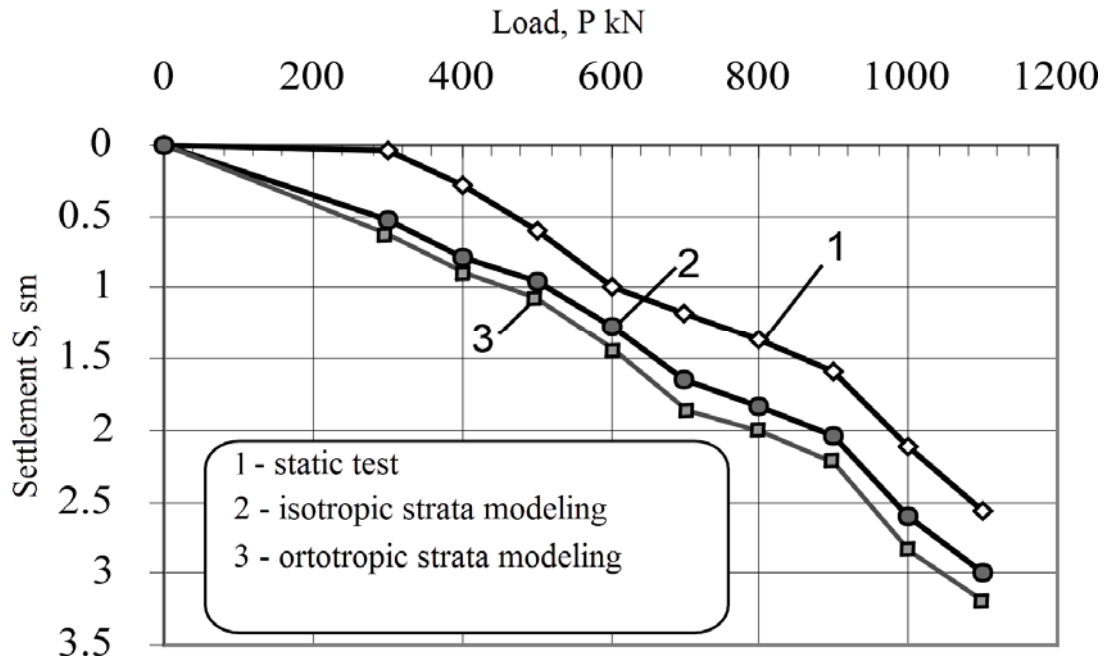


Fig. 5.19 - Graphs of the dependence of settling on the loading of a packing pile with a leading well and expansion for: 1 - static tests; 2 - simulation; 3 - the same in the case of transversally isotropic soil at $n_{E, \alpha=90^\circ} = 0.8$ (clause 5.3.2)

The correlation of the values of the deformation module of the soil was taken in accordance with studies [4 - 8, 121] in areas composed of forest soils of natural moisture, $n_{E, \alpha=90^\circ} = 0.8$: for a loam located above the expansion, $E_\theta = E_r = 4.65$ MPa; $E_z = 5.8$ MPa; for clay that falls on and below the expansion, $E_\theta = E_r = 11.2$ MPa; $E_z = 14.0$ MPa. The values of the coefficient in expression (5.18) were taken the same as in 5.1.

The comparison of the simulated graphs of the dependence of the loading pad $S = f(P)$ on the isotropic base (position 2) and the transversally isotropic medium (position 3) is shown in Fig. 5.19. From it it is seen that the value of the precipitation of the pile in the second case, that is, $E_\theta = E_r < E_z$ provided that some (approximately 10%) is greater in the case when $E_\theta = E_r = E_z$. This result does not deny the well-known regularities of soil mechanics and the conclusions of other researchers [3, 9, 11, 14, 21, 24, 53, 93]. We also note that in simulation for both an isotropic medium and anisotropic soil, none of the CEs reached its limit state.

Thus, with known values of the module of deformation of the soil in the plane of isotropy and in the direction perpendicular to it it is possible by mathematical modeling to estimate the VAT of the orthotropic foundations of foundations.

6. APPLIED PROBLEMS OF ASSESSMENT OF ANISOTROPIC ENVIRONMENT INTERACTION WITH CONSTRUCTIONS (ENGINEERING DECISIONS)

6.1. Resolution of the side pressure of homogeneous anisotropic soils on closely spaced walls

Artificial clogs from a stone, soils, environments, in particular soil, waste dredging, in water areas and water approaches are sharply heterogeneous and anisotropic [59] under the natural conditions of rock accumulation and litigation. In addition, both factors (heterogeneity and anisotropy) to a large extent depend on the construction technology of filling the filling - the nature and sequence of the formation of the soil massif. In practice, this is confirmed by the actual inability to create a perfectly homogeneous and isotropic soil massif.

Given these factors should proceed from the most unfavorable conditions when performing construction work. An ideally homogeneous isotropic soil, as a rule, is simulated with ideal balls with centers in the nodes of a regular spatial grid [19]. The real soil environment is by no means the same. Therefore, existing theories for determining lateral pressures on closely spaced walls, including the theory of H. Janssen, require development to account for heterogeneity and anisotropy.

Characterization and classification of structural models of discrete soil environments. Formation of soil massifs is a complex multifactorial phenomenon. When setting tasks, researchers have some simplifications for soil modeling.

The number of properties (parameters) of the soil environment involved in the construction of its discrete model determines the number of isotropies or anisotropies in its qualitative and quantitative characteristics to be studied.

In this regard, it is advisable to draw attention to the classification of discrete environments, which is contained in Table. 4.1 [58].

Generalization of the theory of H. Janssen for isotropic filling. In addition to parallel closely spaced walls in the practice of building, often there are sloping and curved closely spaced walls. We summarize H. Janssen's decision [85] on the inclination, and then on the curvilinear walls of arbitrary curvature (Fig. 6.1).

The obtained generalizations in some cases must degenerate into the theory of H. Janssen for this purpose, we will deduce for the beginning of H. Janssen's solution for a plane problem.

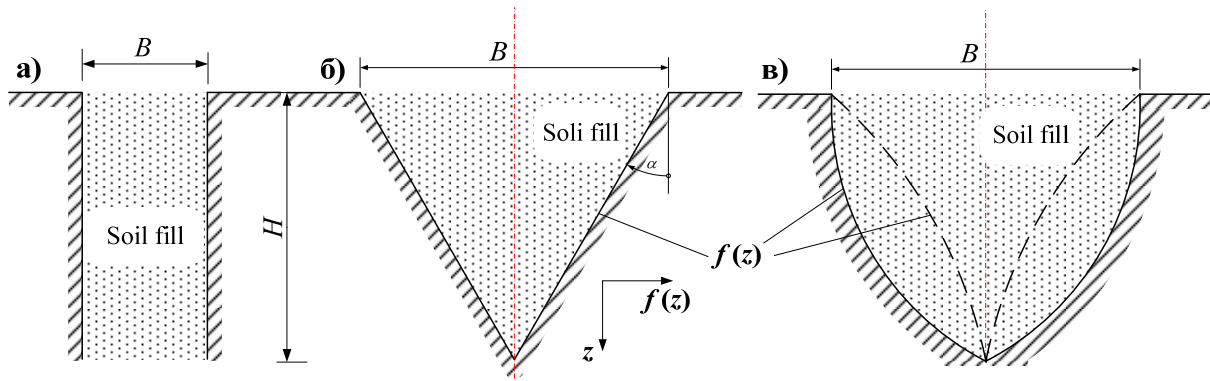


Fig. 6.1 - Different forms of closely spaced walls: a - vertical; b - inclined; in - curvilinear

The theory of H. Janssen for a plane problem. To compare the theoretical results, we use the theory of H. Janssen for a plane problem (see its schematic diagram in Figure 6.2). When calculating we take the following assumptions and preconditions [85]:

- closely spaced vertical walls;
- the surface of the filling is horizontal;
- the vertical stress σ_z in an arbitrary horizontal plane is filled with material (medium) with a horizontal roof of the filler evenly, tangential stresses are absent;
- the friction of the filling medium behind the walls is determined by the coefficient of friction $k_m = tg\delta$, where δ is the angle of friction of the medium on the material of the wall;
- the lateral pressure σ_x at the perimeter of the cross-section at the z value is determined by the lateral pressure coefficient and the dependence $\sigma_x = \sigma_z \cdot \lambda$.

Consider the calculation scheme shown in Fig. 6.2.

Equilibrium in the direction of the z axis, $F_z = 0$:

$$\sigma_z \cdot B - (\sigma_z + d\sigma_z) \cdot B + dG - 2\tau \cdot dz = 0, \quad (6.1)$$

$$\sigma_z B - \sigma_z B - d\sigma_z B + \gamma \cdot B \cdot dz - 2\lambda \cdot tg\delta \cdot \sigma_z dz = 0, \quad (6.2)$$

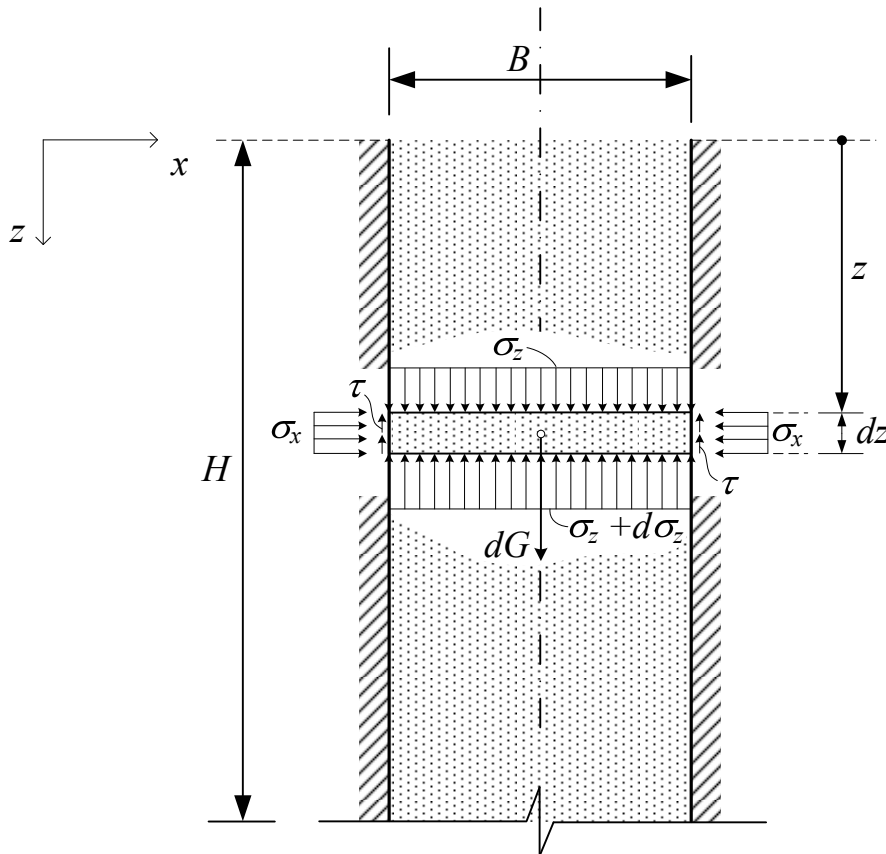
$$d\sigma_z \cdot B + 2 \cdot \lambda \cdot tg\delta \cdot \sigma_z dz = \gamma \cdot B \cdot dz \quad | : dz : B, \quad (6.3)$$

$$\frac{d\sigma_z}{dz} + \frac{2 \cdot \lambda \cdot tg\delta}{B} \sigma_z = \gamma. \quad (6.4)$$

Possible general solution of the obtained differential equation:

$$\sigma_z = e^{-\int \frac{2\lambda tg\delta}{B} dz} \left(\int \gamma e^{\int \frac{2\lambda tg\delta}{B} dz} dz + C \right), \quad (6.5)$$

$$\sigma_z = e^{-\frac{2\lambda tg\delta}{B} \cdot z} \left(\gamma \frac{B}{2\lambda tg\delta} e^{\frac{2\lambda tg\delta}{B} \cdot z} + C \right). \quad (6.6)$$



P Fig. 6.2 - Scheme for the decision of H. Janssen

Consider the equilibrium of the infinitesimal element of the soil (Fig. 6.3)

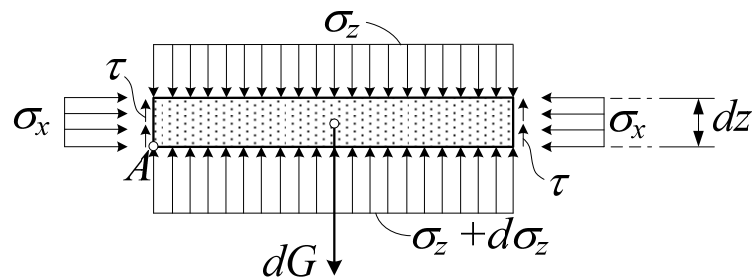


Fig. 6.3 - Equilibrium of the infinitesimal element of isotropic soil

Under the boundary conditions: $z = 0, \sigma_z = 0$ - we have:

$$0 = e^0 \left(\gamma \frac{B}{2\lambda \operatorname{tg} \delta} e^0 + C \right), \quad C = -\frac{\gamma B}{2\lambda \operatorname{tg} \delta}, \quad (6.7)$$

$$\sigma_z = e^{-\frac{2\lambda \operatorname{tg} \delta}{B} z} \left(\gamma \frac{B}{2\lambda \operatorname{tg} \delta} \cdot e^{\frac{2\lambda \operatorname{tg} \delta}{B} z} - \frac{\gamma B}{2\lambda \operatorname{tg} \delta} \right). \quad (6.8)$$

Ultimately, we obtain the law of distribution of vertical and horizontal pressure:

$$\sigma_z = \frac{\gamma B}{2\lambda \operatorname{tg} \delta} \left(1 - e^{-\frac{2\lambda \operatorname{tg} \delta}{B} z} \right), \quad (6.9)$$

$$\sigma_x = \sigma_z \cdot \lambda = \frac{\gamma B}{2\operatorname{tg} \delta} \left(1 - e^{-\frac{2\lambda \operatorname{tg} \delta}{B} z} \right). \quad (6.10)$$

Expressions (6.9) and (6.10) are solutions for vertical and lateral pressures in the theory of H. Janssen for a plane problem.

Generalization of the plane problem of H. Janssen for flat sloping walls. The prerequisites for this solution remain the same as above, except that the normal pressure on the wall σ_α on the z -value is determined by the normal pressure factor λ_α : $\sigma_\alpha = \sigma_z \cdot \lambda_\alpha$.

Consider a flat problem in the calculation scheme in Fig. 6.4. Width B in this case changes with depth. We find its function $B(z)$ (Fig. 6.5).

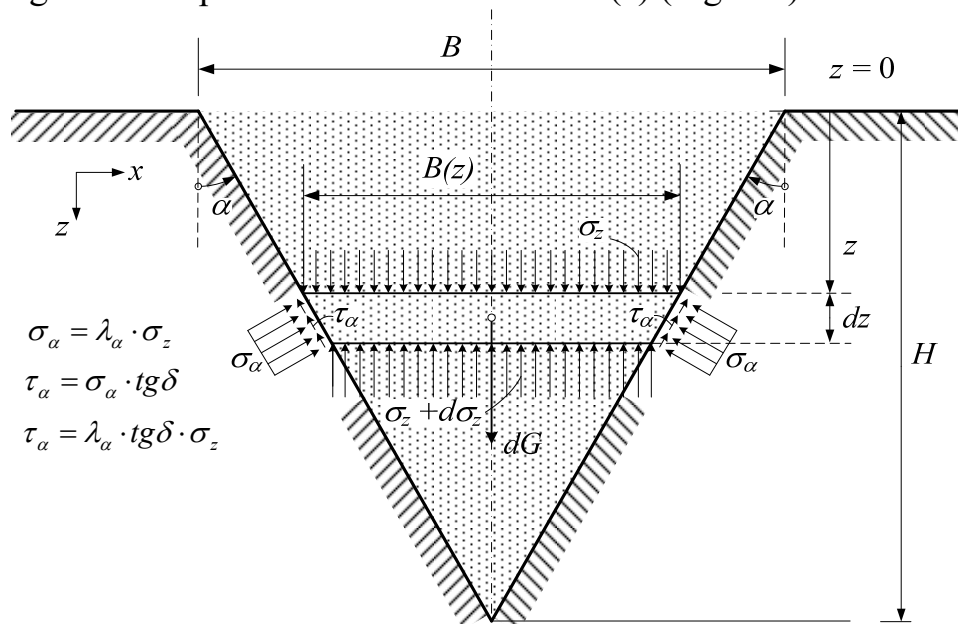


Fig. 6.4 - Estimated pattern of pressure of soil on closely located sloping walls

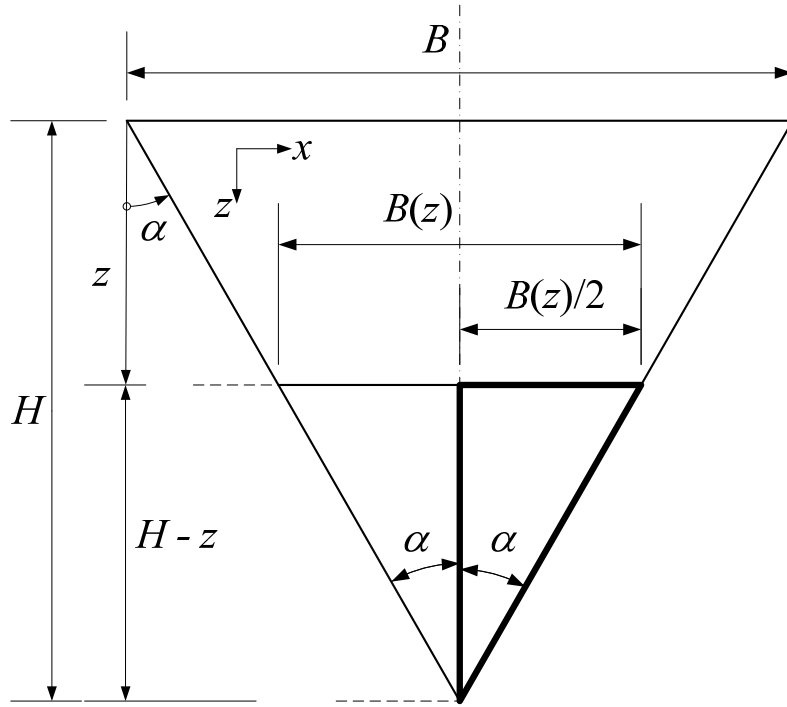


Fig. 6.5 - The calculation scheme of the width function

From the circuit diagram on fig. 6.5 it is obvious that:

$$\operatorname{tg} \alpha = \frac{B(z)/2}{H-z}, \quad (6.11)$$

$$B(z) = 2 \operatorname{tg} \alpha (H-z). \quad (6.12)$$

Find the force of gravity dG acting on the infinitesimal element of the soil (Fig. 6.6).

$$dG = \gamma \cdot \frac{1}{2} (B(z) + B(z+dz)) \cdot dz, \quad (6.13)$$

$$dG = \gamma \cdot \frac{1}{2} (2 \operatorname{tg} \alpha (H-z) + 2 \operatorname{tg} \alpha (H-z-dz)) \cdot dz, \quad (6.14)$$

$$dG = \gamma \cdot \frac{1}{2} (4 \operatorname{tg} \alpha (H-z) - 2 \operatorname{tg} \alpha \cdot dz) \cdot dz, \quad (6.15)$$

$$dG = \gamma \cdot \frac{1}{2} \cdot 4 \operatorname{tg} \alpha (H-z) \cdot dz, \quad (6.16)$$

$$dG = \gamma \cdot 2 \operatorname{tg} \alpha (H-z) \cdot dz. \quad (6.17)$$

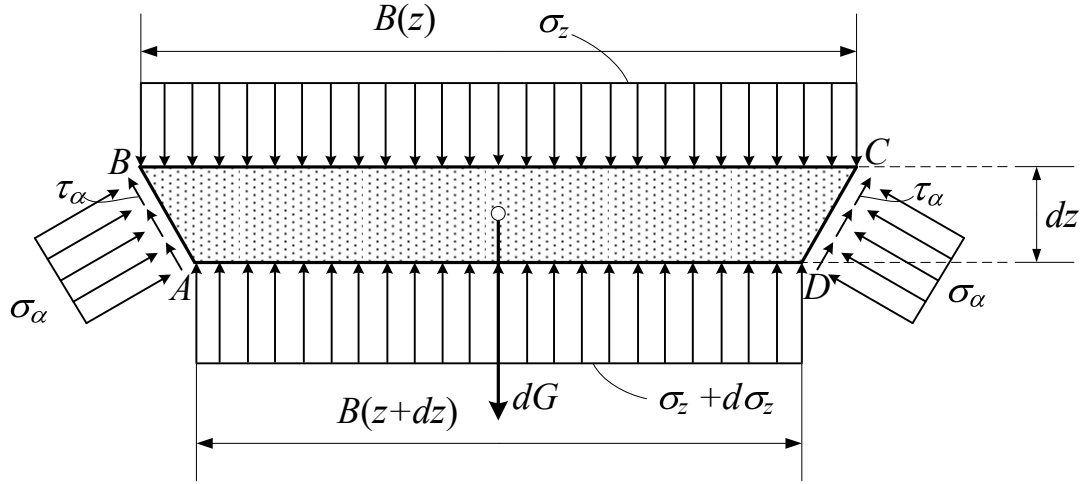


Fig. 6.6 - Infinitesimal element of isotropic soil with inclined position of walls

We set the equilibrium equation for the infinitesimal element (Fig. 6.6) in the direction of the z axis, $F_z = 0$:

$$\sigma_z \cdot B(z) + dG = 2\sigma_\alpha \cdot \sin \alpha \frac{dz}{\cos \alpha} + 2\tau_\alpha \cdot \cos \alpha \cdot \frac{dz}{\cos \alpha} + (\sigma_z + d\sigma_z) \cdot B(z + dz) , \quad (6.18)$$

$$2\sigma_z \operatorname{tg} \alpha (H - z) + 2\gamma \cdot \operatorname{tg} \alpha (H - z) dz = 2\lambda_\alpha \cdot \operatorname{tg} \alpha \cdot \sigma_z dz + 2\lambda_\alpha \cdot \operatorname{tg} \delta \cdot \sigma_z dz + (\sigma_z + d\sigma_z)(2\operatorname{tg} \alpha (H - z) - 2\operatorname{tg} \alpha dz), \quad (6.19)$$

$$2\sigma_z \operatorname{tg} \alpha (H - z) + 2\gamma \cdot \operatorname{tg} \alpha (H - z) dz = 2\lambda_\alpha \cdot \operatorname{tg} \alpha \cdot \sigma_z dz + 2\lambda_\alpha \cdot \operatorname{tg} \delta \cdot \sigma_z dz + \sigma_z \cdot 2\operatorname{tg} \alpha (H - z) - \sigma_z \cdot 2\operatorname{tg} \alpha dz + d\sigma_z \cdot 2\operatorname{tg} \alpha (H - z) - d\sigma_z \cdot 2\operatorname{tg} \alpha dz, \quad (6.20)$$

$$2\gamma \cdot \operatorname{tg} \alpha (H - z) dz = (2\lambda_\alpha g \alpha \sigma_z + 2\lambda_\alpha g \delta \cdot \sigma_z - 2\operatorname{tg} \alpha \cdot \sigma_z) dz + d\sigma_z \cdot 2\operatorname{tg} \alpha (H - z) \quad | : 2dz, \quad (6.21)$$

$$\gamma \cdot \operatorname{tg} \alpha (H - z) = (\lambda_\alpha \operatorname{tg} \alpha + \lambda_\alpha \operatorname{tg} \delta) \cdot \sigma_z + \operatorname{tg} \alpha (H - z) \frac{d\sigma_z}{dz} \quad | : \operatorname{tg} \alpha (H - z). \quad (6.22)$$

As a result, we obtain an ordinary differential equation of the first order

$$\frac{d\sigma_z}{dz} + \frac{\lambda_\alpha \operatorname{tg} \delta + \lambda_\alpha \operatorname{tg} \alpha - \operatorname{tg} \alpha}{\operatorname{tg} \alpha \cdot (H - z)} \cdot \sigma_z = \gamma . \quad (6.23)$$

His joint decision can be written in the form

$$\sigma_z = e^{-\int p(z) dz} \left(\int Q(z) e^{\int p(z) dz} dz + C \right) . \quad (6.24)$$

In our case

$$p(z) = \frac{\lambda_\alpha \operatorname{tg} \delta + \lambda_\alpha \operatorname{tg} \alpha - \operatorname{tg} \alpha}{\operatorname{tg} \alpha (H - z)} = \frac{A}{(H - z)}, \quad (6.25)$$

$$\text{где } A = \frac{\lambda_a \operatorname{tg} \delta + \lambda_a \operatorname{tg} \alpha - \operatorname{tg} \alpha}{\operatorname{tg} \alpha}, \quad Q(z) = \gamma.$$

We solve the integrals in the expression (6.24)

$$\int p(z) dz = \int \frac{A}{(H-z)} dz = -A \ln(H-z). \quad (6.26)$$

We get a substitute for a general solution

$$\sigma_z = e^{A \ln(H-z)} \left(-\gamma \frac{(H-z)^{-A+1}}{-A+1} + C \right). \quad (6.27)$$

Further transformations and simplifications we obtain:

$$\sigma_z = (H-z)^A \cdot (-\gamma) \cdot \frac{(H-z)^{-A+1}}{1-A} + (H-z)^A \cdot C, \quad (6.28)$$

$$\sigma_z = -\gamma \cdot \frac{(H-z)}{1-A} + (H-z)^A \cdot C. \quad (6.29)$$

Under the boundary conditions $z=0, \sigma_z=0$ we have::

$$0 = -\gamma \frac{H}{1-A} + H^A \cdot C. \quad (6.30)$$

$$C = \gamma \cdot \frac{H}{1-A} H^{-A} = -\gamma \frac{H^{1-A}}{A-1}. \quad (6.31)$$

We substitute constant C into equation (6.29):

$$\sigma_z = -\gamma \frac{(H-z)}{1-A} + (H-z)^A \cdot (-\gamma) \frac{H^{1-A}}{A-1}, \quad (6.32)$$

$$\sigma_z = -\gamma \frac{H-z}{1-A} - \gamma \frac{1}{A-1} \cdot H^{1-A} \cdot H^A \left(1 - \frac{z}{H}\right)^H, \quad (6.33)$$

$$\sigma_z = \gamma \frac{H-z}{A-1} - \gamma \frac{H}{A-1} \left(1 - \frac{z}{H}\right)^A. \quad (6.34)$$

In the expression (6.34) we put the brackets $\frac{\gamma}{A-1}$

$$\sigma_z = \frac{\gamma}{A-1} \left(H-z - H \left(1 - \frac{z}{H}\right)^A \right). \quad (6.35)$$

It is known that $A = \frac{\lambda_a \operatorname{tg} \delta + \lambda_a \operatorname{tg} \alpha - \operatorname{tg} \alpha}{\operatorname{tg} \alpha}$ and $H = \frac{B}{2 \operatorname{tg} \alpha}$,

$$\sigma_z = \frac{\gamma}{\lambda_\alpha \operatorname{tg} \delta + \lambda_\alpha \operatorname{tg} \alpha - \operatorname{tg} \alpha} \left(H - z - H \left(1 - \frac{z}{H} \right)^{\frac{\lambda_\alpha \operatorname{tg} \delta + \lambda_\alpha \operatorname{tg} \alpha - \operatorname{tg} \alpha}{\operatorname{tg} \alpha}} \right), \quad (6.36)$$

$$\sigma_z = \frac{\gamma \operatorname{tg} \alpha}{\lambda_\alpha \operatorname{tg} \delta + \lambda_\alpha \operatorname{tg} \alpha - 2 \operatorname{tg} \alpha} \left(\frac{B}{2 \operatorname{tg} \alpha} - z - \frac{B}{2 \operatorname{tg} \alpha} \left(1 - \frac{2z}{B} \cdot \operatorname{tg} \alpha \right)^{\frac{\lambda_\alpha \operatorname{tg} \delta + \lambda_\alpha \operatorname{tg} \alpha - \operatorname{tg} \alpha}{\operatorname{tg} \alpha}} \right), \quad (6.37)$$

$$\sigma_z = \frac{\gamma}{\lambda_\alpha \operatorname{tg} \delta + \lambda_\alpha \operatorname{tg} \alpha - 2 \operatorname{tg} \alpha} \left(\frac{B}{2} - z \operatorname{tg} \alpha - \frac{B}{2} \left(\left(1 - \frac{2z}{B} \operatorname{tg} \alpha \right)^{\frac{1}{\frac{2z}{B} \operatorname{tg} \alpha}} \right)^{-\frac{2z}{B} (\lambda_\alpha \operatorname{tg} \delta + \lambda_\alpha \operatorname{tg} \alpha - \operatorname{tg} \alpha)} \right). \quad (6.38)$$

In the theory of mathematical analysis it is proved that

$$\lim_{\alpha \rightarrow \infty} \left(1 + \frac{1}{\alpha} \right)^\alpha = e, \text{ а также } \lim_{\alpha \rightarrow 0} (1 + \alpha)^{\frac{1}{\alpha}} = e. \quad (6.39)$$

Calculate the boundary of the expression (6.38). In doing so, we use the formula (6.39) to solve the "second remarkable limit." By parameter α can act not only a variable, but also a complex function, which in our case tangent, that is

$$\lim_{\alpha \rightarrow 0} (1 + \operatorname{tg} \alpha)^{\frac{1}{\operatorname{tg} \alpha}} = e. \quad (6.40)$$

If we calculate the boundary $\lim_{\alpha \rightarrow 0} \sigma_z$ in the expression (6.38), which means that the turning of the sloping walls is in the vertical position, we obtain

$$\lim_{\alpha \rightarrow 0} \sigma_z = \frac{\gamma}{\lambda \operatorname{tg} \delta} \cdot \left(\frac{B}{2} - \frac{B}{2} e^{-\frac{2z}{B} \lambda \operatorname{tg} \delta} \right), \quad (6.41)$$

due to the fact that $\lambda_\alpha \rightarrow \lambda$ for $\alpha \rightarrow 0$. We carry the brackets $B / 2$ and in the end we have

$$\lim_{\alpha \rightarrow 0} \sigma_z = \frac{\gamma B}{2 \lambda \operatorname{tg} \delta} \left(1 - e^{-\frac{2 \lambda \operatorname{tg} \delta}{B} z} \right). \quad (6.42)$$

As should be expected, this particular case is the expression (6.10), that is, the formula H. Janssen for the plane problem. This transition is clearly illustrated in Fig. 6.7.

Generalization of the H. Janssen solution for curvilinear walls under the condition of a plane problem. When calculations of normal pressure on a wall of arbitrary curvature inevitably there is a problem of determining the normal pressure factor. It is known that the coefficient of lateral pressure depends on the angle of the slope of the retaining wall α [112]. The variation of the lateral

pressure coefficient according to the Coulomb's theory, depending on the angle of the slope of the wall, is graphically plotted in Fig. 6.8.

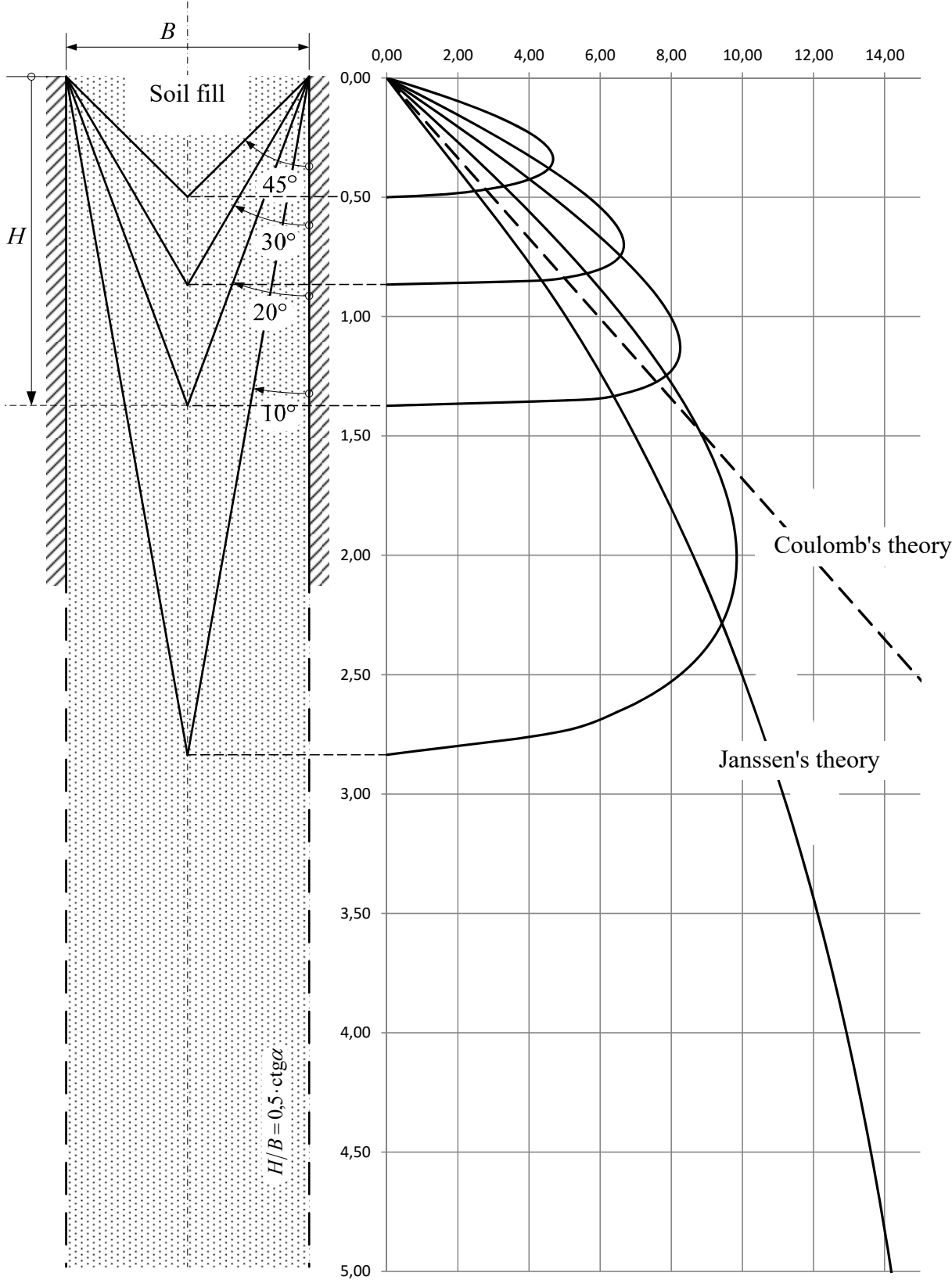


Fig. 6.7 - Graphs of normal pressure at different angles of inclination of closely spaced walls

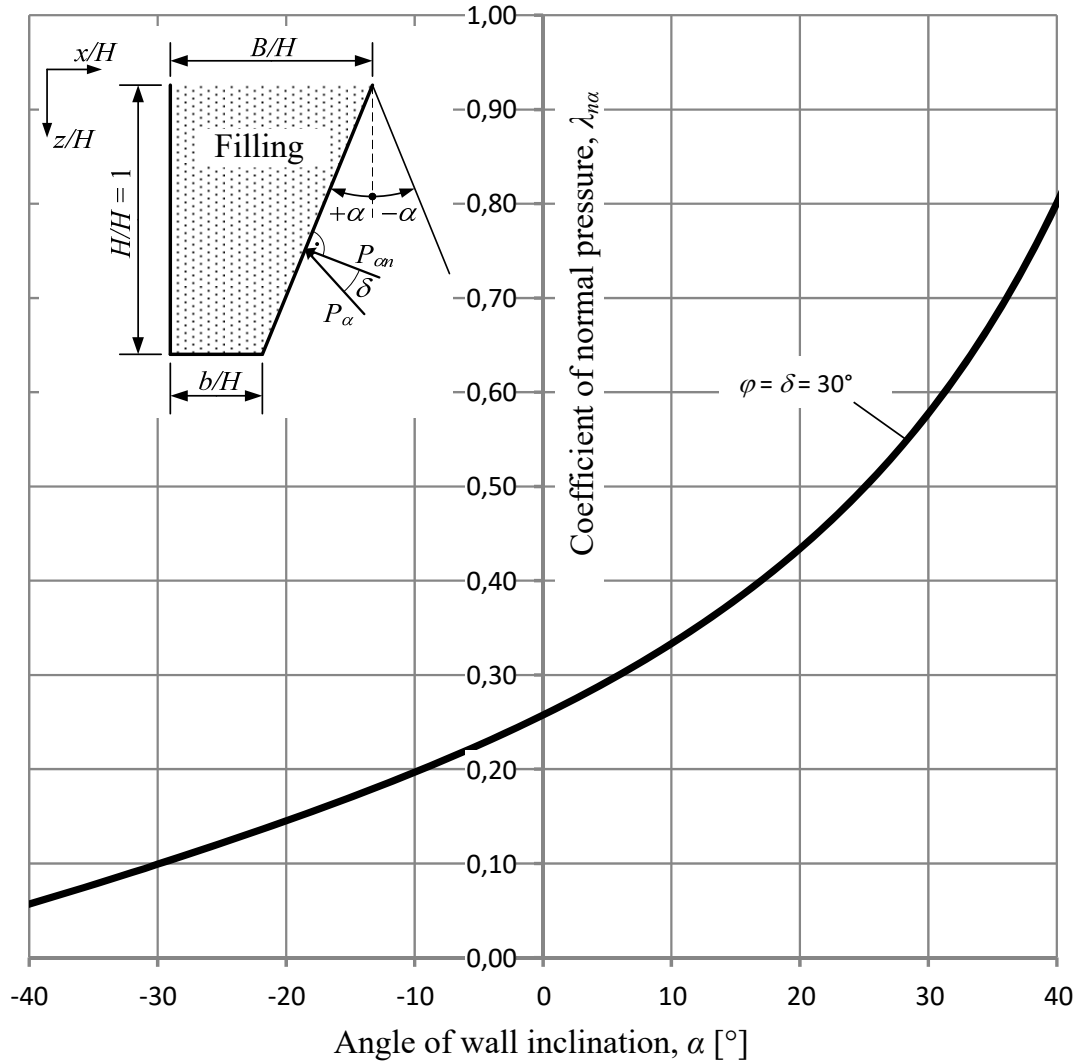


Fig. 6.8 - The coefficient of normal pressure, depending on the angle of the slope of the wall

Fig. 6.8 shows the nature of the change in the normal pressure factor, which increases with an increase in the angle of the wall relative to the vertical. In the case of a wall of arbitrary curvature, the angle of inclination varies depending on the depth, that is, the lateral pressure coefficient is the depth function

$$\lambda_{cn} = \lambda_{cn}[f'(z)] = \lambda_{cn}(z) \quad (6.43)$$

In equation (6.43), the vyzaz $f(z)$ is a function of the shape of the curved wall. It should be noted that the active force of pressure acts at an angle δ to the normal on the wall, and therefore the lateral pressure coefficient on the Coulomb's theory is additionally multiplied by the cosine of the angle δ .

Consider the walls of different curvatures - straight (flat) $f_1(z)$, convex $f_2(z)$ and concave $f_3(z)$. In the end, we will compare the normal vents to the convex and concave wall with respect to the pressures on a flat wall at an angle

of 35° to the vertical for a plane symmetric problem. In fig. 6.9 shows the right side of the calculation scheme.

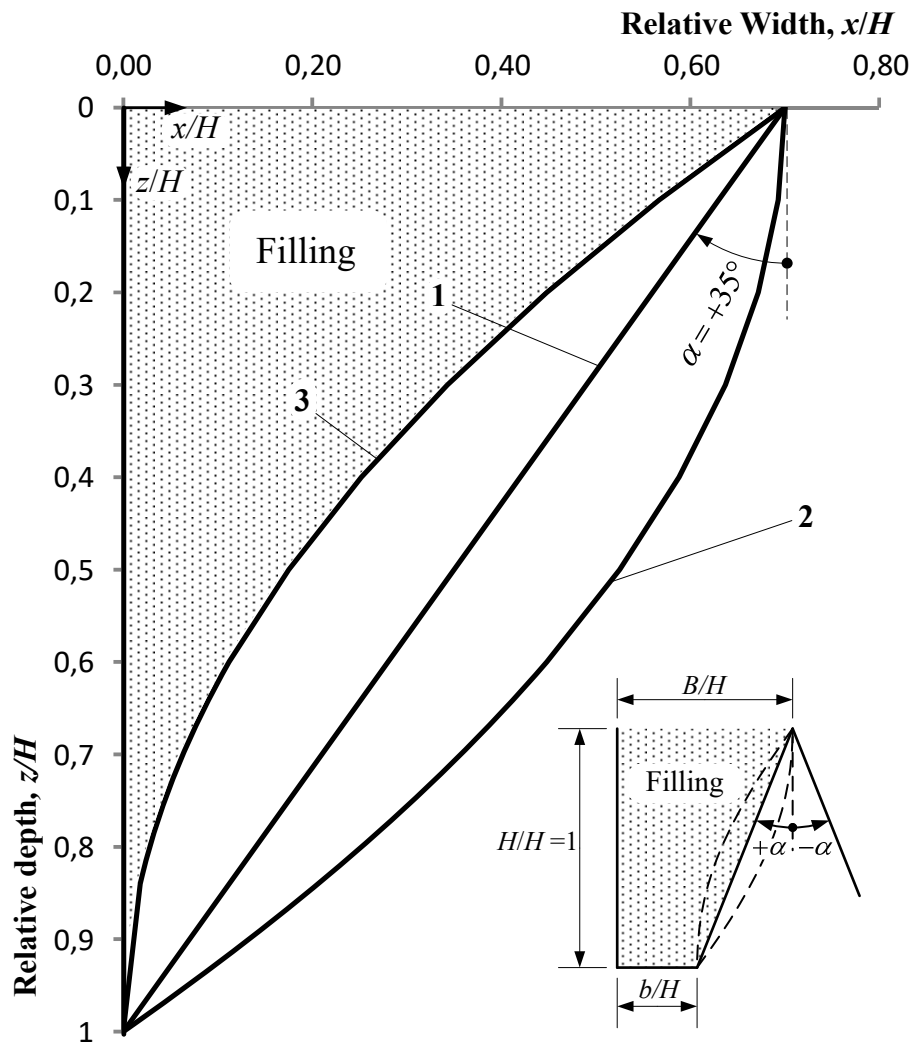


Fig. 6.9 - Scheme, cross section (right side)

As a model material, an isotropic freezing medium with the following characteristics is considered: the internal friction angle $\varphi = 30^\circ$, the friction angle of the medium behind the wall $\delta = 30^\circ$ in the relative coordinates x / H and z / H , with H - the height of the retaining wall.

The following preconditions are taken into account:

- the surface of the filling is horizontal;
- vertical stress σ_z in an arbitrary horizontal plane of the filling medium - uniform;
- there are no tangential stresses on the horizontal planes;
- the friction of the filling medium behind the walls at each point is determined by the coefficient of friction $k_m = \text{tg}\delta$, where δ is the angle of friction of the medium on the material of the wall;

- the normal pressure σ_{an} at the perimeter of the cross-section at z is determined by the normal pressure coefficient λ_{an} and the dependence $\sigma_{an} = \sigma_z \cdot \lambda_{an}$

In fig. 6.10 shows a two-dimensional wedge-shaped infinitely small element with curved side walls.

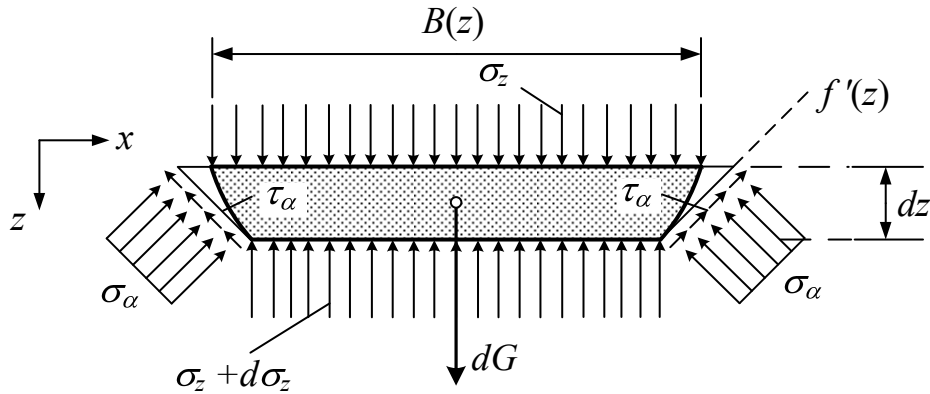


Fig. 6.10 - Infinitesimal element of isotropic soil and effects on it

From the equilibrium condition of the infinitesimal volume element (Fig. 6.10), we get the inhomogeneous linear first-order differential equation

$$\frac{d\sigma_z}{dz} + \frac{\lambda_{an} \text{tg} \delta + \lambda_{an} f'(z) + f'(z)}{f(z)} \sigma_z = \gamma, \quad (6.44)$$

where σ_z - normal pressure at the contact boundary; $f(z)$ - a function that describes the retaining wall; γ - specific gravity of filling.

By the solution of equation (6.44) we obtain the distribution of vertical pressures depending on the relative depth z / H . We solve the differential equation (6.44) numerically using the previously obtained solution for a flat inclined wall (6.45) in the case of a concave and convex wall described by a quadratic function (Figure 6.9)

$$\sigma_z = \gamma \cdot \frac{(H - z)}{A - 1} + (H - z)^A \cdot C, \quad (6.45)$$

where $A = \lambda_{an} \left(\frac{\text{tg} \delta}{\text{tg} \alpha} + 1 \right) - 1$; H - height of the retaining wall; C - constant, which is clear from the conditions of the task; γ - specific gravity of filling.

In fig. 6.11 shows the results of calculations. Clearly, in the case of a convex wall (Fig. 6.11, c, case 2) has a maximum normal stresses that this form of unwanted wall on the other hand is the most profitable form of concave shape (case 3).

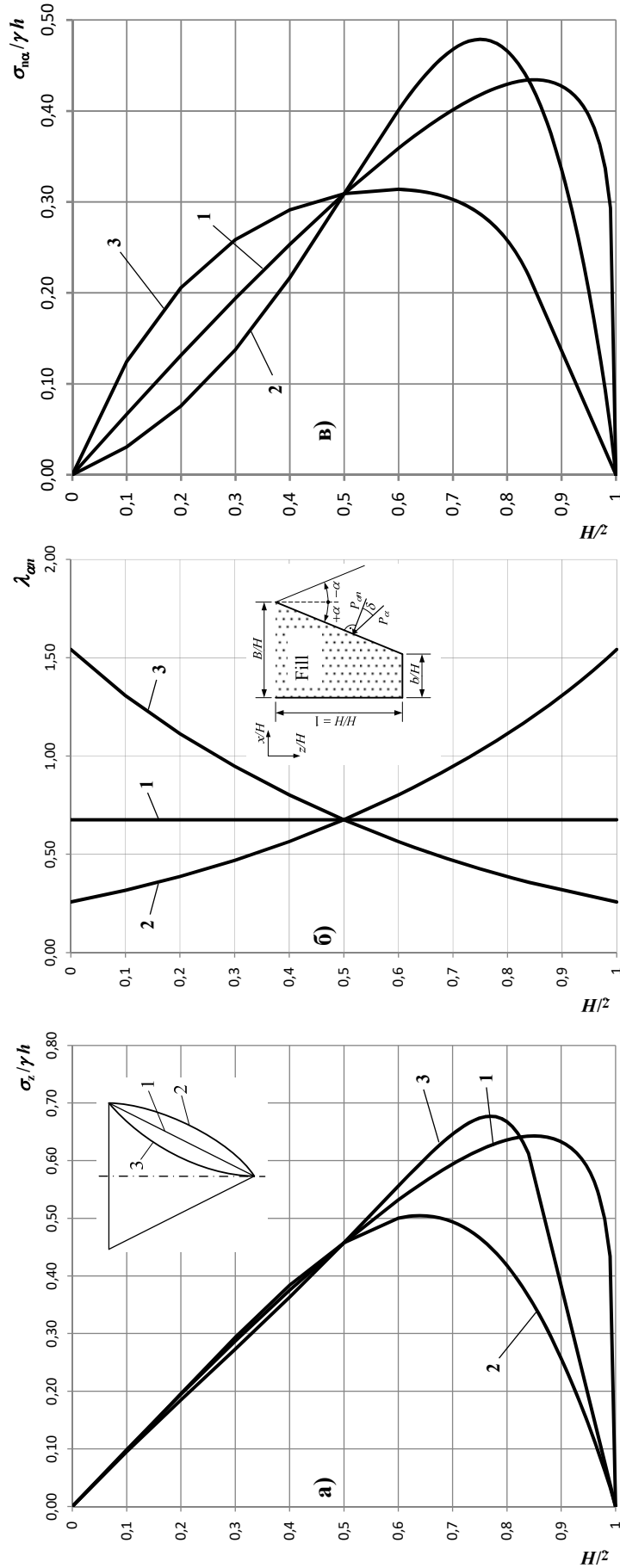


Fig. 6.11 - Charts: a - relative vertical pressure;
 b - normal pressure factor; in - relative normal pressure on curved retaining
 walls: 1 - flat wall, 2 - convex wall, 3 - concave w

It is because of the nature of the change in the normal pressure factor, which is not constant, in the case of 2 the maximum of normal pressure is lower (deeper) than in case 3. Comparison of the curves in Fig. 6.11, c shows that the maximum normal stress, depending on the curvature of the wall, can vary up to about 50%, which is a significant difference.

At first glance the results in Fig. 6.11, in may seem contradictory, since the vertical stress in the case of a convex wall is much less than in the case of a concave wall, given the relation $\sigma_{n\alpha} = \lambda_{n\alpha} \cdot \underline{\sigma}_z$, it seems that in the case of a convex wall, the distribution of normal pressures is more favorable, but on Fig. 6.11, b it is seen that the rate of increase of the coefficient of normal pressure on the wall is not constant, which explains the logic of the results obtained.

The lateral pressure of a homogeneous anisotropic soil on closely spaced walls.

Decision of RN Nedderman RM Nedderman [99] in his work, following the direction of V. Eri and I.P. Prokofiev, by graph-analytical method, solved the problem of determining lateral pressures in closely spaced walls to infinite depths.

The basis of the decision is the following prerequisites:

- closely spaced walls are vertical and rigid;
- the surface of the filling is horizontal;
- areas of sliding - planes;
- the friction of the filling medium behind the walls is constant and is determined by the angle of external friction δ , the friction of the environment behind the walls and on the sliding platforms is fully activated;
- the filling medium is homogeneous and isotropic;
- the force on the left wall E (z) is equal to the previously calculated force on the right wall, that is E (z) = E (h = z) - the principle of symmetry.

The calculation scheme is shown in Fig. 6.12, a. For convenience calculations are considered two coordinate vertical axes: the left - h, and to the right - z, which are connected by dependence (6.17)

$$z = h - B \operatorname{tg} \alpha, \quad (6.46)$$

where B is the distance between the walls; α - angle of inclination of the platform to slip horizontally.

To the depth h0 (Fig. 6.12, a), that is, before the sliding area does not cross the opposite wall, the lateral pressure is calculated according to the classical Coulomb theory.

Consider the equilibrium of forces acting on the prism of slipping ABCD (Fig. 6.11, a). It acts on the force of gravity W, the reaction force of the left and right walls E (h) and E (z), and the reaction force R on the AD slide area. We design all operating forces on the horizontal and vertical axis

$$\Sigma F_x = 0; E(h)\cos\delta - E(z)\cos\delta - R\sin(\alpha(h) - \varphi) = 0, \quad (6.47)$$

$$\Sigma F_z = 0; E(h)\sin\delta + E(z)\sin\delta + R\cos(\alpha(h) - \varphi) - W = 0.$$

By the solution of the system of equations (6.47) we obtain an expression for determining the desired reaction of the left wall or the force of side pressure on the wall - E (h)

$$E(h) = \frac{(W - E(z)\sin\delta)\operatorname{tg}(\alpha - \varphi) + E(z)\cos\delta}{\cos\delta + \operatorname{tg}(\alpha - \varphi)\sin\delta}. \quad (6.48)$$

Because $E(z) = E(h = z)$ (Fig. 6.12), where $E(h = z)$ has already been calculated, then, using formula (6.48), we can calculate the force $E(h)$ for any of any desired depth.

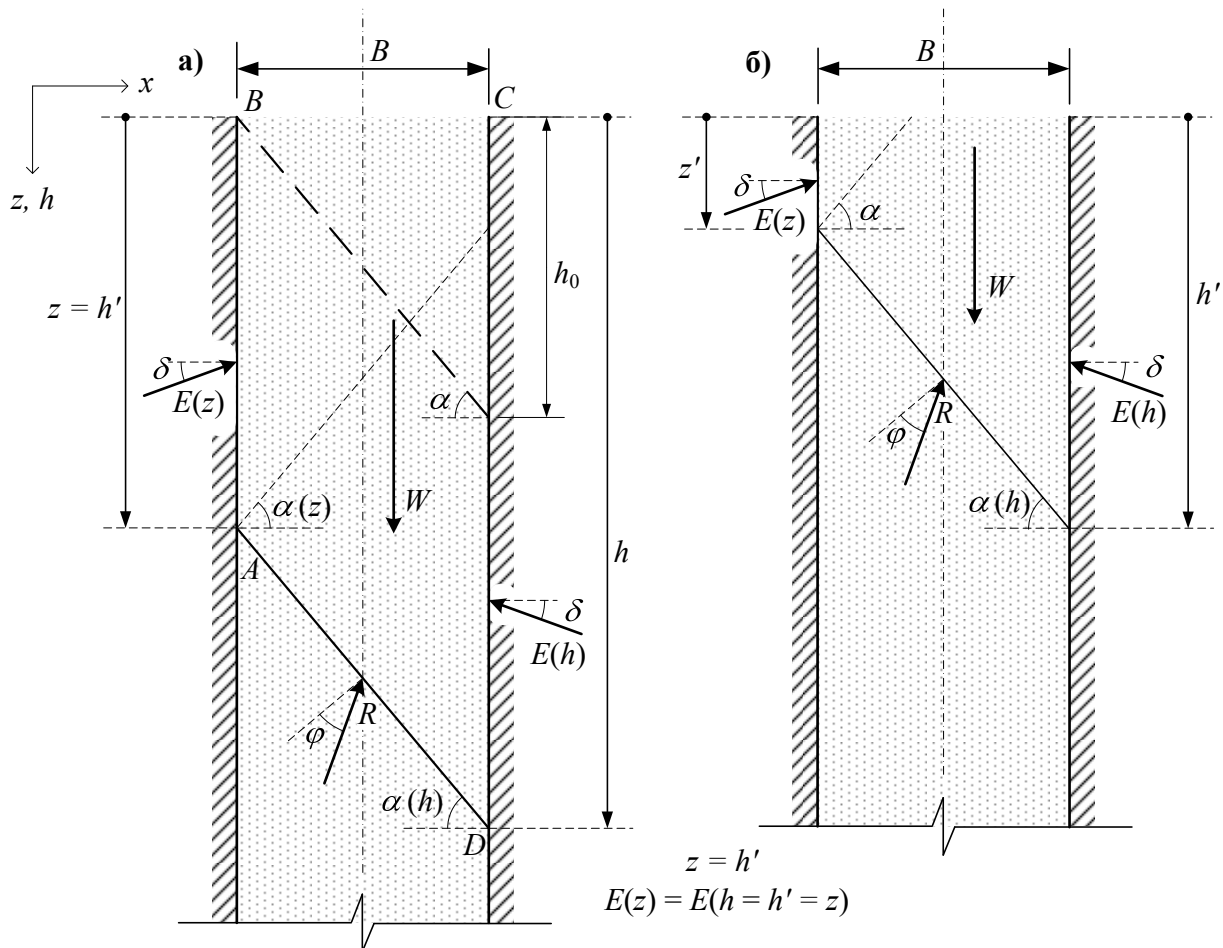


Fig. 6.12 - Scheme of RN Nedderman

For a quantitative comparison of the solution of H. Janssen and the method of prism collapse (RN Nedderman's decision), an algorithm (Figure 6.13) and a

program within the Microsoft Office Excel software program, Visual Basic for Applications, have been developed.

Comparison of the results of calculations is shown in Fig. 6.14.

To the depth h_0 , where the effect of closely spaced walls has no effect, the pressure on H. Janssen is up to 10% higher than the pressure on the Coulomb.

In the future, the numerical difference from the exponential curve of the results of the calculations on the theory of H. Janssen is very small, up to 1.5%.

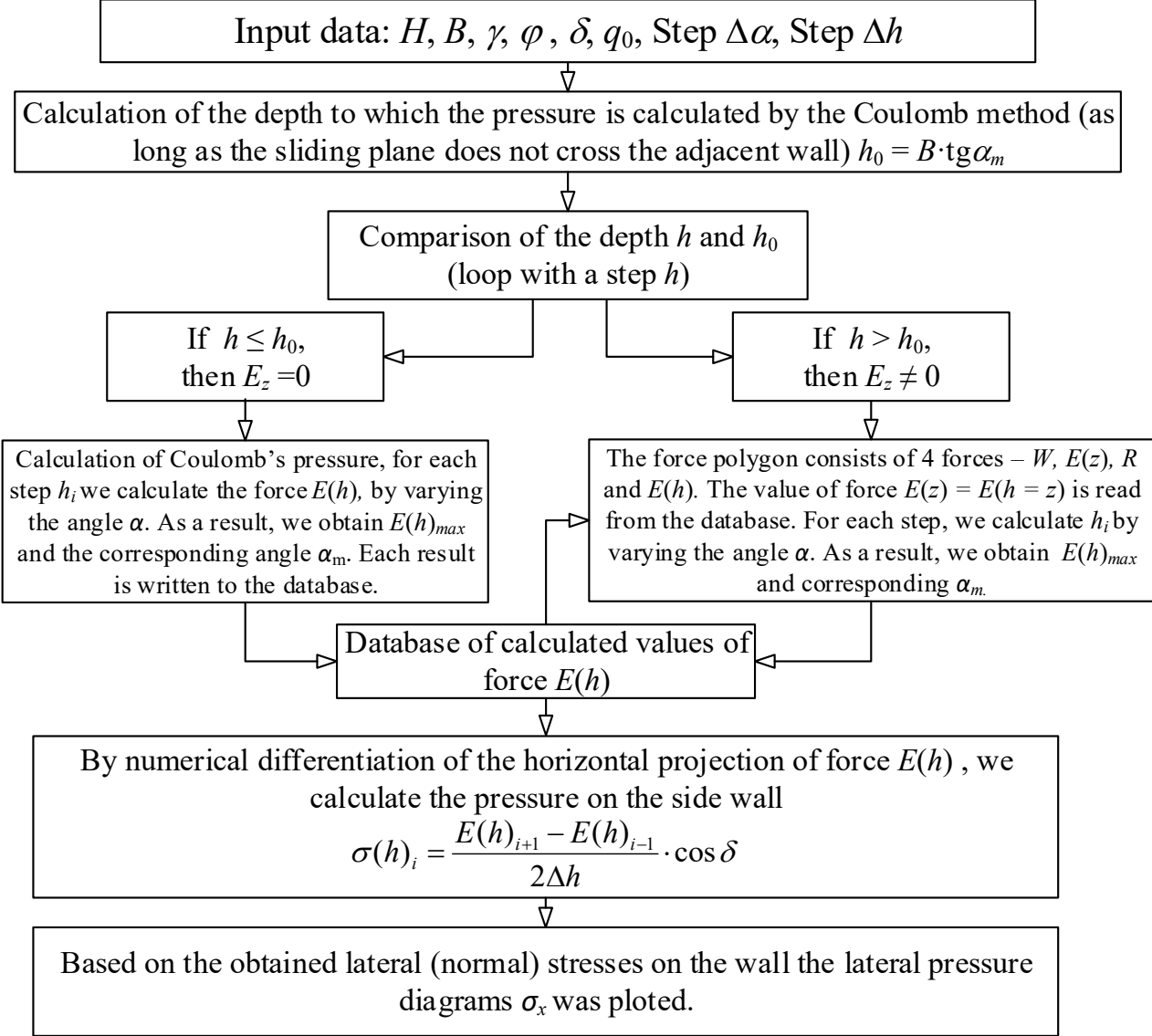
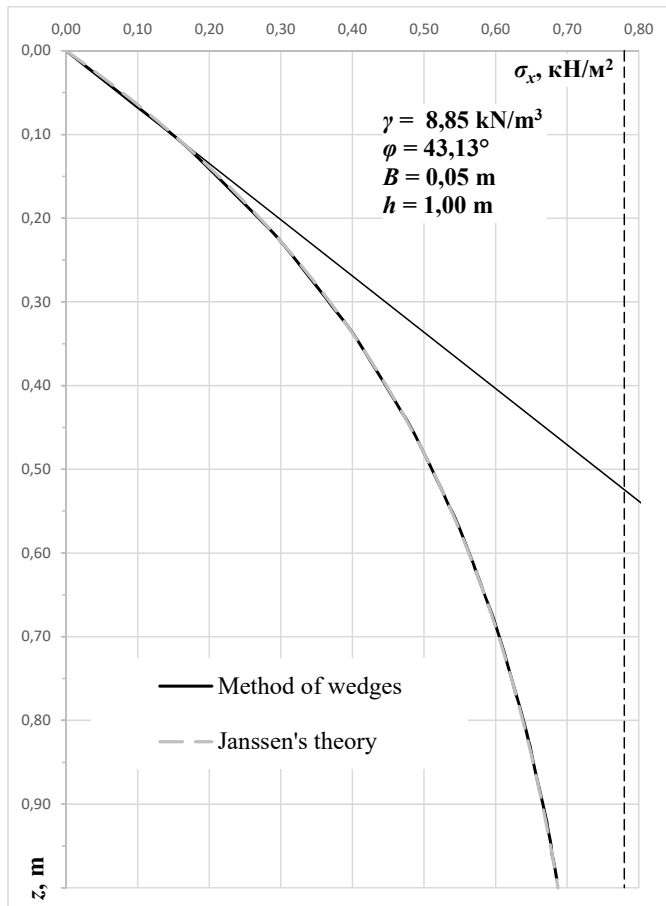


Fig. 6.13 - Calculation Algorithm for the Decision of RM Nedderman

In the decision of RM Neddermana without the influence of loading on the surface of the filler the nature of the pressure increase is monotonous and consists of a series of approximately linear sections.

On the other hand, the distribution of pressure on the theory of H. Janssen has a smooth exponential character and approaches the final value - the boundary of H. Janssen.



z	$\sigma_x, \text{ kN/m}^2$		%
	Janssen	Nedderman	
0,05	0,0789	0,0744	-5,72
0,10	0,1498	0,1487	-0,73
0,15	0,2135	0,2108	-1,27
0,20	0,2707	0,2691	-0,61
0,25	0,3222	0,3211	-0,35
0,30	0,3685	0,3672	-0,36
0,35	0,4101	0,4102	0,03
0,40	0,4475	0,4465	-0,23
0,45	0,4811	0,4820	0,18
0,50	0,5113	0,5110	-0,05
0,55	0,5385	0,5388	0,07
0,60	0,5629	0,5630	0,03
0,65	0,5848	0,5845	-0,06
0,70	0,6045	0,6052	0,12
0,75	0,6223	0,6226	0,05
0,80	0,6382	0,6390	0,13
0,85	0,6525	0,6524	-0,01
0,90	0,6654	0,6661	0,11
0,95	0,6770	0,6777	0,10

Fig. 6.14 Comparison of pressure variations by H. Janssen and R. M. Nedderman

Despite a fundamentally different approach, both solutions give small numerical differences in the absence of loading, which indicates the reliability of both methods. But if loading on the surface of the filler adds significant qualitative and quantitative differences to the epic. In the decision of RM Nedderman lateral pressure increases linearly with depth to some its value h_0 , and then acquire a changing nature. In this case, the slope of the scenes is not constant, but varies from ascending to falling and back in approximately linear regions [99].

An analytical solution (by the method of characteristics [81]) in this case is much closer to the method of prism collapse, which is not surprising, because the basic prerequisite of H. Janssen for the uniform distribution of stresses in horizontal sections is far from reality. The premise of flat sliding platforms in the prism of the collapse method is more realistic [99]. Thus, we arrive at the conclusion that the conformity of solutions in the absence of loading is satisfactory, but if the loading exists, then using the method of H. Janssen should keep in mind the fact of the differences between these solutions.

Generalization of the decision of RM Nedderman for a homogeneous anisotropic filling. The solution of the problem for a homogeneous anisotropic filling at different conditions of laying the bulk material is reduced to the equilibrium of the trapezoid prism in terms of the plane problem (Fig. 6.15).

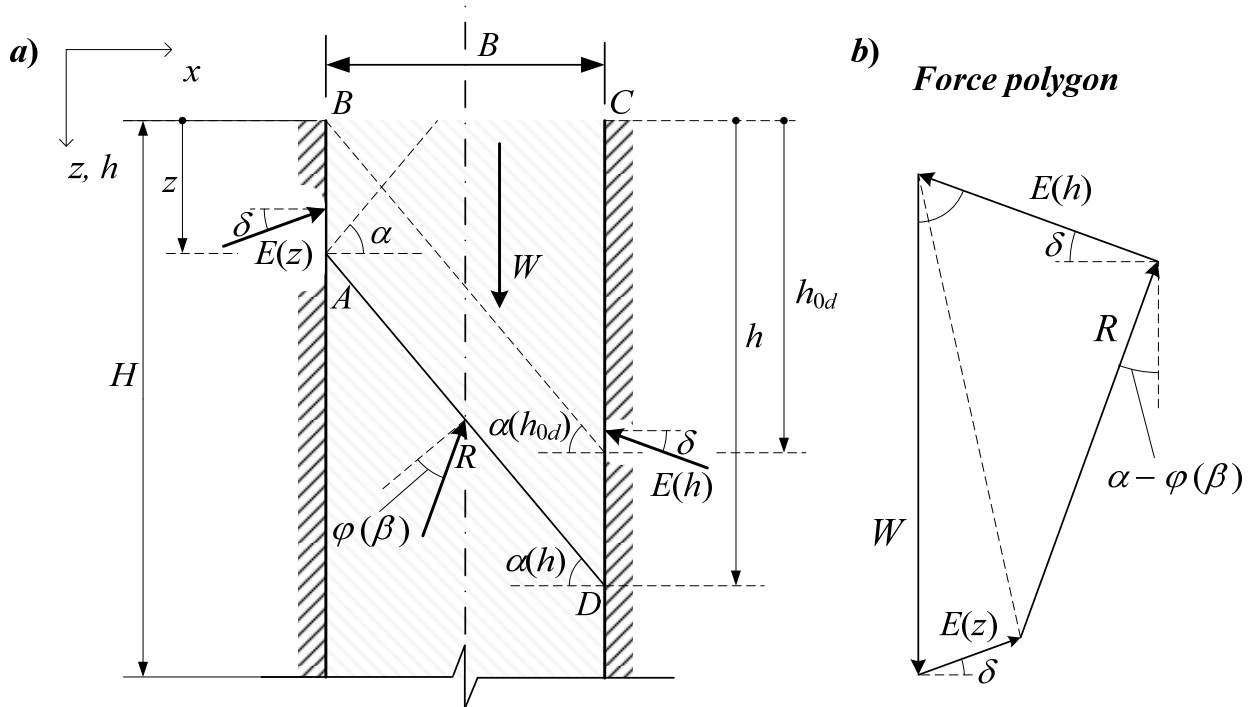


Fig. 6.15 - Scheme for determining lateral pressure

The anisotropy of the bulk material filling at the angle of internal friction is taken into account in accordance with the offer of OV. Schools [60].

The basis of the theory is the following prerequisites:

- closely spaced walls are vertical and rigid;
- the surface of the filling is horizontal;
- the friction of the filling medium behind the walls is constant and is determined by the angle of external friction $\delta(\theta) = \text{const}$.;
- the friction of the environment behind the wall and in the areas of sliding is fully activated;
- a loose filling medium - homogeneous and anisotropic;
- homodographs of anisotropic properties are symmetric and have two axis of symmetry;
- Hodographs of the angle of internal friction and specific coupling satisfy the dependences: $\varphi_n(\beta) = \varphi_n(\beta + \pi)$ and $c_n(\beta) = c_n(\beta + \pi)$.

Like the solution for isotropic soil, consider the equilibrium of forces acting on the prism of the slippage of ABCD (Fig. 6.15, a).

It has the force of gravity W , the force of reaction of the left and right walls $E(h)$ and $E(z)$ and the reaction force R on the AD slide area. The value sought is the force $E(h)$ acting on the right wall.

After projection of forces on the coordinate axes, we obtain the expression (6.49), which is practically identical to formula (6.48), except that the angle of internal friction is defined by the initial hodograph $\varphi = \varphi(\beta)$.

$$E(h) = \frac{(W - E(z) \sin \delta) \operatorname{tg}(\alpha - \varphi(\beta)) + E(z) \cos \delta}{\cos \delta + \operatorname{tg}(\alpha - \varphi(\beta)) \sin \delta} . \quad (6.49)$$

The angle of friction on the wall in directions, as shown in the second section, is the constant value, $\delta(\beta) = \text{const}$. The angle of the orientation of the slider area α is related to the angle β of the site orientation in the hodograph of the expression (6.50). From the method of constructing the hodograph, which is clearly illustrated in Fig. 6.16, it follows that at different angles of filling θ the timeframe of the internal friction angle is transformed in a certain way

$$\beta = 180^\circ - \alpha . \quad (6.50)$$

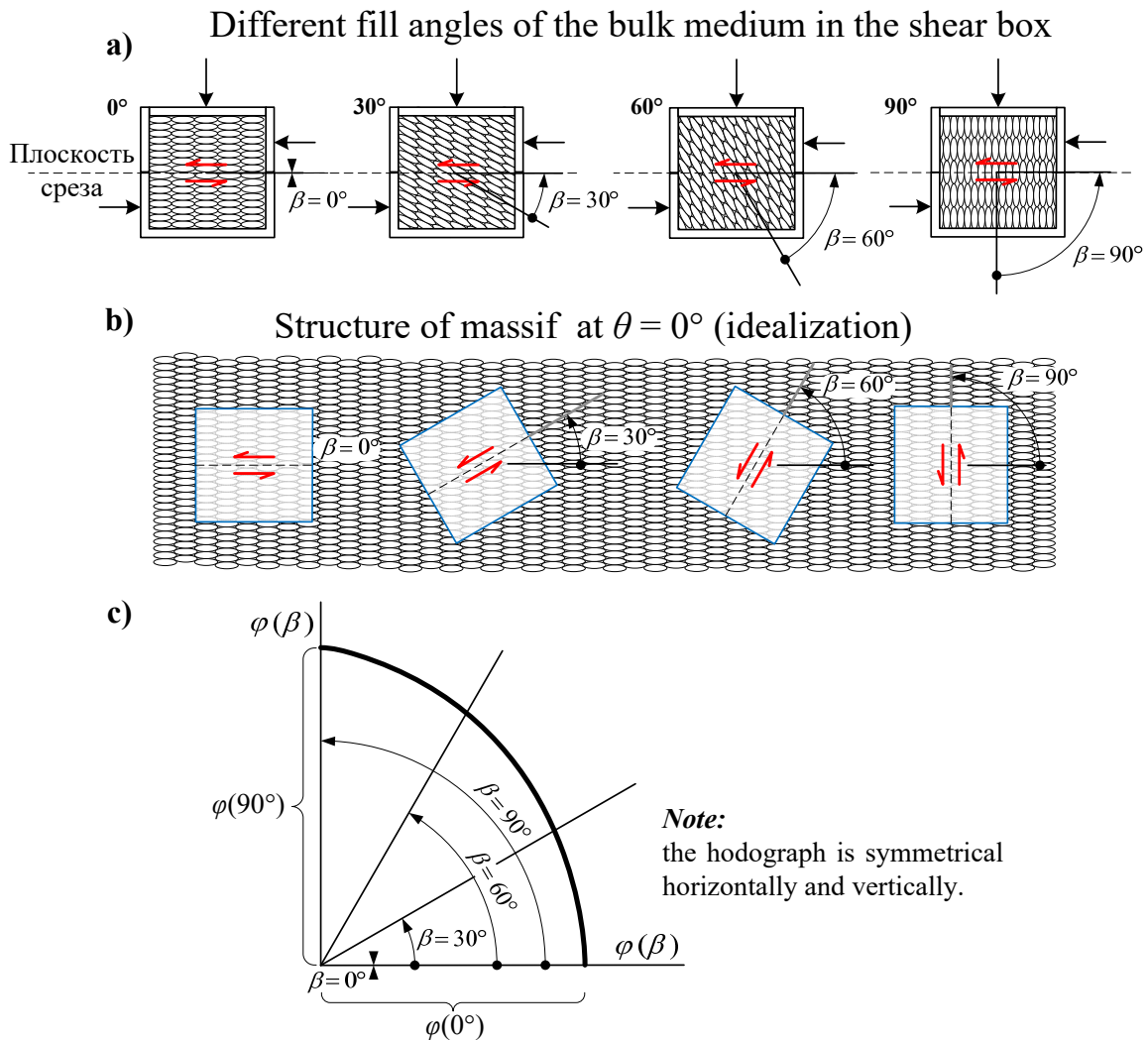


Fig. 6.16 - Method of obtaining the hodograph: a - filling in the cutting chamber; b - samples in the array of bursts; b - the hodograph of the angle of internal friction

The samples, filled in the cutoff clip at an angle β (Fig. 6.16, a), correspond to the angle of sampling β in an array with a horizontal particle orientation, that

is, at $\theta = 0^\circ$ (Fig. 6.16, b), while the hodograph $\varphi = \varphi(\beta)$ looks like it is shown in Fig. 6.16, b.

In the ideal case of oriented fill, every flat particle in the array will be oriented at a given angle of filling θ (Fig. 6.16, b). Due to the fact that the technique of filling the cutters was the same as when filling the model for anisotropic filling carried out at an angle of filling θ , the new, transformed hodograph obtained by turning the original hodograph onto the angle θ corresponds in the same direction (Fig. 6.17).

The solution of the problem for individual cases at the angles of filling of 0° , 90° and 180° is elementary, and it can be carried out according to the algorithm for isotropic filling (Fig. 6.13), taking into account changes in the angle of internal friction in accordance with the output hodograph φ with variation of the angle of orientation of the prism of collapse α .

This is true because in these cases the geometric symmetry and strength symmetry (symmetry of the hodographs of strength) coincides with the vertical axis.

In this case, the equality of forces of active lateral pressure on the left and right walls remains, $E(z) = E(h = z)$.

But in the general case of oriented fill, when the fill angle is in the range $0^\circ < \theta < 180^\circ$, the picture of equilibrium acquires a completely different, asymmetric character (Fig. 6.18).

In this case, the lateral pressure on the left and right walls is different due to the disturbance of the symmetry of strength, respectively, $h_{0l} \neq h_{0d}$ and $\alpha_l \neq \alpha_d$ (Fig. 6.18). It is precisely because of this that an algorithm for isotropic fill requires some correction.

The side pressure forces in the initial section to the depth h_0 do not affect the adjacent wall calculated according to the Coulomb's theory, taking into account the anisotropy of strength [57], with $E(z = h_{0l}) \neq E(h = h_{0d})$.

It should be noted that due to similarity, the angle of orientation of the sliding area α_{lc} and α_{dc} in this interval remains constant.

Let's consider the progression of sliding planes in an array with depth (Fig. 6.19). Unlike the isotropic sample repetition array, the prisms of collapse occur "through the step" (Fig. 6.19, case 1 and 4, case 2 and 5).

Given this feature, we can construct a new algorithm for calculating the side pressure for a homogeneous anisotropic soil with different orientation of the filling θ to an arbitrary depth h .

An enlarged block diagram of the calculation algorithm is shown in Fig. 6.20.

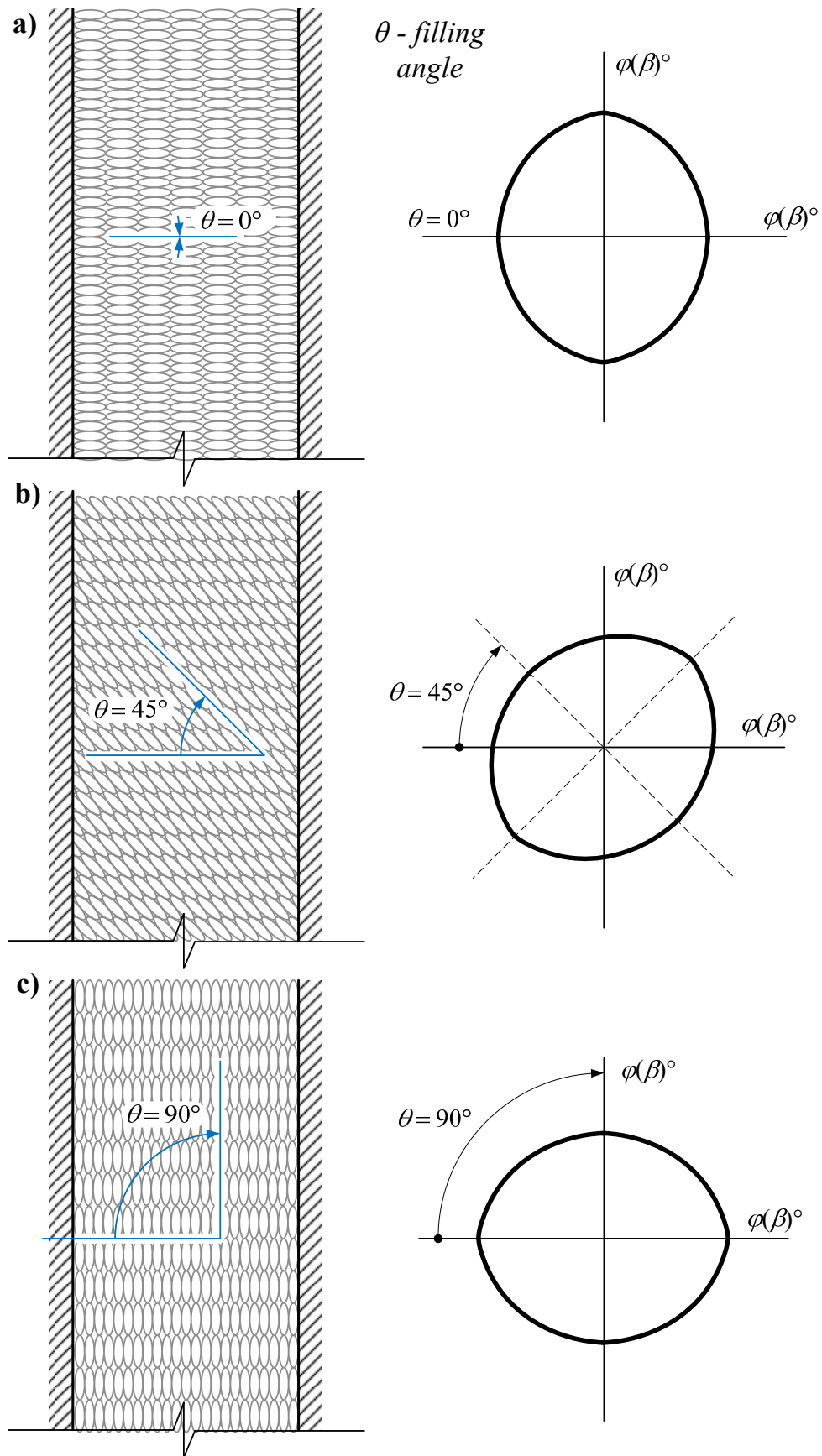


Fig. 6.17 - Hodograph transformation of anisotropy at different angles of filling θ : a - 0° ; B - 45° ; B - 90°

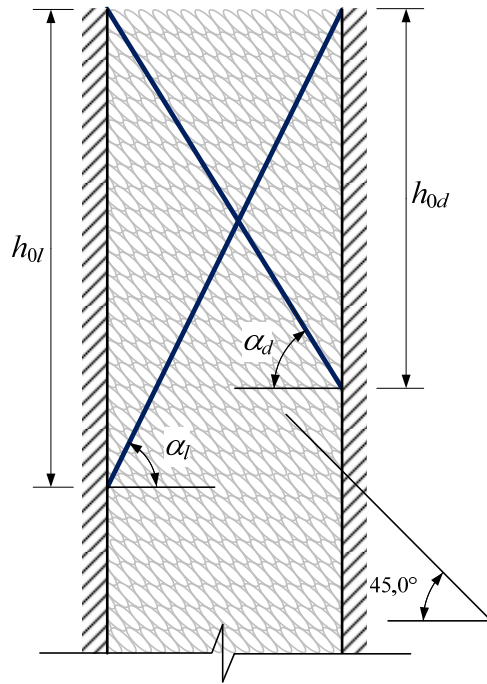


Fig. 6.18 - Asymmetry of the prism of slip at $0^\circ < \theta < 180^\circ$

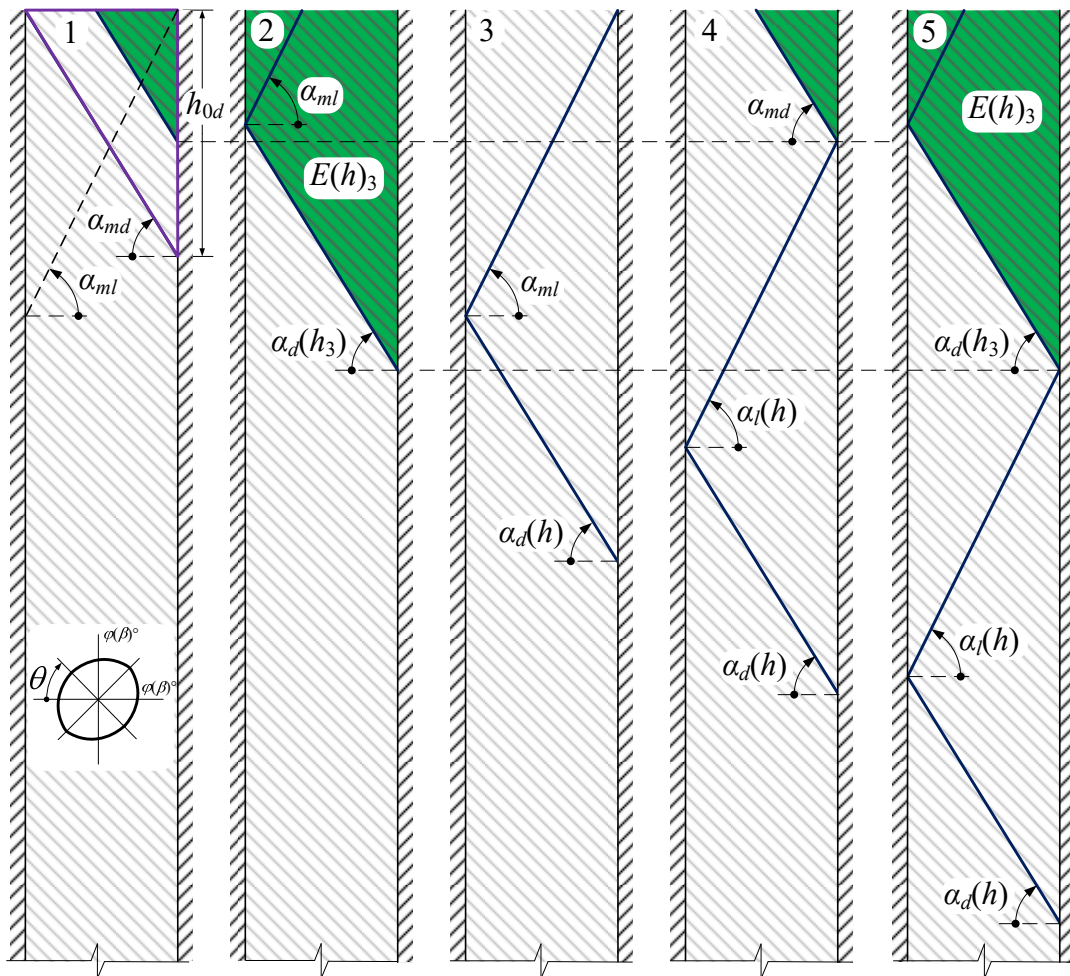


Fig. 6.19 - The order of progress of sliding platforms

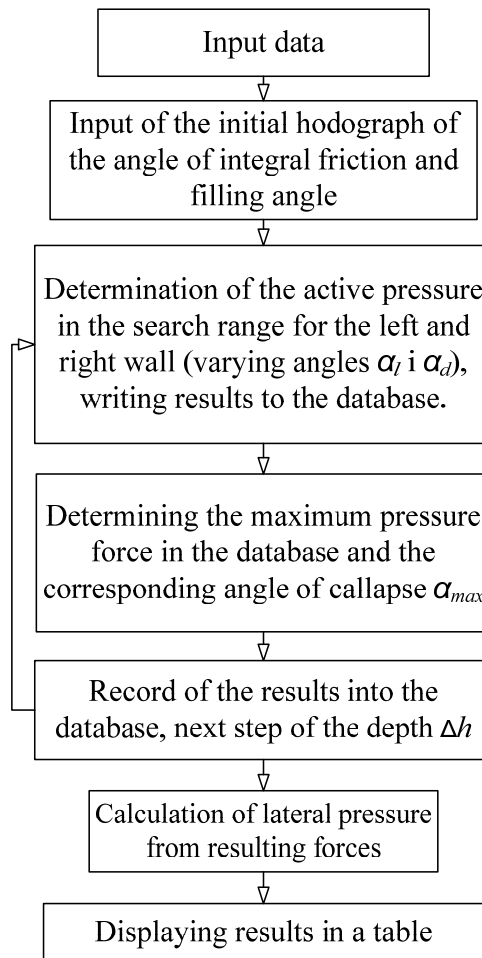


Fig. 6.20 - An enlarged block diagram of the algorithm for anisotropic filling

Analysis of calculation results for different conditions. For numerical analysis of the results of the theory, a computer program has been developed within the framework of Microsoft Office Excel, which is compiled in the Microsoft Visual Basic for Applications computer language.

The program allows you to calculate the side pressure at different angles of material filling. The corners of the filling can vary in the range from 0° to 180° , and the depth of calculation is not limited.

When assigning the hodographs $\varphi(\beta) = \text{const}$, the results obtained correspond to an isotropic fill, which allows to make calculations under the program for isotropic congestion. Hourographs in the program can be approximated by quadratic functions.

The calculations used the initial data from the anisotropy hodographs for rice and composite material.

The lateral pressure was calculated for the angles of filling 0° , 45° and 90° for comparison with experimental data.

The results of calculations and comparisons are shown in Fig. 6.21 - 6.23.

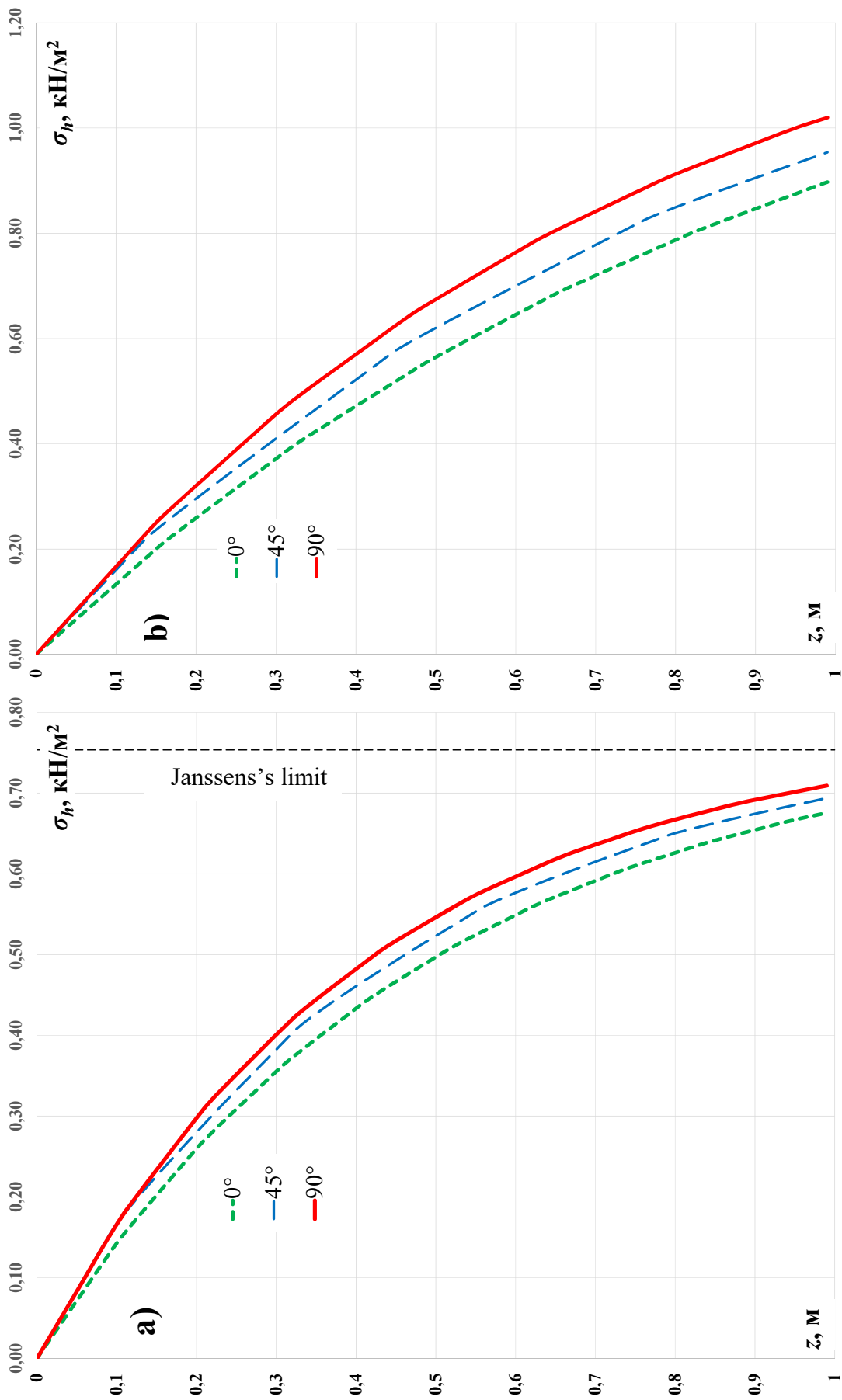


Fig. 6.21 - Results of theoretical calculations of lateral pressure at different angles of filling of 0° , 45° and 90° : a - rice; b - composite material

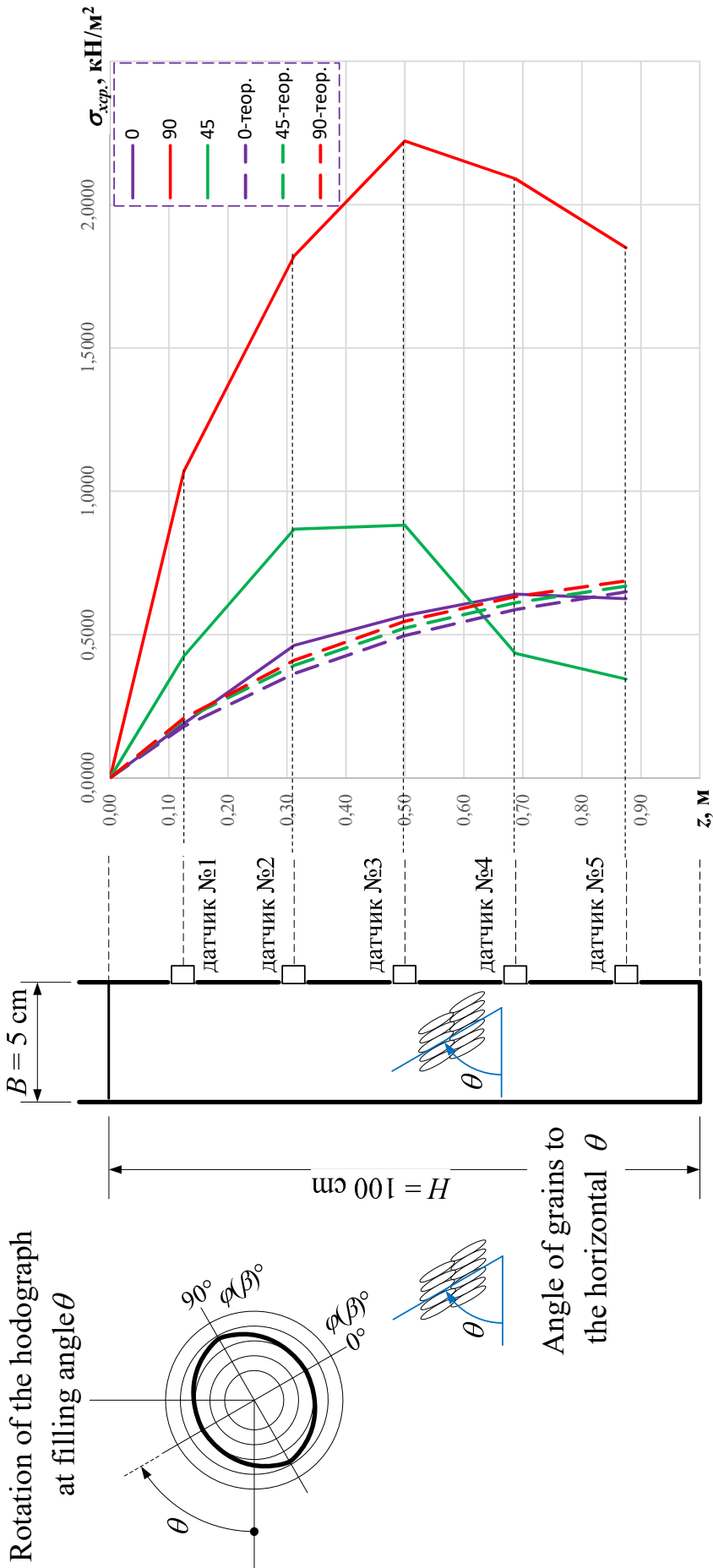


Fig. 6.22 - Comparison of theoretical calculations and experimental data for rice

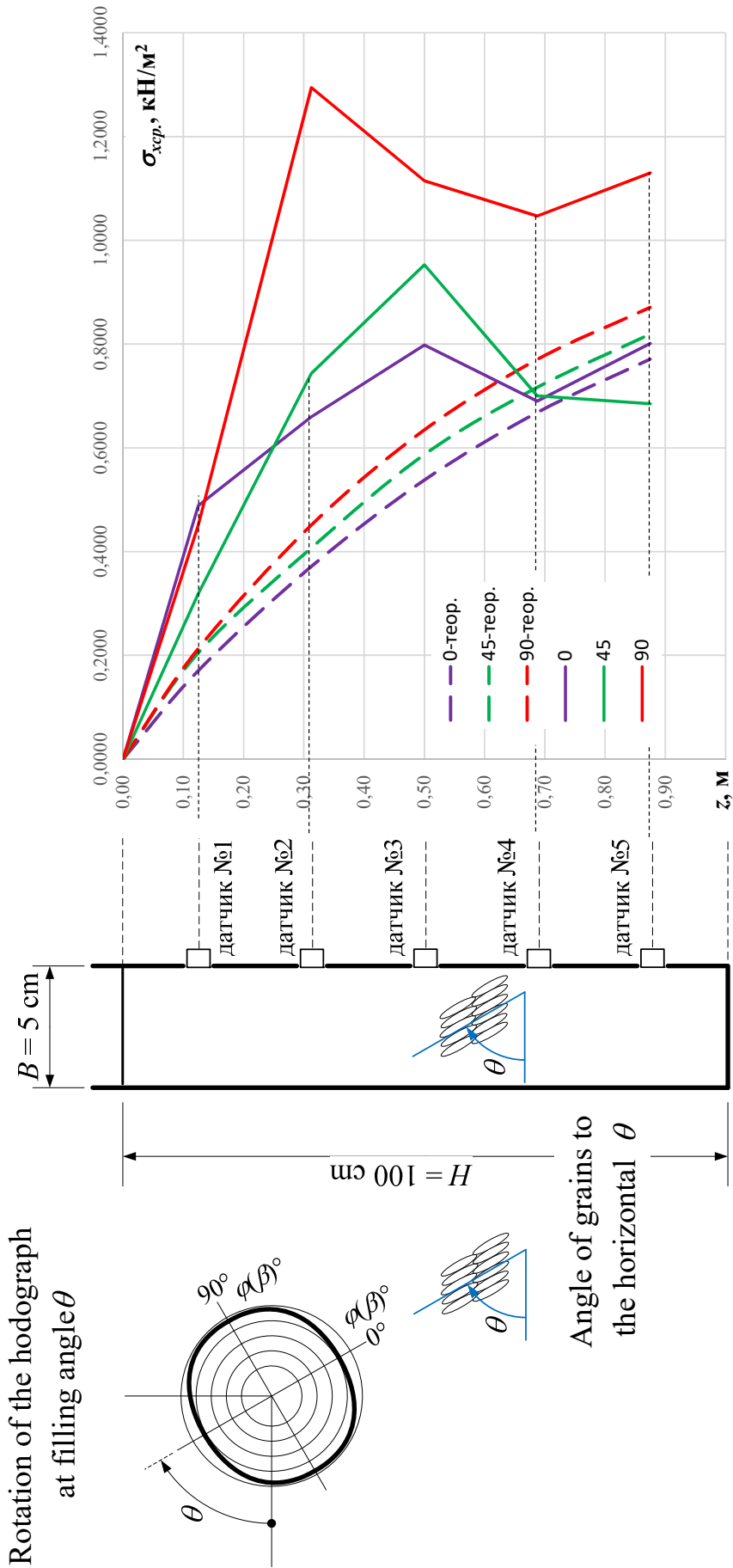


Fig. 6.23 - Comparison of theoretical calculations and experimental data for a composite medium

The analysis of the graphs (Figure 6.21) shows that the side pressures depend essentially on the orientation of the plane of the hodograph θ , and, consequently, on the strength indicators in directions. Compared to an isotropic medium, the abatement reaches 15% for rice and 25% for the composite medium, which confirms the need to take into account anisotropy of strength when designing spacers with closely spaced walls.

Differences in the pressure for the outgoing hodographs of rice at the filling angles $\theta = 0^\circ$ and 90° are significant (Fig. 6.21 a), they are maximum at a depth of 0.11 m and equal to 16.62%.

In case of filling of composite material (Fig. 6.21, b), the rupture of the values is higher and reaches 25.24% at a depth of 0.13 m, and at the depth of 1 m the corresponding differences make 4.98% and 13.65%.

At filling angles $\theta = 0^\circ$ and 45° to the depth of influence according to the Coulomb h_0 , where the sliding area touches the opposite wall, the difference for rice is approximately, as in the case of $\theta = 0^\circ$ and 90° , 17.72% to a depth of 0,08 m, the further reduction is substantially reduced and approximately twice smaller than at $\theta = 90^\circ$.

For a composite material, the rupture of values at $\theta = 0^\circ$ and 45° is 20.29% to a depth of 0.13 m, and then decreases and drops to 6.3% at a depth of 1 m

For both loose media, the horizontal pressure difference $\Delta\sigma_h$ is not constant, and decreases with depth. The trend of the growth of the pressure curves shows the approximation of this difference to zero with increasing depth.

Experimental curves show a similar tendency, but at a much lower rate (Figures 6.22 and 6.23).

Comparison of experimental and theoretical data (Figures 6.22 and 6.23) in both cases shows qualitative convergence

But quantitatively at $\theta = 0^\circ$ and 90° , the differences in the values of experimental pressures exceed calculated, for rice they averaged 16.62%, which is much less than the difference of experimental pressures 294%, and in the case of composite fill, the differences in about 1,8 times higher than in theoretical calculations and make up 44.2%.

Apparently, the difference in experimental data is due to several factors - the intrusion of particles into the space between particles due to the action of gravity forces, which occurs when the model is rotated to the vertical position and the dynamic effects of rotation of the model, which are not taken into account in theoretical calculations.

In general, the results allow us to formulate the following conclusions:

1. When the graph $\varphi(\beta) = \text{const}$ solution degenerates into a solution for isotropic soil, the principle of conformity is observed;
2. When coincidence of geometric symmetry and strength symmetry with respect to vertical values of pressure on both walls are equal;

3. When the angle of filling θ increases from 0° to 90° , the pressure on the wall increases, at which angle θ is supported by its edge
4. The variability at different angles of filling θ decreases with increasing depth;
5. Experimental and theoretical data show qualitative convergence, but the quantitative results of measurements are times higher, which is explained by the squeezing of particles into space (pores) between honests and through dynamic influence;
6. Forming homographs of durability, by improving the technology of creating soil entrainment can significantly reduce the pressure of soil.

Thus, the following conclusions are possible.

1. An analytical generalization of the classical solution for determining the lateral pressures of isotropic soil on closely spaced walls - the theory of H. Janssen on the inclination of the wall and the walls of arbitrary curvature for a plane symmetric problem is obtained. With zero curvature and angle orientation of the wall $\alpha = 90^\circ$ the solution degenerates into H. Janssen's solution, which indicates compliance with the principle of compliance; in the case of a convex wall there is a maximum normal stress, that is, this form of the wall is undesirable; on the other hand, the most advantageous form is a concave shape, which is appropriate to be introduced into the design practice.
2. Approximate solution of the definition of lateral pressure on closely spaced walls for a homogeneous anisotropic filling at different angles of filling θ on the basis of Coulomb's theory for a plane problem, using the solution of RM Neddermann and the theoretical proposition on taking into account the anisotropic properties of the material A.V. Shkola
3. A program for calculating the side pressure of a homogeneous anisotropic soil on closely spaced walls in the Algorithmic language Visual Basic for Applications within Microsoft Office Excel 2013. The program allows you to determine the lateral pressure at arbitrary given hodographs at the corners of the internal friction and corners of the filling θ .
4. The calculated results are analyzed and compared with the given measurements. At different angles of filling, the theoretical results showed differences in side pressures up to 25%. Comparison with the results of measurements showed qualitative convergence, and in absolute values measured pressure exceeds the calculated values.

6.2. Deformation anisotropy calculation in determination of settling of bases and foundations

An advanced analytical approach is proposed to take into account certain geotechnical effects, in particular those that are characteristic for the consolidation of foundations.

At the same time, the method of layer-summing was adopted as the basic one, recommended by DBN B.2.1-10-2009 [15] for the practical calculations of settling of foundations of foundations.

The subsidence of the base in it is determined using a calculation scheme in the form of a linearly deformed semispace by the formula

$$S = \beta \sum_{i=1}^n \frac{\sigma_{zp,i} h_i}{E_i}, \quad (6.51)$$

where β - coefficient equal to 0.8; $\sigma_{zp,i}$ - average value of additional pressure in the elementary layer of soil; h_i, E_i - respectively, the thickness and deformation module of a layer of soil; n - the number of elementary layers within the compressible layer.

Possible ways of clarifying the calculation of settling basics by layer summing one of the authors in conjunction with AV Yakovlev [7] considers the calculation:

- 1) the variability of the deformation module of the soil throughout the range of pressure that perceives the basis of the load;
- 2) coefficient of soil strength;
- 3) deformation anisotropy of soils;
- 4) the regularities of the change in the value of the deformation module of the soil for the depth of the array under the foundations and within the limits of artificial bases, which are reduced with the consolidation of the soil.

In the explanations to [15] among the characteristics necessary for the design of the bases, we refer to the deformation module, which is proposed to determine for the soil of the natural state or taking into account the possibility of increasing the humidity, in the pressure interval of $\sigma = 0.1 - 0.2$ MPa, that is, the deformation module is accepted as a constant.

But in other pressure intervals, in accordance with the definition of the compression curve, the value of this module is not the same (see, for example, Section 5.1).

So, in tabl. 6.1, typical examples of defining characteristics of deformation of clay soil are given, depending on the standard pressure levels for different loamy density.

According to the results of compression tests, according to the standard method of DSTU B B.2.1-4-96 [16] samples of wood semi-solid loam with a natural moisture content of $w = 0.24$ and a porosity coefficient of $e = 0.86$ in the

range of voltages from 0 to 2.7 MPa, the growth value of the deformation module from 3 to 22 MPa was obtained.

It is expedient to take into account the variation of the soil deformation module, based on the known dependence between deformations and stresses, which has the highest probability in the power form

$$\Delta h = b(\sigma_i / \sigma_0)^a . \quad (6.52)$$

Table 6.1 - Examples of variability of deformation module values by the results of compression tests loam

Place of sampling of soil	Porosity coefficient e	Humidity w, %	Modulus of deformation of soil, MPa E, , in intervals of vertical pressure, MPa σ ,			
			0 - 0.05	0.05 - 0.1	0.1 - 0.2	0.2 - 0.3
in an array of natural structure	1.45	25	0.765	1.06	1.19	0.53
	1.27	18	1.83	1.35	1.03	0.81
	0.74	20	5.43	4.85	9.52	6.25
	0.67	16	5.95	5.21	10.4	6.40
	0.56	15	5.56	6.49	7.81	13.0
in a grant pillow	0.48	16	17.0	10.5	12.2	16.2
	0.46	14	24.1	11.4	14.0	22.8
under the NPSP	0.60	19	13.2	9.7	12.7	9.80

In the case of compression tests in expression (6.52) Δh is the deformation of the sample from the voltage at the achievement of conditional stabilization (according to DSTU B V.2.1-4-96 is the rate of deformation 6.25·10⁻⁴ mm / h).

Empirical coefficients: - dimensionless value, which fluctuates within rather narrow limits, for example for clay soils of Poltava region a = 0.6-1.5.

The proportionality factor b has a linear dimension that corresponds to the dimension Δh and varies in a much larger range from a few units to several dozen. The value b is closely related to the coefficient of soil porosity e₀.

Using (6.52) it is easy to adjust the equation of the compression curve:

$$e_\sigma = e_0 - \frac{b(\sigma_i / \sigma_0)^2}{h} (1 + e_0), \quad (6.53)$$

where e₀ and e_σ - respectively, the coefficients of soil porosity at σ = 0 and σ = σ_i, and h - the height of the sample.

In any vertical pressure interval, based on (6.53) and classical expressions of soil mechanics, the coefficient of compressibility

$$m_0 = \frac{\left[e_0 - \frac{b(\sigma_H / \sigma_0)}{h} (1 + e_0) \right] - \left[e_0 - \frac{b(\sigma_K / \sigma_0)}{h} (1 + e_0) \right]}{\sigma_K - \sigma_H}, \quad (6.54)$$

where σ_H and σ_K - the vertical stresses of the beginning and end of the interval. After simplification, we have an expression

$$m_0 = \frac{b(1 + e_0) \left[(\sigma_K / \sigma_0)^a - (\sigma_H / \sigma_0)^a \right]}{h(\sigma_K - \sigma_H)}. \quad (6.55)$$

The given coefficient of compression is equal to

$$m_v = \frac{b \left[(\sigma_K / \sigma_0)^a - (\sigma_H / \sigma_0)^a \right]}{h(\sigma_K - \sigma_H)}. \quad (6.56)$$

Finally, the formula for determining the deformation module has the form:

$$E = \frac{\beta_z \cdot h \cdot (\sigma_K - \sigma_H)}{b \left[(\sigma_K / \sigma_0)^a - (\sigma_H / \sigma_0)^a \right]}. \quad (6.57)$$

where β_z - the coefficient taking into account the absence of transverse expansion of the soil in the compressor device (not to be confused with the coefficient in formula (6.51)) and which is calculated according to the known formula (5.29) of DSTU B V.2.1-4-96 depending on the coefficient of transverse deformation (Poisson coefficient) ν . In the absence of experimental data, clause 5.4.7.5 of the State Standard B of V.2.1-4-96 allows taking depending on the type and condition of the soil.

The coefficient β_z depends on the indices of the physical and mechanical properties of the coherent soil. It can be determined by the formula [7]

$$\beta_z = \frac{0.5 \cdot \sigma_1 \cdot (1 - \sin \varphi_{II}) - c_{II} \cdot \cos \varphi_{II}}{\sigma_1 - c_{II} \cdot \cos \varphi_{II}}, \quad (6.58)$$

where σ_1 - vertical pressure acting under the sole of the foundation for conditions $b = 0$; φ_{II} , c_{II} - the angle of internal friction and specific gravity for water-saturated coherent soil.

Then, for the method of layer summing, the settling of the base will be

$$S = \beta \cdot \sum_{i=1}^n \frac{(\sigma_n + \sigma_k) \cdot 0.5 \cdot h_i}{\beta_z \cdot h \cdot (\sigma_n - \sigma_k)} \cdot b \cdot [\sigma_n^a - \sigma_k^a]. \quad (6.59)$$

Equation (6.59) is final and, taking into account the expressions (6.57) and (6.58), allows us to improve the calculation of settling of the foundations of the foundations of buildings

Now, with the help of the expression (6.59), having the values H_c of additional stresses on the boundary of the auxiliary layers, which are divided into compressive thickness, it is quite easy to take into account the variability of the deformation module by the nature of the additional pressure diagram.

Of course, if there are within the compression layer different layers of soil properties, the parameters a and b should be set separately for each layer.

Here is a fairly simple example of this calculation: for separate foundations of different sizes with depth of laying $d = 2$ m, under the sole of which acts the average pressure $p = 250$ kPa.

At the base - the forest loam, which in the water-saturated state has strength indicators $\varphi_{II} = 22^\circ$, $c_{II} = 15$ kPa

In tabl. 6.2 contains data on the averaging of six long compression tests of loam, conducted prior to the achievement of the standard rate of conditional stabilization ($v = 6.25 \cdot 10^{-4}$ mm / h). Sample height $h = 35$ mm

Table 6.2 - Summary of compression test loam

	Vertical pressure, MPa						
	0.00	0.05	0.10	0.15	0.20	0.25	0.30
Deformation Δh , mm	0.00	0.18	0.45	0.67	0.96	1.20	1.40
Porosity coefficient, e	0.843	0.833	0.821	0.808	0.794	0.780	0.765

The processing of the results by expression (6.52) gave the following parameters of the compression curve with a rather high probability (with a coefficient of correlation $r = 0.998$):

$$b = 5.87; \quad a = 1.146; \quad \Delta h = 5.87 \cdot \sigma^{1.146}.$$

In pressure intervals from 0.1 to 0.2 MPa and 0.2 to 0.3 MPa, $\beta = 0.5$ compression modules of deformation, respectively: $E = 3.4$ and 3.2 MPa

These values are usually used to calculate the subsidence for the DBN B.2.1-10-2009 [15].

If we consider the subsidence for (6.59) taking into account the variability and depending on the values of the additional pressure, then we have the data contained in Table. 6.3.

Table 6.3 - Summary of Determination of Detaching of Individual Square Foundations by (6.59)

z, m	b	1.5 m			2.1 m			2.7 m			3.3 m		
	σ_{zp}	216.0 кПа			216.0 кПа			216.0 кПа			216.0 кПа		
	σ_1	231.3 кПа			223.8 кПа			216.4 кПа			209.0 кПа		
β_z	0.803			0.805			0.808			0.811			
	σ^{cep} , кПа	E, МПа	S, см	σ^{cep} , кПа	E, МПа	S, см	σ^{cep} , кПа	E, МПа	S, см	σ^{cep} , кПа	E, МПа	S, см	
0	168	5.43	2.5	187	5.36	2.8	196	5.33	2.9	203	5.23	3.11	
1	83.7	6.02	1.11	118	5.58	1.69	147	5.60	2.1	160	5.52	2.32	
2	35.3	6.82	0.37	60.3	6.32	0.76	85.2	6.03	0.71	107	5.86	1.46	
3	22.2	7.3	0.13	33.9	6.87	0.39	51.5	6.48	0.64	69	6.24	0.88	
4	$\sum S = 4.11 (7.1)^*$			21.3	8.05	0.12	33.5	6.91	0.39	47	6.60	0.57	
5				$\sum S = 5.76 (10.2)^*$			25.1	7.10	0.14	33	6.94	0.38	
6							$\sum S = 6.88 (13.1)^*$			26	7.18	0.14	

$$\sum S = 8.86 (15.6)^*$$

* In brackets - settling on the recommendations of the DBN B.2.1-10-2009]

So, we recommend such an algorithm for the forecast of precipitation.

1. Conducting compression tests of samples of clay soil with the obligatory fulfillment of conditions for stabilization of deformations.
2. Approximation of compression results by degree dependence (6.52) and determination of parameters a and b .
3. Tests of samples of clay soil on shifts and determination of strength indicators and further critical pressure.
4. Calculation of lateral expansion parameters $\beta_z \cdot v$
5. Calculation of additional pressure according to the DBN scheme V.2.1-10-2009 [15].
6. Determination of the values of the deformation module taking into account the additional pressure curve within the compression layer.
7. Calculation of the subsidence based on the variation of the lateral expansion parameters and deformation modules.

Consequently, in comparison with the traditional method of using the general deformation module, the expression (6.57), together with the refined coefficient, can increase the value E .

This increase, in particular, for water-saturated clay soils, provides grouSSS for limiting the use of coefficients m_k that are usually taken into account when switching from a compression module to a stamp.

In the proposed method, it attracts, in particular, the possibility of taking into account in each case concrete indicators of physical and mechanical properties of the soil, rather than constant quantities, which are assigned only by the number of plasticity.

Numerous experimental data of primary (natural) and secondary (induced, ie, after consolidation or consolidation of soil) soil anisotropy justify the need to take this effect into account in order to clarify the calculation of sedimentation of the bases.

Some rather typical examples of deformation anisotropy of soils from the author's practice are given in Table. 6.4.

In this case, the coefficients of anisotropy were determined by the formula

$$n_{E_{\perp}} = E_{\perp} / E_{\parallel}, \quad (6.60)$$

where E_{\parallel} - the deformation of the soil in the case of orientation of the rings when removed at an angle $\alpha = 0^\circ$ relative to the horizontal plane; E_{\perp} - the same with $\alpha = 90^\circ$

The deformation anisotropy of the soil bases is proposed to be taken into account by determining the additional pressure in formula (6.51) by the expression

$$\sigma'_{zp,i} = \sigma_{zp,i} / \sqrt{n_{E\perp}} \quad (6.61)$$

For the conditions for calculating the settling of a separate foundation, considered above, at 0.8 the value of precipitation will increase by about 10%.

Table 6.4 - Coefficients of deformation anisotropy of soils

Type of soil Location	sampling	Porosity coefficient e	Humidity w, %	Deformation module E _z , MPa	coefficient n _{E⊥}
forest loam	natural array	1.10	16.5	1.5	0.93
		1.07	22.5	3.7	0.91
		0.87	27.5	5.4	0.87
		0.83 – 0.96	13 – 20	2.8	0.7 – 0.9
		0.825	19	5.6 – 6.0	0.7 – 0.9
loam	bulk foundation *	1.0 – 1.05	24	1.9	0.75
	bulk foundation **	0.8 – 0.86	25	2.8	0.86
loam	soil pillow	0.44 – 0.57	14 – 21	13.7 – 18.7	0.62 – 0.89
forest loams	under the sole of the foundation ***	1.04	22.5	3.9	0.92
		0.85	27.5	6.9	0.82
loam	under the NPSP	0.60	19	12.7	0.76

* - time of flooding about 40 years;

** - the retention time more than 10 years;

*** - the operating time of about 100 years at a ratio of the average pressure under the sole of the foundation to the calculated resistance of the soil

The regularities of changing the values of the deformation modulus of the soil at the depth of the densified zone, the use of which increases the accuracy of calculating settling of foundations reduced by the consolidation of their bases, can be obtained rationally within the framework of the first stage of simulation using the "PRIZ-Pile" complex (see Section 5).

Thus, it is possible to clarify the calculation of the settling of the bases by the method of layer summing taking into account: the variability of the deformation module of the soil throughout the range of pressure that perceives the basis of the load; coefficient β_z of soil strength; deformation anisotropy of soils; the regularities of the change in the value of the deformation modulus of the soil for the depth of the array under the foundations and within the artificial bases reduced by the consolidation of the soil, etc.

CONCLUSIONS

1. The method of physical modeling of a bulky anisotropic medium is developed, in particular, the technology of oriented soil filling in the cutting clip (shifts), for which, in accordance with BS 1377: 1990 Clause 4, a special clamping cutter for cutting material of 11 cm x 11 cm and height has been designed and manufactured. 9 cm. A model installation with closely spaced, rigid parallel walls was created for measuring side pressure on the basis of weight strain gauges with the possibility of oriented material filling in the axis of the structure.

2. The method of natural research of parameters of natural and induced anisotropy of the foundations of foundations created with consolidation of soil is developed.

3. For example, the formation of these properties of the array at the location of the piling piles in the pierced wells has been experimentally established that the geometrical dimensions of the consolidation and depletion zones of the foundations, reduced with the possibility of squeezing the soil in different directions, and the parameters of the soil within them are significantly influenced by: the characteristics of the natural I will become the soil; the directions of its displacement by the foundation (working body); geometric dimensions of the foundations.

4. The conducted trench experiments of the direct cut revealed a significant anisotropy of the strength characteristics as a consequence of the technology (orientation) of the filling. With orientations of particles $\beta = 0^\circ$ and 90° for rice, the angle of internal friction differs by 19.09%, and for the composite material φ is 11.67%. Measurement of lateral horizontal pressures under different filling conditions revealed a significant influence of the filling technology (material loading angle θ) on lateral pressure for various dry loose bulk materials. The largest difference in measured side pressures was on the filling of 0° and 90° , for rice it amounted to an average of 294%, and for composite material an average of 44%.

5. For the evaluation of the bases of VAT, during the formation of the bases of consolidation and their subsequent work, a program complex has been created in which the solution of the axisymmetric problem of the ITU by stepwise-iterative methods in the physical and geometrically nonlinear formulation with the representation of the soil isotropic or orthotropic medium is implemented. The use of eight-node isoparametric axial-symmetric CEs with properties that vary considerably in shape and volume makes it possible to use both a rectangular and curvilinear network of CEs, and taking into account these changes - the determination of displacements, stresses and given properties of soil at each step of the arrangement and loading of foundations. Simulation of their construction consists in the task of moving the nodes of the grid CE with the estimation of the SSS of the array. At the stage of their work, further

consideration is given to the consolidation of the soil, its transition to the plastic state, the possibility of slipping the lateral surface of the foundation on the ground.

6. For cases where the values of soil anisotropy coefficients differ significantly $n_\alpha = 1.0$, the accuracy of calculations of the bases of VAT may be increased by the use of an orthotropic or transversally isotropic medium in their physical ratios

7. The solution of tasks for determining the lateral pressures on the near-placed walls in the conditions of a plane problem for a homogeneous anisotropy on the displacement resistance of the medium, taking into account the filling technology on the basis of the classical Coulomb theory and the solution of RM Nedderman

8. It is possible to clarify the calculation of the settling of the bases by the method of layer summing taking into account: the variability of the deformation modulus of the soil throughout the range of pressure, which perceives the basis of the load; coefficient β_z of soil strength; deformation anisotropy of soils; the regularities of the change in the magnitude of the deformation of the soil for the depth of the array under the foundations and within the artificial bases, which are reduced with the consolidation of the soil.

REFERENCE

1. Аніскін А. Бічний тиск сипучого анізотропного середовища на близько розміщені стінки з врахуванням технологічних факторів: автореф. дис. ...канд. техн. наук: 05.23.02 / А. Аніскін. – Одеса: ОДАБА, 2017. – 23 с.
2. Болдырев Г.Г. Методы определения механических свойств грунтов: монография / Г.Г. Болдырев. – Пенза: ПГУАС, 2008. – 696 с.
3. Бугров А.К. Анизотропные грунты и основания сооружений / А.К. Бугров, А.И. Голубев. – СПб.: Недра, 1993. – 245 с.
4. Винников Ю.Л. Експериментальні дослідження анізотропії лесового суглинку в межах ґрунтової подушки / Ю.Л. Винников // Науковий вісник будівництва: Зб. наукових праць. – Вип. 7. – Харків: ХДТУБА, ХОТВ АБУ, 1999. – С. 260 – 263.
5. Винников Ю.Л. Исследования анизотропии лессовидных грунтов вокруг фундаментов впробитых скважинах / Ю.Л. Винников // Изв. вузов. Стр-во, 1999. – №4. – С. 123 – 128.
6. Винников Ю.Л. Математичне моделювання взаємодії фундаментів з ущільненими основами при їх зведенні та наступній роботі: Монографія / Ю.Л. Винников. – Полтава: ПолтНТУ імені Юрія Кондратюка, 2016. – 280 с., вид. друге, переробл. і доповн.
7. Винников Ю.Л. Моделювання процесів ущільнення ґрунту при вісесиметричному напружено-деформованому стані основ: Автореф. дис. ... д-ра техн. наук: 05.23.02 / Ю.Л. Винников. – К.: КНУБА, 2005. – 38 с.
8. Винников Ю.Л. Про деякі закономірності наведеної анізотропії глинистих ґрунтів / Ю.Л. Винников // Будівельні конструкції: Міжвід. наук.-техн. зб. – Вип. 53. – Кн. 1. – К.: НДІБК, 2000. – С. 78 – 81.
9. Габибов Ф.Г. Теория и практика улучшения свойств структурно-неустойчивых глинистых грунтов при решении геотехнических и инженерно-геоэкологических проблем / Ф.Г. Габибов. – Баку: Изд-во «Элм», 2014. – 422 с.
10. Гениев Г.А. Плоская деформация анизотропной сыпучей среды / Г.А. Гениев // Строительная механика и расчет сооружений, 1986. – № 5. – С. 33 – 35.
11. Гениев Г.А. Прочность и пластичность анизотропных материалов / Г.А. Гениев, А.С. Курбатов, Ф.А. Самедов. – М.: Интербук, 1993. – 188 с.
12. Гольдштейн М.Н. Механические свойства грунтов. – М.: Стройиздат, 1971 – 1979. – Т. I. – 1971. – 368 с.; Т. II. – 1973. – 375 с., Т. III. – 1979. – 304 с.
13. Горшков А.Г. Теория упругости и пластичности / А.Г. Горшков, Э.И. Старовойтов, Д.В. Гарлаковский. – М.: ФИЗМАТЛИТ, 2002. – 416 с.
14. Грунтоведение / В.Т. Трофимов, В.А. Королев, Е.В. Вознесенский и др. под ред. В.Т. Трофимова. – М.: Изд-во МГУ, 2005. – 1024 с.
15. ДБН В.2.1-10-2009. Основи та фундаменти будівель і споруд. Основні положення проектування. Зі змінами №1 і №2. – К.: Мінрегіонбуд України. – 2009. – 161 с.
16. ДСТУ Б В.2.1-4-96. Ґрунти. Методи лабораторного визначення характеристик міцності і деформованості / Державний комітет України у справах містобудування та архітектури. – К.: МНТКС, 1997. – 101 с.
17. Зоценко М.Л. Фундаменти, що споруджуються без виймання ґрунту: Монографія / М.Л. Зоценко, Ю.Л. Винников. – Полтава: ПолтНТУ імені Юрія Кондратюка, 2019. – 346 с.
18. Інженерна геологія. Механіка ґрунтів, основи та фундаменти: підручник / М.Л. Зоценко, В.І. Коваленко, А.В. Яковлєв, О.О. Петраков, В.Б. Швець, О.В. Школа, С.В. Біда, Ю.Л. Винников. – Полтава: ПолтНТУ, 2004. – 568 с.
19. Кандауров И.И. Механика зернистых сред и ее применение в строительстве / И.И. Кандауров. – М.: Стройиздат, 1966. – 319 с.

20. Каплер А.А. Монтаж, наладка и эксплуатация автоматических устройств / А.А. Каплер. – М.: Машиностроение, 1969. – 310 с.
21. Капустянский С.М. Упругопластическая дилатансионная модель анизотропных сред / С.М. Капустянский // Изв. АН СССР. Физика Земли. – 1985. – №8. – С. 50 – 59.
22. Клейн Г.К. Строительная механика сыпучих тел / Г.К. Клейн. – М.: Стройиздат, 1977. – 256 с.
23. Клованич С.Ф. Метод конечных элементов в нелинейных задачах инженерной механики / С.Ф. Клованич – Запорожье: ООО «ИПО «Запорожье». – 2009. – 400 с.
24. Коробова О.А. Методика численного решения задач о напряженно-деформированном состоянии анизотропных грунтов оснований / О.А. Коробова // Изв. вузов. Стр-во. – 2010. – №4. – С. 122 – 126.
25. Коробова О.А. Результаты экспериментальных исследований анизотропных лессовидных грунтов / О.А. Коробова // Изв. вузов. Стр-во. – 2003. – №2. – С. 128 – 130.
26. Кушнер С.Г. Расчет деформаций оснований зданий и сооружений / С.Г. Кушнер. – Запорожье: ООО «ИПО Запорожье», 2008. – 496 с.
27. Лехницкий С.Г. Теория упругости анизотропного тела / С.Г. Лехницкий. – М.: Наука, 1977. – 416 с.
28. Малышев М.В. Прочность грунтов и устойчивость оснований сооружений / М.В. Малышев. – М.: Стройиздат, 1994. – 228 с.
29. Месчян С.Р. Экспериментальные основы реологии глинистых грунтов / С.Р. Месчян. – Ереван: Гитутюн, 2008. – 807 с.
30. Можаровский В.В. Моделирование ударного взаимодействия анизотропных конструкций с использованием метода граничных элементов / В.В. Можаровский и др. // Математическое моделирование в механике деформируемых тел. Методы граничных и конечных элементов: Тр. XVI междунар. конф. – Т. 1, СПб, СПбГАСУ, 1998. – С. 60.
31. Молев М.О. Упрощенные динамические модели анизотропных оснований и их использование / М.О. Молев // Известия вузов. Стр-во и арх-ра. – 1987. – №3. – С. 41 – 45.
32. Геотехнічні властивості штучних основ для об'єктів гірничо-збагачувального комплексу: Монографія / Ю.Л. Винников, М.О. Харченко, Р.М. Лопан, С.М. Манжалій. – Полтава: ПолтНТУ імені Юрія Кондратюка, 2017. – 266 с.
33. Определяющие законы механики грунтов // Сб. ст.; Пер. с англ. / Под ред. В.Н. Николаевского – М.: Мир, 1975. – 230 с.
34. Орнатский Н.В. Механика грунтов / Н.В. Орнатский. – М.: Изд-во МГУ, 1962. – 447 с.
35. Осипов Ю.Б. Анизотропия механических свойств глинистых грунтов / Ю.Б. Осипов, А.И. Вайтекунене // Инженерная геология, 1979. – №4. – С. 106 – 112.
36. Парамонов В.Н. Метод конечных элементов при решении нелинейных задач геотехники / В. Н. Парамонов. – СПб. : Геореконструкция, 2012. – 264 с.
37. Посібник з проектування та влаштування набивних паль у пробитих свердловинах / М.Л. Зоценко, Ю.Л. Винников та ін. // ПолтНТУ, ДП НДІБК. – К., 2014. – 70 с.
38. Перельмутер А.В. Расчетные модели сооружений и возможность их анализа / А.В. Перельмутер, В.И. Сливкер. – М.: Изд-во СКАД СОФТ, 2011. – 736 с.
39. Разоренов В.Ф. Пенетрационные испытания грунтов / В.Ф. Разоренов. – М.: Стройиздат, 1980. – 248 с.
40. Рогаткина Ж.Е. Влияние анизотропности глинистых грунтов на их физико-механические свойства / Ж.Е. Рогаткина // Основания, фундаменты и механика грунтов. 1967. – №1. – С. 14 – 15.

41. Садовский С.С. Исследование анизотропии прочностных характеристик намывных песчаных грунтов / С.С. Садовский // Проектирование и строительство объектов на пойменно-намывных и заболоченных территориях БССР. – Мн., 1981. – С. 15 – 16.
42. Сидоров Н.Н. Сопротивление сдвигу песка при малых нормальных давлениях / Н.Н. Сидоров // Исследования деформаций и прочности оснований: сб. тр. ЛИИЖТ, 1967. – Вып. 272. – С. 3 – 9.
43. Соколов Б.А. Влияние текстуры и влажности на анизотропию прочности глинистых грунтов / Б.А. Соколов // Материалы II научн. конф. МГУ: сер. Гидрогеология. – М., 1975. – С. 45 – 51.
44. Справочник геотехника. Основания, фундаменты и подземные сооружения / Под ред. В.А. Ильичева и Р.А. Мангушева. – М.: Изд-во АСВ, 2014. – 728 с.
45. Тер-Мартirosян З.Г. Механика грунтов / З.Г. Тер-Мартirosян. – М.: АСВ, 2009. – 550 с.
46. Тиунов С.В. Численное моделирование стабилметрических испытаний анизотропных грунтов / С.В. Тиунов // Основания и фундаменты: Респ. межвед. науч.-техн. сб. – Вып. 22. – К.: Будівельник, 1989. – С. 90 – 93.
47. Федоровский В.Г. Современные методы описания механических свойств грунтов. Обзор / В.Г. Федоровский. – М.: ВНИИИС, 1985. – 73 с.
48. Филимонов В.А. Исследования анизотропии прочностных свойств намывных несвязных грунтов и золы / В.А. Филимонов // Известия ВНИИГ, 1974. – Т. 106. – С. 280 – 286.
49. Харр М.Е. Основы теоретической механики грунтов / М.Е. Харр. – М.: Стройиздат, 1971. – 317 с.
50. Хейдар А. Влияние анизотропности грунтовых оснований на несущую способность эксплуатируемых портовых сооружений: дис. ... канд. техн. наук: 05.22.19 / А. Хейдар. – Одесса: ОМИ, 1990. – 151 с.
51. Цимбал С.Й. Експериментальні дослідження анизотропії відносної просадочності лесових ґрунтів / С.Й. Цимбал, Н.М. Богославець // Основи і фундаменти. – 2008. – Вип. №31. – С. 20 – 24.
52. Цымбал С.И. Методика розрахунків осідання основи стрічкових фундаментів з урахуванням анизотропії ґрунтів і змінного модуля деформації / С.И. Цымбал, Л.Ч. Меуленер // Основи і фундаменти. – 2001. – Вип. 26. – С. 99 – 105.
53. Цытович Н.А. Механика грунтов: Краткий курс: Учебник. Изд. 5-е / Н.А. Цытович. – М.: КД «ЛИБРОКОМ», 2009. – 272 с.
54. Черный Г.И. Деформационная анизотропия грунтов в зоне действия взрыва и устойчивости бортов взрывных выемок / Г.И. Черный // Взрывные работы в грунтах и горных породах. – К.: Наукова думка, 1982. – С. 34 – 38.
55. Шапиро Д.М. Метод конечных элементов в строительном проектировании / Д.М. Шапиро. – Воронеж: «Научная книга», 2013. – 181 с.
56. Шаповал В.Г. Особенности взаимодействия несомого водонасыщенного основания с расположенными на нем зданиями и сооружениями / В.Г. Шаповал, П.Н. Нажа, А.В. Шаповал. – Дн-вск: Пороги, 2010. – 251 с.
57. Школа А.В. Активное давление связного анизотропного грунта при плоской поверхности скольжения / А.В. Школа, Е.В. Гришко // Морская гидротехника и механизация перегрузочных работ в портах: сб. научн. трудов ОИИМФ. – М.: Мортехинформреклама, 1992. – С. 32 – 36.
58. Школа А.В. Боковое давление анизотропных грунтов на сооружения / А.В. Школа. – Одесса: МАГ ВТ, 2012. – 219 с.
59. Школа А.В. Боковое давление анизотропных сыпучих сред на близкорасположенные крутые наклонные стенки. Решения осесимметричной и плоской

- задач / А.В. Школа, А. Анискин, Б. Солдо // 3б. наук. праць, Серія: Галузеве машинобудування, будівництво. – Вип. 4(34). – Т. 2. Полтава: ПолтНТУ, 2012. – С. 141 – 148.
60. Школа А.В. Диагностика портовых сооружений / А.В. Школа. Одесса: Астропринт, 2010. – 592 с.
61. Школа А.В. Экспериментальные исследования естественной прочностной анизотропии лессовых грунтов / А.В. Школа // Тр. 3 Української конф. з механіки ґрунтів і фундаментобудування. Т. 2, Одеса: ОДАБА. 1997. – С. 334 – 336.
62. Allahverdizadeh P. Influence of highly anisotropic properties on probabilistic slope stability / P. Allahverdizadeh, D. Griffiths, G. Fenton // Proc. of XVI ECSMGE Geotechnical Engineering for Infrastructure and Development. – Edinburg. – 2015. – P. 1555 – 1559.
63. Amadei B. Rock anisotropy and the theory of stress measurements / B. Amadei. – Berlin: Springer, 1983. – 478 p.
64. Arthur I.R.F. Inherent anisotropy in a sand / I.R.F. Arthur, B.K. Menzies // Geotechnique, 1972. – V. 22. – № 1. – P. 115 – 128.
65. Bazant Z.P. Micromechanics Model For Creep of Anisotropic Clay / Z.P. Bazant, I.K. Ozaydin, R.J. Krizek // J. of Engineering Mechanics Division, Proc/ of the American Society of Civil Engineers, 1975. – Vol. 101. – № EM 1. February. – P. 57 – 78.
66. Brown C.J. Experiments on a square platform steel silo / C.J. Brown, E.H. Lahlouh, J.M. Rotter // Chemical Engineering Science, 2000. – Vol. 55. – P. 4399 – 4413.
67. British Standard 1377. Methods of Test for Soils for Civil Engineering Purposes. British Standards Institution. – London. – 1990.
68. Bucklin R.A. Slip-stick frictional behavior of wheat on galvanized steel / R.A. Bucklin, M. Molenda, T.C. Bridges, I.J. Ross // Trans. of the ASAE. – 1996. – Vol. 39(2). – P. 649 – 653.
69. Casagrande A. Shear failure of anisotropic soils / A. Casagrande, N. Carillo // Contributions to soil mechanics, 1941 – 1953. – P. 122 – 135.
70. Chau K. Numerical Methods / K. Chau // Proc. of the 18th Intern. Conf. on Soil Mechanics and Geotechnical Engineering. – Paris. – 2013. – P. 647 – 654.
71. Cudny M. Influence of anisotropic stiffness in numerical analyses of tunneling and excavation problems in stiff soils / M. Cudny, E. Partyka // Proc. of the 19th Intern. Conf. on Soil Mechanics and Geotechnical Engineering (Sep. 17 – 22, 2017 / COEX, Seoul, Korea) – ed. by W. Lee, J.-S. Lee, H.-K. Kim, D.-S. Kim. – Seoul. – 2017. – P. 707 – 710.
72. Duncan I.M. Strength variation along failure surface in clay / I.M. Duncan, H.B. Seed // J. Soil Mech. and Found. Div. ASCE, 1966. – V. 92. – № SM 6. – P. 81 – 104.
73. Dunstan T. The influence of grading on the anisotropic strength of sand / T. Dunstan // J. Geotechnique, 1972. – Vol 22. – No 3. – P. 529 – 532.
74. Ewertowska-Madej Z. Anizotropia wytrzymałości kaolinu sedleckiego w aparacie bezpośredniego scinania / Z. Ewertowska-Madej // IBW, Polskiej AN. Gdansk rozprawy hydrotechniczne. Zeszyt 30. – 1972. – S. 121 – 124.
75. Fu Z.Y. Quantifying the influence depth of dynamic compaction using the discrete element method / Z.Y. Fu, M.B. Jaks, A. Deng // Proc. of the XVI ECSMGE Geotechnical Engineering for Infrastructure and Development. – Edinburg. – 2015. – P. 3851 – 3856.
76. Gallego E. Simulation of silo filling and discharge using ANSYS and comparison with experimental data / E. Gallego, A. Ruiz, P.J. Aguado // Computers and Electronics in Agriculture, 2015. – Vol. 118. – P. 281 – 289.
77. Gazarek M. Granulometrijski sastav šljunaka i pijesaka i teški minerali u pijescima dravskog bazena od Ormoža do Đurđevca / M. Gazarek // Rudarsko – geološko – naftni zbornik, 1990. – Vol. 2. – S. 67 – 73.

78. Gazetas G. Stresses and displacements in cross-anisotropic soils / G. Gazetas. – J. Geotechnical Eng. Division. Proc. ASCE, 1982, vol.108, №4. – P. 532 – 553.
79. Guo P. Modified direct shear test for anisotropic strength of sand / P. Guo // J. of geotechnical and geoenvironmental engineering, 2008. – Vol. 134 (9). – P. 1311 – 1318.
80. Henke S. Numerical modeling of pile installation / S. Henke, J. Grabe // Proc. of the 17th Intern. Conf. on Soil Mechanics and Geotechnical Engineering (Alexandria, 2009). – Amsterdam: IOS Press, 2009. – P. 1321 – 1324.
81. Horn R.M. Analysis of the Stress Distribution in Two-Dimensional Bins by the Method of Characteristics / R.M. Horn, R.M. Nedderman // Powder Technology, 1974. – Vol. 14. – P. 93 – 102.
82. Hsiao-Sung H.J. Wall stresses developed by granular material in cylindrical bins: Magister dissertation / H.J. Hsiao-Sung, 1970. – 130 p.
83. Innovative projects in difficult soil conditions using artificial foundation and base, arranged without soil excavation / P. Kryvosheiev, G. Farenjuk, V. Tytarenko, I. Boyko, M. Kornienko, M. Zotsenko, Yu. Vynnykov, V. Siedin, V. Shokarev, V. Krysan // Proc. of the 19th Intern. Conf. on Soil Mechanics and Geotechnical Engineering (Sep. 17 – 22, 2017 / COEX, Seoul, Korea) – ed. by W. Lee, J.-S. Lee, H.-K. Kim, D.-S. Kim. – Seoul. – 2017. – P. 3007 – 3010.
84. Investigation of the effect of the deformation anisotropy on the stress-strain state of the soil basement / L. Nuzhdin and all // Proc. of the 19th Intern. Conf. on Soil Mechanics and Geotechnical Engineering (Sep. 17 – 22, 2017 / COEX, Seoul, Korea) – ed. by W. Lee, J.-S. Lee, H.-K. Kim, D.-S. Kim. – Seoul. – 2017. – P. 789 – 792.
85. Janssen H.A. Getreidedruck in Silozellen: Z. Ver. Dt. Ing / H.A. Janssen, 1895. – Vol. 39. – P. 1045 – 1049.
86. Krizek R.I. Fabric effects on strength and deformation on kaolin clay / R.I. Krizek // Proc. of the IXth ICSMFE. Tokyo, 1977. – Vol. 1. – P. 169 – 176.
87. Kulatilake H. Development of a New Peak Shear Strength Criterion for Anisotropic Rock Joints / H. Kulatilake // Geotechnical Problems of Construction, Architecture and Geoenvironment on Boundary of XXI Century. – Proc. of the First Central Asian Geotechnical Symposium. – Astana, 2000. – Vol. II. – P. 746 – 749.
88. Lo K.Y. Shear strength properties of two stratified clays / K.Y. Lo, V. Milligan // J. of Soil Mech. and Found. Div. proc. 93, 1967. – № SM1. – P. 1 – 15.
89. Lo K.Y. Strength anisotropy and time effects of two sensitive clays / K.Y. Lo, J.P. Morin // Canadian Geotechnical J., 1972. – № 9. – P. 261 – 277.
90. Loh A.K. Directional Variation in Undrained Shear Strength and Fabric of Winnipeg Upper Brown clay / A.K. Loh, R.T. Holt // Canadian geotechnical J., 1974. – Vol. 9. – №3. – P. 430 – 437.
91. López Bravo E. Formulation of a frictional-cohesive soil model by the Discrete Element method / E. López Bravo et al. // Revista Ciencias Técnicas Agropecuarias, 2013. – Vol. 22. – No. 3. – P. 12 – 17.
92. Magnan J. Mesure des parametres d'elasticite anisotrope de l'argile molle organique de cubzac dans le domaine surconsolide / J. Magnan, M. Piyal // Revue française de geotechnique. – 1985. – №33. – P. 5 – 18.
93. Manjriker A. Foundation Engineering / A. Manjriker, I. Gunarante. – New York: Taylor and Francis, 2006. – 608 p.
94. Mechi J. Geotechnical Engineering Examples and Solutions Using the Cavity Expanding Theory / J. Mechi. – Budapest: Hungarian Geotechnical Society. – 2013. – 221 p.
95. Molenda M. Anizotropia kąta tarcia wewnętrzznego ziarna pszenicy / M. Molenda, M. Stasiak // Inżynieria Rolnicza, 2001. – №2. – S. 245 – 251.

96. Molenda M. Effect of Filling Method on Load Distribution in Model Grain Bins / M. Molenda, J. Horabik, I.J. Ross // Transaction of American Society of Agricultural Engineers, 1996. – Vol. 39(1). – P. 219 – 224.
97. Molenda M. Loads in model grain bins as affected by filling methods / M. Molenda, J. Horabik, I.J. Ross // Proc. of American Society of Agricultural Engineers, 1993. – Vol. 36(3). – P. 915 – 919.
98. Molenda M. Stress and deformation of wheat in direct shear test / M. Molenda, J. Horabik, I.J. Ross // Int. Agrophysics, 1998. – Vol. 12. – P. 115 – 118.
99. Nedderman R.M. Statics and Kinematics of Granular Materials / R.M. Nedderman // New York: Cambridge University Press, 1992. – 352 p.
100. Nguyen D. Finite Element Methods: Parallel-Sparse Statics Eigen-Solution. – Springer, 2006. – 533 p.
101. Nishimura S. Laboratory study of anisotropy of natural London Clay: PhD dissertation / S. Nishimura. – London: Imperial College London, 2005. – 412 p.
102. Novskiy A. Investigation of anisotropic properties of shell limestone by models of bored pile in laboratory-like environments / A. Novskiy, V. Novskiy, V. Vivcharuk // Technical J., 2015. – Vol. 9(2). – P. 151 – 152.
103. Numerical methods in geomechanics // Proc. of the 5 Intern. symposium, NUMOG V, Davos, 1995 / Ed. by G.N. Pande. – Rotterdam: Balkema, 1995. – 720 p.
104. Numerical methods in geotechnical engineering // Proc. of the third European conf., Manchester, 7-9 September 1994 / Ed. by I.M. Smith. – Rotterdam: Balkema, 1994. – 444 p.
105. Numerical simulation of consolidation problem / K. Edip, M. Garevski, V. Sheshov, J. Bojadjeva // Proc. of the XVI ECSMGE Geotechnical Engineering for Infrastructure and Development. – Edinburg. – 2015. – P. 3847 – 3850.
106. Oda M. Experimental study of anisotropic shear strength of sand by plan strain test / M. Oda, I. Koishikawa, T. Niguchi // Soil and Found, 1978. – V. 18. – №1. – P. 25 – 38.
107. Plaxis 3D Foundation. Reference Manual. Version 1.5 / R. Brinkgreve et al. – Delft: Delft University of Technology. – 2006. – 152 p.
108. Plaxis 3D Foundation. Material Models Manual. Version 1.5 / R. Brinkgreve et al. – Delft: Delft University of Technology. – 2006. – 65 p.
109. Rahardjo H. Hydraulic Anisotropy Behavior of Compacted Soil / H. Rahardjo, A. Satyanaga, L.E. Choon // Proc. of the 19th Intern. Conf. on Soil Mechanics and Geotechnical Engineering (Sep. 17 – 22, 2017 / COEX, Seoul, Korea) – ed. by W. Lee, J.-S. Lee, H.-K. Kim, D.-S. Kim. – Seoul. – 2017. – P. 1241 – 1244.
110. Reimbert M.L. Silos - Theory and Practice / M.L. Reimbert, A.M. Reimbert. – Claustal, Germany: Trans Tech Publication, 1st Edition, 1976. – 250 p.
111. Sergeev E.M. Structural aspects of shearing resistance of clays / E.M. Sergeev, V.T. Osipov // Proc. of the IXth ICSMFE. Tokyo, 1977. – Vol. 1. – P. 193 – 198.
112. Schulze D. Untersuchungen zur gegenseitigen Beeinflussung von Silo und Austragorgan, Dissertation / D. Schulze. – Fakultät für Maschinenbau und Elektrotechnik der Technischen Universität Carolo-Wilhelmina zu Braunschweig, 1991. – 212 s.
113. Sperl M. Experiments on Corn Pressure in Silo Cells – Translation and Comment of Janssen's Paper from 1895 / M. Sperl // Granular Matter, 2006. – No. 8. – P. 59 – 65.
114. Tong Z. DEM Simulation of Biaxial Compression Experiments of Inherently Anisotropic Granular Materials and the Boundary Effects / Z. Tong, L. Zhang, M. Zhou // J. of Applied Mathematics. – Vol. 2013. – Article ID 394372. – P. 1 – 13.
115. Tong Z. Experimental investigation of shear strength of saSSS with inherent fabric anisotropy / Z. Tong et al. // Acta Geotechnica, 2014. – Vol. 9. – P. 257 – 275.
116. Vynnykov Yu.L. Features of the mathematical modeling of foundations interaction with compacting soils, with anisotropic properties / Yu.L. Vynnykov, O. Aniskin // Academic

- Journal. Series: Industrial Machine Building, Civil Engineering. – Poltava: Poltava National Technical Yuri Kondratyuk University. – 2017. – Is. 1 (48)'. – P. 156 – 164.
117. Yang Z.X. Quantifying and modelling fabric anisotropy of granular soils / Z.X. Yang, X.S. Li, J. Yang // *Geotechnique*, 2008. – Vol. 58. – No 4. – P. 237 – 248.
118. Yong R.N. Anisotropic behavior of sensitive clay / R.N. Yong, V. Sylvestry // *Canad. Geot. J.*, 1979. – Vol. 10. – P. 335 – 350.
119. Zhang K. Recent developments in geomaterial's stress-induced anisotropy research at Hohai university: testing, modeling and application / K. Zhang, J. Zhu, F.N. Charkley // *Proc. of the 19th Intern. Conf. on Soil Mechanics and Geotechnical Engineering (Sep. 17 – 22, 2017 / COEX, Seoul, Korea)* – ed. by W. Lee, J.-S. Lee, H.-K. Kim, D.-S. Kim. – Seoul. – 2017. – P. 997 – 1000.
120. Zienkiewicz O. The finite element method. Fifth edition / O. Zienkiewicz. – V. 2. Solid Mechanics – Butterworth-Heinemann, 2000. – 459 p.
121. Zotsenko N. Anisotropic Soil Medium of Foundation Compaction Zone / N. Zotsenko, Y. Vynnykov // *Problemy Naukovo – Badawcze Budownictwa. T. VII. – XLIV Konf. Nauk. Krynica'98 – Poznan – Krynica*, 1998. – P. 193 – 201.
122. Zotsenko N.L. Long-Term Settlement of Buildings Erected on Driven Cast-In-Situ Piles in Loess Soil / N.L. Zotsenko, Y.L. Vinnikov // *Soil Mechanics and Foundation Engineering*. – July 2016, Volume 53, Issue 3, pp 189 – 195 (First Online: 31 August 2016. DOI: 10.1007/s11204-016-9384-6. © Springer Science+Business Media New York 2016).
123. Zotsenko M. Modern practice of determination of strength characteristics of cohesive soils by penetration methods / M. Zotsenko, Y. Vynnykov, A. Yakovlev // *Proc. of XIVth Danube – European Conf. on Geotechnical Eng.* – Bratislava: Slovak University of Technology. – 2010. – P. 245 – 253.